

The pes planus foot type and its evolutionary significance: the use of radiographic measurements of the talus and calcaneus in the interpretation of hominin pedal remains

David Agoada

A dissertation

submitted in partial fulfillment of the
requirements for the degree of

Doctor of Philosophy

University of Washington

2018

Reading Committee:

Patricia A. Kramer, Chair

Daniel Eisenberg

Donald Grayson

Program Authorized to Offer Degree:

Anthropology

©Copyright 2018

David Agoada

University of Washington

Abstract

The pes planus foot type and its evolutionary significance: the use of radiographic measurements of the talus and calcaneus in the interpretation of hominin pedal remains

David Agoada

Chairperson of the Supervisory Committee:

Patricia Ann Kramer, PhD

Department of Anthropology

This dissertation explores the relationship between the morphology of the talus and calcaneus, as expressed by certain measurement variables, and the medial arch height in the foot of modern humans. Features seen in fossil hominins pedal remains have been postulated as similar to that found in the pes planus foot type. Since pes planus (flatfoot) can only be identified in a functional, intact, weight-bearing foot, radiographs were used to examine this relationship. However, before radiographic measurements of the talus and calcaneus could be analyzed in the same manner as physical bone, the relationship between measurements taken from a physical bone and its radiographic image had to be identified. Two separate studies using limbs amputated for medical reasons were undertaken to examine this relationship. In the first study selected linear measurements were performed on each skeletonized talus and calcaneus. Corresponding landmarks were identified on the radiographic images and the

distances between these points determined. Using the measurements taken from the physical bone, the accuracy of the radiographic measurements was evaluated. Most sagittal and transverse plane measurements were associated ($r^2 = 0.20 - 0.88$, $p < 0.001$). In the second study, selected angular measurements were performed on both bone and radiograph and evaluated in a similar manner. As in the first study, most transverse and sagittal plane measurements were associated ($r^2 = 0.35 - 0.78$, $p < 0.001$). The results of these two studies indicated that selected linear and angular measurements of the talus and calcaneus taken from radiographic images could be compared quantitatively to the physical bone, demonstrating that they provide useful information concerning both bones. The third study examined the relationship between arch height and talar and calcaneal morphology using a collection of weight-bearing radiographs ordered for medical evaluation. Selected variables derived from the first two studies were employed to examine this relationship. The results of the third study indicated that most angular measures of the calcaneus are associated with arch height to some degree ($r^2 = 0.17 - 0.44$). However, angular measurements of the talus and linear measurements of both the talus and calcaneus either did not correlate with arch height or were weakly associated. These results demonstrated that the relationship between the morphologies of these bones and the biomechanics of the modern human foot is complex, requiring further investigation. The three studies presented here suggest that selected measurements of the talus and calcaneus taken from radiographic imaging of weight-bearing radiographs can provide valuable information on the morphologies of the talus and calcaneus in the pes planus foot of modern humans that can be used in the interpretation of hominin pedal remains. From the results of the third study, hypotheses were developed concerning the pes planus foot type: that

the shape of the talus does not play a major role in pes planus; variations in the “locking mechanism” of the calcaneocuboid joint may account for variations in arch height in modern humans; variations in the shape of the calcaneus are related to arch height and pes planus. These hypotheses should help stimulate further investigation concerning both the evolution of the bipedal hominin and the analysis of foot type in osteological collections of ancient as well as recent human populations. There is still much work to be done in the understanding of the relationship between the biomechanical function of the human foot and the morphology of the talus and calcaneus.

Table of Contents

Chapter 1: Introduction..... 1

 Evolution of the human foot: Historical review..... 3

 Functional anatomy of the human foot 5

 The foot and joint motion in the gait cycle 10

 Pes Planus foot type..... 12

 Definition and classification..... 12

 Clinical methods of evaluation..... 16

 Radiographic imaging of the human foot..... 18

 Positioning technique and terminology for standard radiographic views..... 19

 The significance of osteologic variability of the talus and calcaneus as it relates to foot type classification..... 20

 Pes planus and evolution of the human foot 25

 Hypothesis and Goals..... 28

 Chapter 1: Literature cited 31

 Chapter 1: List of Figures..... 43

Chapter 2: The relationship between linear osteological and radiographic measurements of the human calcaneus and talus 75

 Preface..... 75

 Abstract 75

 Introduction 76

 Materials and Methods 83

 Results 85

 Discussion 86

 Chapter 2: Appendix..... 91

 Talus bone measurements 91

 Sagittal plane measurements (Figure 1)..... 91

 Transverse plane measurements (Figures 3a and 3b) 92

 Talus radiographic measurements..... 93

 Lateral view measurements (Figures 2a and 2b) 93

 AP view measurements (Figures 4a and 4b) 94

 Calcaneus bone measurements..... 94

 Sagittal plane measurements (Figure 5)..... 95

Transverse plane measurements (Figures 7a and 7b)	96
Calcaneus radiographic measurements	96
Lateral view measurements (Figures 6a and 6b)	96
AP view measurements (Figures 8a and 8b)	97
Chapter 2: Literature cited	99
Chapter 2: List of Tables	102
Chapter 2: List of Figures	105
Chapter 3. The relationship between angular osteological and radiographic measurements of the human talus and calcaneus	123
Preface	123
Abstract	123
Introduction	124
Materials and Methods	129
Results	133
Discussion	134
Conclusions	140
Chapter 3: Appendix.....	143
Talus bone and radiographic measurements	143
Talus transverse plane measurements	143
Talus sagittal plane measurements.....	145
Calcaneus bone and radiographic measurements	146
Calcaneus transverse plane measurements	146
Calcaneus sagittal plane measurements	147
Chapter 3: Literature cited	151
Chapter 3: List of Tables	154
Chapter 3: List of Figures	158
Chapter 4. Radiographic measurements of the talus and calcaneus in the adult pes planus foot type	172
Preface	172
Abstract	172
Introduction	173
Materials and Methods	182
Results	185

Discussion	187
Conclusion	196
Chapter 4: Appendix.....	198
Angular variables of the foot lateral view	198
Linear variables of the foot lateral view.....	199
Angular variables of the foot AP view	200
Linear variables of the talus lateral view.....	200
Angular variables of the talus lateral view	201
Linear variables of the talus AP view	202
Angular variables of the talus AP view.....	202
Linear variables of the calcaneus lateral view.....	203
Angular variables of the calcaneus lateral view	204
Linear variables of the calcaneus AP view.....	206
Angular variables of the calcaneus AP view	206
Chapter 4: Literature cited	208
Chapter 4: List of Tables	216
Chapter 4: List of Figures.....	231
Chapter 5: Evolution of the human foot, areas of future investigation, and conclusions	241
Summary of results from Chapters 2, 3, and 4: Implications	241
Areas of future investigation: Hypotheses concerning requirements for the foot in obligate bipedalism and striding gait	243
Areas of future investigation: Recommendations for future areas of research concerning the interpretation of fossil hominin pedal remains.....	258
Areas of future investigation: Recommendations for further studies of the morphology of the talus, calcaneus and other bones of the modern human foot.....	259
Conclusions	261
Chapter 5: Literature cited	263
Chapter 5: List of Figures.....	266
Appendix A: Tarsal anatomy.....	276
Talus (astragalus)	276
Radiographic anatomy of the talus.....	278
Calcaneus (os calcis).....	279

Radiographic anatomy of the calcaneus	281
Appendix A: Literature cited	283
Appendix B: Further Details Materials and Methods Chapters 2 and 3	284
Appendix B: Literature cited	286
Appendix B: List of Tables	287
Appendix C: Raw data	292
Chapter 2: (Tables 1a-2)	292
Chapter 3 (Tables 3-4b)	295
Chapter 4 (Tables 5a-10b)	298
Appendix D Statistical Data	312
Chapter 2 Statistical analysis calcaneus	312
Chapter 2 Statistical analysis talus	319
Chapter 3 Statistical analysis calcaneus	328
Chapter 3 Statistical analysis talus	340
Chapter 4 Descriptive statistical analysis	345
Chapter 4 Linear regression analysis	351

Acknowledgements

There are so many people who assisted me, supported me, and encouraged me in attaining this degree. It is a long list that spans the decades. Many are lost to the haze of time. I'd like to thank the physical anthropology faculty during my early years at UW, including Drs. Laura Newell, Marshall T. Newman, Peter Nute, Richard Klein, John Rensberger, and my fellow graduate students, some who became movers and shakers in the profession, including Nina, Ed, Jay, Dave, Phil, Ken, and Dr. Lew Tarrant, my anatomy guru. Thank you to Drs. Mark Levinson and Richard Pelman. A special thank you to Keith Smith and Steve Rose, who remain my friends to this day. Thank you to Dr. Jean Turnquist, my gross anatomy prof who encouraged my research interests in physical anthropology while I was a student at PCPM. A special thank you to Dr. Bruce Hirsch who supported the early work on my dissertation research project and served as a member of my first reading committee. A special thank you to Nancy Belyea, my medical assistant and friend who helped me in the preparation of the specimens used in this study and was always there for moral support and encouragement. Acknowledgement to the forensic anthropology faculty at BU for instructing me on much of the basics that were necessary for my research and data collection. A special nod to Dr. Don Siwek. Thank you to Drs. Sarah Reel, Ivan Birch, Steve Wachter, Wes Vernon and Michael Nirenberg, my forensic podiatry colleagues, for their support and encouragement.

Thank you to Dr. Don Grayson and Dr. Dan Eisenberg for agreeing to be members of my reading committee and taking the time to go through my writings. Thank you to Catherine Ziegler for all her time and effort in getting me reinstated. I could not have gotten to this point without her efforts.

Most importantly, a very special acknowledgement to Dr. Patricia Kramer, who gave me this opportunity. Over the last seven long years her time, patience and knowledge allowed me to develop my passion into a workable, successful dissertation project. Thank you so much. I could not have done it without you! I am forever in your debt.

And of course, thank you to my sons Joseph and Keith, who are always there with unconditional love and support. They have forever inspired me to work hard, do good, and be the best I can. Thank you to Jen, the newest member of our family, for her support, encouragement, and help in getting this document done. And finally, to Clara, my long-suffering wife through this entire 46-year process, who noted that Moses took less time to lead the children of Israel to the promised land than it did for me to complete my studies.

Dedication

This dissertation is dedicated to the memory of Dr. Daris Swindler, the former chairman of my graduate committee, who always had faith in me, and though I left the graduate program to become a podiatrist, allowed me to return 10 years later to resume my studies. He always supported me and understood when I had to leave the program for the second time, as my practice and family grew. I would like to think of myself as the 20th member of that elite group of individuals who make up his graduate students. Daris, mentor and friend, this is for you.

Chapter 1: Introduction

“The investigation of man’s origin and evolution has necessarily been based largely upon indirect evidence provided by comparative studies of living forms, for the more direct evidence of paleontology is still relatively slight, fragmented and too often ambiguous. Recent years have witnessed the discovery of a considerable number of fossil hominids, many of them obviously more primitive than modern man, and of numerous fossils of other primates. But these, instead of simplifying the phylogenetic story, have merely served to demonstrate its complexity, so that the apparent course of man’s evolution is actually more obscure than it was a few decades past (Straus, 1949 p. 200).”

Since the middle of the 19th century, theories have been advanced to explain how the striding bipedal gait of modern humans, and the foot configuration associated with that form of locomotion, evolved. Until the mid 20th century, pedal remains were limited largely to later fossil hominins such as those associated with Neandertals (Trinkaus, 1983), requiring theories on the evolution of bipedalism to be based largely on comparative studies using non-human primates and variations seen in the feet of modern humans (Morton, 1935; Wood-Jones, 1944). Discoveries of postcranial material in the later part of the 20th century provided information concerning the bipedal locomotion of early hominins, though associated pedal material, while important, continued to be limited and open to interpretation (Day and Wood, 1968; Susman, 1983; Clarke and Tobias, 1995; Kidd et al., 1996). Recent additions to the pedal hominin fossil record have only added to the confusion concerning the form, function and evolution of the human foot (Lovejoy et al., 2009; Jungers et al., 2009a; Zipfel et al., 2011; DeSilva et al., 2013;

Harcourt-Smith et al., 2015). One important trajectory of thought that has been proposed is that the foot of our hominin ancestors was functionally similar to the foot of modern individuals with excessive pronation associated with a medial longitudinal arch that is close to or in contact with the ground on full weight-bearing (Morton, 1935; DeSilva, 2010; DeSilva and Throckmorton, 2010; DeSilva et al., 2014; DeSilva et al., 2015), termed the pes planus foot type (Helfet and Lee, 1980; Staheli, 1999).

The talus (Figures 1a-1f; 2a-2b), calcaneus (Figures 3a-3; 4a-4b) and their articulations as components of the subtalar and midtarsal joints, play major roles in the biomechanics of the foot and thus are recognized as being important elements in excessive pronation of the foot. The examination of the relationship of these bones to each other, and to the foot as a whole, should assist in the understanding of the pes planus foot in modern humans, as well as in the interpretation of the hominin pedal fossil record.

Humans are the only living primates whose form of locomotion is classified as obligate bipedalism (Begun, 2004). While the human foot has evolved from a grasping organ adapted to arboreal life to a stable platform for habitual bipedal gait on the ground, the sequence of adaptive events that resulted in the modern human foot is unknown, and the functional anatomy of those fossil hominins believed to be associated with that evolutionary pathway unclear.

Evolution of the human foot: Historical review

Three general areas of investigation have been employed over the years to assist in understanding the evolution of bipedalism in general, and the human foot in particular: comparative primate anatomy, medical studies in modern humans, and the fossil record.

Comparative anatomy using non-human primates has been one area of investigation, with emphasis on the feet of human's closest extant relatives, the gorilla (*Gorilla*) and chimpanzee (*Pan*) (Schultz, 1950; Lewis, 1962; Schultz, 1963; Lewis, 1964; Schultz, 1969; Preuschoft, 1970; Preuschoft, 1971; Lewis, 1980a; Lewis, 1980b; Lewis, 1980c; Lewis, 1983; Langdon, 1986; Tocheri et al., 2011; Dunn et al., 2014). Some studies based on upper and lower limb comparative anatomy have suggested, however, that the ancestors of human bipedalism may be better demonstrated functionally by the arboreal gibbon (*Hylobates*) and orangutan (*Pongo*) than by the terrestrial knuckle-walking gorilla and chimpanzee (Vereecke et al., 2005; Crompton et al., 2008; Crompton et al., 2010). The problem with the use of living nonhuman primates as models is no extant primate species ambulates in a manner similar to that of modern human bipedalism, limiting their use in the interpretation of the hominin fossil record.

A second area of investigation has been the application of modern human anatomy, medicine, and biomechanics to better understand how the ancestral human foot functioned and how habitual bipedal gait may have evolved. It is interesting to note that some of the earliest investigators, such as Dudley Morton (Morton, 1935) were trained physicians who used their clinical knowledge of the human foot to investigate the evolution of the human foot to understand the etiology of various pedal problems, as well as to help shed light on the ancestral condition from which the human foot evolved. Applying what is known about human foot

biomechanics and foot dysfunction continues to be important in the interpretation of the known fossil material in reconstructing the evolution of human bipedalism. In the medical literature, the flat foot, or pes planus foot type, has been associated with painful symptomatology. The etiology of the most common forms of pes planus has been ascribed to the retention of more “primitive” characteristics from our human ancestors. Alfred Krogman (Krogman, 1951) described pes planus as a “scar” of human evolution, observing, “Our fallen arch trouble, our bunions, our calluses, and our foot miseries generally hark back to the fact that our feet are not yet healed by adaptation and evolutionary selection into really efficient units.” While most forms of pes planus may be part of the normal range of human variation, its association with clinical problems has resulted in widespread investigation by both the medical and scientific communities.

A third area of investigation has been the fossil record itself. Since the fossil record for the time period during which human bipedalism evolved was essentially unknown until the mid 20th century, evidence for the evolutionary development of the human foot from a non-human primate type of foot was once based largely on features that were considered retention of ancestral (and often pathological) traits in the foot of modern humans (for example see: Morton ,1922, 1924a, 1924b, 1924c, 1927, 1928, 1935).

The fossil pedal record has exploded in the last 20 years and now includes dozens of remains (Harcourt-Smith and Aiello, 2004; Kidd, 2004; Kidd and Oxnard, 2005; Gebo and Schwartz, 2006; DeSilva, 2009; Jungers et al., 2009a; Jungers et al., 2009b; Zipfel et al., 2009; DeSilva and Papkyrikos, 2011; Zipfel et al. ,2011; Pablos et al., 2013; Berger et al., 2015; Boyle and DeSilva, 2015; DeSilva et al., 2015).

While the fossil record is the actual documentation of how the proposed hominin ancestors were structured, the fragmentary nature of the fossil record necessitates the reliance on the first two areas of investigation to understand the locomotor abilities of these ancestral forms and to postulate the evolutionary steps that lead to modern human bipedalism.

Functional anatomy of the human foot

The fragmentary nature of the fossil record, and the limited utility of nonhuman primates as locomotor models, necessitates reliance on investigations of the variation seen in the foot of modern humans and how that variation affects foot biomechanics to understand the structure and function in modern humans and in the reconstruction of the fossil hominin foot. The ability of the foot to go from a flexible adaptive structure at heel strike to a rigid lever for support and propulsion is a hallmark of human bipedal gait (Root et al., 1977). The flattening of the medial border on weight-bearing in the flexible anthropoid ape foot is in contrast to the arch formation seen in most human feet with weight-bearing (Morton, 1935), though flattening of the arch is also seen in humans with the more flexible pes planus foot type.

To understand the potential functional significance of the variation in arch height of the human foot, a review of the relationship between joint structure, biomechanics, and bipedal gait is necessary. The following terminology will be used in this study to describe foot joint motions (from Sgarlato, 1971) (See Figures 5a-5e):

Abduction – Motion occurring on the transverse plane during which the distal aspect of the foot or part of the foot moves away from the midline of the body about a vertical axis of rotation localized at the proximal aspect of the foot or part.

Adduction – Motion as above where the distal part of the foot moves toward the midline of the body.

Inversion – Motion occurring on the frontal plane during which the plantar aspect of the foot or part of the foot is tilted so as to face more toward the midline of the body. (A position of fixed inversion is termed varus).

Eversion – Motion as above where the plantar aspect of the foot is tilted so as to face further away from the midline of the body. (A position of fixed eversion is termed valgus).

Dorsiflexion – Motion occurring on the sagittal plane during which the distal aspect of the foot or part of the foot moves toward the tibia about an axis of rotation localized at the proximal aspect of the part.

Plantarflexion – Motion as above where the distal aspect of the foot or part of the foot moves away from the tibia.

Pronation – A triplanar motion consisting of simultaneous movement of the foot or part of the foot in the direction of abduction, eversion, and dorsiflexion. The axis of this motion passes from a position posterior, lateral and plantar to anterior, medial and dorsal direction.

Supination – A triplanar motion consisting of simultaneous movement of the foot or part of the foot in the direction of adduction, inversion and plantarflexion. The axis of motion is the same as in pronation.

Most of the major joints of the human foot are modified ginglymus, or hinged, joints. As hinged joints, they have one plane of motion, perpendicular to their axes of motion; however, because joint axes are often angled to the three anatomical planes, joint motion occurs at angles to these planes. Since joint motion terminology typically describes motion in the anatomical planes, this relationship of the joints to the anatomical planes makes the description of foot motion complicated.

The major joints of the human foot involved with gait to be considered here are the ankle, subtalar, midtarsal, and first metatarsophalangeal. As a complicated structure, with 26 bone and 33 joints (Figures 6a and 6b), the actual function of these joints, and the interplay of other joints in foot biomechanics and movement is more complex than presented here.

The ankle is a hinged joint; however, due to the angle of the ankle joint axis to the anatomical planes, the motion of the ankle is not pure dorsiflexion and plantarflexion but rather is triplanar. The result is that the ankle joint rotation forces the subtalar joint and midtarsal joint into more supination during propulsion. For proper functioning of the foot during the propulsive portion of the stance phase of gait, a minimum of 10° of ankle dorsiflexion when the knee is extended is necessary (Root et al., 1977).

The subtalar joint is made up of the articulation between the talus and calcaneus and includes the posterior, middle, and anterior facets. The axis of motion has been described as oblique, going from a lateral, plantar, and posterior direction proximally, to medial, dorsal, anterior direction, averaging 42° from the transverse plane and 16° from the sagittal plane (Figures 7a and 7b) (Manter, 1941; Root et al., 1977), with a wide range of variation (Sarraffian and Kelikian, 2011). Because of the relationship of the axis of motion to the planes of the foot,

the axis is pronatory-supinatory. From a neutral position, the normal subtalar joint can supinate twice as much as it can pronate. In open chain (non-weight-bearing) pronation of the subtalar joint, the calcaneus abducts, everts and dorsiflexes (with the talus being fixed in the ankle mortise) (Figure 5d). In closed chain (weight-bearing) pronation, the calcaneus everts while the talus adducts (allowing the leg to internally rotate) and plantarflexes. This motion is observed as calcaneal (rearfoot) eversion (Figure 5e). Open and closed chain supination is the opposite, with the calcaneus inverting in closed chained motion. The talus is fixed in the ankle mortise, so talar motion allows the leg to externally rotate in relation to the calcaneus (Elftman and Manter, 1935; Elftman, 1960; Inman, 1976; Root et al., 1977).

The midtarsal joint is composed of the talonavicular and calcaneocuboid articulations. These articulations function as one joint. The midtarsal joint has two different axes of motion, both pronatory-supinatory (Root et al., 1977). Average values for the oblique axis has been reported as 57° from the sagittal plane (medially oriented) and 52° from the transverse plane (dorsally oriented) while average values for the longitudinal axis of motion have been described as directed 9° from the sagittal plane and 16° from the transverse plane (Figures 8a and 8b) (Manter, 1941; Sarrafian and Kelikian, 2011). Variation has been noted in the angulation of these axes, which may result in functional abnormalities (Root et al., 1977). To accommodate the ground and allow the arch to depress with weight-bearing, when the subtalar joint pronates, pronation takes place at the oblique midtarsal joint axis and supination takes place at the longitudinal midtarsal joint axis.

Forefoot eversion and inversion occur mainly at the longitudinal midtarsal axis, while forefoot adduction-abduction and dorsiflexion-plantarflexion occur mainly at the oblique

midtarsal joint axis. The midtarsal joint exhibits its greatest range of motion (“unlocked”) when the subtalar joint is maximally pronated. The midtarsal joint is restricted (“locked”) when the subtalar joint is supinated (Root et al., 1977). Elftman (1960) explained this mechanism in the following way: Subtalar joint pronation produces a parallelism between the longitudinal axes of the articular surfaces of the head of the talus and anterior aspect of the calcaneus. This allows greater freedom and range of midtarsal joint motion. Subtalar joint supination produces obliquity between these two surfaces which causes locking to occur with attempted midtarsal joint motion. With the locking of the midtarsal joint, the foot becomes a rigid lever for propulsion. The unlocked midtarsal joint results in a foot (i.e., a pronated foot) that is not only more flexible for shock absorbency but can also more easily adapt to variations in terrain. It is also less stable.

The first metatarsal-phalangeal joint has two distinct axes of motion: transverse and vertical. The range of motion along the vertical axis is small, only becoming important in pathology. Sagittal plane motion of the first metatarsal-phalangeal joint is very important in normal motion locomotion, where the joint functions as a “ginglyoarthroidial” joint (Root et al., 1977). The joint acts as a ginglymus joint for the first 20 to 30° of dorsiflexion. Since in propulsion, a total of 65° of dorsiflexion is necessary at toe off, the first metatarsal head must glide in a plantar direction relative to the base of the proximal phalanx, an arthroial type of motion. This motion is facilitated, in part, by a second metatarsal that is longer than the first. The longer second metatarsal will maintain ground contact, allowing the shorter first metatarsal to plantarflex while the hallux is planted firmly against the ground by its intrinsic

muscles during propulsion. A lack of full dorsiflexion at the first metatarsal-phalangeal joint can result in pain and disability during gait.

The foot and joint motion in the gait cycle

The foot can be thought of as having four main functions in gait where joint movement and motion is of major importance: allows transverse motion of the leg to occur with the foot planted on the ground; acts as a mobile adaptor to the ground surface; acts as a rigid lever for forward propulsion; and acts as a shock absorber to prevent the force of ground contact from being transmitted proximally (Root et al., 1977).

The gait cycle for a particular limb can be divided into two phases, stance and swing (Root et al., 1977). During stance phase, the foot bears the weight of the body. Stance phase occupies 62% of the gait cycle in normal walking while the swing phase is approximately 38% of the total gait cycle. The stance phase of gait is divided into three parts: contact (from the time of heel strike to when the full foot is on the ground); midstance (from the time the entire foot is on the ground to when the heel is lifted); propulsion (from the raising of the heel to when the hallux leaves the ground). The osseous movements of the foot during the gait cycle have been described by different investigators (Sgarlato, 1971; Root et al., 1977; Mann, 1978). The motion of the subtalar joint is of great importance in bipedal gait. At heel strike, the calcaneus is slightly inverted. Following heel strike, the subtalar joint undergoes a small amount of pronation and the calcaneus everts 2 to 4°. This pronation unlocks the midtarsal joint, allowing adaptation of the foot to the terrain and cushioning the shock of ground contact. It also allows internal rotation of the leg to take place. Going into midstance, the subtalar joint begins to

supinate from the pronated position, passing neutral position before the end of midstance.

Into propulsion, the subtalar joint continues to resupinate and the calcaneus inverts. The first ray begins to plantarflex until the final propulsive thrust where the foot leaves the ground.

Stability of the foot during gait is the result of a number of factors. Most important is an enlarged calcaneus when compared to other extant primates, especially at the heel, to absorb shock and support the increased load placed on the foot by bipedal locomotion (Latimer and Lovejoy, 1989). The other tarsal bones are also enlarged to support the increased weight-bearing on the single limb. The intertarsal joints also are structured for reduced flexibility. The stability of the medial longitudinal arch of the foot, made up of the calcaneus, talus, navicular, medial cuneiform, and first metatarsal, along with associated joints, ligaments, and tendons, is maintained in weight-bearing, by the osseous and ligamentous structure of the foot (Figure 9). Much of the arch support and motion of the foot in normal gait takes place with minimal muscle activity by either the extrinsic or intrinsic foot muscles (Basmajian and Stecko, 1963). The rigidity of the rearfoot and midfoot provides a stable platform for the fibularis (peroneus) longus tendon as it wraps around the cuboid bone which, in turn, stabilizes the first metatarsal at its base and the forefoot.

The ability of the foot to go from a flexible shock absorber to a stable platform during the stance phase of gait has been ascribed to a “windlass mechanism,” relying on minimal contraction of the triceps surae, forward momentum, and passive dorsiflexion of the metatarsophalangeal joints to tighten the plantar aponeurosis (Hicks, 1954; Griffin et al., 2015) (see Chapter 5). The plantar aponeurosis thus plays an important role in maintaining the integrity of the medial longitudinal arch throughout the stance phase (Griffin et al., 2015). The

more the ligaments supporting the arch are stretched, the more strain is placed on the muscles of the foot to function during normal walking and running at times when they should normally be at rest. Consequently, variations in foot structure that increase ligamentous stretching potentially affect foot function.

Pes Planus foot type

Definition and classification

Distinct differences in foot configuration concerning the height of the medial longitudinal arch in weight-bearing have been well documented in the medical literature. Foot types based on arch height range from the pes planus (flatfoot) to pes cavus (high arch) (Figures 10a and 10b). The pes planus foot has been defined in various ways. Most commonly, the pes planus foot type has been described as a foot with the medial margin of the plantar aspect of the foot in contact with the ground. However, others have described it as having a more variable morphology. Staheli (1999) defined flatfoot simply as a condition in which the foot has an increased contact area with the ground. Helfet and Lee (1980) described it as a condition in which the medial longitudinal arch is lower than “normal” when bearing the weight of the body. The term “pes planovalgus” is sometimes used to describe a more complex form of pes planus, where both the arch is flat in the sagittal plan and the heel is in a more pronounced everted (valgus) position in the frontal plane (Helfet and Lee, 1980). The problem with these definitions, and thus identifying a pes planus foot type, is knowing how low the arch must be for a foot to be defined as a flatfoot when the entire medial foot is not in contact with the ground.

Pes planus is a commonly recognized human foot variation. Children characteristically have a pes planus appearing foot at birth; most juvenile flat feet are said to develop arches by four to five years of age. In one study, 80% of children examined in Israel had flatfeet (Helfet and Lee, 1980). Prevalence of flat foot in a Nigerian primary school population (ages 6 to 10 years) found that the number of children diagnosed with flat foot had a prevalence rate of 22.4% (Ezema et al., 2014). Isbigbi et al. (2005) reported the results of the analysis of the dynamic footprints obtained from population samples of Kenyan and Tanzanian individuals between 12 and 18 years of age. Among their findings, 45% of Kenyans had a low arch compared with 20% of Tanzanians. While more common in children than in adults, it is unknown as to what percentage of children with pes planus will retain the foot type as adults. Pes planus is seen more often in certain adult population groups (Krogman, 1962). Harris and Beath (1947) examined Canadian men for military induction and found 22% had pes planus. Steward (1970) reported that among Black West Africans 29% had severely flat feet. Helfet and Lee (1980) reported that about one third of all adults have flatfeet (not always bilaterally equal). However, variations in prevalence of pes planus as reported in the literature might be the result of differences in the accepted definition of pes planus as well as the methodology used in determining pes planus and how the populations under study were identified.

There have been different proposals for pes planus classification on the basis of etiology, clinical features, natural history, and potential for causing disability (Page, 1983; Lepow and Valenza, 1989; Staheli, 1999; Lee et al., 2005; Giza et al., 2007; Richie, 2007; Benedetti et al., 2010; Bubra et al., 2015). Classification systems based on etiology divide pes planus into two categories: congenital and acquired (Page, 1983). There are also classification

systems based on structure and symptomatology, categorizing pes planus as either pathologic or physiologic (Staheli, 1999). Pes planus may be considered pathologic when it is structurally “abnormal,” either due to congenital or acquired etiology, and causes significant symptomatology. Certain forms of pes planus, such as peroneal spastic flatfoot due to tarsal coalition, congenital vertical talus, talipes calcaneovalgus, peroneal spastic flatfoot, talipes calcaneovalgus, accessory navicular, ligamentous laxity, and generalized dysplasia are congenital pathologic conditions (Lee et al., 2005). Medial arch collapse that results from dysfunction caused by bone fracture or traumatic rupture of the posterior tibial tendon, systemic arthritis problems, and neuromuscular imbalance are examples of acquired pathologic conditions. Research has supported the common belief that pes planus feet tend to be flexible while pes cavus feet tend to be stiff (Zifchock et al., 2017).

Physiologic flatfoot is described as a benign condition that, while tending to disappear by the end of childhood, may be retained into adulthood (Staheli, 1999). The clinical signs of this category of flexible flatfoot include a “normal” appearing non-weight-bearing arch with some degree of reduction of the arch height in stance (Page, 1983; Lee et al., 2005). The flexible flatfoot (and any other variation in arch height) may be considered within the range of normal variation when there are no abnormal causative factors. These forms of pes planus in themselves may not produce significant symptomatology or disability (Staheli, 1999).

Adult flexible flatfoot is thus a continuation of a pediatric condition characterized by partial or complete absence of the medial arch (Lee et al., 2005). However, the adult flexible flatfoot may progress from an asymptomatic “physiologic” pes planus, to a more rigid “pathologic” adult acquired pes planus (Richie, 2007). Thus, the congenital flexible flatfoot has

the potential to result in an acquired rigid pes planus with weakening and rupture of the posterior tibial tendon, progressive collapse of the medial arch, development of arthritic changes, and increased symptomatology (Lee et al., 2005; Richie, 2007). Posterior tibial tendon dysfunction is the most common cause of adult acquired foot disease with tendon degeneration beginning before the clinical manifestations are apparent (Giza et al., 2007; Richie, 2007; Bubra et al., 2015). Factors that may also result in excessive reduction in arch height and cause symptomatology, in addition to posterior tibial tendon dysfunction, include compensated forefoot varus, compensated flexible forefoot valgus, ankle equinus, lower limb torsional, and anything that contributes to a medial shift in weight-bearing such as genu valgum, obesity, and wide base of gait (Lee et al., 2005).

The relationship between physiologic flexible flatfoot and habitual wearing of shoe gear is unclear. Some population studies suggest that shoe gear does not play a primary role in the development (or retention) of pes planus (Thompson and Zipfel, 2005; D'Aout et al., 2009; Abolarin et al., 2011). Others provide evidence that suggests that shoe wearing in early childhood is detrimental to the development of a normal longitudinal arch (Rao and Joseph, 1992) or that shoe wearing reduces the prevalence of flatfoot (Alakja, 1979; Phillips, 1999). Over the years the medical community has also been divided as to whether supportive shoe gear (and the appropriate orthotic support) has a role in the prevention of flexible pes planus in the adult (Phillips, 1999; Staheli, 1999). Wood-Jones (1944) stated (p.254) "The rigidity of the boot-wearing arch, like the rigidity of the Chinese lady's bound arch, is an acquired rigidity; it is not an inherent condition of the normal human foot." In other words, a rigid arch is secondary to shoe gear; the human arch is actually more mobile. It has also been suggested that

endurance running in minimal support footwear makes greater use of the spring-like function of the longitudinal arch, putting increased demand on the intrinsic muscles supporting the arch, thus strengthening the foot against arch flattening (Miller et al., 2014). Certainly, there is evidence that foot binding combined with restrictive shoe gear severely limits the growth and development of the foot, resulting in both soft tissue and osseous deformities causing life-long disability. The effect of shoe gear on foot configuration, especially the more restrictive type of shoes, needs further investigation (Lautzenheiser and Kramer, 2013).

Clinical methods of evaluation

Evaluating a patient for pes planus usually includes clinical examination and radiographic evaluation (Menz, 1998). The clinical examination may involve observing the foot non-weight-bearing, in stance and in gait, together with testing joint range of motion and arch height measurements. Taking footprints or using other methods to capture the pressure pattern of the weight-bearing foot may also be employed. Standard radiographs include weight-bearing anterior-posterior (AP), lateral, and oblique views. Specialized views, such as the Harris-Beath calcaneal axial projection, may also be obtained if a tarsal coalition is suspected (Lee et al., 2005). Other imaging modalities, such as CT scanning and MRI, may also be ordered when necessary to assist with diagnosis and treatment planning.

Footprints have been widely used in the evaluation of pes planus (James, 1939; Harris and Beath, 1948; Steward, 1970; Cavanagh and Rogers, 1987; Didia et al., 1987; Agoada, 1989; McCrory et al., 1997; Isbigbi et al., 2005; Chen et al., 2006; Roy et al., 2012; Gutierrez-Vilahué et al., 2016). It is usually assumed that a flatfoot (pes planus) will always produce a footprint

without the presence of the medial arch. However, studies have found that the feet of some individuals described as "pes planus" on physical examination produced footprints that did not display loss of the medial arch (Agoada, 1989; Menz, 1998; Wearing et al., 2004). Menz (1998) reviewed different clinical techniques for evaluating foot type reported in the literature (arch height, footprint indices, the valgus index, and navicular drop). He observed several feet that appeared clinically flat, but when lateral weight-bearing radiographs were obtained, the feet would not be classified as low arched. He concluded that footprints and clinical examination alone might not accurately indicate sagittal plane arch height (Menz, 1998).

The radiographic features of pes planus have been widely discussed in the literature for many decades (Kaplan and Symonds, 1945; Bonnet and Baker, 1946; Cavanagh and Rogers, 1987; Lepow and Valenza, 1989; McCrory et al., 1997; Menz, 1998; Lee et al., 2005; Menz and Munteanu, 2005; Younger et al., 2005; Murley et al., 2009; Bourdet et al., 2013; Sanner et al., 2015) (*Figure 10a*). The accuracy of classifying a foot as pes planus using weight-bearing radiographs has been compared to other methods of evaluation, including weight-bearing pedal prints and clinical examination. Radiographs provide the most valid representation of skeletal foot alignment (Saltzman and Nawoczinski, 1995; Menz and Munteau, 2005; Murley et al., 2009; Benedetti et al., 2010). Menz and Munteanu (2005) consider the reliability of the radiographic measurements as the "gold standard" when correlating clinically determined measurements with those from radiographic images. The radiographic analysis of flexible pes planovalgus demonstrates the complexity of the structural variation associated with this form of pes planus (Bourdet et al., 2013).

Radiographic imaging of the human foot

Plain radiographs of the foot provide accurate information on the morphology of the individual bones, as well as angular relationships between bones (Christman, 2015).

Radiographs document the osteology of a weight-bearing human foot and allow for foot type classification. Plain radiographs are a medically approved form of non-invasive examination in individuals where trauma has occurred, where trauma is suspected, where surgical treatment is planned, or where bone appearance, arthritic or joint relationships need to be evaluated to arrive at a diagnosis of the condition so that a treatment program can be formulated. While CT and MRI scans will give more information about bony structure, they are more expensive tests that are less often performed on a routine basis. In addition, due to x-ray exposure, CT scans are not usually ordered, unless absolutely necessary when other forms of evaluation, such as plain radiographs or MRI scans would not provide enough information. Since plain radiographs are commonly performed, their availability makes them useful for studying human variation where large sample sizes are crucial. Foot radiographs have a long history of use as part of the clinical examination when evaluating a patient with a foot problem (Kaplan and Symonds, 1945; Bonnet and Baker, 1946; Templeton et al., 1965; Rhea et al., 1983; Shereff and Johnson, 1983; Smith and Staple, 1983; Floyd et al., 1984; Takai, 1984).

As noted, standard views in an initial radiographic foot evaluation usually include the anterior-posterior (AP or dorso-plantar) view to assess structures from the transverse plane of the foot, and the lateral view to assess structures from the sagittal plane. While other views may be ordered depending upon the medical concern to be evaluated, the AP and lateral views produce images with the least amount of distortion that most closely correlates with the size

and shape of the actual bone. Thus, bones of the foot are best assessed in the AP and lateral views (Christman, 2015). However, all three anatomic planes need to be considered when evaluating the appearance of the bone produced on the two-dimensional radiographic image being studied. Using standard plain radiographs, the frontal-plane position of a bone cannot be directly evaluated; assessments of the talus and calcaneus in the frontal plane require logical analysis and reasoning while looking at both the AP and lateral views (Christman, 2015).

Positioning technique and terminology for standard radiographic views

The AP and lateral standardized views are taken with the foot either weight-bearing or non-weight-bearing, depending upon the medical concern and whether the foot type and bony relationships need to be evaluated in the normal standing position. Weight-bearing lateral and AP views are best for establishing standardized criteria for biomechanical classification based on the relationships of the bones of the foot to each other (Gamble and Yale, 1975; Lautzenheiser and Kramer, 2013). However, both weight-bearing and non-weight-bearing views should be useful in taking linear and angular measurements of individual bones, if the radiograph was taken with the foot in a standardized position.

In taking the AP view, the foot rests flat on the radiographic image receptor with the x-ray beam (tubehead) usually angled 15° from the vertical directed posteriorly. The central ray is usually directed at the second metatarso-cuneiform joint (Gamble and Yale, 1975; Christman, 2015). The radiographic image receptor is closest to the plantar aspect of the foot (and thus the calcaneus) (Gamble and Yale, 1975).

In the lateral non-weight-bearing view, the radiographic image receptor is flat (horizontal) on the table, the tubehead is oriented vertically, i.e., 0° to film. In the weight-bearing, the radiographic image receptor is vertical and the tubehead is horizontal. The central ray position is usually aimed at the lateral cuneiform/cuboid (Gamble and Yale, 1975; Christman, 2015). In the lateral view, the medial aspect of the foot is against the radiographic image receptor, thus the talus is closer to it than the calcaneus. The outline of the borders and surfaces of bony structures may be referred to as the “margins” of the bone (Christman, 2014).

The significance of osteologic variability of the talus and calcaneus as it relates to foot type classification

“The information derived from the Canadian Army Foot Survey and from previous studies leads us to the conclusion that, in the foot more than any other part of the body, variations in the shape of the skeletal units and in their relationship to one another profoundly modify the stability, the shape, and the function of the foot... It is incorrect to assume that there is uniformity of bony structure in all feet, or that the support provided by the architecture of the foot is virtually the same in every case. The tarsal bones, especially the talus and calcaneus, vary in their shape, in their position relative to each other, and in the manner in which they articulate with one another” (Harris and Beath, 1948, p. 132).

The talus and calcaneus are recognized as important elements in the structure, function, and integrity of the human foot (Elftman and Manter, 1935; Morton, 1935; Hicks, 1953; Elftman, 1960; Close et al., 1967; Inman, 1976; Root et al., 1977; DeSilva et al., 2013). The range of variation in size and shape of these tarsal elements in modern humans is well

documented and has been employed to statistically analyze skeletal remains in both modern and ancient osteologic collections (Steele, 1976; Introna et al., 1997; White and Folkens, 2000; Murphy, 2002a,b; Harris and Case, 2012). In reviewing the descriptions of the osteology of the talus and calcaneus (Appendix A; *Figures 1a-1f; 3a-3f*), the amount of variation in size, shape and angulation of the surfaces, borders, and features of these bones is readily apparent. Bony variation in morphology of the human foot has been well documented in the literature for both of these bones (Laidlaw, 1904; Sewell, 1904a; Sewell, 1904b; Laidlaw, 1905; Sewell, 1905; Sewell, 1906; Harris and Beath, 1947; Harris and Beath, 1948; Lisowski, 1967; Day and Wood, 1968; Oxnard, 1972; Lisowski et al., 1974; Lisowski et al., 1976; Oxnard and Lisowski, 1980; Deloison, 1985; Lamy, 1986; Kelikian, 2011; Heard-Booth, 2014) and the talocalcaneal articulations (Last 1952; Smith, 1958; Bunning, 1964; Bunning and Barnett, 1965; Cahill, 1965; Bojsen-Moller and Flagstad, 1976). However, the significance of this variation has received less attention, especially as it relates to foot type and foot biomechanics. There have been few studies that directly examined the relationship between the morphology of the talus and calcaneus with foot type.

Forefoot varus is a frontal plane structural position where the forefoot is in an inverted structural position, rather than being perpendicular relative to the rearfoot at the level of the midtarsal joint (Grumbine, 1987) (*Figures 11a and 11b*). To compensate for this varus position and bring the medial aspect of the forefoot down to the weight-bearing surface, the subtalar joint will pronate. The result may be a pes planus foot, depending upon the amount of pronation available by the subtalar joint for compensation and the degree of forefoot pronation (Root et al., 1977; Grumbine, 1987). Forefoot varus has been described as due to inadequate

frontal plane torsion of the head and neck of the talus that should occur during normal ontogeny of the foot (Valmassy, 1996). However, this has not been documented in the literature. McPoil et al. (1987) investigated the relationship between clinically measured forefoot varus and the amount of talar neck adduction and torsion. Their study suggested that the degree of forefoot varus (or forefoot valgus) is not specific to variations in head and neck anatomy.

Anderson et al. (1997) attempted to answer the question as to whether the shape of the talus is associated with pes planus. Using CT scan measurements, they found statistically significant differences when comparing ratios of talar length with talar width, talar length with talar height, and head length with head width. The tali from the flatfoot group were narrower in width and shorter in height when compared with overall length and had heads that were more elongated in the transverse plane than tali in feet with a normal appearance. Of note is the small sample size (pes planus n=10; control n=10) and that the pes planus population used in this study were surgical candidates for correction of pes planus, thus representing the most severe form of the pes planus “deformity.” Peeters et al. (2013) also conducted a study with a small sample size, using 10 “clinically diagnosed” “flatfeet” and 15 “non-flatfeet,” examining the relationship of the talus and the navicular using CT scan imaging. Their study defined the criteria for a flatfoot classification in general terms (besides heel valgus of greater than 7°) stating the classification was based on “clinical evaluation by an experienced foot surgeon....” They found from their measurements that the ratio of the talar and navicular articular surface height was decreased in the flatfoot group. They also found that the talar head was wider in the flatfoot group and faced more “proximally” than in the non-flatfoot group. They concluded

from their results that the morphological differences in the talus and navicular articular surfaces between the flatfoot and non-flatfoot group would explain the medial arch “collapse” and forefoot adduction found in the flatfoot. They did not address the differences in the overall shape of the talus between the two groups.

Morton (1935) noted that, in the frontal plane, the superior aspect of the calcaneus presents an almost level surface with the sustentaculum tali in humans. This relationship is in contrast to that of the gorilla with a more medial declination of the sustentaculum tali contributing to the medial displacement of weight on the ground and the flattening of the foot in apes. Morton also noted that the upper surface of the calcaneus in apes has an oblique slant anteriorly and plantarly in the sagittal plane. Both of these features of the sustentaculum tali result in a decrease in the medial deviation of body weight in the human foot when compared to that of the ape foot. Mahato (2011) studied the relationship between the talus and calcaneus using fifty-two articulated skeletons of the foot collected from medical schools in India. The bones were described as “free from gross bony deformities.” The author found strong correlations for certain parameters between linear and angular measurements of the sustentaculum tali of the calcaneus and the talus but concluded that the sustentaculum tali primarily ‘sustains’ the talus without assisting in sharing the load distribution at the talo-calcaneo-navicular joint at the medial aspect of the foot.

The work of Harris and Beath (1947, 1948) is one of a few studies to examine the functional relationship between bony morphology and foot configuration for the calcaneus and talus. They created the term “hypermobile flatfoot with short Achilles tendon” to identify what they described as a “severe and disabling” type of flexible flatfoot. This form of pes planus is

present beginning in childhood and young adult life, is the result of abnormalities of the talus and calcaneus that cause instability of the tarsus. This is a congenital deformity associated with a prolonged history of some degree of foot disability extending back to childhood and is the result of an abnormal relationship of the talus to the calcaneus, especially with reference to the manner in which the head of the talus is supported by the anterior end of the calcaneus. The manner in which the proximal bones interlock influences the range of motion of the more distal tarsal bones. They studied the foot radiographs of 3,619 Canadian soldiers and found that a major difference between the flexible flatfoot and normal foot was support of the talar head by the sustentaculum tali. In the flexible flatfoot, the sustentaculum tali was narrow and short while normally broad, rounded, and running forward to the anterior margin of the talus in the normal foot. In the flatfoot, the head and neck of the talus were short and were facing medially and anteriorly. They compared the morphology of the talus and calcaneus collected from 200 cadavers (the feet were not examined before the foot was skeletonized and bones disarticulated) and the foot radiographs of the military recruits and found the same features of the sustentaculum tali in some of the calcanei as seen in the flexible flatfoot of the military recruits. They concluded that this variation in the morphology of the sustentaculum tali, present in both the radiographs of living subjects and the osteology of the calcaneus dry bones reinforced their believe that the “inadequate support” of the talar head by the sustentaculum tali is a “basic cause” of the flexible flatfoot. Variations in the articular facets of the subtalar joint have also been postulated as being related to excessive subtalar joint pronation and foot type (Harris and Beath, 1948; Bruckner, 1987). However, these are morphologic features that could not be evaluated using plain radiographs of the foot.

The calcaneocuboid joint (CCJ) has also been studied in relationship to the structure of the anterior calcaneus in terms of foot type and function. A relatively flat CCJ is seen in pes planus; a more sellar (or saddle shaped) shaped CCJ is seen in the cavus foot (Landry and Agoada, 1986; DeSilva et al., 2014; Heard-booth, 2015). It has been concluded that variations in the calcaneocuboid joint can, at least in part, produce a functionally less stable foot as seen in a lower arch. Volger and Bojsen-Moller (2000) postulated that since the cuboid like the talus has no muscle attachments; it is also dependent on its soft tissue attachments and articulations with other bones, including the anterior calcaneus with its overlapping anterior process. Elftman and Manter (1935) believed that stability of the human foot is maintained, in part, by the presence of an anteromedial process of the calcaneus, which prevents excessive subtalar joint eversion (pronation), and which is absent in apes (see Chapter 5).

Pes planus and evolution of the human foot

Modern human foot “disorders,” such as the hypermobile flatfoot, have been related to our evolutionary history (Keith, 1928; Morton, 1935; Wood-Jones, 1944; Krogman, 1951; Lapidus, 1960; Krogman, 1962; Olson and Seidel, 1983). Common complaints in individuals with hypermobile flatfoot include arch pain, aching and fatigue feeling of the feet and legs, and leg and foot cramping, all aggravated by prolonged standing and activity (Helfet and Lee, 1980). This “hyperpronated” foot configuration has been associated with joint instability, medial arch pain, posterior tibial tendinitis, hallux valgus, bunion deformity, osteoarthritis in the joints of the foot, as well as creating medial knee pain, hip pain, and back pain (Root et al., 1977). While the hypermobile flatfoot can produce serious arch strain and biomechanical problems, the

percentage of individuals with significant disability who have this foot configuration is unclear (DeSilva and Throckmorton, 2010). Although most individuals with the pes planus may be able to walk and run without significant restriction, they may require more energy to do so than those who do not have pes planus, putting them at somewhat of an evolutionary disadvantage in long distance walking and running (Bramble and Lieberman, 2004). As noted, despite early beliefs that the medial longitudinal arch is held in position only by the power of muscles (Hoke, 1931) the effects of muscle activity on the height of the arch are now considered to be limited (Basmajian and Bentzon, 1954; Basmajian and Stecko, 1963; Gray and Basmajian, 1968; Gray, 1969; Bojsen-Moller and Flagstad, 1976).

A hallmark of the modern human's striding bipedal gait is how little intrinsic and extrinsic muscle action is needed to support the longitudinal medial arch in stance, the arch being maintained by joint configuration and ligamentous, capsular and passive tendinous attachments (Hicks, 1954; Hicks, 1956; Griffin et al., 2015). However, before the attainment of the modern striding gait, muscle action must have played a more important role in supporting the medial arch (Lovejoy et al., 2009) as it does in modern humans with pes planus due to excessive pronation (Cartmill and Smith, 2009). If the strain is excessive, muscle fatigue, discomfort and damage can result (Cartmill and Smith, 2009). Natural selection may have played upon excessive pronation and medial column flexibility, selecting for those individuals with the most efficient foot configuration for striding bipedal gait and against those individuals (at least to some degree) with the less efficient hypermobile flatfoot configuration. This is a process that probably continues to evolve while preserving variability in the amount of flexibility seen in the wide range of medial arch height seen in modern humans. There has been

renewed interest in understanding the relationship foot function and morphology in the interpretation of the structure of fossil hominid pedal remains (DeSilva and Gill, 2013; Lautzenheiser and Kramer, 2013).

None of the studies of the talus and calcaneus looked at the bones of an intact weight-bearing human foot of known foot type to examine the individual bone morphology. These studies also were unable to compare the physical bone with its radiographic image when proposing relationships between talus or calcaneus morphology and foot type. Thus, the size, shape and angular relationships within the talus and calcaneus of the modern foot have not been studied in sufficient detail to explain how the variability of these elements is associated with the pes planus foot. Studying the structural variability of the talus and calcaneus as it related to excessive pronation and arch height should be useful in the interpretation of pedal elements of both the modern human foot and those from the hominin fossil record in the understanding of how the modern human foot functions as well as its evolutionary history.

Hypothesis and Goals

While plain radiographs of the foot have been used to provide information concerning a bone's length, shape, and angular relationships to other bony structures in the intact foot, there have been few studies that have demonstrated the accuracy of *within bone* measurements taken from radiographic images by comparing these measurements to the actual physical bone. If plain radiographs of the weight-bearing foot are to be used in the same manner as the physical bone in evaluating the talus and calcaneus in the pes planus foot type, the accuracy of measurements taken from plain radiographs must first be demonstrated. Once this is done, the osteology of the modern pes planus foot type in living individuals can be described and evaluated quantitatively, as well as qualitatively, for both the physical bone and its radiographic image. In addition, the results of such studies can be used in the investigation of isolated hominin pedal remains.

The hypothesis of this dissertation is that there are linear and angular measurements of the talus and calcaneus in modern humans that can be used to help identify a foot as pes planus. To investigate this hypothesis, measurements from an articulated, weight-bearing foot of known foot type are necessary. Since this requires the intact foot of a living individual capable of weight-bearing, such an investigation can only be performed using radiographic images, such as those that can be provided by standard weight-bearing views of the foot. However, as noted above, first the relationship between radiographic image of the talus and calcaneus and the physical bone must be established. Thus, to support examination of this hypothesis, the following steps need to be performed:

1. The association between selected linear measures between the talus, calcaneus, and its radiographic image must be established (Chapter 2).
2. The association between selected angular measures between the talus, calcaneus, and its radiographic image must be established (Chapter 3).
3. Using weight-bearing radiographs and the same variables as in 1 and 2, the association between these variables and foot type must be established (Chapter 4).

Measurements taken from steps 1 and 2 that demonstrate a close relationship between measurement of the physical bone and its radiographic image would signify that those measurements can be analyzed in the same manner for either the physical bone or its radiographic image. Therefore, any of those linear and angular variables that are associated with foot type as demonstrated by step 3 would support this hypothesis and can be used in the evaluation of either an individual isolated bone, or when examining the radiograph of an intact foot. Chapters 2 and 3 demonstrate an association between measurements taken from the talus and calcaneus with that of their radiographic images. (See Appendix B for a detailed description of the population used for these studies and the methodology for bone preparation.) Chapter 4 provides information on the relationship (or lack of relationship) between these measurements and arch height.

The information derived from this study can potentially be used to help identify foot type and function of an individual from an isolated talus or calcaneus. With recognition of the association of measurements of the talus and calcaneus with the pes planus foot type, the analysis of the individual bones can be used to postulate how a skeletonized individual “walked

in life.” The osteology of the talus and calcaneus in the pes planus foot type of modern humans can then be described quantitatively and evaluated functionally. The results from Chapter 2, 3 and 4 can be applied to the studies on modern human foot biomechanics. In addition, finding similarities in fossil hominin pedal remains could then be used in the interpretation of relevant hominin fossil pedal remains as described in the literature. Such information would assist in the functional analysis of these remains and in the understanding of the bipedal gait of our hominin ancestors.

When evaluating the relationship between osteologic form and function, the question arises as to whether the morphologic changes seen in the talus and calcaneus, even if associated with foot function, help create the pes planus or rather are the result of the interaction of bone and soft tissue that occur with the pes planus foot type. The question then becomes how much can the talus or calcaneus be remodeled? Wolff’s law suggests that when a bone’s position is changed relative to applied stress, it would, in time, reshape itself. However, alternatively, if the altered bone shape is present initially, what effects do soft tissue constraints have on preventing further deformity or on causing symptoms (Anderson et al., 1997)? The goal of this study is ultimately to look at the relationship between pes planus and measurements of the talus and calcaneus, and how that relationship may be used in the understanding of form and function, not necessarily on assigning cause and effect.

Chapter 1: Literature cited

- Abolarin T, Aiyegbusi A, Tella A, and Akinbo S. 2011. Predictive factors for flatfoot: The role of age and footwear in children in urban and rural communities in South West Nigeria. *The Foot* 21:188-192.
- Agoada D. 1989. The relationship of human footprints to actual foot configuration. *Am J Phys Anthropol* 75:181-182.
- Alakja TD, 1979. 1979. Prevalence of flat foot in school children in Benin City, Nigeria. *Trop Doct* 9:192-194.
- Anderson JG, Harrington R, and Ching RP. 1997. Alterations in talar morphology associated with adult flatfoot. *Foot Ankle Int* 18:705-709.
- Basmajian JV, and Bentzon JW. 1954. An electromyographic study of certain muscles of the leg and foot in the standing position. *Surg Gynecol Obstet* 98:662-666.
- Basmajian JV, and Stecko G. 1963. The role of muscles in arch support of the foot. *J Bone Joint Surg* 45A:1184-1190.
- Begun DR. 2004. Knuckle-walking and origin of human bipedalism. In: Meldrum DJ, and Hilton CE, editors. *From Biped to Strider: The Emergence of Modern Human Walking, Running, and Resource Transport*. New York: Kluwer Academic/Plenum Publishers.
- Benedetti MG, Berti L, Straudi S, Ceccarelli FC, and Giannini S. 2010. Clinicoradiographic assessment of flexible flatfoot in children. *J Am Podiatr Med Assoc* 100:463-471.
- Berger LR, Hawks J, de Ruiter DJ, Churchill SE, Schmid P, Delezene LK, Kivell TL, Garvin HM, Williams SA, DeSilva JM et al. 2015. *Homo naledi*, a new species of the genus *Homo* from the Dinaledi Chamber, South Africa. *eLIFE* 4:e09560.
- Bojsen-Moller F, and Flagstad KE. 1976. Plantar apneurosis in the internal architecture of the ball of the foot. *J Anat* 121:599-611.
- Bonnet WL, and Baker DR. 1946. Diagnosis of pes planus by x-ray. *Radiology* 46:36-45.
- Bourdet C, Seringe R, Adamsbaum C, Glorion C, and Wicart P. 2013. Flatfoot in children and adolescents. Analysis of imaging findings and therapeutic implications. *Orthop Trauma: Surg Res* 99:80-87.
- Boyle EK, and DeSilva JM. 2015. A Large *Homo erectus* Talus from Koobi Fora, Kenya (KNM-ER 5428), and Pleistocene Hominin Talar Evolution. *PaleoAnthropol* 1(1-13).

- Bramble DM, and Lieberman DE. 2004. Endurance running and the evolution of Homo. *Nature* 432:345-352.
- Bruckner J. 1987. Variations in the human subtalar joint. *J Orthopedics Sports Phys Therapy* 8:489-494.
- Bubra PS, Keighley G, Rateesh G, and Carmody D. 2015. A population of patient-specific adult acquired flatfoot deformity models before and after surgery. *J Family Med Primary Care* 4:26-29.
- Bunning PSC. 1964. Some observations on the West African calcaneus and the associated talocalcaneal interosseous ligamentous apparatus. *Am J Phys Anthropol* 22:467-472.
- Bunning PSC, and Barnett CH. 1965. A comparison of adult and foetal talocalcaneal articulations. *J Anat Lond*:71-76.
- Cahill DR. 1965. The anatomy and function of the contents of the human tarsal sinus and canal. *Anat Rec* 153:1-18.
- Cartmill C, and Smith FH. 2009. *The Human Lineage*. Hoboken: John Wiley and Sons, Inc.
- Cavanagh PR, and Rodgers MM. 1987. The arch index: A useful measure from footprints. *J Biomechanics* 20:547-551.
- Chen C, Huang M, Chen T, Weng M, Lee C, and Wang G. 2006. The correlation between selected measurements from footprint and radiograph of flatfoot. *Arch Phys Med Rehabil* 87:235-240.
- Christman RA. 2015. *Foot and Ankle Radiology*. Second edition. Philadelphia: Wolters Kluwer.
- Christman RA. 2014. Radiographic Anatomy of the Foot and Ankle—Part 1 The Distal Leg. *J Am Podiatr Med Assoc* 104:402-412.
- Clarke RJ, and Tobias PV. 1995. Sterkfontein member 2 foot bones of the oldest South African hominid. *Science* 269:521-524.
- Close J, Inman VT, P.M. P, and Todd FN. 1967. The function of the subtalar joint. *Clin Orthop Relat Res* 50:159-179.
- Crompton RH, Sellers WI, and Thorpe SKS. 2010. Arboreality, terrestriality and bipedalism. *Phil Trans R Soc B* 365:3301-3314.

- Crompton RH, Vereecke EE, and Thorpe SKS. 2008. Locomotion and posture from the common hominoid ancestor to fully modern hominins, with special reference to the last common panin/hominin ancestor. *J Anat* 212:501-543.
- D'Aout K, Pataky TC, De Clercq D, and Aerts P. 2009. The effects of habitual footwear use: foot shape and function in native barefoot walkers. *Footwear Sci* 1:81-94.
- Day MH, and Wood BA. 1968. Functional affinities of the Olduvai hominid 8 talus. *Man* 3:440-455.
- Deloison Y. 1985. Comparative study of calcanei of primates and Pan-Australopithecus-Homo relationship. In: Tobias PV, editor. *Hominid Evolution: Past, Present and Future*. New York: Alan R. Liss, Inc. p 143-147.
- DeSilva JM. 2008. Vertical climbing adaptations in the anthropoid ankle and midfoot: implications for locomotion in Miocene catarrhines and Plio-pleistocene hominins. Ph.D. dissertation, Department of Anthropology, University of Michigan, Ann Arbor, MI.
- DeSilva JM. 2009. Functional morphology of the ankle and the likelihood of climbing in early hominins. *Proc Natl Acad of Sci USA* 106:6567-6572.
- DeSilva JM. 2010. Revisiting the "midtarsal break". *Am J Phys Anthropol* 141:245-258.
- DeSilva JM, Bonneannee R, Swanson Z, Gill CM, Sobel M, Uy J, and Gill SV. 2015. Midtarsal break variation in modern humans: Functional causes, skeletal correlates, and paleontological implications. *Am J Phys Anthropol* 156:543-552.
- DeSilva JM, Gill CM, Swanson Z, Bonneannee R, and Gill SV. 2014a. Reconstructing foot form and function in early hominins using modern human models. *Am J Phys Anthropol* 153:104-105.
- DeSilva JM, and Gill SV. 2013. Brief communication: A midtarsal (midfoot) break in the human foot. *Am J Phys Anthropol* 151:495-499.
- DeSilva JM, Holt KG, Churchill SE, Carlson KJ, Walker CS, Zipfel B, and Berger LR. 2013. The lower limb and mechanics of walking in *Australopithecus sediba*. *Science* 340:1232999-1-1232999-5.
- DeSilva JM, and Papakyrikos A. 2011. A case of valgus ankle in an early Pleistocene hominin. *Int J Osteoarchaeol* 21:732-742.
- DeSilva JM, and Throckmorton ZJ. 2010. Lucy's flat feet: the relationship between the ankle and rearfoot arching in early hominins. *PloS one* 5(12):e14432.

- DeSilva JM, Zipfel B, Van Arsdale AP, and Tocheri MW. 2010. The Olduvai hominid 8 foot: adult or subadult? *J Hum Evol* 58:418-423.
- Didia BC, Omu ET, and Obuoforibo AA. 1987. The use of footprint contact index II for classification of flat feet in a Nigerian population. *Foot Ankle* 7:285-289.
- Dunn RH, Tocheri MW, Orr CM, and Jungers WL. 2014. Ecological divergence and talar morphology in gorillas. *Am J Phys Anthropol* 153:526-541.
- Eftman H. 1960. The transverse tarsal joint and its control. *Clin Orthop* 16:41-45.
- Eftman H, and Manter J. 1935. The Evolution of the Human Foot, with Especial Reference to the Joints. *J Anat* 70:56-67.
- Ezema CI, Abaraogu UO, and Okafor GO. 2014. Flat foot and associated factors among primary school children: A cross-sectional study. *Hong Kong Physio* 32:13-20.
- Floyd EJ, Ransom RA, and Dailey JM. 1984. Computed tomography scanning of the subtalar joint. *J Am Podiatr Med Assoc* 74:533-537.
- Gamble FO, and Yale I. 1975. *Clinical Foot Roentgenology*, 2nd edition. New York: Krieger Publishing.
- Gebo DL, and Schwartz GT. 2006. Foot bones from Omo: implications for hominid evolution. *Am J Phys Anthropol* 129:499-511.
- Giza E, Cush G, and Schon LC. 2007. The flexible flatfoot in the adult. *Foot Ankle Clin N Am* 12:251-271.
- Gray EG. 1969. The role of leg muscles in variations of the arch in normal and flat feet. *Phys Ther* 49:1084-1088.
- Gray EG, and Basmajian JV. 1968. Electromyography and cinematography of leg and foot ("normal and flat) during walking. *Anat Rec* 161:1-15.
- Griffin NL, Miller CE, Schmitt D, and D'Aout K. 2015. Understanding the evolution of the windlass mechanism of the human foot from comparative anatomy: Insights, obstacles, and future directions. *Am J Phys Anthropol* 156:1-10.
- Grumbine NA. 1987. The varus components of the forefoot in flatfoot deformities. *J Am Podiatr Med Assoc* 77:14-20.

- Gutierrez-Vilahué L, Massó-Ortigosa N, Rey-Abella F, Costa-Tutusaus L, and Guerra-Balic M. 2016. Reliability and validity of the footprint assessment method using Photoshop CS5 software in young people with Down syndrome. *J Am Podiatr Med Assoc* 106:207-213.
- Harcourt-Smith WE, and Aiello LC. 2004. Fossils, feet and the evolution of human bipedal locomotion. *J Anat* 204:403-416.
- Harcourt-Smith WE, Throckmorton ZJ, Congdon KA, Zipfel B, Deane AS, Drapeau MSM, Churchill SE, Berger LR, and DeSilva JM. 2015. The foot of *Homo naledi*. *Nat Commun* 6:8432. Doi: 10.1038/ncomms9432:1-8.
- Harris RI, and Beath T. 1947. *An Investigation of foot ailments and Canadian Soldiers*. Ottawa: New York Academy of Medicine.
- Harris RI, and Beath T. 1948. Hypermobility flat-foot with short tendo Achillis. *J Biomech* 31A:116-150.
- Harris SM, and Case DT. 2012. Sexual dimorphism in the tarsal bones: Implications for sex determination. *J Forensic Sci* 57(2): 295–305.
- Heard-Booth AN. 2014. Using calcaneal morphology to predict medial longitudinal arch height in fossil hominins. *Am J Phys Anthropol* 153:139.
- Helfet AJ, and Lee DG. 1980. *Disorders of the Foot*. Philadelphia: J.B. Lippincott Company.
- Hicks JH. 1953. The mechanics of the foot I The joints. *J Anat* 87:345-357.
- Hicks JH. 1954. The mechanics of the foot II the plantar aponeurosis and the arch. *J Anat* 88:25-31.
- Hicks JH. 1956. The mechanics of the foot IV. The action of the muscles on the foot in standing. *Acta Anat* 27:180-192.
- Hoke M. 1931. An operation for the correction of extreme relaxed flat feet. *J Bone Joint Surg* 13:773-783.
- Inman VT. 1976. *The Joints of the Ankle*. Baltimore: The Williams and awilkins Company.
- Introna F, Di Vella G, Campobasso CP, and Dragone M. 1997. Sex determination by discriminant analysis of calcanei measurements. *J Forensic Sci* 42(No 4):725-728.
- Isbigbi PS, Msamati BC, and Shariff MB. 2005. Arch index as a predictor of pes planus. *J Am Podiatr Med Assoc* 95:273-276.

- James CS. 1939. Footprints and feet of natives of the Solomon Islands. *Lancet* 234:1390-1394.
- Jungers WL, Harcourt-Smith WE, Wunderlich RE, Tocheri MW, Larson SG, Sutikna T, Due RA, and Morwood MJ. 2009a. The foot of *Homo floresiensis*. *Nature* 459:81-84.
- Jungers WL, Larson SG, Harcourt-Smith WE, Morwood MJ, Sutikna T, Awe RD, and Djubiantono T. 2009b. Descriptions of the lower limb skeleton of *Homo floresiensis*. *Journal of human evolution* 57:538-554.
- Kaplan M, and Symonds M. 1945. Pes planus: a method of mensuration. *Radiology* 44:355-356.
- Keith A. 1928. The history of the human foot and its bearing on orthopaedic practice. *J Bone Joint Surg* 11:10-32.
- Kelikian AS. 2011. *Sarraffian's Anatomy of the Foot and Ankle*. Philadelphia: Wolters Kluwer / Lippincott Williams & Wilkins.
- Kidd RS. 1998. The past is the key to the present: thoughts on the origins of human foot structure, function and dysfunction as seen from the fossil record. *The Foot* 8:75-84.
- Kidd RS. 2004. *On the nature of morphology: Selected canonical variates analysis of the hominoid hindtarsus and their interpretation*. Cambridge, UK: Cambridge University Press.
- Kidd RS, O'Higgins P, and Oxnard CE. 1996. The OH8 foot: a reappraisal of the functional morphology of the hindfoot utilizing a multivariate analysis. *J Hum Evol* 31:269-291.
- Kidd RS, and Oxnard CE. 2005. Little foot and big thoughts - a re-evaluation of Stw573 foot from Sterkfontein, South Africa. *J Comparative Hum Biol* 55(3):189-212.
- Krogman WM. 1951. The scars of human evolution. *Sci Amer* 185:54-57.
- Krogman WM. 1962. Man's posture: Where from? Where to? *Clin Orthop* 25:98-109.
- Laidlaw PP. 1904. The varieties of the os calcis. *J Anat Physiol* 38:133-143.
- Laidlaw PP. 1905. The os calcis. Part II. *J Anat Physiol* 39 (Pt 2):161-177.
- Lamy P. 1986. The settlement of the longitudinal plantar arch of some African Plio-Pleistocene hominids: a morphological Study. *J Hum Evol* 15:31-46.
- Landry M, and Agoada D. 1986. The significance of the calcaneocuboid joint in the evolution of human bipedality. *Abstr. Am J Phys Anthropol* 69:225.

- Langdon JH. 1986. *Functional Morphology of the Miocene Hominoid Foot*. Basel: Karger.
- Lapidus PW. 1960. The author's bunion operation from 1931 to 1959. *Clin Orthop* 16:119-135.
- Last RJ. 1952. Specimens from the Hunterian Collection: 7. The subtalar joint (Specimens S 100 and S 1002). *J Bone Joint Surg* 34B:116-119.
- Latimer B, and Lovejoy CO. 1989. The calcaneus of *Australopithecus afarensis* and its implications for the evolution of bipedality. *Am J Phys Anthropol* 78:369-386.
- Lautzenheiser SG, and Kramer PA. 2013. Linear and angular measurements of the foot of modern humans: A test of Morton's foot types. *Anat Rec* 296:1526–1533.
- Lee MS, Vanore JV, Thomas JL, Catanzariti AR, Kogler G, Kravitz SR, Miller SJ, and Gassen SC. 2005. Diagnosis and treatment of adult flatfoot. *The J Foot Ankle surg: official publication of the American College of Foot and Ankle Surgeons* 44:78-113.
- Lepow GM, and Valenza PL. 1989. Flatfoot overview. *Clin Podiatric Med Surg* 6:477-489.
- Lewis OJ. 1962. The comparative morphology of m. flexor accessorius and the associated long flexor tendons. *J Anat Lond* 96:321-333.
- Lewis OJ. 1964. The tibialis posterior tendon in the primate foot. *J Anat Lond* 98:209-218.
- Lewis OJ. 1972. The evolution of the hallucial tarsometatarsal joint in the anthropoidea. *Am J Phys Anthropol* 37:13-34.
- Lewis OJ. 1980a. The joints of the evolving foot. Part I. The ankle joint. *J Anat* 130:527-543.
- Lewis OJ. 1980b. The joints of the evolving foot. Part II. The intrinsic joints. *J Anat* 130:833-857.
- Lewis OJ. 1980c. The joints of the evolving foot. Part III. The fossil evidence. *J Anat* 131:275-298.
- Lewis OJ. 1983. The evolutionary emergence and refinement of the mammalian pattern of foot architecture. *J Anat* 137:21-45.
- Lisowski FP. 1967. Angular growth changes and comparisons in the primate talus. *Folia Primat* 7:81-97.
- Lisowski FP, Albrecht GH, and Oxnard CE. 1974. The form of the talus in some higher primates: A multivariate study. *Am J Phys Anthropol* 41:191-215.
- Lisowski FP, Albrecht GH, and Oxnard CE. 1976. African fossil tali: Further multivariate morphometric studies. *Am J Phys Anthropol* 45:5-18.

- Lovejoy CO, Latimer B, Suwa G, Asfaw B, and White TD. 2009. Combined prehension and propulsion: The foot of *Ardipithecus ramidus*. *Science* 326:72-79.
- Mahato NK. 2011. Morphology of sustentaculum tali: Biomechanical importance and correlation with angular dimensions of the talus. *The Foot* 21:179-183.
- Mann RA. 1978. *Duvries' Surgery of the Foot*. St. Louis: C.V. Mosby Co.
- Manter J. 1941. Movements of the subtalar and transverse tarsal joints. *Anat Rec* 80:397-410.
- McCrary JL, Young MJ, Boulton AJM, and Cavanagh PR. 1997. Arch index as a predictor of arch height. *The Foot* 7:79-81.
- McPoil T, Cameron J, and Adrian MJ. 1987. Anatomical characteristics of the talus in relation to forefoot deformities. *J Am Podiatr Med Assoc* 77:77-81.
- Menz HB. 1998. Alternative techniques for the clinical assessment of foot pronation. *J Am Podiatr Med Associ* 88:119-129.
- Menz HB, and Munteanu SE. 2005. Validity of 3 clinical techniques for the measurement of static foot posture in older people. *J Orthop Sports Phys Ther* 35:479-486.
- Miller EE, Whitcome KK, Lieberman DE, Norton HL, and Dyer RE. 2014. The effect of minimal shoes on arch structure and intrinsic foot muscle strength. *J Sport Health Sci* 3:74-85.
- Morton DJ. 1922. Evolution of the human foot I. *Am J Phys Anthropol* V:305-336.
- Morton DJ. 1924a. Evolution of the human foot II. *Am J Phys Anthropol* VII:1-52.
- Morton DJ. 1924b. Evolution of the longitudinal arch of the human foot. *J Bone Joint Surg* 6:56-90.
- Morton DJ. 1924c. Mechanism of the normal foot and of flat foot Part I. *J Bone Joint Surg* 7:368-406; 356-390.
- Morton DJ. 1927. Metatarsus atavicus The identification of a distinctive type of foot disorder. *J Bone Joint Surg AM* 9:531-544.
- Morton DJ. 1928. Hypermobility of the first metatarsal bone: the interlinking factor between metatarsalgia and longitudinal arch strains. *J Bone Joint Surg X*:187-196.
- Morton DJ. 1935. *The Human Foot: Its Evolutionary Development, Physiology and Functional Disorders*. New York: Columbia University Press.

- Murley GS, Menz HB, and Landorf KB. 2009. A protocol for classifying normal- and flat-arched foot posture for research studies using clinical and radiographic measurements. *J Foot Ankle Res* 2:22
- Murphy AMC. 2002a. The calcaneus: sex assessment of prehistoric New Zealand Polynesian skeletal remains. *Forensic Sci Int* 129:205-208.
- Murphy AMC. 2002b. The talus; sex assessment of prehistoric New Zealand Polynesian skeletal remains. *Forensic Sci Int* 128:155-158.
- Olson TR, and Seidel MR. 1983. The evolutionary basis of some clinical disorders of the human foot: a comparative survey of the living primates. *Foot Ankle* 3:322-341.
- Oxnard CE. 1972. Some African fossil foot bones: A note on the interpolation of fossils into a matrix of extant species. *Am J Phys Anthropol* 37:3-12.
- Oxnard CE, and Lisowski FP. 1980. Functional articulation of some hominoid foot bones: implication for the Olduvai (Hominid 8) foot. *Am J Phys Anthropol* 52:107-117.
- Pablos A. 2015. The foot in the Homo fossil record. *Mitteilungen der Gesellschaft für Urgeschichte* 24(11-28).
- Pablos A, Martinez I, Lorenzo C, Gracia A, Sala N, and Arsuaga JL. 2013. Human talus bones from the Middle Pleistocene site of Sima de los Huesos (Sierra de Atapuerca, Burgos, Spain). *J Hum Evol* 65:79-92.
- Page JC. 1983. Symptomatic flatfoot. Etiology and diagnosis. *J Am Podiatr Med Assoc* 73:393-399.
- Peeters K, Schreur J, Burg F, Behets C, Van Bouwel S, Dereymaeker G, Vander Sloten J, and Jonkers I. 2013. Altered Talar and Navicular Bone Morphology Is Associated with Pes Planus Deformity: A CT-Scan Study. *J Orthop Res* 31:282-287.
- Phillips RD. 1999. Planovalgus foot deformity revisited (Letter to the editor). *J Am Med Assoc* 89:265-269.
- Preuschoft H. 1970. Functional anatomy of the lower extremity. In: Bourne GH, editor. *The Chimpanzee*. Basel: Karger. p 221-294.
- Preuschoft H. 1971. Body posture and mode of locomotion in Early Pleistocene hominids. *Folia Primat* 14:209-240.
- Rao UB, and Joseph B. 1992. The influence of footwear on the prevalence of flat foot. *J Bone Joint Surg* 74B:525-527.

- Rhea JT, De Luca SA, and Sheehan J. 1983. Radiographic anatomy of the tarsal bones. *Med Radiog Photog* 59:2-8.
- Richie HR. 2007. Biomechanics and clinical analysis of the adult acquired flatfoot. *Clin Podiatric Med Surg* 24:617-644.
- Root ML, Orien WP, and Weed JH. 1977. *Normal and Abnormal Function of the Foot*. Los Angeles: Clinical Biomechanics Corporation.
- Roy H, Bhattacharya K, Deb S, and Ray K. 2012. Arch index: An easier approach for arch height (a regression analysis). *Al Ameen Med Sci* 5:137-146.
- Saltzman CL, and Nawoczenski DA. 1995. Complexities of foot architecture as a base of support. *J Orthop Sports Phys Ther* 21:354-360.
- Sanner WH, and Whitney KA. 2015. Foot segment relationships and bone morphology. In: Christman RA, editor. *Foot and Ankle Radiology*. Philadelphia: Wolters Kluwer. p 209-234.
- Sarrafian SK, and Kelikian AS. 2011. Functional Anatomy of the Foot and Ankle. In: Kelikian AS, editor. *Sarrafian's Anatomy of the Foot and Ankle*. Philadelphia, PA: Wolters Kluwer/Lippincott Williams & Wilkins. p 507-643.
- Schultz AH. 1950. The physical distinction of man. *Proc Am Phil Soc* 94:428-449.
- Schultz AH. 1963. Relations between the lengths of the main parts of the foot skeleton in primates. *Folia Primat* 1:150-171.
- Schultz AH. 1969. *The Life of Primates*. New York: Universe Books.
- Sewell RBS. 1904a. A study of the astragalus: Part II. *J Anat Physiol* 38:423-433.
- Sewell RBS. 1904b. A study of the astragalus: Part I. *J Anat Physiol* 38:233-247.
- Sewell RBS. 1905. A study of the astragalus: Part III. *J Anat Physiol* 39:74-88.
- Sewell RBS. 1906. A study of the astragalus: Part IV the caput. *J Anat Physiol* 40:152-161.
- Sgarlato TE. 1971. *A Compendium of Podiatric Biomechanics*. San Francisco: California College of Podiatric Medicine.
- Shereff MJ, and Johnson KA. 1983. Radiographic anatomy of the hindfoot. *Clin Orthop Relat Res* 177:16-22.

- Smith JW. 1958. The ligamentous structures in the canalis and sinus tarsi. *J Anat* 94:616-621.
- Smith RW, and Staple TW. 1983. Computerized tomography (CT) scanning technique for the hindfoot. *Clin Orthop Relat Res* 177:34-38.
- Staheli LT. 1999. Planovalgus foot deformity. *J Am Podiatr Med Assoc* 89:94-99.
- Steele DG. 1976. The estimation of sex on the basis of the talus and calcaneus. *Am J Phys Anthropol* 45:581-588.
- Stewart SF. 1970. Human gait and the human foot: An ethnological study of flatfoot. *Clin Orthop Relat Res*:111-132
- .
- Straus WLJ. 1949. The riddle of man's ancestry. *Q Rev Biol* 24:200-223.
- Susman RL. 1983. Evolution of the human foot: evidence from Plio-Pleistocene hominids. *Foot Ankle* 3:365-376
- .
- Takai S. 1984. Structural components of the arch of the foot analyzed by radiogrammetric and multivariate statistical methods. *Acta anat* 119:161-164.
- Templeton AW, McAlister WH, and Zim ID. 1965. Standardization of terminology and evaluation of osseous relationships in congenitally abnormal feet. *Am J Roentgenol Radium Ther Nucl Med* 93:374-381.
- Thompson ALT, and Zipfel B. 2005. The unshod child into womanhood—forefoot morphology in two populations. *The Foot* 15:22-28.
- Tocheri MW, Solhan CR, Orr CM, Femiani J, Frohlich B, Groves CP, Harcourt-Smith WE, Richmond BG, Shoelson B, and Jungers WL. 2011. Ecological divergence and medial cuneiform morphology in gorillas. *J Hum Evol* 60:171-184.
- Trinkaus E. 1975. *A Functional Analysis of the Neandertal Foot*. Philadelphia, PA: University of Pennsylvania.
- Trinkaus E. 1983. Functional aspects of Neandertal pedal remains. *Foot Ankle* 3:377-390.
- Valmassy RL. 1996. *Clinical Biomechanics of the Lower Extremities*. Chapter 2 Pathomechanics of lower extremity function. St. Louis: Mosby, Inc.
- Vereecke E, D'Aout K, Van Elsacker L, De Clercq D, and Aerts P. 2005. Functional analysis of the gibbon foot during terrestrial bipedal walking: Plantar pressure distributions and three-dimensional ground reaction forces. *Am J Phys Anthropol* 128:659-669.

Volger HW, and Bojsen-Moller F. 2000. Tarsal functions, movement, and stabilization mechanisms in foot, ankle, and leg performance. *J Am Podiatr Med Assoc* 90:112-125.

Wearing SC, Hills AP, Byrne NM, Hennig EM, and McDonald M. 2004. The arch index: a measure of flat or fat feet? *Foot Ankle Int* 26:820-825.

White TD, and Folkens PA. 2000. *Human Osteology*. San Diego: Academic Press.

Wood-Jones F. 1944. *Structure and Function as seen in the Foot*. Baltimore: Williams and Wilkins Company.

Younger AS, Sawatzky B, and Dryden P. 2005. Radiographic assessment of adult flatfoot. *Foot Ankle Int* 26:820-825.

Zifchock RA, Theriot C, Hillstrom HJ, Song J, and Neary M. 2017. The relationship between arch height and arch flexibility. *J Am Podiatr Med Assoc* 107:119-123.

Zipfel B, DeSilva JM, and Kidd RS. 2009. Earliest complete hominin fifth metatarsal-Implications for the evolution of the lateral column of the foot. Volger HW, and Bojsen-Moller F. 2000. Tarsal functions, movement, and stabilization mechanisms in foot, ankle, and leg performance. *J Am Podiatric Med Assoc* 90:112-125.

Zipfel B, DeSilva JM, Kidd RS, Carlson KJ, Churchill SE, and Berger LR. 2011. The foot and ankle of *Australopithecus sediba*. *Science* 333:1417-1420.

Chapter 1: List of Figures

- Figure 1a. Right talus superior surface.
- Figure 1b. Right talus lateral surface.
- Figure 1c. Right talus medial surface.
- Figure 1d. Right talus posterior surface.
- Figure 1e. Right talus inferior surface.
- Figure 1f. Right talus anterior surface.
- Figure 2a. Radiograph right talus AP view.
- Figure 2b. Radiograph right talus lateral view.
- Figure 3a. Right calcaneus anterior surface.
- Figure 3b. Right calcaneus superior surface.
- Figure 3c. Right calcaneus lateral surface.
- Figure 3d. Right calcaneus posterior surface.
- Figure 3e. Right calcaneus inferior surface.
- Figure 3f. Right calcaneus medial surface.
- Figure 4a. Radiograph right calcaneus AP view.
- Figure 4b. Radiograph right calcaneus lateral view.
- Figure 5a. Abduction-Adduction motion of the foot.
- Figure 5b. Inversion-Eversion motion of the foot.
- Figure 5c. Plantarflexion-Dorsiflexion motion of the foot.
- Figure 5d. Open chain pronation-supination motion of the right foot.
- Figure 5e. Closed chain pronation-supination motion of the right foot.
- Figure 6a. Lateral view of the left foot.
- Figure 6b. AP view of the left foot
- Figure 7a. Subtalar joint axis lateral view of the foot.
- Figure 7b. Subtalar joint axis AP view of the foot.
- Figure 8a. Midtarsal joint axes lateral view of the foot
- Figure 8b. Midtarsal joint axes AP view of the foot.
- Figure 9. Bones of the medial longitudinal arch of the foot.
- Figure 10a. Radiograph pes planus foot type lateral view (top).
- Figure 10b. Radiograph pes cavus foot type lateral view (bottom).
- Figure 11a. Forefoot (blue) to rearfoot (red) position in right weight-bearing foot without forefoot varus (frontal plane posterior heel).
- Figure 11b. Forefoot varus (frontal plane posterior heel weight-bearing).

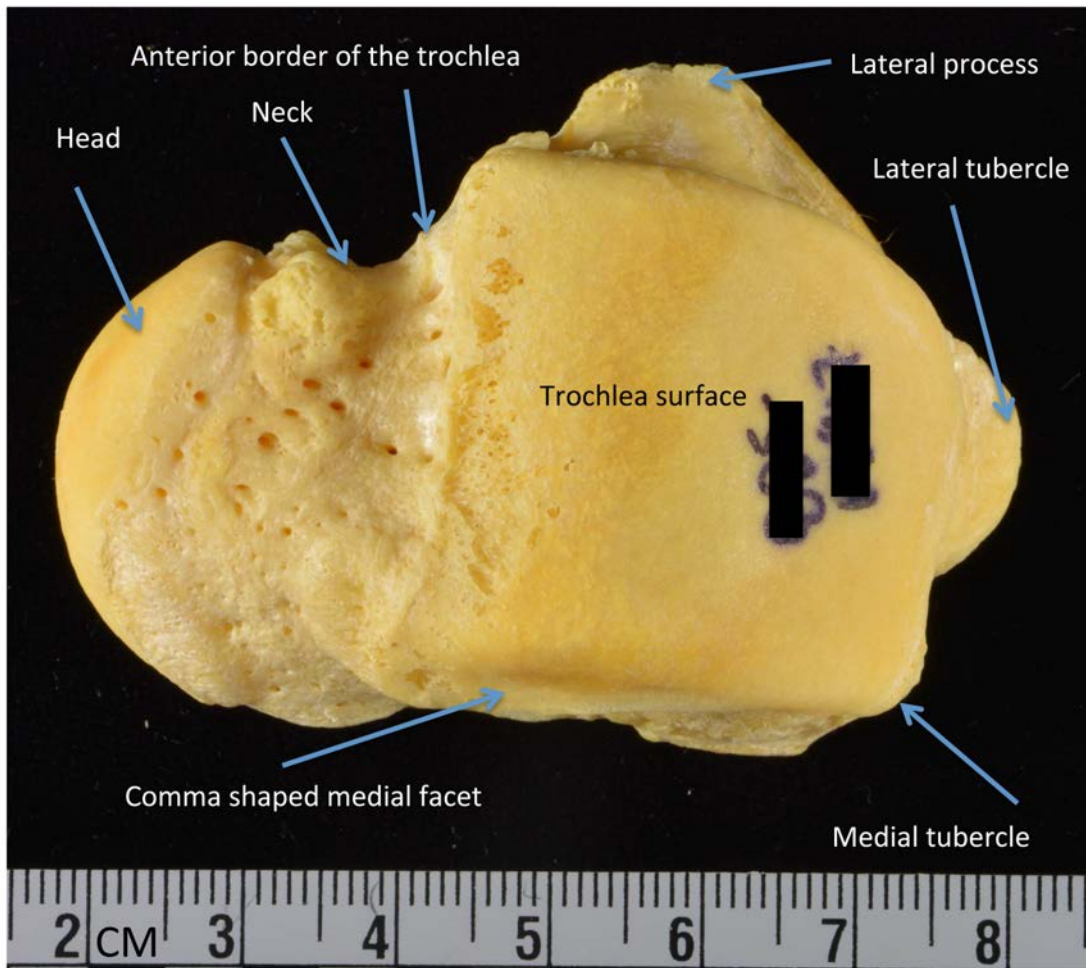


Figure 1a. Right talus superior surface.

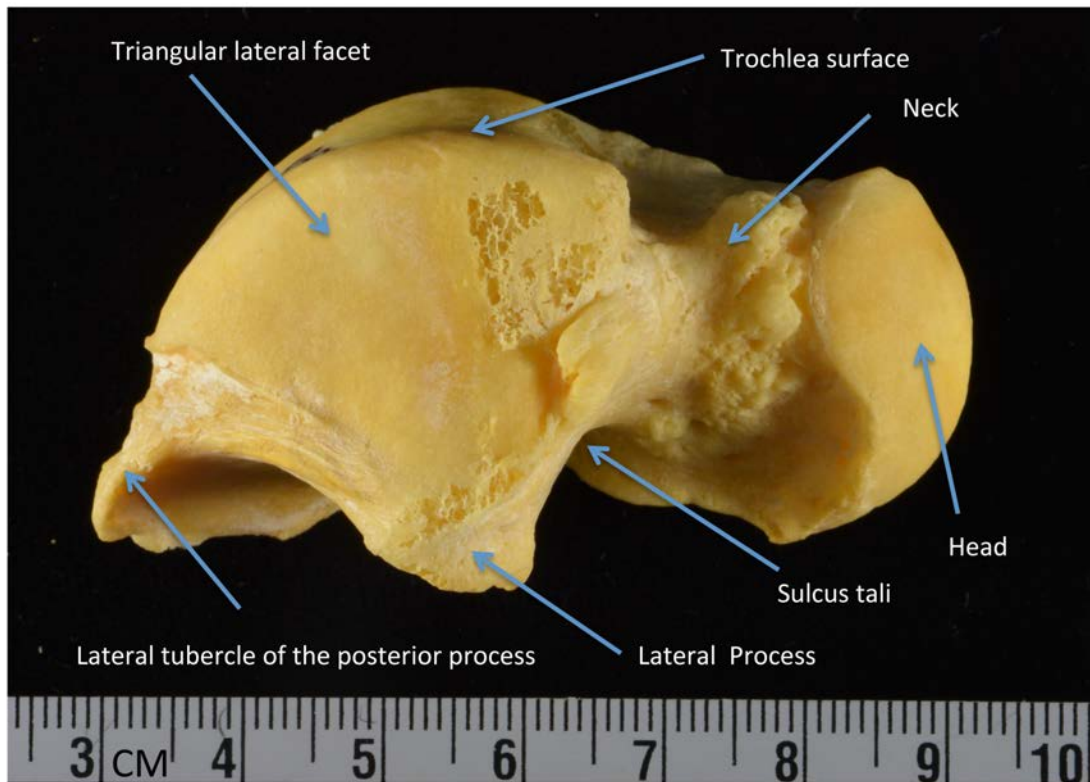


Figure 1b. Right talus lateral surface.

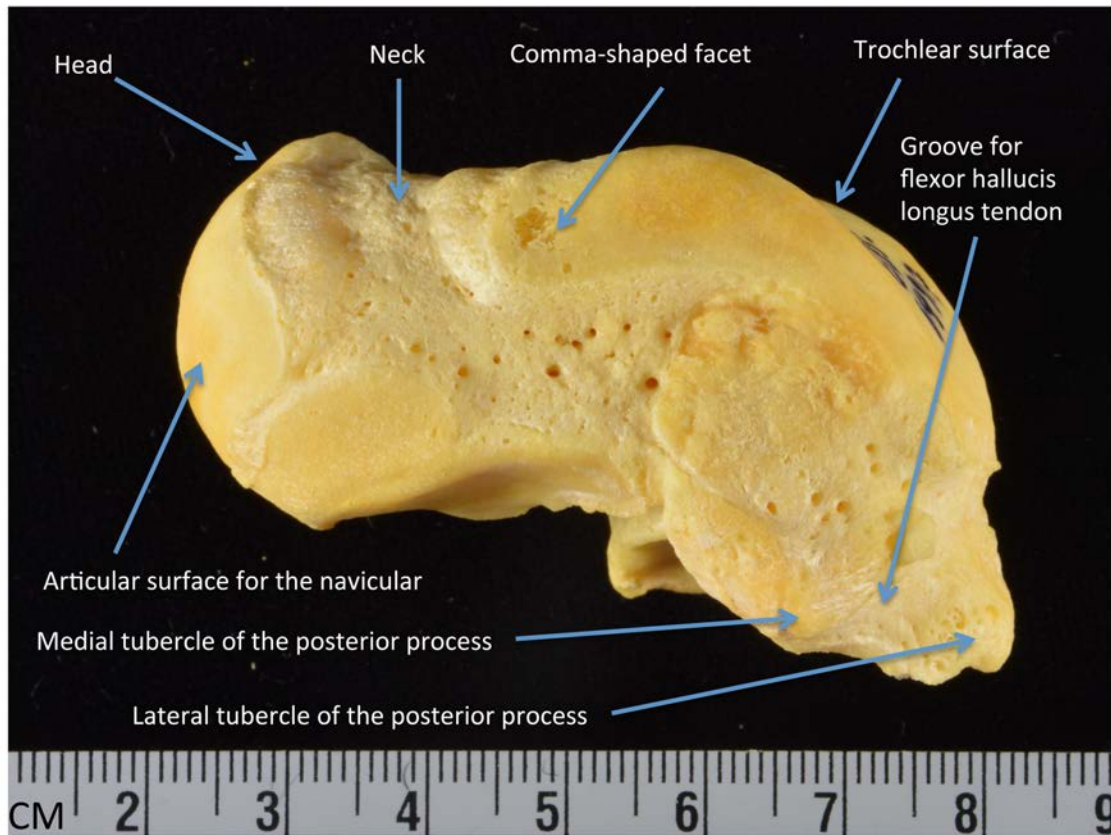


Figure 1c. Right talus medial surface.

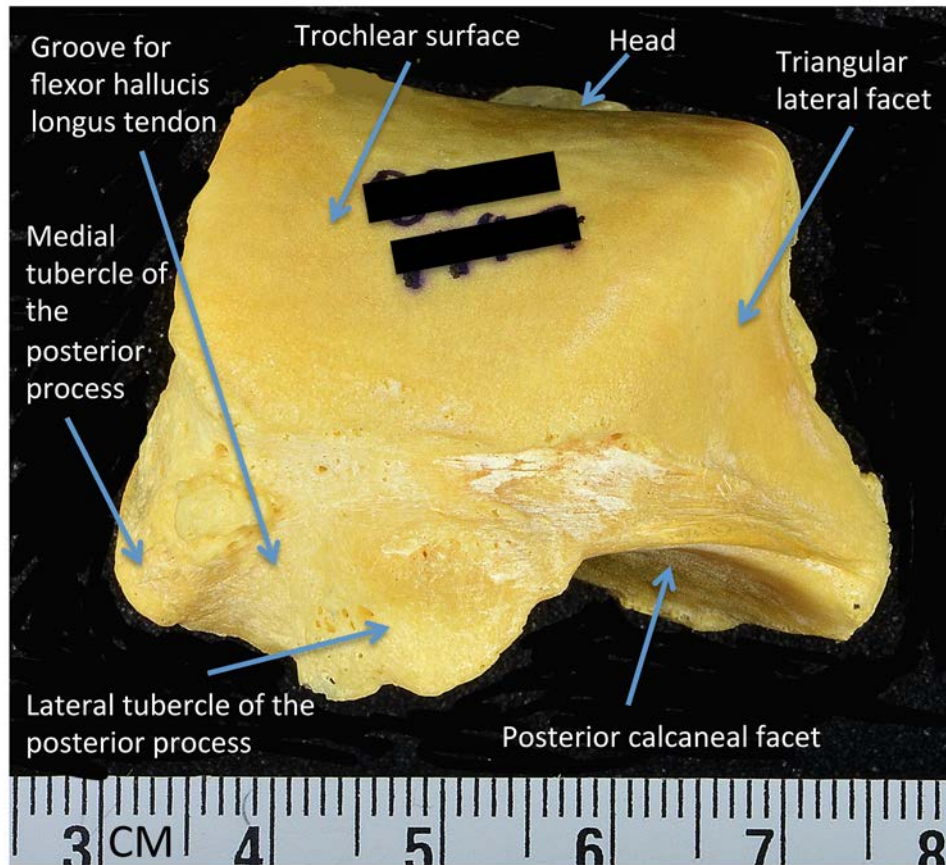


Figure 1d. Right talus posterior surface.

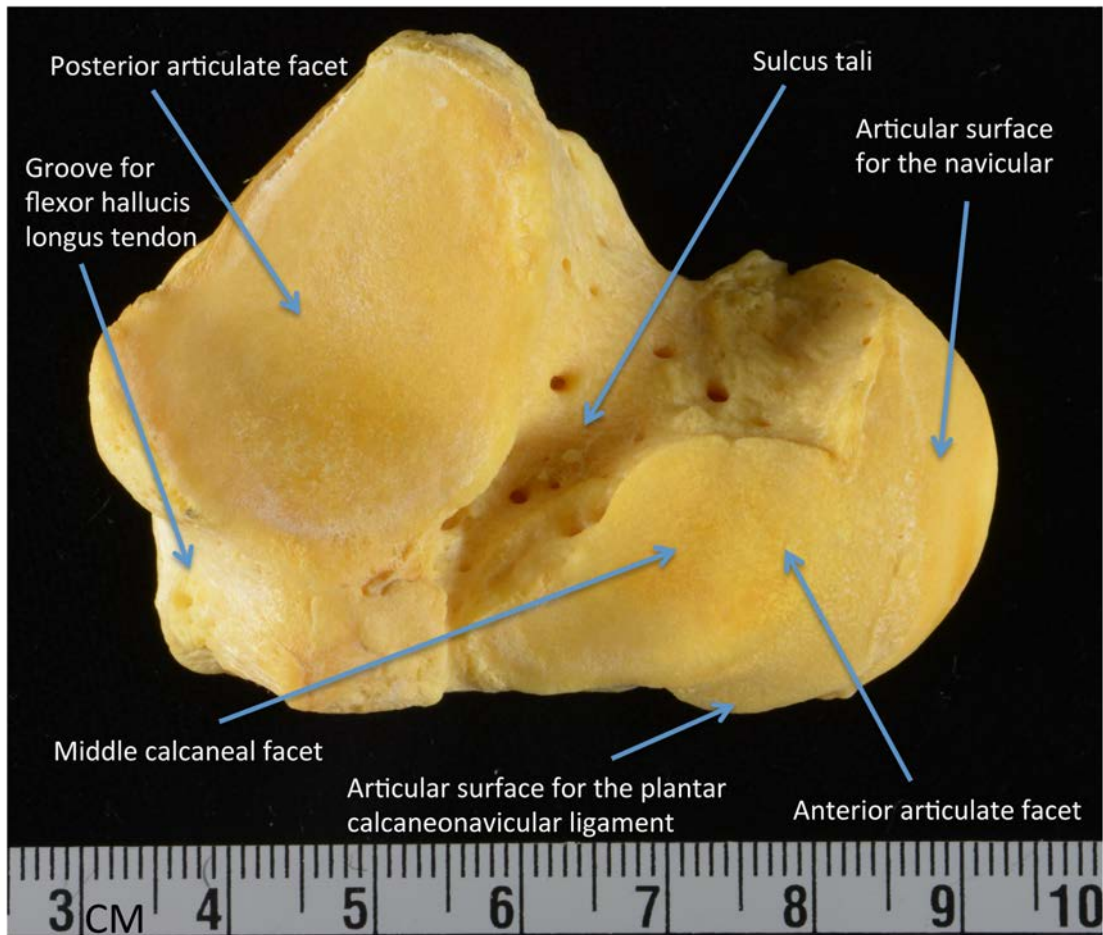


Figure 1e. Right talus inferior surface.

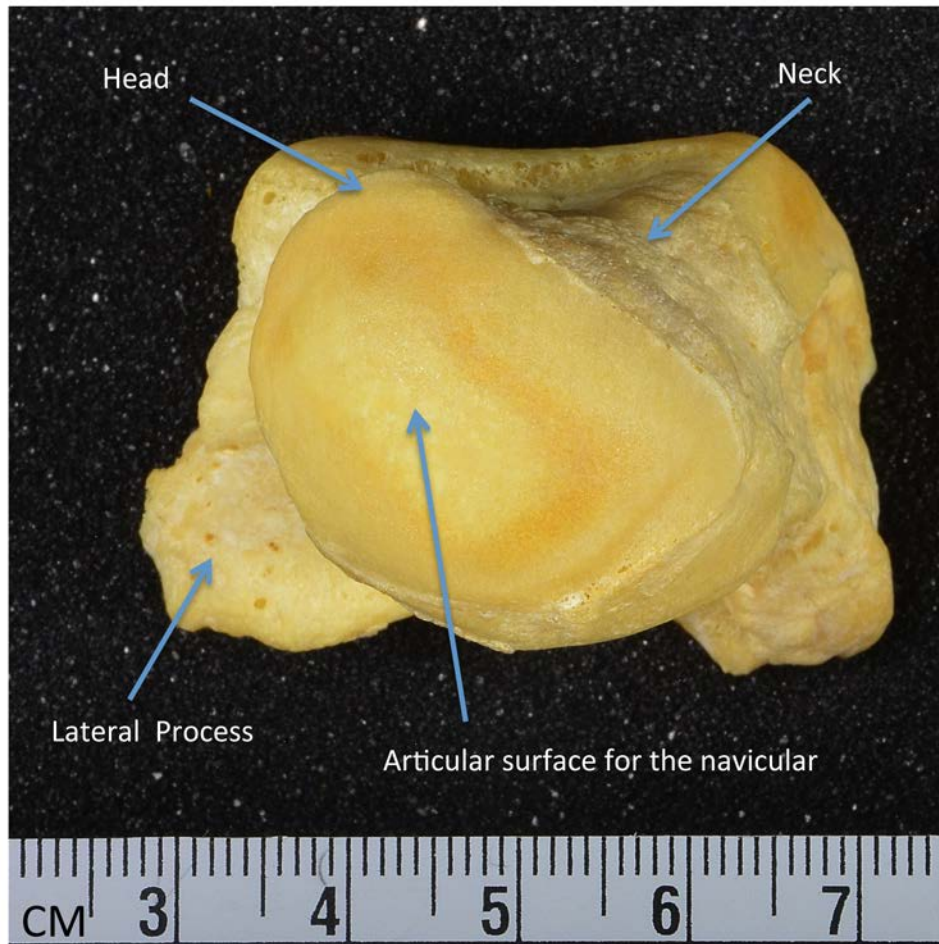


Figure 1f. Right talus anterior surface.

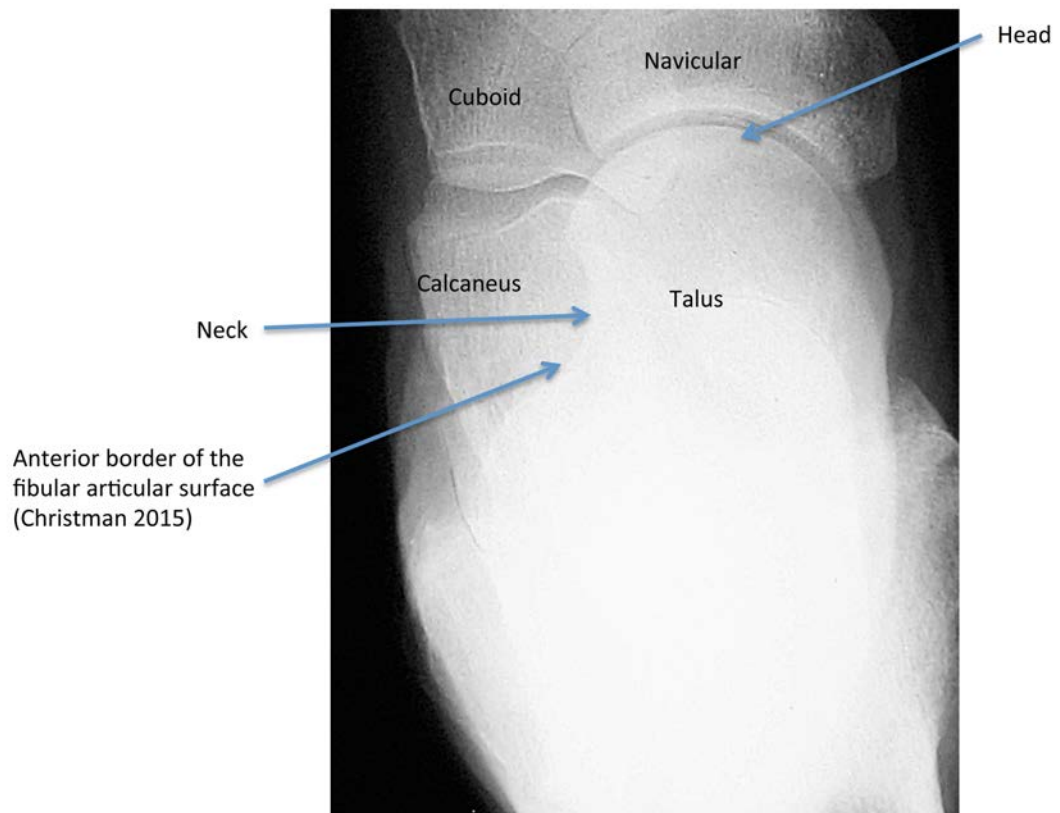


Figure 2a. Radiograph right talus AP view.

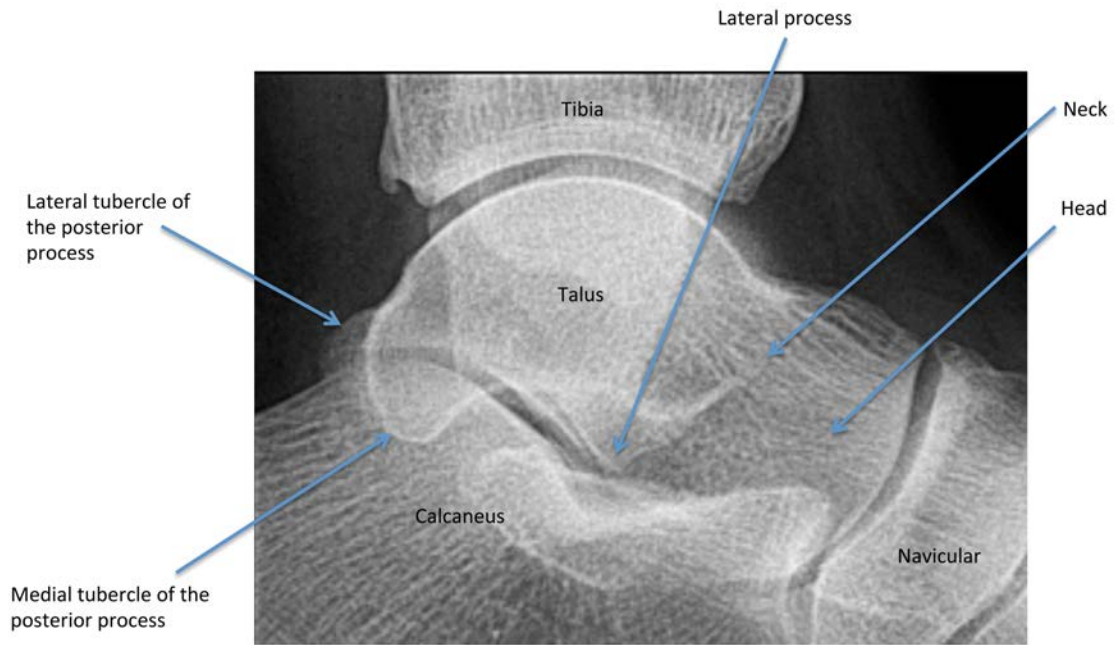


Figure 2b. Radiograph right talus lateral view.

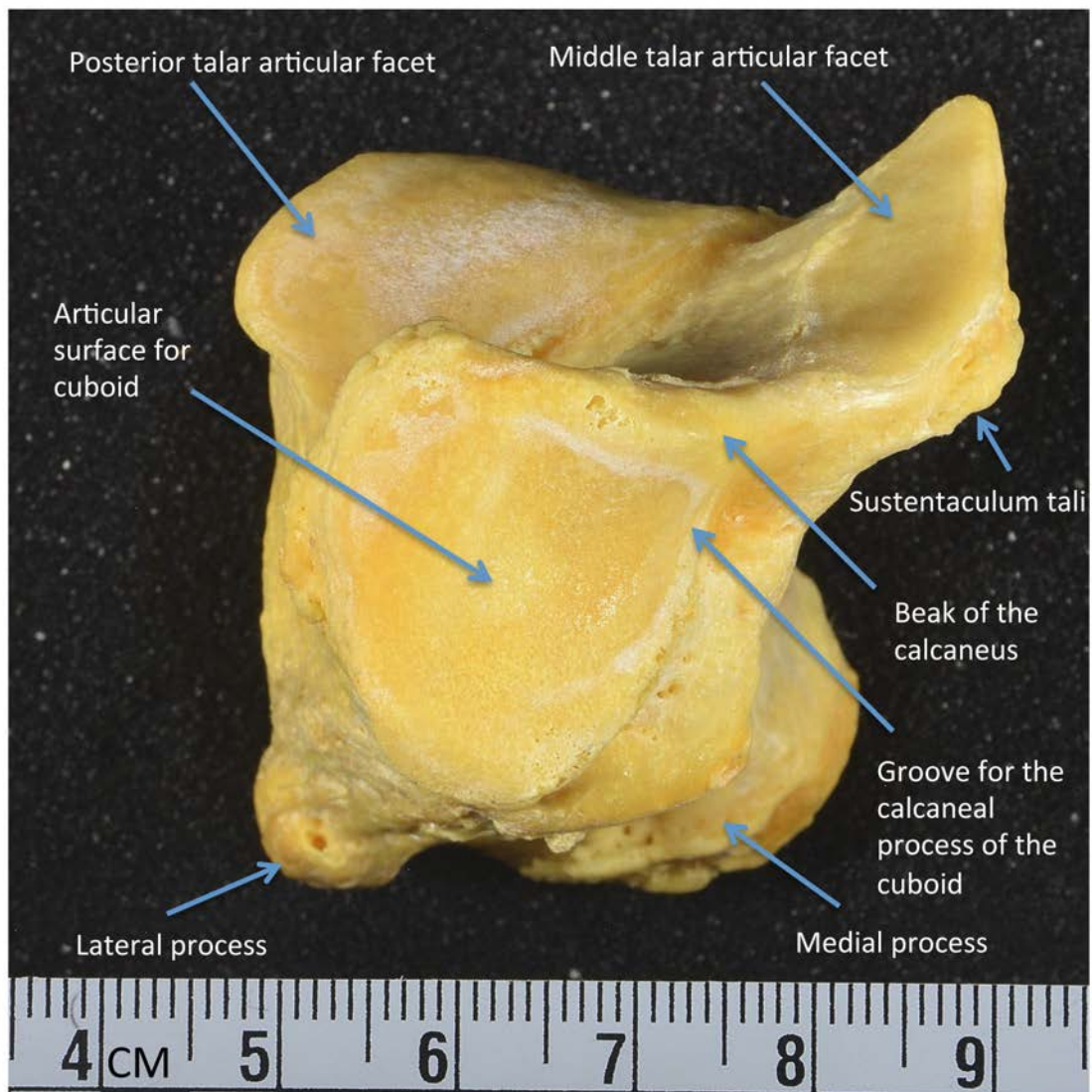


Figure 3a. Right calcaneus anterior surface.

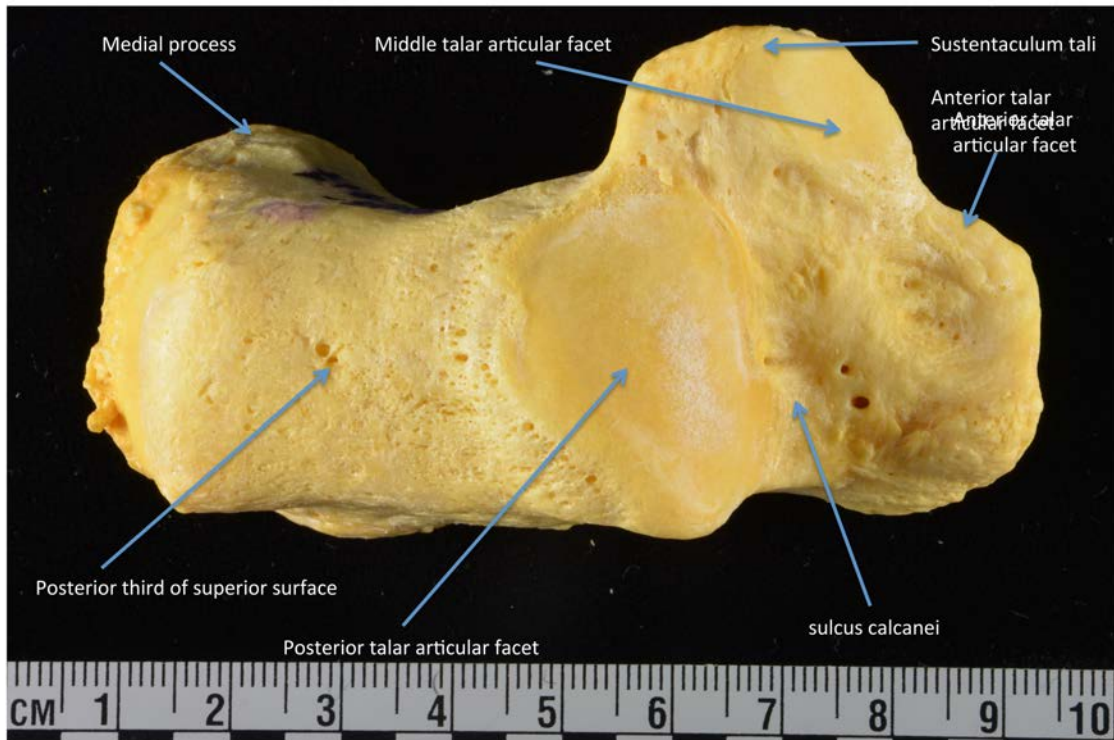


Figure 3b. Right calcaneus superior surface.

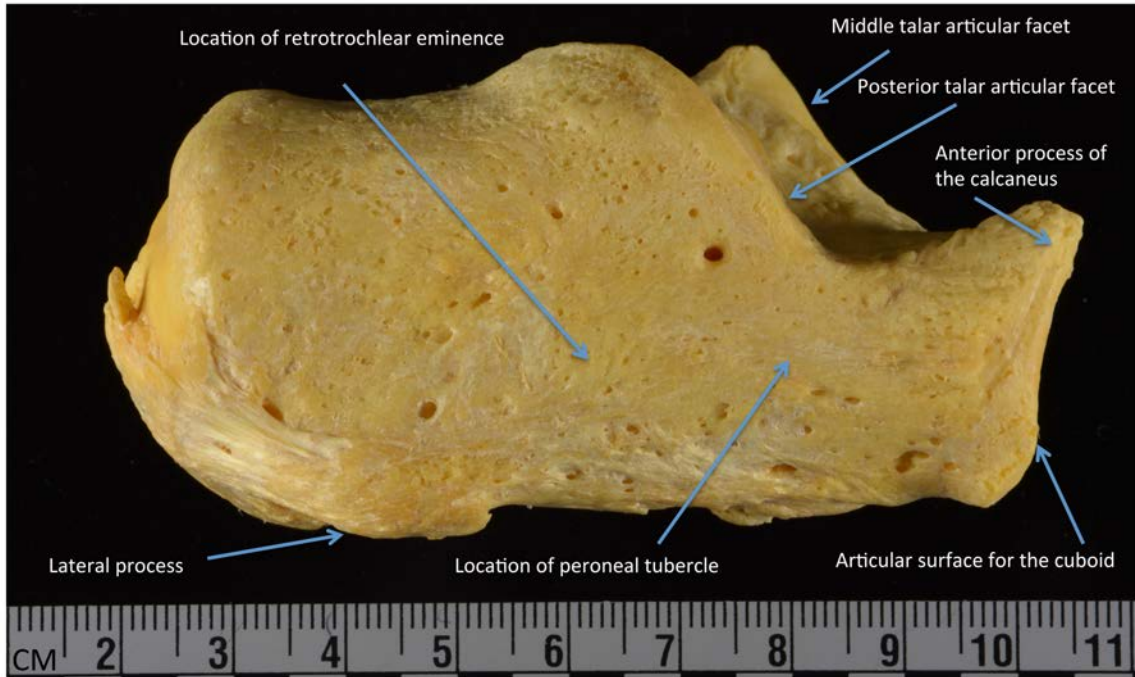


Figure 3c. Right calcaneus lateral surface.

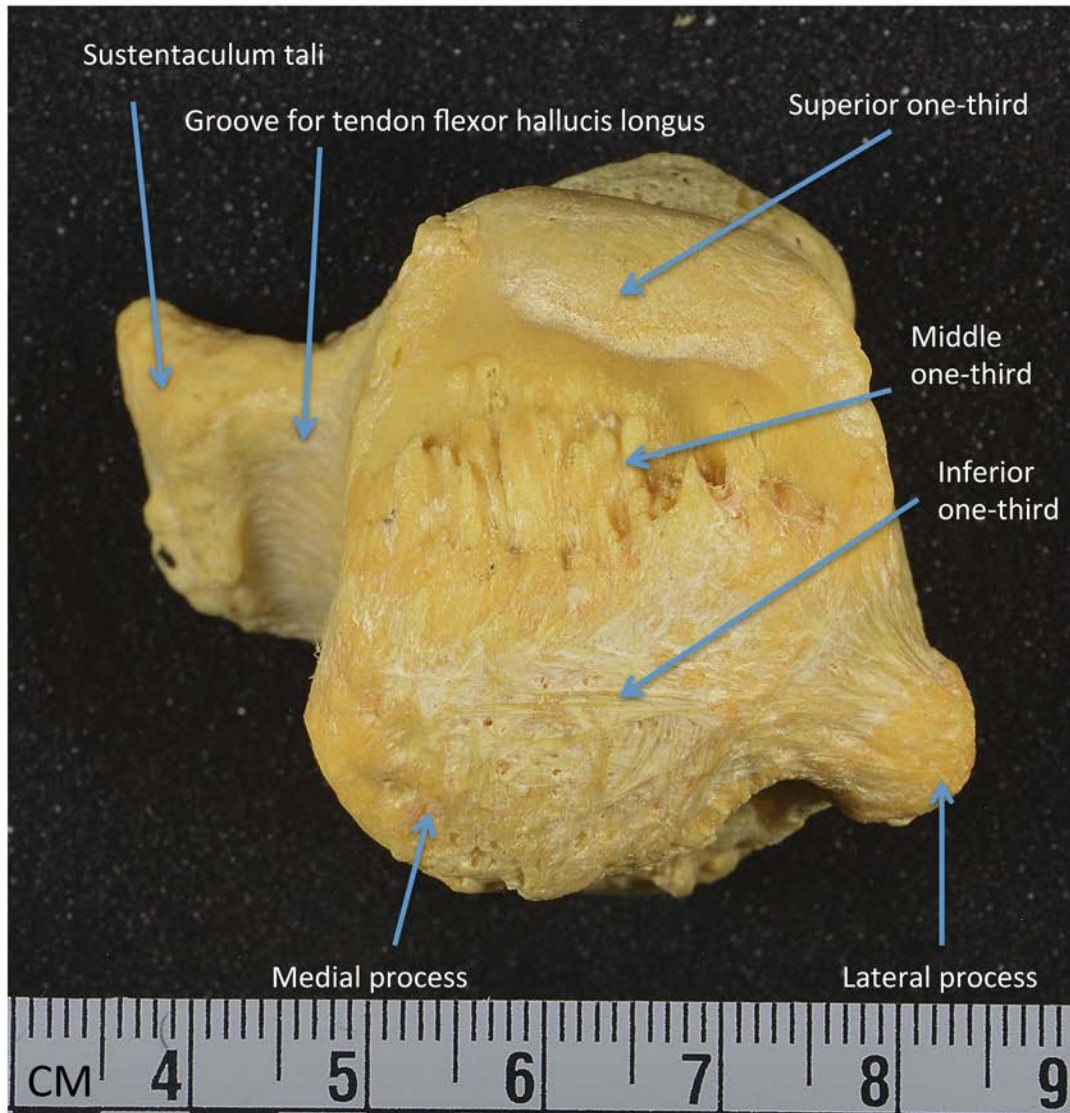


Figure 3d. Right calcaneus posterior surface.

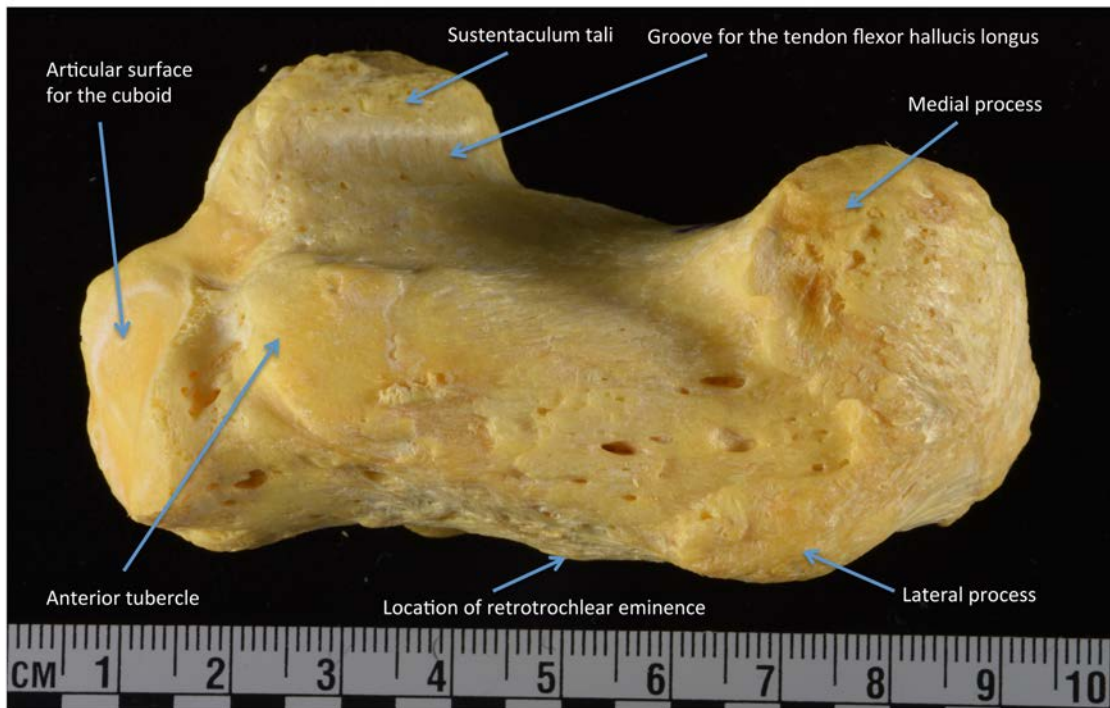


Figure 3e. Right calcaneus inferior surface.

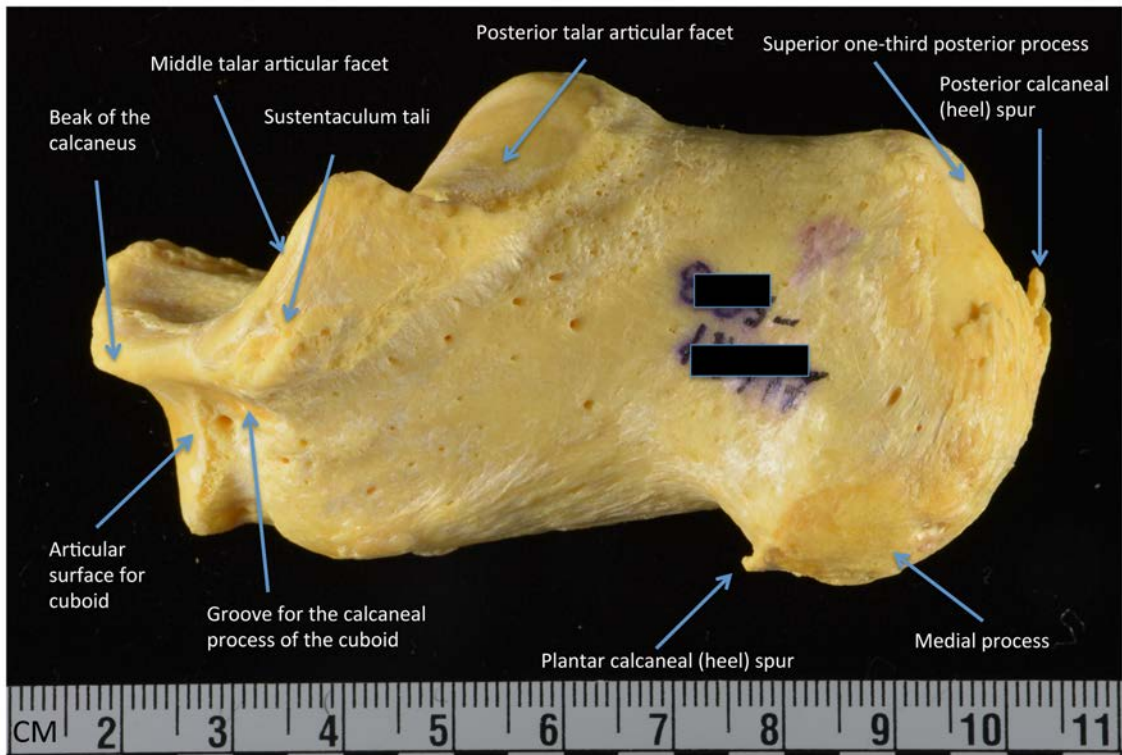


Figure 3f. Right calcaneus medial surface.

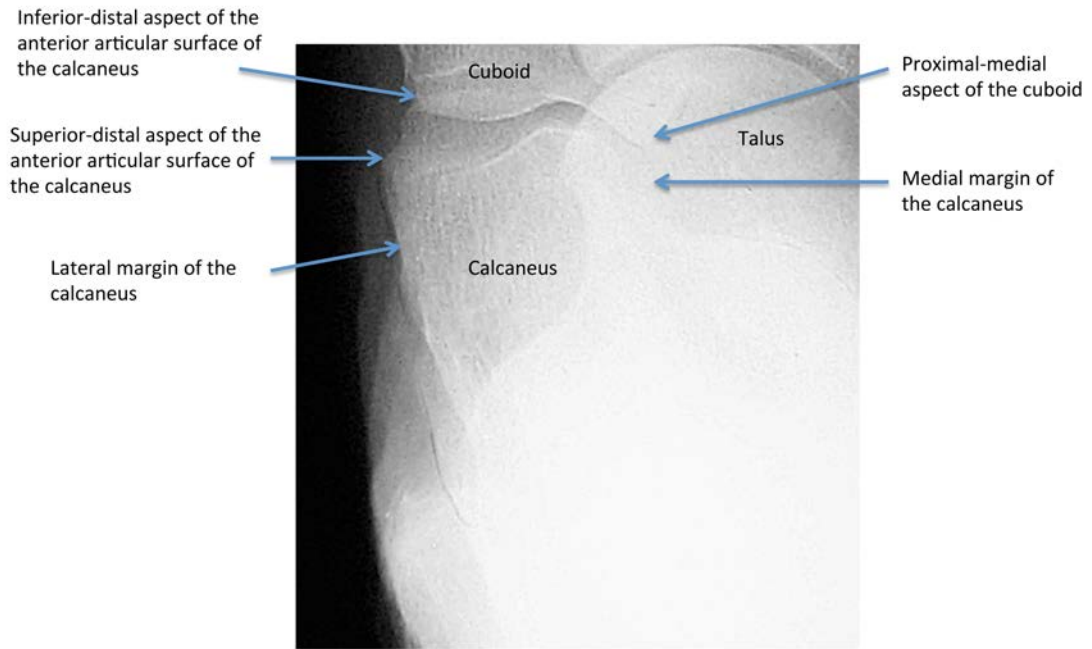


Figure 4b. Radiograph right calcaneus AP view.

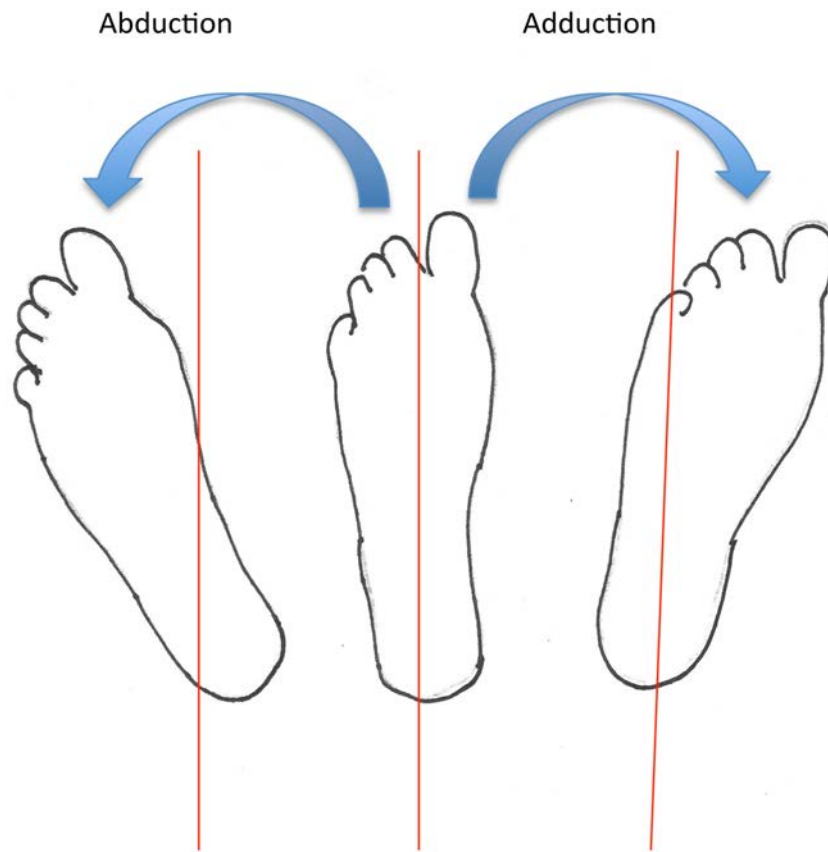


Figure 5a. Abduction-Adduction motion of foot.

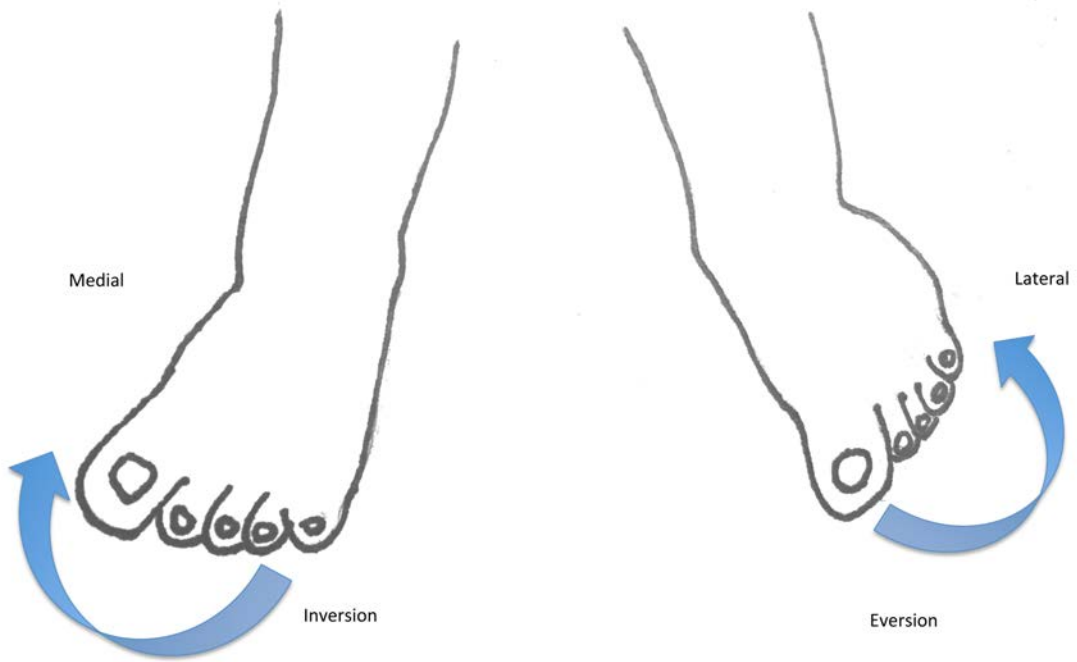


Figure 5b. Inversion- Eversion motion of the foot.

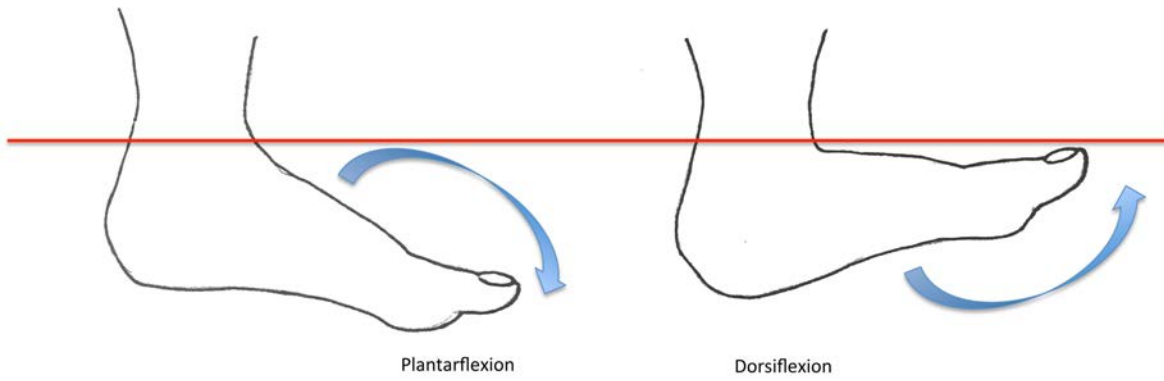


Figure 5c. Plantarflexion-Dorsiflexion motion of the foot.

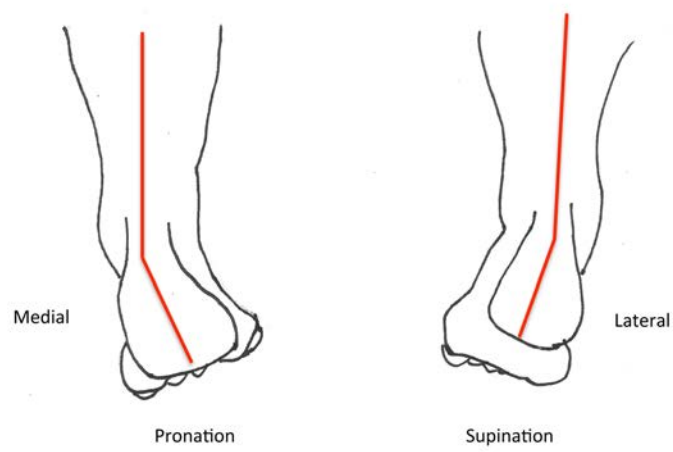


Figure 5d. Open chain pronation-supination motion of the right foot.

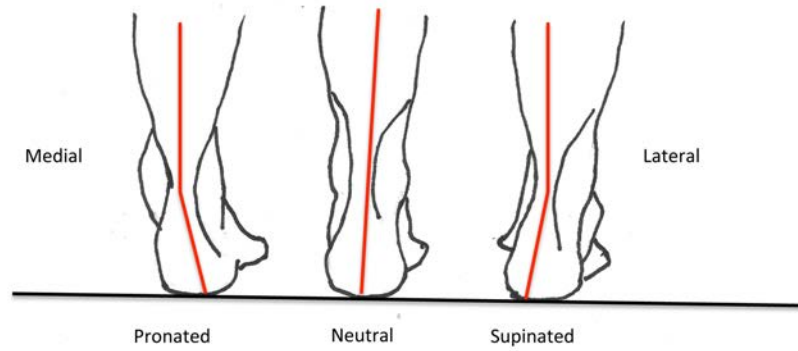


Figure 5e. Closed chain pronation-supination motion of the right foot.



Figure 6a. Lateral view of the left foot.



Figure 6b. AP view of the left foot.



Figure 7a. Subtalar joint axis lateral view of the foot.



Figure 7b. Subtalar joint axis AP view of the foot.



Figure 8a. Midtarsal joint axes lateral view of the foot.



Figure 8b. Midtarsal joint axes AP view of the foot.

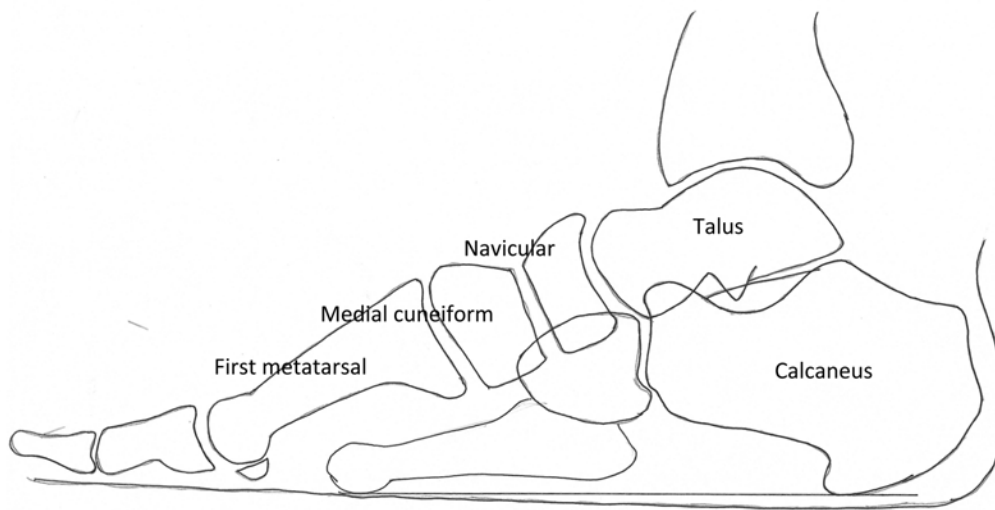


Figure 9. Bones of the medial longitudinal arch of the foot.



Figure 10a. Radiograph pes planus foot type lateral view (top).
Figure 10b. Radiograph pes cavus foot type lateral view (bottom).

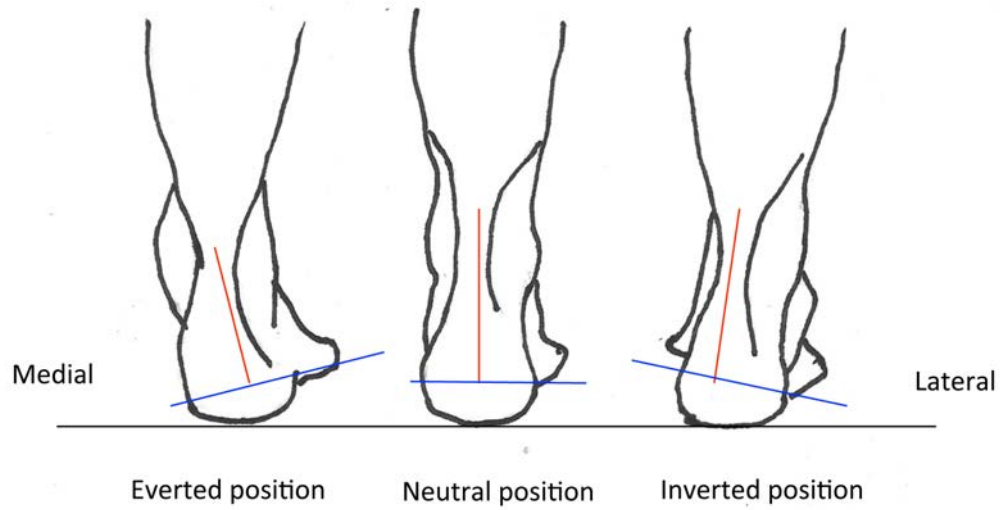


Figure 11a. Forefoot (blue) to rearfoot (red) position in right weight-bearing foot without forefoot varus (frontal plane posterior heel).

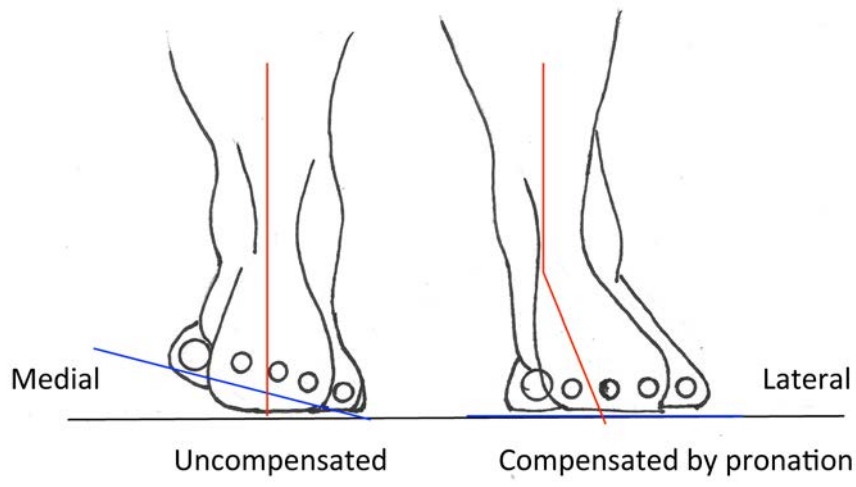


Figure 11b. Forefoot varus (frontal plane posterior heel weight-bearing).

Chapter 2: The relationship between linear osteological and radiographic measurements of the human calcaneus and talus

Preface

The manuscript for this chapter has been published in the *Anatomical Record* (Agoada, 2018). The relationship between linear osteological and radiographic measurements of the human calcaneus and talus. (*Anat Rec* 301:21-33). Changes were made to the manuscript since publication where appropriate for context or consistency in chapter presentation. Additional information concerning the materials and methods used in this study can be found in Appendix B. Appendix C has tables with the measurements used for statistical analysis. More detailed information concerning the statistical analyses can be found in Appendix D.

Abstract

Plain radiographs of the foot are a common form of examination in individuals when medical evaluation is indicated. Their availability makes them useful for studying human variation where large sample sizes are crucial. Calcaneal and talar morphology are critical in the understanding of human foot form and function, but few studies have examined the accuracy of linear measurements of these bones taken from radiographs. If linear measurements are to be used in quantitative analysis, their accuracy must first be demonstrated. For this study, fifty-four human feet from amputated limbs were imaged in standard radiographic views and skeletonized. Selected linear measurements were made on each skeletonized talus and calcaneus. Corresponding landmarks were identified on the

radiographic images and the distances between these points determined. Using the measurements taken from the physical bone, the accuracy of the radiographic measurements was evaluated employing paired Student's *t*-tests and correlation analysis. Most measurements were not significantly different ($p \geq 0.05$). Overall, the sagittal plane measurements were associated ($r^2 > 0.61 - 0.88$, all $p < 0.001$) with the radiographic measurements; transverse plane measurements less strongly associated ($r^2 = 0.20 - 0.63$, $p < 0.001$). These results demonstrate that measurements from radiographic images provide useful information concerning both the calcaneus and talus, indicating that radiographs of living individuals can be evaluated quantitatively and compared to osteology collections of modern humans. This information can be applied to the understanding of functional anatomy of the modern human foot, interpreting the hominin fossil pedal record, and establishing identification in forensic analysis.

Key words: Talus; calcaneus; radiograph; linear measurements.

Introduction

Plain radiographs of the foot provide accurate information on the morphology of the individual bones as well as angular relationships between bones (Christman, 2015). They are a medically approved form of non-invasive examination in individuals where trauma has occurred or is suspected, where surgical treatment is planned, or where bone appearance, arthritic changes, or joint relationships need to be evaluated to arrive at a diagnosis of a condition and to formulate a treatment plan. Computer tomography (CT) and magnetic resonance imaging (MRI) do provide more information about bony structure than plain radiographs. However, CT

requires multiple x-ray projections, exposing the patient to a higher dosage of radiation than plain radiographs. Since there is no known threshold below which the effects of radiation are not harmful, and its effects are cumulative over a lifetime, a diagnostic test subjecting the patient to ionizing radiation exposure must have specific benefits (Christman, 2015). Thus, CT scans are not usually ordered unless absolutely necessary, and only when other forms of evaluation, such as plain radiographs or MRI scan would not provide enough information. In addition, because CT and MRI scans are expensive tests that usually require special approval by insurance providers, they are ordered less often. Since plain radiographs are commonly performed, their availability makes them useful for studying human variation where large sample sizes are necessary.

The talus and calcaneus are recognized as important elements in the structure, function, and integrity of the human foot ((Elftman and Manter, 1935; Morton, 1935; Hicks, 1953; Wood-Jones, 1944; Elftman, 1960; Close et al., 1967; Inman, 1976; Root et al., 1977; DeSilva et al., 2013). The range of variation in size and shape of these tarsal elements in modern humans is well known and has been employed to analyze skeletal remains of both modern and ancient osteological collections (Steele, 1976; Introna et al., 1997; White and Folkens, 2000; Murphy, 2002a,b; Bidmos and Asala, 2003; Bidmos and Dayal, 2003; Bidmos and Asala, 2004; Bidmos and Dayal, 2004; Harris and Case, 2012). While plain radiographs of the foot have been used to provide information concerning the morphology of these bones and their relationships to other bony structures in the foot, few studies have demonstrated the accuracy of the linear measurements of these bones taken from the radiographic images. If a close relationship can be demonstrated between the osteological and radiographic measurements of the calcaneus

and talus, biomechanical and functional analysis of living individuals taken from foot radiographs could then be applied to the understanding of the morphology of the bones themselves (Lautzenheiser and Kramer, 2013).

Standard views of the foot in an initial radiographic evaluation usually include the anterior-posterior (AP or dorsoplantar) view to assess structures from the transverse plane of the foot and the lateral (or lateromedial) view to assess structures from the sagittal plane (Christman, 2015). In the AP view, the image receptor is placed under the foot with the tube head angled posteriorly 15 degrees from vertical, the central beam aimed toward the second metatarso-cuneiform joint. In the lateral view, the medial aspect of the foot is positioned against the image receptor with the tube head angulated vertically (0°) if non weight-bearing, horizontally (90°) if weight-bearing, with the central ray directed at the lateral cuneiform/cuboid region. Occasionally the sagittal plane view is taken through a mediolateral projection with the lateral side of foot against the image receptor and the center beam directed toward the medial cuneiform; however, this is considered a specialized view and is rarely performed routinely. While other views, such as medial and lateral oblique, and dorsoplantar axial, may be ordered depending upon the medical concern to be evaluated, only the AP and lateral views produce images with the least amount of distortion and will most closely correlate with the size and shape of the physical bone. Bones of the foot, therefore, are best assessed in the AP and lateral views (Christman, 2015). All three anatomic planes need to be considered, however, when evaluating the appearance of the bone produced on the two-dimensional radiographic image. For example, using standard plain radiographs, the frontal-plane position

of a bone cannot be directly evaluated; assessments of the talus and calcaneus thus require logical analysis and reasoning while looking at both the AP and lateral views (Christman, 2015).

Steel et al. (1980) reviewed weight-bearing radiographs of 41 pairs of feet taken in standard radiographic technique and found a wide range of variation in linear and angular measurements despite these feet being described as “normal.”

A number of studies have evaluated the accuracy of taking such linear measurements from standard radiographic images of the foot. Most have dealt with the differences in the angular relations between physical bone and its radiographic image in weight-bearing vs. non-weight-bearing views (Hlavac, 1967; Shereff et al., 1990, for example). Shereff et al. (1990) compared selected measurements taken from weight-bearing views with those taken from non-weight-bearing radiographs and found no significant difference in most measurements. They did, however, observe consistent differences in measurements of the length of metatarsals and phalanges, where the bones appeared to be longer with weight-bearing. They postulated that these measurement differences were probably due to variations in the positioning of the x-ray source, the foot, and the radiographic image receptor where, with weight-bearing, these bones move relatively closer to the radiographic image receptor. In addition, metatarsals and phalanges move to a more parallel position in relation to the radiographic image with weight-bearing resulting in an apparent lengthening on the radiographic image.

Lenz et al. (2016) investigated the relationship between the medial eminence width of the first metatarsal and the presence of hallux valgus using radiographs from 43 patients with hallux valgus and 27 patients without. They found that both the first metatarsal head and

medial eminence widths were significantly greater in patients with hallux valgus on the AP view. However, they concluded that this was an artifact of the radiographic image, the result of frontal plane rotation of the first metatarsal head associated with hallux valgus, producing a change in the relationship of the bone to the radiographic image receptor that exaggerated the widths in the AP view. Grady et al. (2015) compared length measurements for the first and second metatarsals measured on the AP and lateral views, with lengths determined by ultrasound-guided measurements. They found that the absolute first metatarsal length measurements were significantly affected by the radiographic view, with the lateral view producing longer, and more accurate, measurements than the AP view.

Saltzman et al. (1994) studied the reliability of radiographic measurements using qualitative vs. quantitative methods. They looked at repeated angular measurements from radiographs, using both intra- and inter- observer comparisons. Measurements were made in two ways: first by a subjective visual assessment, and second by quantitative evaluation made according to strictly defined criteria. They found that greater measurement reliability was obtained with the quantitative methodology, indicating that taking measurements from radiographic images of the foot produce more reliable results than estimating angular relationships by visual estimation alone. Bryant (2001) looked at the effect of taking two slightly different standardized weight-bearing positions at two different times and found no difference in any of the angular values taken from the radiographs.

A few studies have compared the appearance of bone on foot radiographs with that of the physical bone. Christman (2014) compared the radiograph appearance of the talus and calcaneus with that of the physical bone but did not take any measurements. Using

radiographs of the first metatarsal-cuneiform joint taken from different positions, Sanicola et al. (2002) found that, depending on position, the joint can appear to have an inaccurate, abnormal obliquity at the medial cuneiform.

In a review of the literature, there were no studies found that compared foot bone linear measurements with their images taken from standard radiographic views of the intact foot. Riepert et al. (1996) used linear and angular measurements of the calcaneus taken from foot radiographs of 800 patients to investigate quantitatively the degree of sexual dimorphism of the human calcaneus. However, measurement results were not analyzed in relationship to that of the physical bone morphology. Susman (1976) did analyze radiographic images of metacarpals of the human hand. He monitored the accuracy of his radiographic technique by comparing measurements of physical bones with those taken from radiographs. A random sample of 10 measurements was chosen, and a range of large and small measurements was included. Correlation coefficients were computed on the two groups of measurements demonstrating a close relationship ($r = 0.94$ to 0.99) in measurements between the physical bone and its radiographic image.

If selected measurements taken from plain radiographic images of the calcaneus and talus are to be used in statistical studies in the same manner as is done with physical bone, the accuracy of linear measurements from plain radiographs must first be demonstrated. A close association between the measurements of the calcaneus and talus taken from the radiographic images with those from the physical individual bones would establish this relationship. Once this is done, standardized foot radiographs of the modern human foot can be used, and integrated with established osteological collections, to evaluate quantitatively the variability of

the human talus and calcaneus. Such parameters as bone size and shape could be compared statistically within, and between, human population samples. Biomechanical and functional analysis of living individuals could then be combined with the quantitative information concerning the talus and calcaneus obtained from weight-bearing radiographs. If measurements of these relatively complex-shaped bones taken from radiographic images can be used in statistical analysis, it is possible that measurements taken from radiographs of other bones of the foot can be used in the same manner. However, each bone of the foot must first be evaluated separately as described here for the talus and calcaneus, to identify those measurements that can be used for both bone and radiograph, their measuring points, and how the measurements should be taken.

As demonstrated by DeSilva and Throckmorton (2010) skeletal information derived from radiographs of the modern human foot can be used to address questions of functional analysis in a paleontological context. These analyses would provide invaluable information for the assessment of foot form and function in the ancestral hominins, an area where the functional meaning of similarities, and dissimilarities between fossil hominin feet and modern human feet are not completely understood (DeSilva et al., 2014). Determining the accuracy of radiographs will also be useful in a forensic context by assisting in the identification of an unknown individual from pedal remains, using known foot radiographs (Steele, 1976). In addition, the results of this study would be useful in clinical medicine, by adding to the body of knowledge on the accuracy of measurements taken from plain radiographs that can then be applied in such areas as the diagnosis of pathological conditions and planning of surgical procedures.

The goal of this study is to assess the ability to use linear measurements of the talus and calcaneus taken from standard radiographs of the foot for statistical analysis in the same manner as those taken from the physical bone. The null hypothesis is that there are no significant differences in selected linear measurements of the talus and calcaneus with corresponding measurements taken from the standardized radiograph images of these bones.

Materials and Methods

The specimens used for this study were collected between 1986 and 1988 from lower extremity amputations performed at the (then) New England Deaconess Hospital (NEDH) in Boston, MA. The specimens and associated patient information were collected with the written approval of the NEDH Institutional Review Board on Human Studies. These individuals underwent below or above knee amputations for infection or acute ischemia. Information concerning their age, ancestry, sex, stature, and medical condition was recorded. The individuals ranged between 35 and 89 years of age at the time of the amputation. Each amputated limb was sectioned above the ankle and the foot x-rayed in the standardized non weight-bearing fashion (Christman, 2015). Any foot that had evidence of bony destruction due to osteomyelitis in the areas of interest was not included in the study. Each foot was then skeletonized. The lower tibia and fibula, talus, calcaneus, navicular, cuboid, medial, intermediate, and lateral cuneiforms, all five metatarsals, and the proximal and distal phalanges of the hallux were retained. The talus and calcaneus were examined for this study. Any bone that had evidence of previous trauma, severe arthritic changes (that resulted in deformity of that bone), or other abnormal features, was not used. Individual bones with spurring and mild

arthritic changes were included as long as the measuring points were not damaged or obscured, and did not interfere with the determination, or taking, of the defined linear measurements. Any spurs with projections at a 90° angle from the bony surface were not included in the measurements. A total of 32 feet from male individuals and 22 feet from female individuals were collected.

Linear dimensions for the talus and calcaneus, along with the corresponding dimensions from the radiographs, were measured. The definition for each linear measurement is given in the Appendix and illustrated in Figures. 1-8. Measurement definitions and techniques for bone were developed from Steele (1976) and others (Olivier, 1940; Trinkaus, 1975; Gomberg, 1981), modified as necessary). Based on the bony landmarks, corresponding measuring points and measurement techniques for the radiographic image were determined. An “x” at the end of the variable name denotes the radiograph version of the measurement.

Eight osteological measurements for the talus (Figures. 1, 3a, 3b) and six for the calcaneus (Figures 5,7a, 7b) along with their corresponding radiographic measurements (Figures 2b, 4b, 6b, 8b) were chosen. Bone measurements were performed using standard techniques as described in the literature (Bass 2005). Linear measurements were made using a Mitutoyo digital sliding caliper to the nearest 0.01-millimeter. An osteometric board was also used for some of the measurements to the nearest 0.1-millimeter. AP and lateral radiographic views were scanned with a reference scale and digitized. Bony landmarks were identified on the scanned radiographs corresponding to those on the bone. Each scanned radiograph was calibrated and measurements performed using ImageJ (NIH) (<http://imagej.nih.gov/ij/>).

Three months after the original measurements were taken, eleven randomly chosen tali and calcanei and their associated radiographs were re-measured to assess intraobserver error. Intraclass correlation coefficients (ICC) using Pearson product-moment coefficient of correlation (r) between initial and second set of measurements were calculated, and the average ranged from 0.86 and 0.99, results similar to those reported in other examination of foot morphology from radiographs (Lautzenheiser and Kramer, 2013).

Descriptive statistics and Student t -tests comparing physical bone and radiographic measurements were performed to identify the presence of significant differences in measurement dimensions between bone and radiograph. Similar to previous work (from Lautzenheiser and Kramer, 2013), the degree to which measurements were associated was established using ordinary least squares regression and confirmed with reduced major axis analysis. Statistical significance was established using an alpha of 95%. Bonferroni correction for multiple comparisons, which yielded $p < 0.001$ was applied to establish the significance of all pairwise tests. Descriptive statistics and other analyses were computed using Stata (V12, Statacorp, College Station, TX).

Results

Talus (Table 1 and Figures 9a,b)

Descriptive statistics, Student's t -tests, regression coefficients (b), and coefficients of determination (r^2) were derived for the talus. Most measurements taken on the bone are not significantly different from those taken on the radiograph (i.e., $p \geq 0.05$), but some do differ.

Talar skeletal measurements were closely related to the radiographic measurements ($b = 0.989$

– 0.999). Measurements taken from the sagittal plane ($r^2 = 0.62-0.88$, $p < 0.001$) explain more of the variation than those taken from the transverse plane ($r^2 = 0.20-0.63$, $p < 0.001$).

Calcaneus (Table 2 and Figures 10a,b)

Descriptive statistics, Student's *t*-tests, regression coefficients (*b*), and coefficients of determination (r^2) were derived for the calcaneus. Most measurements of the calcaneus were not significantly different ($p \geq 0.05$), and overall the calcaneus skeletal measurements are associated with the radiographic measurements ($b = 0.967 - 1.005$). As in the talus, measurements taken from the sagittal plane ($r^2 = 0.54-0.90$, $p < 0.001$) explain more of the variation than those taken from the transverse plane ($r^2 = 0.26$, $p < 0.001$).

Discussion

The accuracy of measurements of the talus and calcaneus taken from radiographs was examined in this study by comparing the radiographic values with measurements of the physical bone.

As demonstrated, while some of the length measurements of the calcaneus and talus are significantly different, all physical bone measurements are associated with the radiographic measurements. Measurements taken from the sagittal plane explained more of the variation than those taken from the transverse plane (Figures 9-10). Measurement differences and differences in r^2 values between bone and radiograph noted from variable to variable may reflect the amount of distortion that takes place due to the variable's position in relation to the x-ray beam and image receptor. These differences among variables may also be the result of the varying degree of accuracy with which the described measuring point location on bone

corresponds with its paired measuring point location described for the radiograph.

Thus, the most accurate radiographic image of a bone is one where the radiograph is taken with the bone next to, and parallel with, the image receptor and perpendicular to the x-ray beam. Since the bones of the foot are not all parallel to the foot, or each other, it is not possible to have every bone of an intact foot parallel to the image receptor and perpendicular to the x-ray beam when taking a radiograph. Consequently, at least some distortion of a bone's image will be present. In addition, every bone varies in its shape. Thus, each surface of a bone may be angulated to the x-ray beam and image plate differently. As a result, every measurement taken from a radiograph will be affected when compared to the physical dimensions of the bone by distortion to some degree, and some images more than others. Because both the talus and calcaneus are roughly parallel to the axis of the foot in the AP and lateral views, these radiographic views should produce images with minimal distortion and magnification.

Other factors, besides image distortion and magnification, can interfere with the correlation between measurements from the physical bone and its radiographic image. The acceptability of measurements taken from any image is dependent upon precise standardization of positioning technique when the radiograph is created. Any deviation from the "ideal" position may affect the accuracy of such measurements. If the foot is not placed in the proper position for the radiograph, the measurements taken of each bone may be close to the physical measurements or may vary a great deal (Gamble and Yale, 1975). Other factors that can cause problems with accuracy of bone vs. radiographic measurements include errors in properly identifying corresponding landmarks, and changes that may take place in the bone

after the radiographs are taken during processing, storage, and handling. Even the careful use of calipers and other bone measuring devices may affect a bone's delicate measuring points and the ability to accurately identify them.

As noted, the relationship of the talus and calcaneus to the x-ray beam, radiographic image receptor, and to each other, results in bony overlap and variations in presentation, potentially obscuring landmarks. For example, the minimal anterior width of the calcaneus (MinAWCALx) is difficult to measure in the AP view because the medial aspect of the calcaneus may be obscured by the lateral talus. In addition, both the medial and lateral borders of the calcaneus at the level of the cuboid articular facet may be difficult to identify due to overlap of the cuboid. This measurement is thus taken as the distance between the most medial and most lateral points of the calcaneal articular surface of the cuboid (see Appendix). Despite these issues, this study demonstrates that most measurements taken from radiographs accurately represent corresponding measurements from the physical bone (Figures 9-10). Further, radiographic measurements that differ from the physical bone measurements remain correlated. For example, although a significant difference ($p < 0.05$) exists between the radiograph and the physical bone measurements for maximum talar length (MaxLTAL = MaxLTALx) and maximum length of the calcaneus (MLCAL = MLCALx) both variables show a strong association ($r^2 = 0.88 - 0.90$).

The height of the body of the talus (BHTAL) was determined on the physical bone using two different landmarks (BHTALa and BHTALb) in order to determine which method produces better results when compared to the radiograph. A significant difference between the height of the radiograph and the physical bone exists for BHTALa, with the radiographic height greater.

For BHTALb no significant difference between the radiograph and the physical bone was found. In both cases the heights correlated well, although the radiographic height was consistently higher than the physical bone measurement. BHTALb, thus, produces better results than BHTALa.

The greater dimensions on the radiograph when compared to the physical bone seen in the example above (and several other variables) are most likely the results of image magnification due to the distance of the physical bone from the radiographic image receptor. Some measurements are greater for the physical bone than the radiograph. For instance, a significant difference in maximum talar head and neck length (MaxLHNTAL) between the radiograph and the physical bone ($p = 0.02$) exists, with the physical bone length being greater. The lengths are associated ($r^2 = 0.63$). The greater measurement of the physical bone may be the result of the choice of corresponding measuring points.

Length and width measurements taken from the AP view are more difficult to measure accurately than lateral view measurements, as reflected by their lower coefficient of determination values. While no significant difference in maximum width of the talar head (MaxWHTAL) or minimal talar neck width (MinWNTALa, b) between the radiograph and the physical bone exists, the variation in the radiographic width explains only 20% and 36-45%, respectively, of the physical bone (MaxWHTAL $r^2 = 0.20$; MinWHTALa $r^2 = 0.36$; MinWNTALb $r^2=0.45$). Similarly, MinAWCAL exhibited no significant difference in widths between the radiograph and the physical bone exists, but the radiographic width explains only 26% of the physical bone width ($r^2 = 0.26$).

Where some variables produced weaker associations, alternative techniques for measuring these variables on bone and or radiograph were developed and tested. Nonetheless, the results for the anterior process width of the distal calcaneus and the maximum width of the head and neck of the talus may reflect that these measurements are more challenging to obtain from radiographs.

This study demonstrates that linear measures of the talus and calcaneus measured on radiographs accurately reflect the linear dimensions of the physical bones. Collecting quantitative information on these bones from radiographic images of the feet of living humans should help in understanding the association of the morphologic variation of these tarsal elements in modern humans with identifiable foot types, something that currently cannot be performed with confidence using isolated foot bones (DeSilva et al., 2014). Having the ability to treat measurements taken from radiographs in the same manner as those from bone is useful in a forensic context, as well, allowing expansion of the databases on age, sex, and ancestry, which, until now, could only be compiled using osteological collections.

Chapter 2: Appendix

Talus bone measurements

The plane of measurement refers to the plane of the foot in which the measurement was made.

Sagittal plane measurements (Figure 1)

Maximum Talar Length (MaxLTAL)

Definition: The distance between the most posterior aspect (the posterior lateral process of the talus) and the most anterior point of the talar head.

Method: The medial surface of the talus faces the examiner, with the caliper held in the sagittal plane, roughly parallel to the medial border of the trochlear in the sagittal plane. Depending upon the most anterior point, the caliper may not be parallel to the long axis of the talus.

Maximum Height of the Body of the Talus (MaxHBTAL)

Definition: The distance between the most superior point of the lateral border of the trochlear surface and the most inferior point (lateral process of the talar body at the apex) of the lateral surface of the talar body.

Method: The lateral surface of the talus faces the examiner, with the caliper held in the sagittal plane, roughly parallel to the surface of the superior surface of the fibular malleolar facet in the transverse plane. The caliper is also held roughly perpendicular to the long axis of the talus in the sagittal plan.

Height of the Body of the Talus (BHTALa)

Definition: The distance between the most superior point of the medial border of the trochlear surface and most inferior point at the medial aspect of the posterior articular facet for the calcaneus.

Method: The medial surface of the talus faces the examiner with the caliper held in the sagittal plane. One arm of the sliding caliper contacts both the most inferior point of the talar head and the most inferior and medial point of the posterior articular facet for the calcaneus, and the other arm contacts the most superior surface of the medial border of the trochlea. The caliper should be held roughly parallel to the medial surface of the talus in the frontal plane. Although the medial border is not always the high point superiorly, using the same three points consistently helps standardize the measurement.

Height of the Body of the Talus (BHTALb)

Definition: The distance between the most superior point of the medial border of the trochlear surface and most inferior point at the medial aspect of the posterior articular facet for the calcaneus.

Method: Using an osteometric board, the talus is placed perpendicular to the board, medial aspect facing down. Both the inferior surfaces of the posterior articular facet and the talar head should be in contact with the fixed end of the board. The bone may need to be move around to find the maximum height.

Maximum Length Fibular (Lateral) Malleolar Facet of the Talus (MaxLFMTAL)

Definition: The distance between the most anterior aspect of the fibular malleolar facet (talar trochlear) and the most posterior aspect of the facet.

Method: The lateral surface of the talus (talar trochlear) faces the examiner, with the caliper held in the sagittal plane (and parallel to the long axis of the talus in the sagittal plane, or MaxLTAL), roughly parallel to the lateral margin of the trochlea surface in the transverse plane. It is the maximum distance between the two surfaces laterally; the articular surface may not extend to the maximum anterior and posterior extent of the surfaces.

Transverse plane measurements (Figures 3a and 3b)

Maximum Width of the Head of the Talus (MaxWHTAL)

Definition: The distance between the most medial and the most lateral aspects of the navicular articular surface at the anterior aspect of the talus.

Method: The superior surface faces the examiner, with the caliper held in the frontal plane perpendicular to the lateral border of the neck. The caliper is held roughly parallel to the long axis of the talar head.

Minimal Width of the Neck of the Talus (MinWNTALa)

Definition: The shortest distance between the medial and lateral borders of the talar neck.

Method: The inferior surface faces the examiner, with the caliper held in the frontal plane, perpendicular to the lateral border of the talar neck and anterior to the anterior border of the trochlear surface medially.

Minimal Width of the Neck of the Talus (MinWNTALb)

Definition: The shortest distance between the medial and lateral borders of the talar neck.

Method: The superior surface faces the examiner with the caliper held in the frontal plane, roughly perpendicular to the lateral border of the neck laterally to the long axis of the neck, and the most anterior point of the anterior border of the trochlear surface medially, superior to the middle articular facet.

Maximum Length of the Head and Neck of the Talus (MaxLHNTAL) (MaxLHNTAL-1 measurements used)

Definition: The distance between the most anterior point of the head of the talus and the anterior border of the trochlear at its most proximal aspect laterally (i.e., the distance between the most anterior aspect of the head and where the neck flares out onto the talar body at its lateral border).

Method: The superior surface faces the examiner, with the caliper roughly in the transverse plane, parallel to the lateral border of the talar neck.

Talus radiographic measurements

Lateral view measurements (Figures 2a and 2b)

Maximum Talar Length (MaxLTALx)

Definition: The distance between the most posterior point of the posterolateral tubercle (PLT) and the most anterior point of the talus. If a prominent spur, or evidence of an os trigonum (OT), is present, then two measurements are taken, the longer including the spur or trigonum in the measurement.

Maximum Height of the Body of the Talus (MaxHBTALx)

Definition: The distance between the most superior point of the trochlear lateral surface (either medial or lateral) and the most inferior point of the lateral process of the talar body at the apex.

Height of the Body of the Talus (BHTALx)

Definition: The distance between the most superior point of the trochlear surface and most inferior point of the talus.

Method: The most inferior point of the talus is determined in the following way: A line is drawn between the most inferior point of the talar head and the most inferior point of the posteromedial tubercle of the talus. BHTALx is the distance between the superior surface of the talus and the point perpendicular to the line.

Maximum Length of Fibular Malleolar Facet (MaxLFMTALx)

Definition: The distance between the most anterior point of the border of the lateral surface and the most posterior margin of the lateral surface.

Method: Determined by drawing a line roughly parallel to the longitudinal axis of the talus. The most anterior aspect is the point where the neck and body meet; the most posterior point is where this line transects the posterior border.

AP view measurements (Figures 4a and 4b)

Maximum Width of the Head of the Talus (MaxWHTALx)

Definition: The distance between the most medial and the most lateral points of the head of the talus.

Minimum Width of the Neck of the Talus (MinWNTALx) (from MinWNTALx-1)

Definition: The shortest distance between the medial and lateral borders of the talar neck, perpendicular to the long axis of the lateral border.

Method: The measured line is drawn between the narrowest point on the lateral border and where it traverses the medial border.

Maximum Length of the Head and Neck of the Talus (MaxLHNTALx)

Definition: The distance between the most anterior point of the head of the talus and the point where the base of the neck is widest (flares out) at the body of the talus at the lateral border of the neck.

Method: A straight line is drawn parallel to the lateral border of the talar neck. A second line is drawn perpendicular to the first, traversing the widest point of the talar neck at the lateral border (where it flares out to become continuous with the body). MaxLHNTALx is measured as the distance between the most anterior aspect of the head and the second line drawn, perpendicular to that line.

Calcaneus bone measurements

The plane of measurement refers to the plane of the foot in which the measurement was made.

Sagittal plane measurements (Figure 5)

Maximum Length of the Calcaneus (MLCAL)

Definition: The distance between the most posterior point of the calcaneal tuberosity and the most anterior point on the superior margin (Calcaneal beak or anterior process) of the articular surface for the cuboid.

Method: The lateral surface of the calcaneus faces the examiner with the caliper held in the sagittal plane, parallel to the axis of the bone in the sagittal plane, and parallel to the lateral surface of the calcaneus in the transverse plane; or taken with an osteometric board, the lateral side held parallel to the board and inferior surface facing down. If a posterior spur is present, it is included in the measurement unless the spur projects posteriorly; if it does, the spur's length is not included in the measurement.

Maximum Length of the Calcaneus (MLCAL-2)

Definition: The distance between the most posterior point of the calcaneal tuberosity and the most anterior point of the lateral surface of the calcaneus distally.

Method: The lateral surface of the calcaneus faces the examiner with the caliper held in the sagittal plane, parallel to the axis of the bone in the sagittal plane, and parallel to the lateral surface of the calcaneus in the transverse plane. If a posterior spur is present, it is included in the measurement unless the spur projects posteriorly; if it does, the spur's length is not included in the measurement.

Maximum Body Height of the Calcaneus (BHCAL)

Definition: The greatest projected height of the calcaneus, measured between the most inferior point of the calcaneal tuberosity and the most superior point of the posterior articular facet.

Method: The measurement is taken between the highest point of the posterior articular process and a line parallel to the long axis of the calcaneus projected from the most inferior point of the calcaneal tuberosity. The lateral surface of the calcaneus faces the examiner, with the caliper held in the sagittal plane, roughly perpendicular to the long axis of the body of the calcaneus. Or this measurement can be taken with an osteometric board, the lateral surface of the body facing down, the longitudinal axis of the body perpendicular to the board (the bone may need to be moved around to find the maximum height). The use of the osteometric board is preferred if the arms of the caliper are too short and cannot contact either the superior or inferior points comfortably. A plantar spur, if present, may be the most inferior aspect of the calcaneus.

Minimum Body Height of the Calcaneus (MinBHCAL)

Definition: The minimal distance between the superior border of the calcaneus posterior to the posterior articular facet superiorly and anterior to the calcaneal tuberosity inferiorly.

Method: The lateral surface of the calcaneus faces the examiner, with the caliper held in the frontal plane, roughly perpendicular to the lateral surface of the calcaneus in both the frontal and transverse planes. The measurement is taken between the most inferior point of the superior border of the body of the calcaneus posterior to the posterior articular facet superiorly, and the most superior point of the inferior border, anterior to the calcaneal tuberosity.

Minimum Anterior Height of the Calcaneus (MinAHCAL)

Definition: The minimal distance between the superior and inferior borders of the calcaneus, anterior to the posterior articular facet.

Method: The measurement is taken with the lateral surface of the calcaneus facing the examiner, the caliper held in the frontal plane, roughly perpendicular to the long axis of the calcaneus, posterior to the cuboid articular facet superiorly and the most anterior point of the inferior margin of the cuboid articular surface inferiorly.

Transverse plane measurements (Figures 7a and 7b)

Minimum Anterior Width of the Calcaneus (MinAWCAL)

Definition: The minimal distance between the medial and lateral borders of the calcaneus, anterior to the posterior articular facet (or the widest distance between the medial and lateral borders of the cuboid articular facet).

Method: The inferior surface of the calcaneus faces the examiner, with the caliper held in the frontal plane. The caliper is also held roughly parallel to the cuboid articular surface. (Any articular surface that extends beyond the medial border, at either its midpoint, or superiorly toward the sustentaculum tali, is not included in defining the widest point at the medial border.)

Calcaneus radiographic measurements

Lateral view measurements (Figures 6a and 6b)

Maximum Length of the Calcaneus (MLCALx)

Definition: The distance between the most anterior point of the calcaneus and the most posterior point of the calcaneal tuberosity, measured roughly parallel to the long axis of the calcaneus.

Maximum Length of the Calcaneus (MLCAL- 2x)

Definition: The distance between the anterior border of the lateral surface of the calcaneus, at the point where it begins to curve superiorly, and the most posterior point of the calcaneal tuberosity, measured roughly parallel to the long axis of the calcaneus.

Body Height of the Calcaneus (BHCALx)

Definition: The greatest projected height, measured from the most inferior point of the calcaneal tuberosity to the most superior point of the posterior articular facet.

Method: Measurement is taken from a line extended distally from the plantar aspect of the calcaneal tuberosity, parallel to the long axis of the calcaneus. BHCALx is measured perpendicular to this line.

Minimum Body Height of the Calcaneus (MinBHCALx)

Definition: The minimum distance between the superior border of the calcaneus posterior to the posterior articular facet superiorly, and the line representing the most superior point of the inferior border of the lateral surface, anterior to the calcaneal tuberosity.

Minimum Anterior Height of the Calcaneus (MinAHCALx)

Definition: The distance between the most inferior point of the anterior border of the calcaneus, and the superior border of the lateral surface, just posterior to the articular face for the cuboid, and anterior to the superior prominence of the lateral surface. This measurement is roughly perpendicular to the long axis of the calcaneus.

Method: A straight line is drawn from the most inferior point of the calcaneal tuberosity distally roughly parallel to the long axis of the calcaneus. A second line is drawn perpendicular to this line, going through the most inferior point to the superior border of the distal calcaneus. MinAHCALx is measured along that line as the distance from the most inferior point of the distal aspect of the calcaneus to where it transects the superior border of the distal aspect of the calcaneus.

AP view measurements (Figures 8a and 8b)

Minimal Anterior Width of the Calcaneus (MinAWCALx-1)

Definition: The distance between the medial and lateral borders of the calcaneus, at the level of the cuboid articular facet. (If the medial border of the calcaneus is difficult to identify, the point

that is the most medial aspect of the calcaneocuboid joint may be used.) The measurement points for this variable are difficult to identify, and with $icc's\ p > 0.05$, this variable as representative of anterior width of the calcaneus was not used to test the association with MinAWCAL.

Minimal Anterior Width of the Calcaneus (MinAWCALx)

Definition: The distance between the medial and lateral borders of the calcaneus, at the level of the cuboid articular facet.

Method: Since the medial and lateral borders of the calcaneus may be difficult to identify, this measurement is taken as the distance between the most medial (and proximal) and most lateral (and distal) points of the calcaneal articular surface on the *cuboid*.

Chapter 2: Literature cited

- Agoada D. 2018. The relationship between linear osteological and radiographic measurements of the human calcaneus and talus. *Anat Rec* 301:21-33.
- Bass WM. 2005. *Human Osteology. A Laboratory and Field Manual*. Fifth edition. Columbia, Mo: Missouri Archaeological Society.
- Bidmos MA, Asala SA. 2003. Discriminant function sexing of the calcaneus of the South African Whites. *J Forensic Sci* 43:1213-1218.
- Bidmos MA, Asala SA. 2004. Sexual dimorphism of the calcaneus of South African Blacks. *J Forensic Sci* 49:446-450.
- Bidmos MA, Dayal MR. 2003. Sex determination from the talus of South African Whites by discriminant function analysis. *Am J Forensic Pathol* 24:322-328.
- Bidmos MA, Dayal MR. 2004. Further evidence to show population specificity of discriminant function equations for sex determination using the talus of South African Blacks. *J Forensic Sci* 49:1165-1170.
- Bryant JA. 2001. A comparison of radiographic foot measurements taken in two different positions. *J Am Podiatr Med Assoc* 91:234-239.
- Christman RA. 2014. Radiographic anatomy of the foot and ankle – Part 2 The greater tarsus. *J Am Podiatr Med Assoc* 104:493-503.
- Christman RA. 2015. *Foot and Ankle Radiology*. Second edition. St. Louis: Churchill Livingstone.
- Close J, Inman VT, Todd FN. 1967. The function of the subtalar joint. *Clin Orthop Relat Res* 50:159-179.
- DeSilva JM, Gill CM, Swanson Z, Bonneannee R, Gill SV. 2014. Reconstructing foot form and function in early hominins using human models. *Am J Phys Anthropol* 153:104-105.
- DeSilva JM, Holt KG, Churchill SE, Carlson KJ, Walker CS, Zipfel B, Berger LR. 2013. The lower limb and mechanics of walking in *Australopethicus sediba*. *Science* 340:1232999-1 - 1232999-5.
- DeSilva JM, Throckmorton ZJ. 2010. Lucy's flat feet: the relationship between the ankle and rearfoot arching in early hominins. *PloS one* 5(12):e14432.
- Elftman H. 1960. The transverse tarsal joint and its control. *Clin Orthop* 16: 41-45.

- Eftman H, Manter J. 1935. Chimpanzee and human feet in bipedal walking. *Am J Phys Anthropol* 7 0: 56-67.
- Gamble FO, Yale I. 1975. *Clinical Foot Roentgenology*. 2nd edition. New York: Krieger Publishing.
- Gomberg DN. 1981. *Form and Function of the Hominoid Foot* (PhD dissertation). Amherst: University of Massachusetts, Amherst.
- Grady J, Trotter KT, Ruff J, Miller SM. 2015. Radiographic investigation of the absolute and relative first metatarsal lengths in the asymptomatic foot. *J Am Podiatr Med Assoc* 105:478-483.
- Harris SM, Case DT. 2012. Sexual dimorphism in the tarsal bones: implications for sex determination. *J Forensic Sci* 57:295-305.
- Hicks JH. 1953. The mechanics of the foot I. The joints. *J Anatomy* 87:345-357.
- Hlavac HF. 1967. Differences in x-ray findings with varied positioning of the foot. *J Am Podiatr Med Assoc* 57:465-471.
- Inman VT. 1976. *The Joints of the Ankle*. Baltimore: The Williams and Wilkins Company.
- Introna F, Di Vella G, Campobasso CP, Dragone M. 1997. Sex determination by discriminant analysis of calcanei measurements. *J Forensic Sci* 42:725-728.
- Jenkins FA. 1986. Personal communication.
- Lautzenheiser SG, Kramer PA. 2013. Linear and angular measurements of the foot of modern humans: A test of Morton's foot types. *Anat Rec* 296:1526-1533.
- Lenz RC, Nagesh D, Park HK, Grady J. 2016. First metatarsal head and medial eminence widths with and without hallux valgus. *J Am Podiatr Med Assoc* 106:323-327.
- Morton DJ. 1935. *The Human Foot: Its Evolutionary Development, Physiology and Functional Disorders*. New York: Columbia University Press.
- Murphy AMC. 2002a. The calcaneus: sex assessment of prehistoric New Zealand Polynesian skeletal remains. *Forensic Sci Int* 129:205-298.
- Murphy AMC. 2002b. The talus: sex assessment of prehistoric New Zealand Polynesian skeletal remains. *Forensic Sci Int* 128:155-158.
- Olivier G. 1940. *Practical Anthropology*. Springfield, IL: Charles C Thomas Pub.

- Riepert T, Drechsler T, Schild H, Nafe B, Mattern R. 1996. Estimation of sex on the basis of radiographs of the calcaneus. *J Forensic Legal Med* 77:133-140.
- Root ML, Orien WP, Weed JH. 1977. *Normal and Abnormal Function of the Foot*. Los Angeles: Clinical Biomechanics Corporation.
- Saltzman CL, Brandser EA, Berbaum KS, DeGnore L, Holmes JR, Katcherian DA, Teasdall RD, Alexander JJ. 1994. Reliability of standard foot radiographic measurements. *Foot Ankle* 15:661-665.
- Sanicola SM, Arnold TB, Osher L. 2002. Is the radiographic appearance of the hallucal tarsometatarsal joint representative of the true anatomical structure? *J Am Podiatr Med Assoc* 92:491-498.
- Shereff MJ, DiGiovanni LD, Bejjani FJ, Hersh A, Kummer FJ. 1990. A comparison of nonweight-bearing and weight-bearing radiographs of the foot. *Foot Ankle* 10:306-311.
- Steel MW, Johnson KA, DeWitz MA, Ilstrup DM. 1980. Radiographic measurements of the normal adult foot. *Foot Ankle* 1:151-158.
- Steele DG. 1976. The estimation of sex on the basis of the talus and calcaneus. *Am J Phys Anthropol* 45:581-588.
- Susman RL. 1976. *Functional and Evolutionary Morphology of Hominoid Manual Rays II – V* (PhD Dissertation). Chicago IL: University of Chicago.
- Trinkaus E. 1975. *A Functional Analysis of the Neanderthal Foot* (PhD Dissertation). Philadelphia PA: University of Pennsylvania.
- White TD, Folkens PA. 2000. *Human Osteology*. San Diego: Academic Press.
- Wilbur AK. 1998. The utility of hand and foot bones for the determination of sex and the estimation of stature in a prehistoric population from West-Central Illinois. *Int J Osteoarchaeol* 8:180-191.
- Wood-Jones F. 1944. *Structure and Function as seen in the Foot*. Baltimore: Williams and Wilkins.

Chapter 2: List of Tables

Table 1. Measurements and descriptive statistics of bone and radiographic measurements for the talus (* different measuring points for bone only; see Appendix. n = 54, degrees of freedom = 53 for all values.)

Table 2. Measurements and descriptive statistics of bone and radiographic measurements for the calcaneus (**different measuring points for both bone and radiograph; see Appendix). n = 54, degrees of freedom = 53 for all values.

Note: The regression coefficient (b) indicates the ratio of radiographic measurement to the bony measurement, i.e., the degree of change associated with measuring on the radiograph.

Description	Variable	Bone			Radiologic (x)			t-test Analysis		Linear Regression Analysis	
		Mean	SEM	SD	Mean	SEM	SD	t	p	b	r ²
Maximum Length	MaxLTAL	60.10	0.713	5.24	62.45	0.803	5.90	-8.533	<0.05	0.999	0.88
Maximum Body Height	MaxHBTAL	32.91	0.370	2.72	33.16	0.449	3.30	-0.888	0.38	0.996	0.62
Body Height*	BHTALa	33.05	0.404	2.97	33.81	0.444	3.26	-4.303	<0.05	0.997	0.84
Body Height*	BHTALb	33.53	0.434	3.19	33.81	0.444	3.26	-1.314	0.19	0.998	0.78
Maximum Length Fibular Malleolar Facet	MaxLFMTAL	32.40	0.391	2.87	32.83	0.384	2.82	-1.721	0.09	0.997	0.61
Maximum Width Talar Head	MaxWHTAL	31.60	0.397	2.92	31.92	0.447	3.51	-0.696	0.49	0.989	0.20
Minimal Width Talar Neck*	MinWNTALa	27.43	0.352	2.56	27.75	0.449	3.30	-0.875	0.39	0.991	0.36
Minimal Width Talar Neck*	MinWNTALb	27.32	0.369	2.72	27.75	0.449	3.30	-1.268	0.21	0.992	0.45
Maximum Length Talar Head and Neck	MaxLHNTAL	25.22	0.415	3.05	24.54	0.464	3.41	2.426	0.02	0.993	0.63

Table 1. Descriptive statistics and analysis of bone and radiographic measurements for the talus (*different measuring points for bone only; see Appendix) (n = 54, degrees of freedom = 53 for all values).

Note: The regression coefficient (b) indicates the ratio of radiographic measurement to the bony measurement, i.e., the degree of change associated with measuring on the radiograph.

Description	Variable	Bone			Radiologic (x)			t-test analysis		Linear Regression Analysis	
		Mean	SEM	SD	Mean	SEM	SD	t	p	b	r ²
Maximum Length**	MLCAL	83.87	0.893	6.56	86.75	0.915	6.72	-9.965	<0.05	0.967	0.90
Maximum Length**	MLCAL-2	82.15	0.917	6.74	83.32	0.918	6.74	-4.113	<0.05	0.986	0.90
Body Height	BHCAL	49.75	0.587	4.31	50.50	0.773	5.68	-1.784	0.08	0.981	0.71
Minimum Body Height	MinBHCAL	39.24	0.497	3.65	38.98	0.520	3.82	1.119	0.26	1.005	0.80
Minimum Anterior Height	MinAHCAL	25.07	0.289	2.12	23.08	0.301	2.21	-0.044	0.96	0.997	0.54
Minimum Anterior Width	MinAWCAL	22.83	0.272	2.00	23.01	0.285	2.09	-0.642	0.52	0.998	0.26

Table 2. Descriptive statistics and analysis of bone and radiographic measurements for the calcaneus (** different measuring points for both bone and radiograph; see Appendix) (n= 54, degrees of freedom = 53 for all values).

Note: The regression coefficient (b) indicates the ratio of radiographic measurement to the bony measurement, i.e., the degree of change associated with measuring on the radiograph.

Chapter 2: List of Figures

- Figure 1. Lateral view of the left talus (flipped horizontally).
- Figure 2a. Lateral radiograph of the left foot.
- Figure 2b. Lateral radiograph view measurements of the left talus.
- Figure 3a. Dorsal view of the left talus.
- Figure 3b. Plantar view of the left talus (flipped horizontally).
- Figure 4a. AP radiograph view of the left foot.
- Figure 4b. AP radiograph view measurements of the left talus.
- Figure 5. Lateral view of the right calcaneus (flipped horizontally).
- Figure 6a. Lateral radiograph of the right foot.
- Figure 6b. Lateral radiograph view measurements of the right calcaneus.
- Figure 7a. Plantar view right calcaneus (flipped).
- Figure 7b. Dorsal view right calcaneus.
- Figure 8a. AP radiograph view right foot.
- Figure 8b. AP radiograph view measurements of the right calcaneus.
- Figure 9a. Transverse plane relationships (MinWNTALa and MinWNTALb) of the talus.
- Figure 9b. Sagittal plane relationships (MaxLTAL and Max HBTAL) of the talus.
- Figure 10a. Transverse plane relationship (MinAWCAL) of the calcaneus.
- Figure 10b. Sagittal plane relationships (MLCAL and MinAHCAL) of the calcaneus.

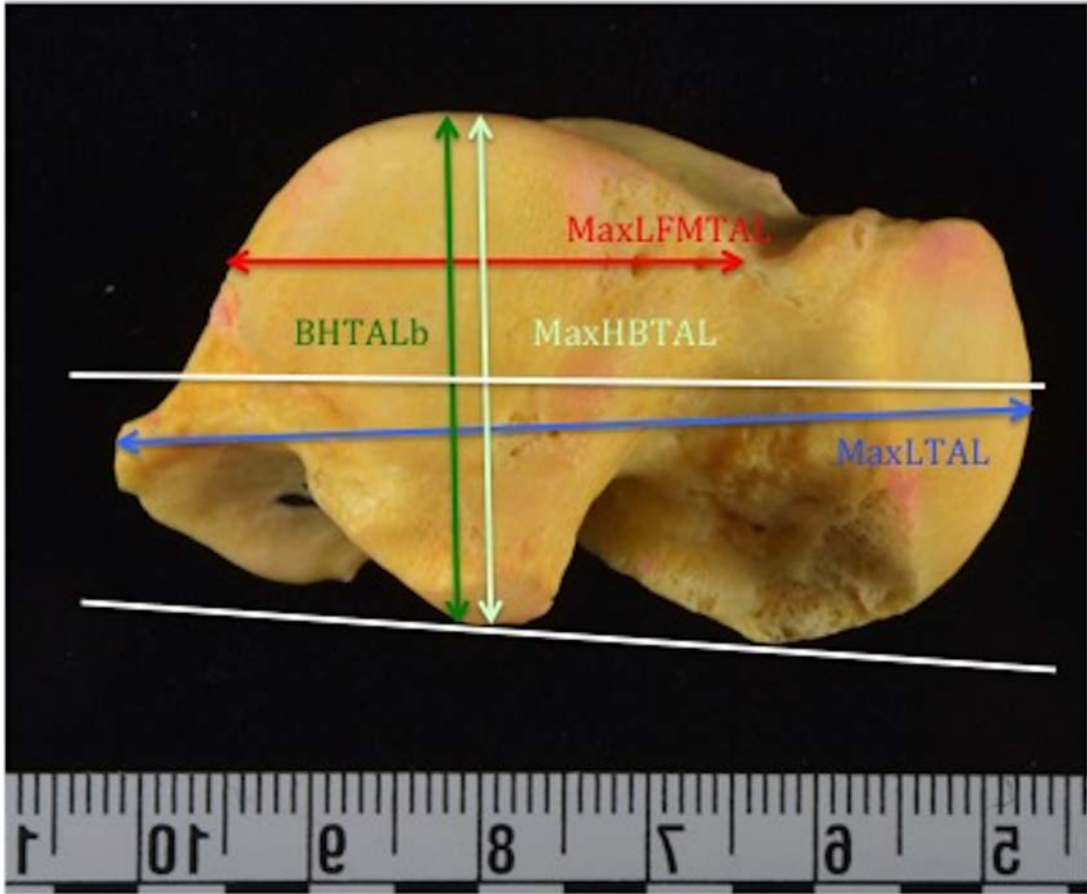


Figure 1. Lateral view of the left talus (flipped horizontally).



Figure 2a. Lateral radiograph of the left foot.

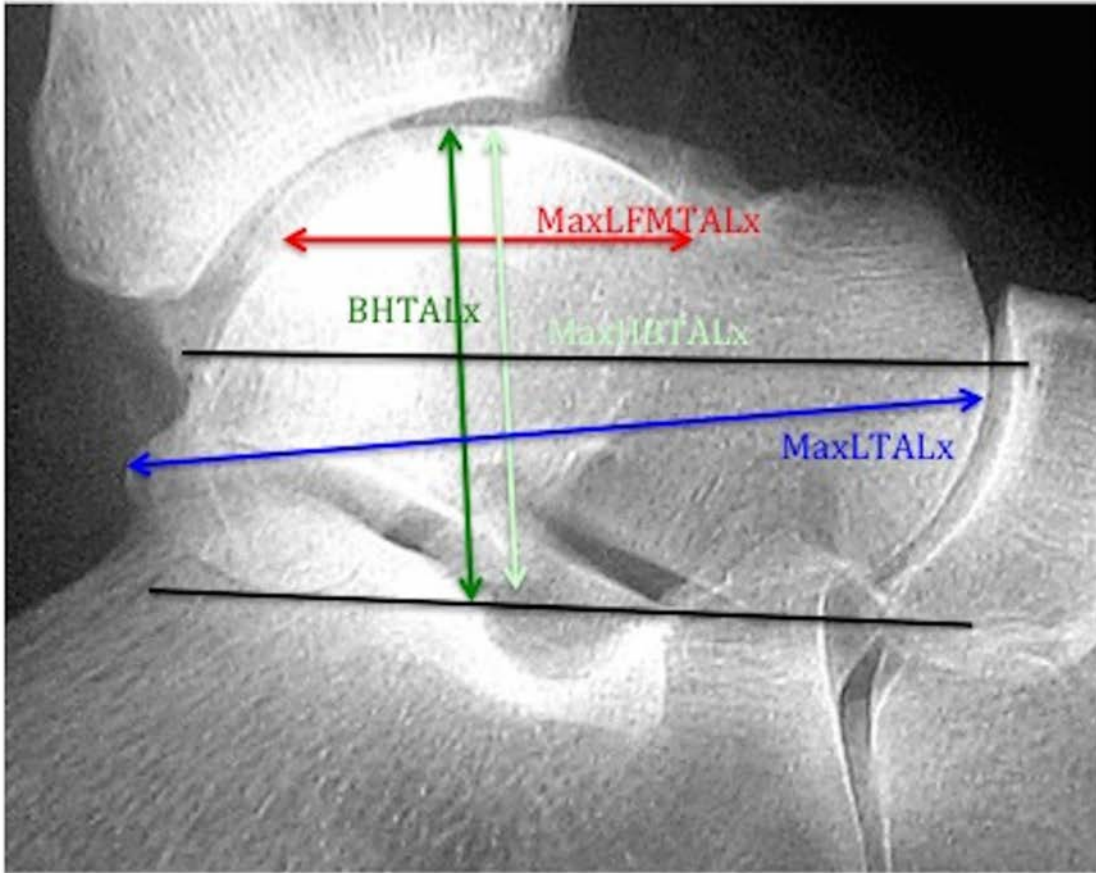


Figure 2b. Lateral radiograph measurements of the left talus.

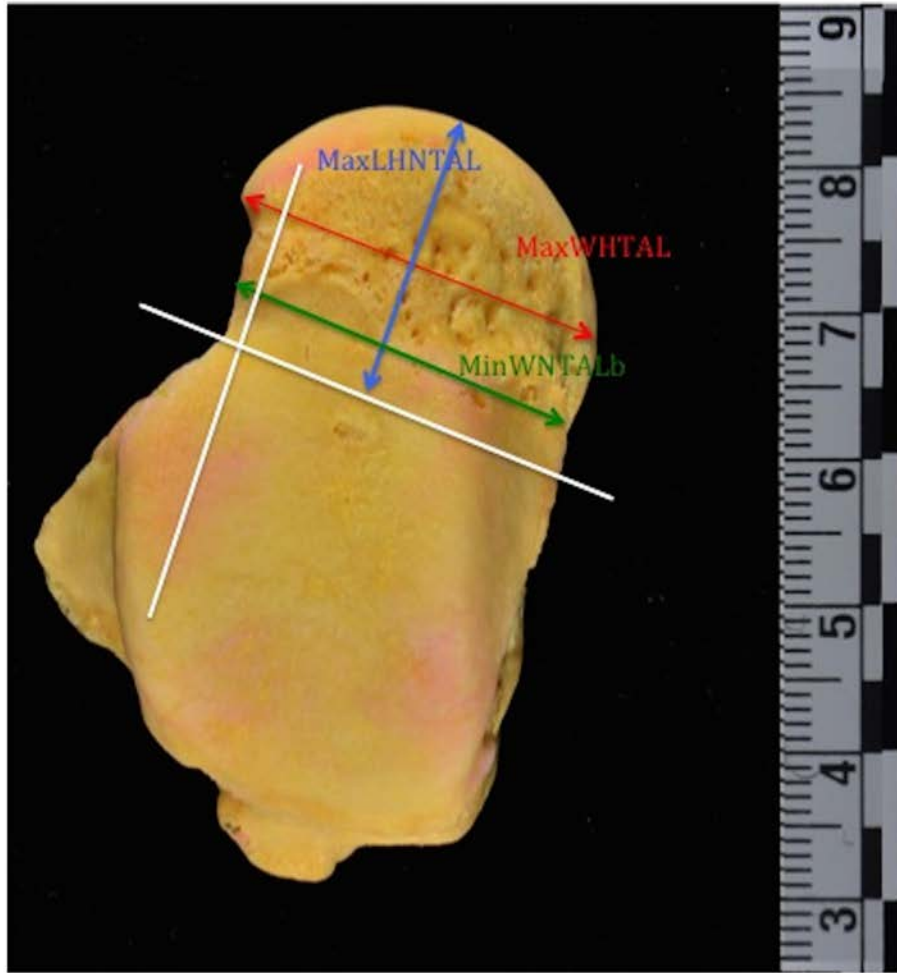


Figure 3a. Dorsal view of the left talus.

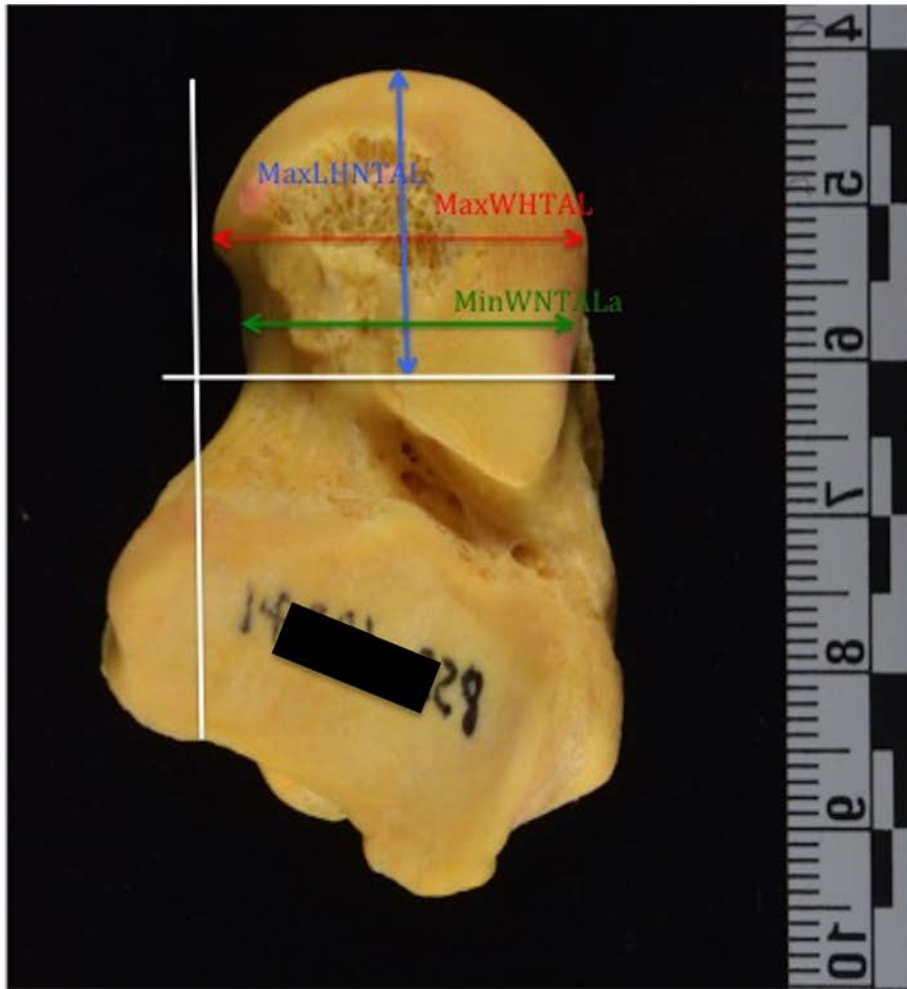


Figure 3b. Plantar view of the left talus (flipped horizontally).



Figure 4a. AP radiograph of the left foot.

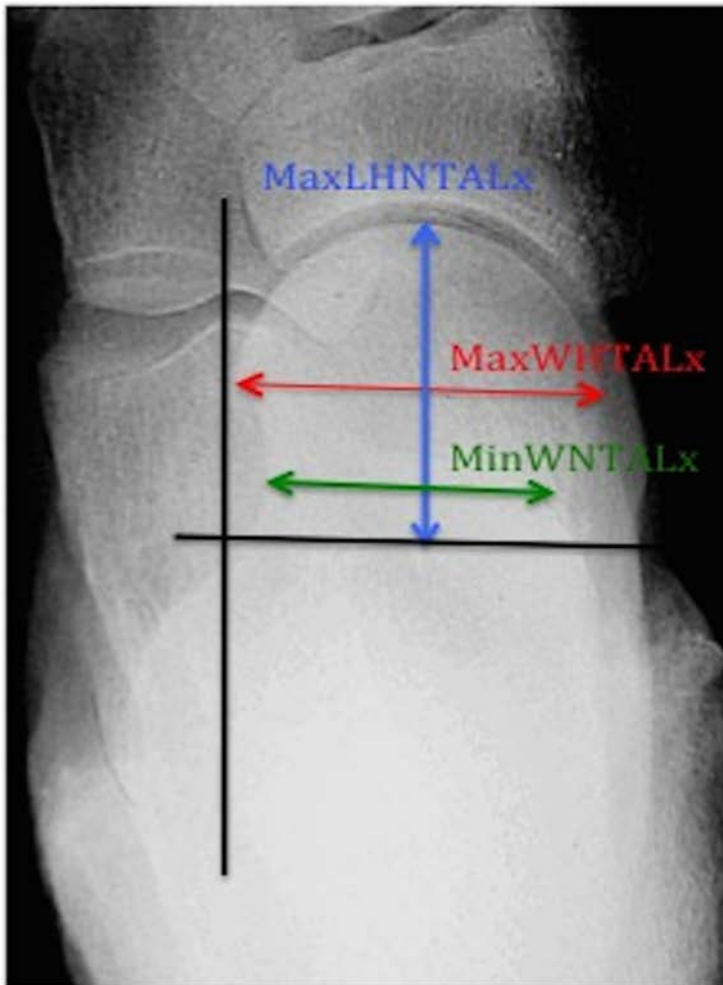


Figure 4b. AP radiograph measurements of the left talus.

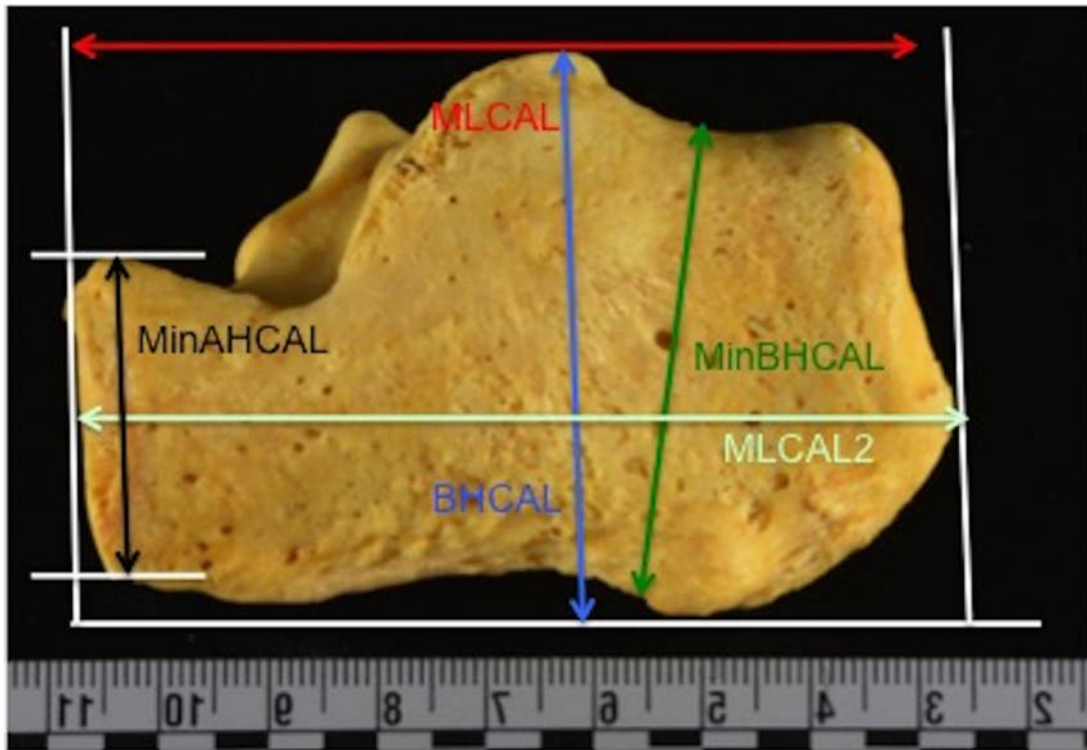


Figure 5. Lateral view of the right calcaneus (flipped horizontally).

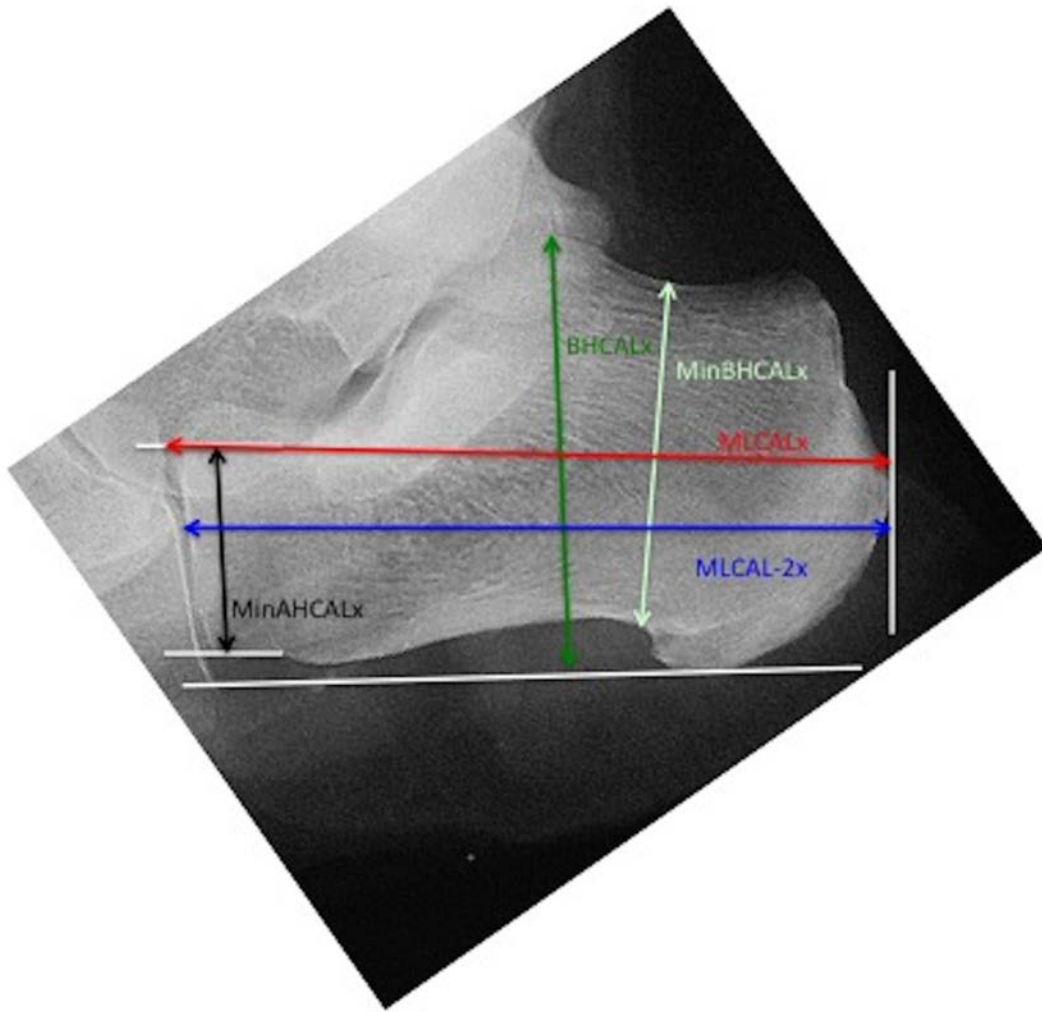


Figure 6b. Lateral radiograph measurements of the right calcaneus.

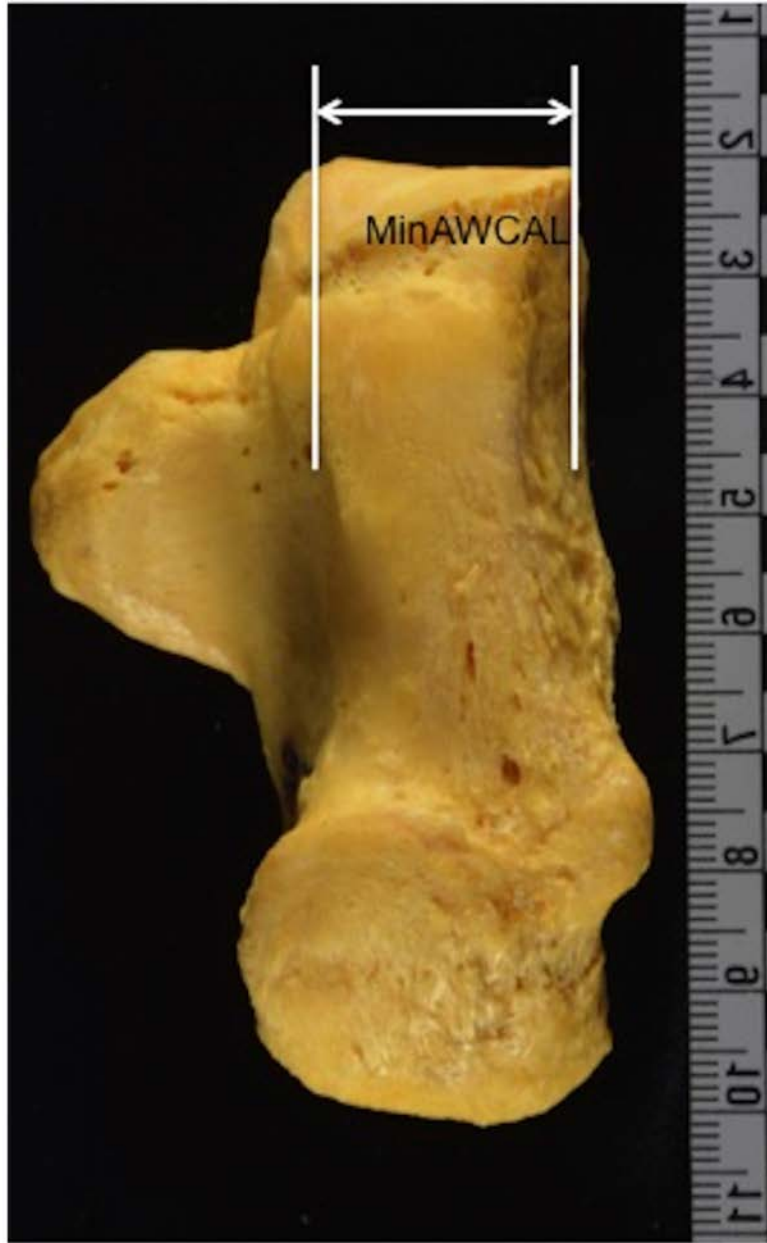


Figure 7a. Plantar view of the right calcaneus (flipped).

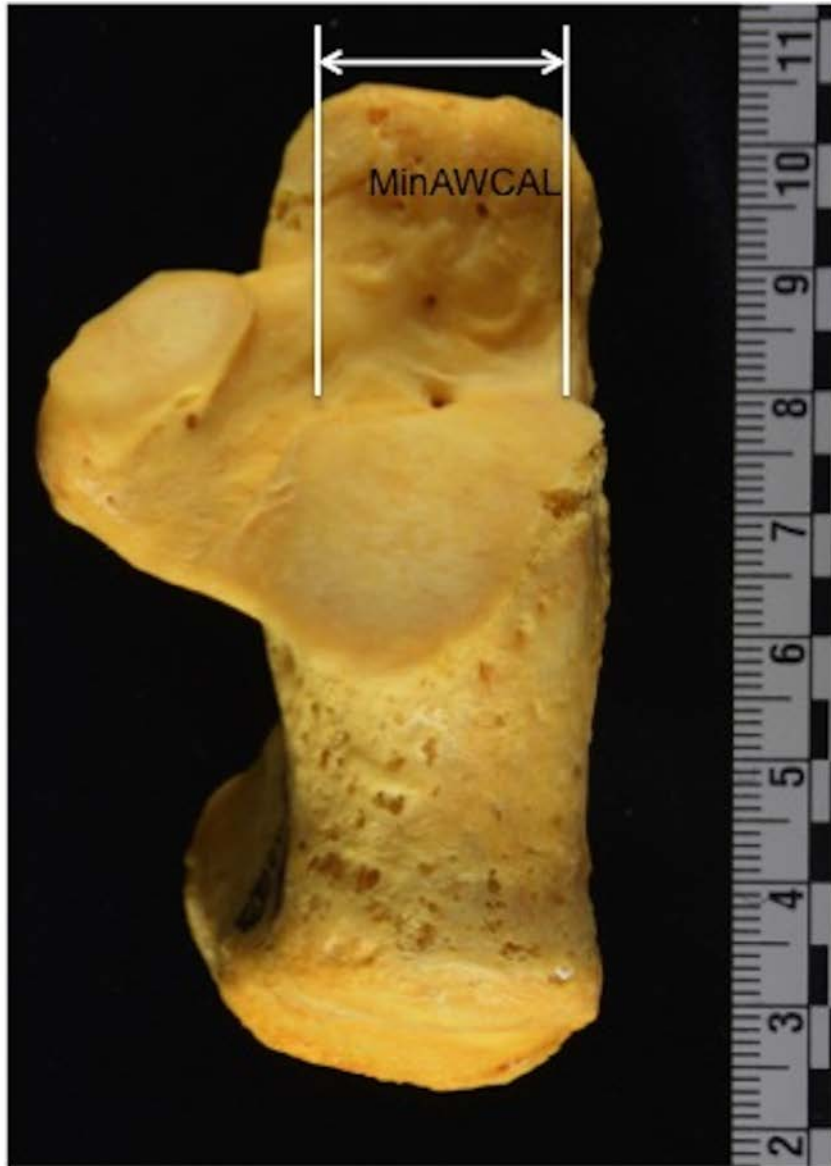


Figure 7b. Dorsal view of the right calcaneus.



Figure 8a. AP radiograph view of the right foot.



Figure 8b. AP radiograph measurements of the right calcaneus.

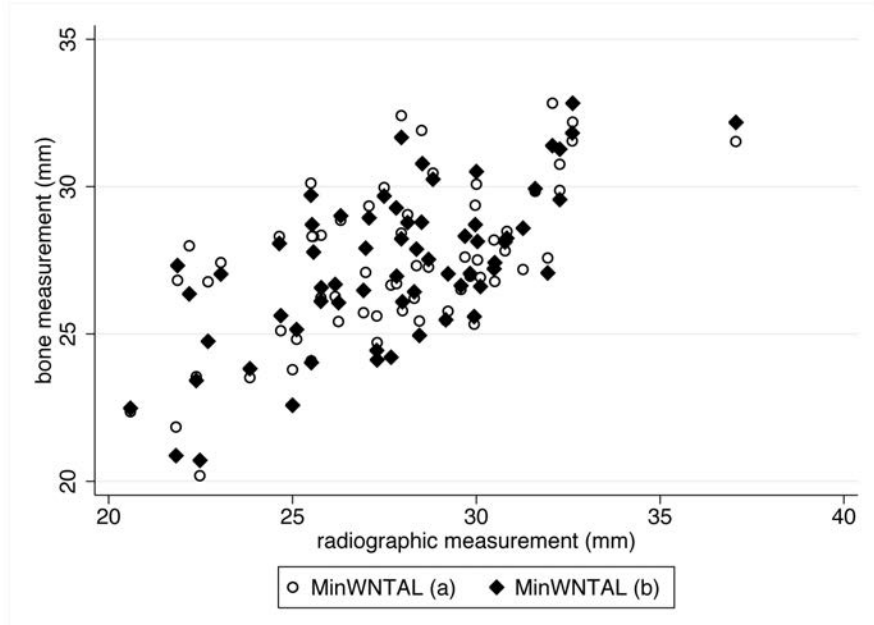


Figure 9a. Transverse plane relationships (MinWNTALa and MinWNTALb) talus.

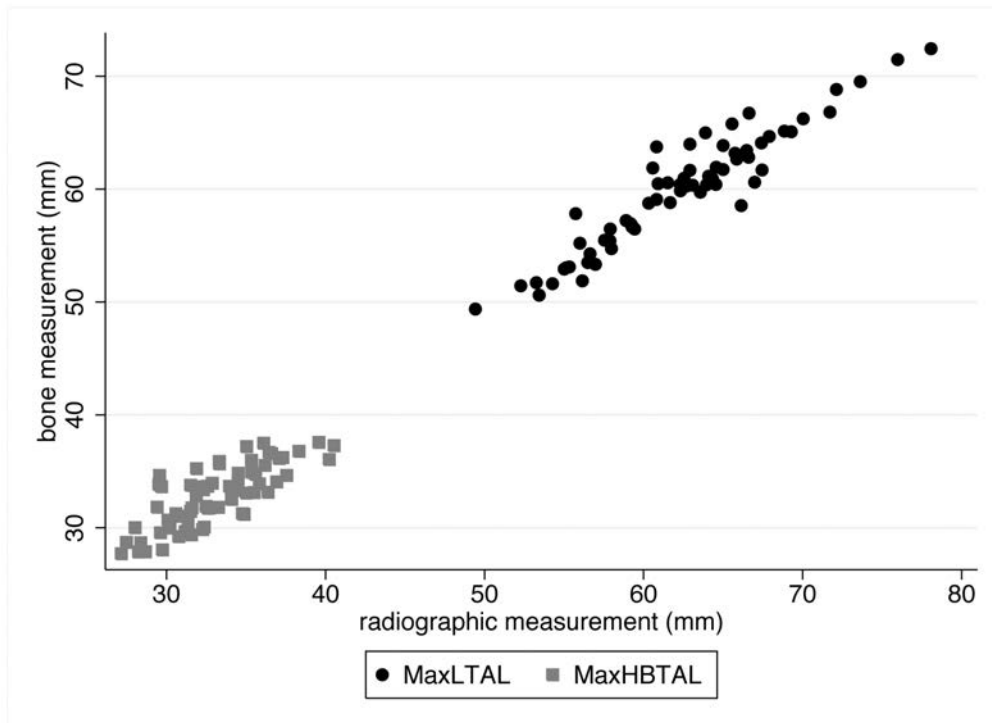


Figure 9b. Sagittal plane relationships (MaxLTAL and MaxHBTAL) of the talus.

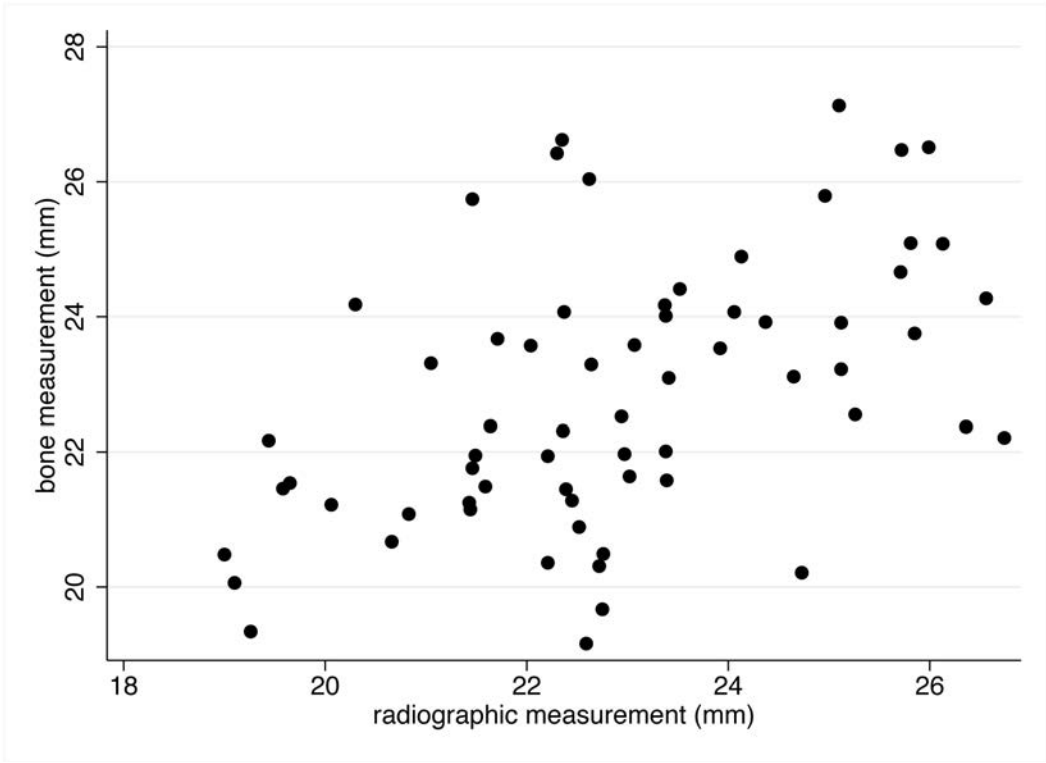


Figure 10a. Transverse plane relationship (MinAWCAL) of the calcaneus.

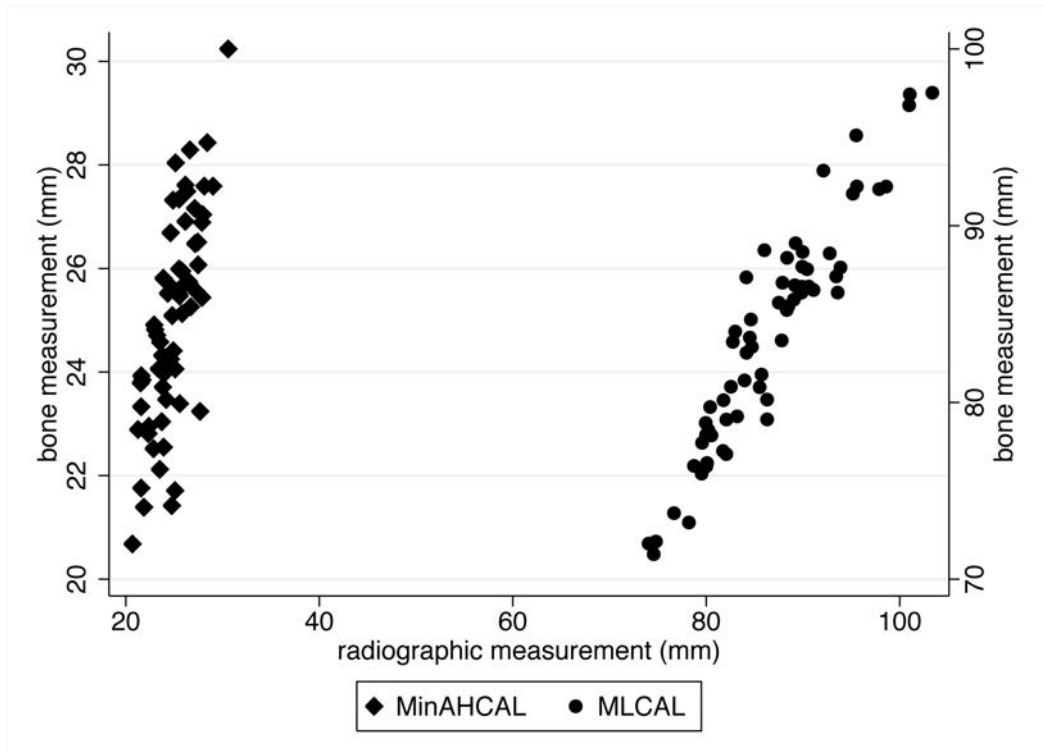


Figure 10b. Sagittal plane relationships (MLCAL and MinAHCAL) of the calcaneus.

Chapter 3. The relationship between angular osteological and radiographic measurements of the human talus and calcaneus

Preface

The manuscript for this chapter, coauthored with Patricia A. Kramer, was submitted to *The Journal of the American Podiatric Medical Association* for publication consideration on November 8, 2017 (revised May 13, 2018). It is currently under review. Changes were made to the manuscript since submission where appropriate for context or consistency in chapter presentation. Additional information concerning the materials and methods used in this study can be found in Appendix B. Appendix C has tables with the measurements used for statistical analysis. More detailed information concerning the statistical analyses can be found in Appendix D.

Abstract

Radiographic imaging of the foot is commonly performed on individuals when medical evaluation is indicated. Angular measurements between bones may be assessed as part of the examination for trauma and foot biomechanics. However, angular relationships between surfaces of the physical bone as they compare to the bone's radiographic image has had limited investigation. For this study, fifty-four human feet from amputated limbs were imaged in standard radiographic views and skeletonized. Selected angular measurements were taken on each skeletonized talus and calcaneus and compared to those taken from radiographic images, employing paired Student's *t*-tests and linear regression analysis. Transverse plane

measurements of the talus were not significantly different ($p \geq 0.05$), associating strongly ($r^2 = 0.67 - 0.75$, all $p < 0.001$). Most transverse and sagittal plane measurements of the calcaneus were not significantly different ($p \geq 0.05$), with transverse plane measurements more strongly associated ($r^2 = 0.70 - 0.77$, all $p < 0.001$) than sagittal plane measurements ($r^2 = 0.35 - 0.78$, all $p < 0.001$). The results indicate that selected angular measurements of the talus and calcaneus taken from radiographic images can be compared quantitatively to the physical bone, demonstrating that angular measurements from radiographic images provide useful information concerning both of these bones. This knowledge can be applied to the understanding of the morphology of the calcaneus and talus as it relates to foot biomechanics when diagnosing problems and formulating treatment plans for foot dysfunction. The results of this study indicate that radiographs of living individuals can be evaluated quantitatively and combined with osteology collections of modern humans, useful in studies where large sample size is crucial. In addition to the understanding of the functional anatomy of the modern human foot, the information derived from this study can also be applied to interpreting the human fossil pedal record.

Key words; talus; calcaneus; radiograph; angular measurements; biomechanics

Introduction

Radiography of the foot has an essential role in the assessment of foot and ankle disorders. Plain radiographs of the foot provide accurate information on the morphology of the individual bones as well as angular relationships between bones (1). They are a medically approved form of non-invasive examination in individuals where trauma has occurred or is

suspected, where surgical treatment is planned, or where bone appearance, arthritic changes, or joint relationships need to be evaluated to arrive at a diagnosis of a condition and to formulate a treatment plan.

Since plain radiographs of the foot are used for medical evaluation of the skeletal structures of the foot, it is important that the radiographic image accurately reflect the morphology of the physical bone. In addition, because plain radiographs are commonly performed, their availability makes them useful for studying human variation where large sample sizes are necessary for statistical analysis.

Standard images from plain radiographs of the foot in an initial radiographic evaluation usually include the dorsoplantar (DP) (or anterior-posterior) view to assess structures from the transverse plane of the foot, and the lateral (or lateromedial) view to assess structures from the sagittal plane (1). While other projections, such as medial and lateral oblique, and dorsoplantar axial, may be ordered depending upon the medical concern to be evaluated, only the DP and lateral projections produce images with the least amount of distortion that should most closely correlate with the size and shape of the physical bone. Thus, bone images of the foot are best assessed in the DP and lateral views (1).

Computer tomography (CT) and magnetic resonance imaging (MRI) do provide more information about bony structure than plain radiographs. However, CT requires multiple x-ray projections, exposing the patient to a higher dosage of radiation than plain radiographs. As a result, CT scans are not usually ordered unless absolutely necessary, and only when other forms of evaluation, such as plain radiographs or MRI scans would not provide enough information. In addition, because CT and MRI scans are expensive tests that usually require special approval

by insurance providers, they are ordered less often. Plain radiographs of the foot thus provide an important and cost-effective source for evaluation of the skeletal elements of the foot, both at the patient and population levels.

The talus and calcaneus are recognized as important elements in the structure, function, and integrity of the human foot. Their role in foot function and pathology has been investigated in experimental and clinical settings (2-10). The range of variation in size and shape of these tarsal elements in modern humans is well known and has been employed to analyze skeletal remains of both modern and ancient osteological collections (11-16)). However there has been little definitive research relating this size and shape variation to foot biomechanics and functional pathology.

There have been several studies reporting angular measurements for the distal tibia, talus and calcaneus taken from the individual bone in the literature (17-28). Measuring the angles of the talus or calcaneus directly from the physical bone is a difficult process. Different measurement techniques have been proposed (see Day and Wood (18); Gomberg (23); Trinkaus (28) for example). However, using modern software programs, taking measurements from photographs of the bone when properly performed, has been shown to be a relatively simple and acceptable method in the determination of angular values for these bones (19-22).

Studies looking at the morphology of the talus and calcaneus in terms of their role in foot biomechanics have, by necessity, relied to a large extent on analyzing radiographic images of the intact foot. There have been very few studies demonstrating the accuracy with which the radiographic images of these bones reflect the morphology of the physical bone. Harris and Beath (4) hypothesized on the role of the talus and calcaneus in the formation of the

hypermobile flatfoot using disarticulated bones and their radiographic images but did not evaluate these findings as they relate to an intact foot and did not do any measurements. Bruckner (17) studied angles of the calcaneus and subtalar joint morphology using disarticulated bones but did not compare the physical bone to images taken from standard radiographic views of the foot. Sarrafian and Kelikian (24) cite several sources for angular measurements of the talus and calcaneus on the physical bone only, some of which would not be possible to reproduce from a radiographic image. Christman (29) described the radiographic appearance of the talus and calcaneus using the physical bones but did not take any measurements.

While standard radiographs of the foot have been used to provide information concerning angular relationships of the talus and calcaneus to each, other bones of the foot, and the plain of support, there have been no studies comparing angular measurements of the individual bone taken from radiographs in the intact foot with that of the physical bone. Angular relationships formed by the surfaces of a bone may provide information on its role in the form and function of the foot, but the accuracy of these measurements taken from radiographic images when compared to the physical bone must first be demonstrated.

Angular measurements of the calcaneus taken from radiographs have been used to assess the foot for calcaneal trauma and pathology (30-34); however, these measurements have not been compared to, or correlated with, measurement values taken of the physical bone. Didia and Dimkpa (35) studied Böehler's angle (which they called the calcaneal angle) in Nigerians using lateral radiographs. They found that Böehler's angle in Nigerians was not significantly related to sex, age, or body side. While they postulated that proper alignment of

the calcaneus is essential for the maintenance of the arches of the foot and bipedal locomotion, they did not discuss any relationship between Böehler's angle and foot biomechanics as demonstrated by the radiographs they examined.

A close association between the measurements of the talus and calcaneus taken from the radiographic images with those from the physical individual bones would help in the interpretation of the radiographic images of the talus and calcaneus when evaluating the appearance of the bone in terms of morphology, pathology, and trauma. Demonstrating a close relationship in angular measurements between the bone and its radiographic image in would be useful in clinical medicine in such areas as biomechanical analysis, the diagnosis of pathological conditions, and the planning of surgical procedures. Such parameters as bone size and shape could be compared statistically within, and between, human population samples. Standardized foot radiographs of the modern human foot could be used, and integrated with established osteological collections, to evaluate quantitatively the variability of these angular measurements of the human talus and calcaneus, providing information that can be applied to the functional morphology of these bones. Biomechanical and functional analysis of living individuals could then be combined with the quantitative information concerning the talus and calcaneus obtained from weight-bearing radiographs. These analyses would also provide invaluable information for the assessment of foot form and function in the ancestral hominins, an area where the functional meaning of similarities, and dissimilarities between fossil hominin feet and modern human feet are not completely understood (36).

The goal of this study is to test the hypothesis that angular measurements of the talus and calcaneus taken from standard radiographs are closely related. A close relationship in measurements between the bone and its radiographic image would demonstrate that both bone and image could be used in the same manner when studying aspects of bone morphology for statistical analysis. The null hypothesis is that there are no significant differences in selected angular measurements of the talus and calcaneus with corresponding measurements taken from the standardized radiograph images of these bones.

Materials and Methods

The specimens for this study were collected between 1986 and 1988 from lower extremity amputations performed at the (then) New England Deaconess Hospital (NEDH) in Boston, MA. The material and associated patient information were collected with the written approval of the NEDH Institutional Review Board on Human Studies. The specimens were from individuals who underwent below or above knee amputations for infection or acute ischemia. Information concerning their age, ancestry, sex, stature, and medical condition was collected. The individuals ranged in age between 35 and 89 years of age at the time of the amputation. Each amputated lower limb was sectioned above the ankle and AP and lateral x-rays taken in the standardized fashion for the non-weight-bearing foot. The foot was then skeletonized. Processing of each limb took place shortly after a pathologist's evaluation and release of the specimen.

The lower tibia and fibula, talus, calcaneus, navicular, cuboid, medial, intermediate, and lateral cuneiforms, all five metatarsals, and the proximal and distal phalanges of the hallux were

retained. The talus and calcaneus were examined for this study. Any bone that had evidence of previous trauma, pronounced abnormal features, or severe arthritic changes that resulted in deformity of that bone, was not used. Individual bones with spurring and mild arthritic changes were included as long as the landmarks were not damaged or obscured, and the arthritic changes did not interfere with the determination of the measuring points or the taking of the defined angular measurements. Any spurs with projections at a 90° angle from the bony surface were not included in the measurements.

A total of 32 feet from male individuals and 22 feet from female individuals were collected. Five angular osteological measurements for the talus and eleven for the calcaneus, along with their corresponding radiographic measurements, were chosen. Measurement definitions and techniques were developed. Based on the bony landmarks identified, corresponding measuring points and measurement techniques for the radiographic image were determined. The definition for each angular measurement is given in the Appendix and illustrated in Figures 1-8. An “x” at the end of the variable name denotes the radiograph version of the measurement.

The bone to be photographed was placed in a tray filled with black art sand to support the bone in the proper relationship to the camera’s lens as described by Christman [55]. The medial, lateral, superior, and inferior sides of each bone were photographed using a Nikon D5200 digital camera and an AF-S DX Nikkor 18-140mm f/3.5-5.6G ED VR lens. The bone was positioned so that the surface being photographed was perpendicular to the camera lens to minimize distortion. A scale was placed in the same plane as the side being photographed to minimize magnification of the image’s measurements. To improve visual identification of the

measuring points, Nikon ViewNX-i software program was used to brighten and sharpen the image. Images were also cropped to center the bone on the photograph. When necessary, to match the radiographic image, the photograph was flipped horizontally. Measurements of the physical bone were taken from the photographic images as described by DeSilva (20). Digital images were imported into the program Image J (NIH) (<http://imagej.nih.gov/ij/>), and the angle created by the designated measuring points was measured with the angle tool to the nearest 0.01 degree.

DP and lateral view radiographs of each foot were taken following the standard protocol as described for patients undergoing a non-weight-bearing clinical examination (1) (Figures 1a and 1b). Each film radiograph was scanned with a reference scale and digitized. Bony landmarks were identified on the scanned radiographs. Scanned radiographs were imported into ImageJ, calibrated using the reference scale, and measured using the angle tool as described above.

Three months after the original measurements were taken, eleven tali and calcanei, and their associated radiographs, were randomly selected to assess repeatability. Intraclass correlation coefficients (ICC) between initial and second set of measurements were calculated. The average difference between the two measures for the talus was $\pm 1.9^\circ$ and for the calcaneus $\pm 1.6^\circ$. The average ICC ranged from $r = 0.86$ to 0.99 for the talus ($p < 0.001$ for all but AnTAL and AnTALpl variables, which were $p < 0.01$) and $r = 0.92$ to 0.99 ($p < 0.001$) for the calcaneus. Similar results assessing reliability have been reported in other radiological studies of foot morphology (37).

Descriptive statistics were calculated on the measurements taken from the actual bones and their radiographic images. Student *t*-test comparing physical bone and radiographic measurements were performed to identify the presence of significant differences in measurement dimensions between bone and radiograph. The degree to which measurements are associated was established using ordinary least squares regression and confirmed with reduced major axis analysis. Regression coefficient (*b*) and coefficient of determination (r^2) values were examined to assess the relationship between measurements. Statistical significance was established using an alpha of 95%. Bonferroni correction for multiple comparisons, which yielded $p < 0.001$, was applied to establish the significance of all pairwise tests. Descriptive statistics and other analyses were computed using Stata (V12, Statacorp, College Station, TX).

In making comparisons between a physical bone and its radiographic image, it should be noted that, while the sagittal and transverse planes are the only planes visualized on these two-dimensional radiographic images all three anatomic planes need to be considered. For example, using standard plain radiographs, the frontal-plane position of a bone cannot be directly evaluated, thus assessments of the talus and calcaneus require logical analysis and reasoning while looking at both the DP and lateral views (29).

Results

Talus

Table 1. Descriptive statistics and analysis of bone and radiographic angular measurements for the talus.

The angle of the head of the talus (measured both dorsally (AHTAL) and plantarly (AHTALpl)) and the angle of the neck of the talus (measured both dorsally (ANTAL) and plantarly (ANTALpl)) are not significantly different from those measured on the radiograph (ANTALx) (i.e., $p \geq 0.05$). These talar skeletal measurements are associated with the radiographic measurements ($r^2 = 0.67 - 0.75$). However, measurements taken of the inclination angle of the neck of the talus (IANTAL) from the sagittal plane were significantly different ($p < 0.05$) from the radiograph measurement (IANTALx) and did not associated as well ($r^2 = 0.46$, $p < 0.001$) as those of the transverse plane. From the results, it would appear that variables measured from either the dorsal or plantar aspects of the physical bone are more closely associated with measurements from the AP radiograph than measurements from either the medial or lateral aspect of the bone are with that taken from the lateral radiograph.

Calcaneus

Table 2. Descriptive statistics and analysis of bone and radiographic angular measurements for the calcaneus.

The anterior angle of the calcaneus measured from both the dorsal (AAAPCALa) and plantar (AAAPCALb) surfaces are not significantly different from those taken from the radiograph (AAAPCALx) ($p \geq 0.05$). These calcaneal skeletal measurements also are strongly associated with the radiographic measurement ($r^2 = 0.70 - 0.77$). Measurements of the

calcaneus taken from the sagittal plane gave more variable results. The angle of inclination of the posterior talar facet (AIPFCAL), the angle of inclination of the middle talar facet (AIMFCAL), and the anterior angle of the calcaneus in the lateral view (AALCAL) were not significantly different from their associated radiographic measurements ($p \geq 0.05$) and strongly associated ($r^2 = 0.64 - 0.73, p < 0.001$). Two other sagittal plane measurements (BTACAL, CACAL) were significantly different from those from the radiograph ($p < 0.05$) but strongly associated ($r^2 = 0.69-0.78, p < 0.001$). The other measurements of the calcaneus in the sagittal plane (GACAL, FACAL, TAPCAL, TADCAL) while not significantly different ($p \geq 0.05$) were not as strongly associated, ranging from $r^2 = 0.35$, to $r^2 = 0.49$ ($p < 0.001$).

Discussion

The angular relationships of the bones of the human foot to each other from radiographic images have been extensively studied in the medical literature, as these angular variations are associated with foot biomechanics and pathomechanics. However, the angles formed by the bony surfaces *that make up* a bone as represented on the radiographic image have been minimally studied, limited mainly to the assessment of trauma to the body of the calcaneus (32-33); or non-traumatic pathology of the calcaneal tuberosity (34). Prior to this study, the relationship between what is seen on the radiographic image of the intact foot and what can be measured on the physical bone for the talus and calcaneus has had little attention.

In this study, the accuracy of angular measurements of the talus and calcaneus taken from radiographs has been examined by comparing those values with measurements of the

physical bone. As demonstrated, while some of the measurements of the talus and calcaneus are significantly different, most are strongly associated with the radiographic measurements.

The angle of the head of the talus and the angle of the neck of the talus measured on the dorsal surface were not significantly different from those measured on the radiograph AP view. These talar skeletal measurements were strongly associated with the radiographic measurements. However, the inclination angle of the neck of the talus (IANTAL) measurement taken for the lateral surface was one of the few measurements that was significantly different and had a smaller coefficient of determination value when compared to the other r^2 values (Figure 10). An attempt was made to develop a variable that would improve the accuracy of this sagittal plane measurement of the talus by measuring the talar inclination angle from the medial surface of the bone (IANTALa) (Figure 4b). These measurement comparisons with IANTALx were also significantly different and resulted in even lower r^2 values. This lack of agreement between the physical bone and radiographic image in inclination angle of the neck could be due to a number of factors. Both the axis of the body and axis of the neck are estimations based on landmarks and surfaces that may be difficult to identify on the radiographic image. The angular measurement taken from the radiograph may be especially sensitive to the position of the talus in relation to the x-ray beam and image receptor. The results suggest that this angular measurement taken from the radiograph should only be used with caution when determining the degree of talar neck plantarflexion, since this radiographic measurement may not accurately represent the physical bone morphology. Determining the talar declination and lateral talocalcaneal angles are important in assessing the degree of subtalar joint pronation when using radiographs in performing a biomechanical analysis (38).

The anterior angle measurements of the calcaneus taken from the transverse plane (AAAPCALa and AAAPCALx) (Figures 1a and 6.) were not significantly different and appeared to be closely associated (Figure 11). This was surprising, due to the difficulty in determining the longitudinal axis of the calcaneus from radiographs where the posterior surface is obscured, necessitating the use of the lateral border to determine this axis (1). This would seem to indicate that the lateral border is an appropriate proxy of the calcaneal longitudinal axis.

Most angular measurements taken from the radiographic lateral view of the calcaneus were not significantly different and were closely associated with those taken from the bone. Böehler's angle (BTACAL) (Figure 12) and compression angle of the calcaneus (CACAL), both used to assess for the presence of calcaneal fracture, and thus morphology, were significantly different; however measurements of both angles taken from bone were closely associated with those from the radiographic image, suggesting that these may be useful angles in determining the presence of a compression fracture, though the actual degrees of deformity of the physical bone may need to be adjusted by the appropriate coefficient.

As noted, Böehler's angle measured from a radiographic image is one of the few foot bone angles that have been widely investigated by other researchers. In the study presented here, the Böehler's angle average was 28.52° (range 15.45°-37.22°) for bone and 30.55° (range 17.56°-38.92°) for the radiograph. Lautzenheiser and Kramer (37) studied Böehler's angle in weight-bearing radiographs and found an average value of 32.82° for women and 34.07° men (with a population range 18.65° to 44.90°). Khoshhal et al. (33) found the average Böehler's angle in a Saudi population was 31.21° (range 16°-47°). Didia and Dimkpa (35) reported an

average of 32.8° (range 28° to 38°) in a Nigerian population. They also looked at the range of variation for Böhler's angle, reviewing the literature prior to their 1999 study. They noted that Böhler's angle had never been reported to be less than 15° or more than 40°. The average radiographic value for this study was only slightly less than that reported in the literature. However, as demonstrated in this study, and other more recent investigations, the maximum range of 40° is exceeded in several populations.

Gissane's angle (GACAL), also used to assess for a calcaneal fracture from a lateral radiograph, as well as the frontal angle of the calcaneus (FACAL) did not display significant differences between measurements taken from bone and radiographic image; however, both did not appear to be as closely associated with the measurement taken from their radiographic image ($r^2 = 0.35$ and 0.39 respectively) as did the BTACAL/BTACALx measurements. This suggests that the GACAL (Figure 13) and FACAL measurements may not be as useful as the BTACALx measurements in evaluating the bone morphology of the calcaneus using radiographic images and thus may not always reflect the actual damage to the physical bone accurately.

The tuber angle of the plantar calcaneus (TAPCAL) and tuber angle of the distal calcaneus (TADCAL) were also not significantly different from their radiographic counterparts. They were not as closely associated as were other calcaneal angles from the sagittal plane (AIPTFCAL, AIMTFCAL, and AALCAL). However, their r^2 values (0.47 - 0.49) showed a closer association between bone and radiograph measurement than either the GACAL or FACAL ($r^2 = 0.35$ - 0.39), indicating that these tuber angle variables may be more useful angles in quantitatively describing physical bone morphology, but still need to be used with some degree of caution. Of note is that all the angles that produced lower coefficient of determination

values were based in part on measuring points that did not have a parallel surface available to assist in determining the superior arm of the angle (GACAL, FACAL, TAPCAL, TADCAL).

A number of factors can interfere with the accuracy of bone vs. radiographic image measurements in both the physical bone and its radiographic image. These include errors in identifying corresponding landmarks between bone and radiograph and distortion of the radiographic image. Any deviation from the standardized position may affect the accuracy of such measurements. Thus, measurements taken of each bone may be close to the actual measurements, or may vary a great deal, if the foot is not placed in the proper position for the radiograph (39). The most accurate radiographic image of a bone is one where the radiograph is taken with the bone next to, and parallel with, the image receptor and perpendicular to the x-ray beam. Since the bones of the foot are not all parallel to the foot axis, or to each other, it is not possible for every bone of an intact foot to be parallel to the image receptor and perpendicular to the x-ray beam in a radiograph. There will be at least some distortion of a bone's image. In addition, every bone varies in shape. Thus, each surface of a bone may be angulated to the x-ray beam and image plate differently from another bone. As a result, it would be expected that every bone has the potential of creating a radiographic image altered from the actual dimensions with some images being affected more than others. Because both the talus and calcaneus have relatively complex shapes, even though they tend to be roughly parallel to the axis of the foot in the AP and lateral views, some distortion of the radiographic image, would be expected. This distortion, while potentially present, should be less of a problem with angular measurements taken from photographic images of the physical bone taken in isolation, because the relationship of the bone to the camera is better controlled. In

addition, the bony landmarks used for measuring points are more easily identified on the photograph. However, without regard to how angles are measured, whether from photograph, cast, or the bone itself, some distortion is to be expected (18). These factors may have all come into play in producing measurements with physical bone and radiographic image measurement comparisons resulting in smaller value of determination values as seen in the talar IANTAL and calcaneal GACAL, FACAL, TACALa and TACALb variables. Developing a system to identify features for evaluating the level of potential distortion present on a foot radiograph would be useful when assessing the accuracy of measurements taken from the radiographic image. In addition, the relationship of the talus and calcaneus to the x-ray beam, radiographic image receptor, and each other, may result in bony overlap on the image obscuring landmarks. This is less of a problem when taking measurements from the physical bone in isolation, where bony overlap is not a problem and landmarks are easier to identify.

Despite these issues, this study demonstrates that selected angular measurements taken from radiographs of the talus and calcaneus can accurately represent corresponding measurements taken from the physical bone and may be used when investigating the morphology of these bones. However, of potential concern is the accuracy of certain measurements used in medical evaluation and biomechanical assessment. These would include Böhler's angle (BTACAL) and the compression angle of the calcaneus (CACAL), where measurement values were significantly different, and Gissane's angle (GACAL) and the front angle of the calcaneus (FACAL), where there was not a strong association between radiographic image and the physical bone measurements. The results presented here suggest that these

measurements taken from the radiographic images by themselves may not reflect the morphology of the physical bone accurately when used in making a medical diagnosis.

Two physical bone measurements taken in the transverse plane with potential use in determining bony morphology were not useful for this study because the corresponding landmarks were either too indistinct or obscured by the overlying leg on the radiographs to be identified. One angular measurement is the horizontal angle of the neck of the talus (HANTAL) (Figure 3a), defined as the angle formed by the longitudinal axis of the neck and longitudinal axis of the body, modified as described by Day and Wood (18) (see the Appendix.) Since the medial border of the trochlea surface is not clearly observable on the AP radiograph, this measurement is limited to bone only. Of note, the mean of the horizontal axis of the neck for this study was determined to be 12.4° (S.D. 7.9), smaller than that reported by Day and Wood (18) (19.0° , S.D. 3.4) and Sarrafian and Kelikian (24) (24° , range 10° - 44°). The other measurement is the anterior calcaneocuboid angle of the calcaneus in the AP view (ACCAPCAL) (Figure 7a) (see the Appendix). Defined as the angle created by the inferior border of the calcaneocuboid joint and a line parallel to the lateral border of the calcaneus, its use is limited to the physical bone because the anterior-inferior border of the calcaneus is not clearly observable on AP radiograph.

Conclusions

If angular measurements taken from plain radiographic images are to be used in statistical studies in the same manner as that from the physical bone, the accuracy of angular measurements from plain radiographs must first be demonstrated, as has been done in this

study. The close association between the angular measurements of the calcaneus and talus taken from the radiographic images and physical bone for several important measurements establishes that relationship.

The ability to better understand angular morphology of these bones from radiographs can be important when assessing a patient's foot pathology and developing an appropriate treatment plan. The knowledge derived from this study provides information for the functional analysis of the talus and calcaneus that, until now, could only be performed on weight-bearing radiographs. Such information should also help in understanding the association of the morphologic variation of these tarsal elements as it relates to the biomechanics of the entire foot, something that currently cannot be performed with confidence using isolated foot bones (36). The results of this research can be applied to assist in the interpretation of fossil hominin pedal remains towards an understanding of the evolution of the human foot and bipedal locomotion. In addition, studying osteometric variations in humans can help establish differences in individual skeletons, important in archeology and forensic investigation (35). Being able to use measurements from both radiographic image and the physical bone increases the numbers of individuals available for statistical analysis, necessary in the assessment of variation at the population level.

If angular measurements of these relatively complex-shaped bones taken from radiographic images can be applied to the physical bone, it is possible that angular measurements taken from radiographs of other bones of the foot can be studied in the same manner. However, each bone of the foot must first be evaluated separately as described here

for the talus and calcaneus, to identify those measurements that can be used for bone and radiograph, their measuring points, and how the measurements should be taken.

Chapter 3: Appendix

All angular measurements for each individual bone were taken from photographs, using the photography protocol as described in the *Revealing Hominid Origins Initiative (RHOI)* website (http://rhoi.berkeley.edu/RHOI_photo/RHOI_Photography_Protocol.html; accessed 6-30-2014.). Except where noted, all transverse plane measurements of bone were taken from dorsal (superior) views and all sagittal plane measures of bone were taken from lateral views. All angular measurements were taken from photographs and scanned radiographs with known scale, using ImageJ (<http://imagej.nih.gov/ij/>). An “x” at the end of the variable indicates that the measurement was taken from a radiographic image.

Talus bone and radiographic measurements

Talus transverse plane measurements

Angle of the Head of the Talus (AHTAL) (Figure 2a)

Definition: The angle of the head of the talus in relation to the talar neck.

Method: Using a photo of the dorsal aspect of the bone, a line is drawn between the widest medial and lateral points of the head of the talus *at the point where each begins to taper at the neck*. The angle is formed between this line and a line parallel to the lateral border of the neck of the talus. The lateral border of the neck is parallel to the section before it flares out at its base.

Angle of the Head of the Talus (AHTALpl) (Figure 2b)

Definition: The angle of the head of the talus in relation to the talar neck.

Method: Using a photo of the plantar aspect of the bone, a line is drawn between the widest medial and lateral points of the head of the talus *at the point where each begins to taper at the neck*. The angle is formed between this line and a line parallel to the lateral border of the neck of the talus. The lateral border of the neck is parallel to the section before it flares out at its base.

Angle of the Head of the Talus (AHTALx) (Figures 1a, 3)

Definition: The angle of the head of the talus in relation to the talar neck.

Method: Using the AP radiograph, a line is drawn between the widest medial and lateral points of the head of the talus *at the point where each begins to taper at the neck*. The angle is formed between this line and a line parallel to the lateral border of the neck of the talus. If the most lateral aspect of the talar head is not easily observed, it may be identified as the most

lateral point where the talar head articulates with the navicular. The lateral border of the neck is parallel to the section before it flares out at its base.

Angle of the Neck of the Talus (ANTAL) (Figure 2a)

Definition: The angle of the head of the talus in relation to the talar neck at its base.

Method: Using a photo of the dorsal aspect of the bone, a line is drawn between the widest medial and lateral points of the head of the talus *at the point where each begins to taper at the neck*. The angle is formed between this line and a line parallel to the base of the lateral border of the neck of the talus as it begins to curve laterally. The line thus is parallel to the section of the lateral border of the neck where the neck flares out at its base.

Angle of the Neck of the Talus (ANTALpl) (Figure 2b)

Definition: The angle of the head of the talus in relation to the talar neck at its base.

Method: Using a photo of the plantar aspect of the bone, a line is drawn between the widest medial and lateral points of the head of the talus *at the point where each begins to taper at the neck*. The angle is formed between this line and a line parallel to the base of the lateral border of the neck of the talus as it begins to curve laterally. The line is thus parallel to the section of the lateral border of the neck where it flares out at its base.

Angle of the Neck of the Talus (ANTALx) (Figures 1a, 3)

Definition: The angle of the head of the talus in relation to the talar neck at its base.

Method: Using the AP radiograph, a line is drawn between the widest medial and lateral points of the head of the talus *at the point where each begins to taper at the neck*. If the most lateral aspect of the talar head is not easily observed, it may be identified as the most lateral point where the talar head articulates with the navicular. The angle is formed between this line and a line parallel to the base of the lateral border of the neck of the talus as it begins to curve laterally. The line is thus parallel to the section of the lateral border of the neck where it flares out at its base.

Horizontal Angle of the Neck of the Talus (HANTAL) (Modified from Day and Wood (18)) (Figure 3a)

Definition: The angle formed by the longitudinal axis of the neck and longitudinal axis of the body of the talus in the transverse plan. Referred to as the *declination angle of the talar neck* relative to the body by Sarrafian and Kelikian [50] and *obliquity of the head of the talus* by Sewell [52-53]. Since the medial border of the trochlea is not clearly observable on AP radiograph, this measurement is limited to bone only.

Method: Using a photograph of the dorsal aspect of the bone, the longitudinal axis of the neck is drawn parallel to the lateral border of the neck, as described for AHTAL. The longitudinal axis of the body is parallel to the medial border of the trochlear surface. HANTAL is formed at the intersection of these two axes [52-53].

Talus sagittal plane measurements

Inclination Angle Neck of the Talus (IANTAL) relative to the body (Modified from Day and Wood (18) and Sarrafian and Kelikian (24)) (Figure 4a)

Definition: The angle of inclination of the talar neck relative to the body in the sagittal plane (i.e. the angle between the longitudinal axis of the body of the talus and the longitudinal axis of the talar neck in the sagittal plane).

Method: Using a photo of the lateral surface of the talus, a line is drawn between the most anterior and most posterior points of the fibular trochlear surface of the talus (MaxLFTSTAL). This line is considered parallel to the longitudinal axis of the *body* of the talus. A second line is drawn approximately from the midpoint of the navicular articular surface of the head, through a point midway between the upper and lower borders of the neck. This line should be roughly parallel to the inferior border of the neck. IANTAL is formed at the point where this line intersects the MaxLFTSTAL line. The vertical axis of the body of the talus is perpendicular to MAXLFTSTAL. The longitudinal axis of the neck may or may not intersect at the point where the vertical axis of the body intersects with the longitudinal axis of the body at its midpoint.

Inclination Angle Neck of the Talus (IANTALa) (Medial surface) (Figure 4b)

Definition: The angle of inclination of the talar neck relative to the body in the sagittal plane (i.e. the angle between the longitudinal axis of the body of the talus and the longitudinal axis of the talar neck in the sagittal plane).

Method: A line is drawn joint the most anterior and posterior points of the trochlear surface as viewed from its medial surface. A second line is drawn as described for IANTAL (above). IANTALa is formed where these two lines intersect. *(This angle did not produce significantly better results than IANTAL and so was not used in this study.)*

Inclination Angle Neck of the Talus (IANTALx) (Modified from Day and Wood (18)) (Figures 1b, 5)

Definition: The angle of inclination of the talar neck relative to the body in the sagittal plane (i.e. the angle between the longitudinal axis of the neck of the talus and the longitudinal axis of the body of the talus in the sagittal plane). This line is referred to as the *talar declination angle* on lateral weight-bearing radiographic images where the axis of the talar neck intersects a line parallel to the supporting surface (38).

Method: Similar to that described for IANTAL. The most anterior aspect of the trochlear is the widest point where the neck and body meet anteriorly; the most posterior point is where this line transects the widest point of the posterior border. The line connecting these two points (MaxLFTSTALx) is considered the longitudinal axis of the *body* of the talus. The axis of the neck is determined by a line drawn from the approximately midpoint of the articular surface of the head, through a point midway between the upper and lower borders of the neck. This axis may also be roughly parallel to the inferior border of the neck, if observable. IANTALx is formed by the intersection of these two axes. The longitudinal axis of the neck may or may not intersect the longitudinal axis of the body at the point where the vertical axis intersects the horizontal axis of the body.

Calcaneus bone and radiographic measurements

Calcaneus transverse plane measurements

Anterior Angle AP view of the Calcaneus (AAAPCALa) (Figure 6a)

Definition: The angle created by a line drawn parallel to the distal anterior border of the calcaneus and a line parallel to the lateral border of the distal aspect of the calcaneus, exclusive of any exostosis or bony prominence protruding from the lateral border.

Method: A photograph of the superior surface of the calcaneus is used. The anterior line is drawn parallel to the anterior border, exclusive of where the surface flares anteriorly as part of the anterior articular facet medially, and where the border curves proximally. The lateral line is drawn parallel to the lateral border of the calcaneus, exclusive of any exostosis or bony prominence protruding from the lateral border. The angle is measured where these two axes intersect.

Anterior Angle AP view of the Calcaneus (AAAPCALb) (Figure 6b)

Definition: The angle created by a line drawn parallel to the distal anterior border of the calcaneus and a line parallel to the lateral border of the distal aspect of the calcaneus, exclusive of any exostosis or bony prominence protruding from the lateral border.

Method: A photograph of the inferior surface of the calcaneus is used. The anterior line is drawn parallel to the anterior border, exclusive of where the surface flares anteriorly as part of the anterior articular facet medially, or where the border curves proximally. The lateral line is drawn parallel to the lateral border of the calcaneus, exclusive of any exostosis or bony prominence protruding from the lateral border. The angle is measured where these two axes intersect.

Anterior Angle AP view of the Calcaneus (AAAPCALx) (Figures 1a, 7b)

Definition: The angle created by a line drawn parallel to the distal anterior border of the calcaneus and a line parallel to the lateral border of the distal aspect of the calcaneus, exclusive of any exostosis or bony prominence protruding from the lateral border.

Method: The angle is measured in the same manner as the AAAPCAL bone measurements, using the AP radiograph. The anterior line should be parallel to the calcaneocuboid joint border centrally, before it curves proximally, which represents the anterior border of the calcaneus superiorly. However, the anterior border may be difficult to identify. In that case, the least angulated section of the most distal aspect of the border (usually at the more lateral aspect of the anterior border) may be used. If the anterior border is not clearly observable, a line connected the anterior-medial and anterior lateral borders may also be used. A line parallel to the posterior border of the cuboid may be used if the anterior border of the calcaneus is not observable. The lateral line is drawn parallel to the lateral border of the calcaneus, exclusive of any exostosis or bony prominence protruding from the lateral border. The line is usually parallel to the most proximal portion of the lateral border observable on the AP view. The angle is measured where these two axes intersect.

Anterior Calcaneocuboid AP view of the Calcaneus (ACCAPCAL) (Figure 7a)

Definition: The angle created by the inferior border of the calcaneocuboid joint and a line parallel to the lateral border of the calcaneus.

Method: The photograph of the inferior surface of the calcaneus is used. The anterior line is drawn connecting the most lateral and most medial points of the inferior border of the calcaneocuboid joint roughly parallel to its surface. The lateral line is drawn parallel to the lateral border of the calcaneus, exclusive of any exostosis or bony prominence protruding from the lateral border (see AAAPCAL lateral border description). The angle is measured where these two axes intersect. *(Since the anterior-inferior border of the calcaneus is not clearly observable on AP radiograph, this measurement is limited to bone only.)*

Calcaneus sagittal plane measurements

(Note: The longitudinal axis of the calcaneus in the sagittal plane is a line drawn roughly parallel to the plantar border of the calcaneus, exclusive of the calcaneal tuberosity or any other bony plantar projection or prominence. Depending on the shape of the bone, it may also be parallel to the superior border between the beginning of the flare at its anterior aspect and the beginning of the flare for the calcaneal tuberosity at its posterior aspect. All measurements are taken from a lateral photograph of the calcaneus from bone, or the lateral radiographic view of the foot.)

Angle of Inclination Posterior Talar Facet of the Calcaneus (AIPTFCAL and AIPTFCALx) (Modified from Bruckner (17)) (Figures 8a, 1b, 9a)

Definition: The angle between the posterior talar articular surface and the longitudinal axis of the calcaneus.

Method: A line is drawn from the *highest point* of the posterior talar articular surface through an inferior point just anterior to where the surface curves into the inferior border of the sinus tarsi. A second line is drawn parallel to the longitudinal axis of the calcaneus. This is the angle where these two lines intersect.

Angle of Inclination Middle Talar Facet of the Calcaneus (AIMTFCAL and AIMTFCALx) Figures 8a, 1b, 9a)

Definition: The angle between the middle talar articular surface and the longitudinal axis of the calcaneus. This measurement represents the slope of the sustentaculum tali. It is termed as the angle of inclination of the sustentaculum tali by Sarrafian and Kelikian (24), described as the angle between lines drawn parallel to the surface of the middle articular facet and parallel to the inferior surface of the calcaneus).

Method: A line is drawn parallel to the surface of the middle talar articular facet. The line should be parallel to the slope of the surface at middle section of the middle talar facet that is observable (usually the lower ½ of the midsection of the slope, excluding any extreme slope at the most superior aspect, or reduced slope at the distal aspect, if visible). The angle is created where this line and the line drawn parallel to the longitudinal axis of the calcaneus intersect. If articular surface of the middle articular facet is not clearly observable on radiograph, the radiograph should not be used for this measurement.

Anterior Angle Lateral view of the Calcaneus (AALCAL and AALCALx) (Modified from Bruckner (17)) (Figures 8a, 1b, Figure 9a)

Definition: The angle between the distal anterior border and the longitudinal axis of the calcaneus.

Method: A line is drawn parallel to the anterior border of the lateral surface of the calcaneus. This line usually connects the most superior and inferior points of the anterior surface, though more importantly, should be roughly parallel to the anterior aspect of the calcaneus, usually at its midsection. A second line is drawn from the anterior inferior point of the calcaneus parallel to the longitudinal axis of the calcaneus. The angle is created where these two lines intersect.

Böhler's Tuber Angle of the Calcaneus (BTACAL and BTACALx) (Modified from Sarrafian and Kelikian (24) (Figures 8b, 1b, Figure 9b)

Definition: The angle formed by the anterior and posterior surfaces of the superior border of the calcaneus.

Method: An acute angle is formed anteriorly by a line drawn from the superior aspect of the calcaneal tuberosity and highest point of the calcaneus (which may or may not be the most superior point of the posterior talar articular surface) and a line drawn from the highest point of the calcaneus and the most superior point of the anterior aspect of the calcaneus (lateral or medial).

Gissane's Angle of the Calcaneus (GACAL and GACALx) (modified from Lautzenheiser and Kramer (37)) (Figures 8b, 1b, 9b)

Definition: The angle formed by the posterior talar articular surface and the superior surface anterior to it as seen on the lateral surface of the calcaneus.

Method: One line is drawn from the superior point of the posterior facet of the calcaneus to the inferior point on the posterior facet (Parallel to AIPTFCAL). A second line is drawn from the most inferior point of the posterior articular facet at the inferior border to the most superior point of the anterior border (or to the most superior point just proximal to the anterior border) of the calcaneus. (This line is usually parallel to the superior border). The angle is measured where these lines intersect at the inferior point of the posterior talar articular facet (See Khoshhal et al. [40] for variations on this measurement).

Compression Angle of the Calcaneus (CACAL and CACALx) (modified from Saxena and Weddington (34)) (Figures 8b, 1b, 9b)

Definition: This angle has been used to assess traumatic compression of the posterior subtalar joint by comparing the superior aspect anterior to the posterior border of the posterior talar facet with the longitudinal axis of the calcaneus.

Method: The angle is created by a line connecting the superior surface of the superior point of the calcaneus and the superior aspect of the distal calcaneus (the more inferior line used to create Böehler's angle) and a line parallel to the longitudinal axis of the calcaneus. The angle is created where the two lines intersect.

Front Angle of the Calcaneus (FACAL and FACALx) (Modified from Riepert et al. (40)) (Figures 8b, 1b, 9b)

Definition: The angle created by the superior point of the calcaneal tuberosity.

Method: One line is drawn from the most superior point of the calcaneal tuberosity to the most inferior point of the distal anterior calcaneus. A second line is drawn from the inferior point of the distal anterior calcaneus parallel to the long axis of the calcaneus. The angle is measured where the two lines intersect at the inferior distal anterior aspect of the calcaneus.

Tuber Angle of the Plantar Calcaneus (TAPCAL and TAPCALx) (Modified from Riepert et al. (40)) (Figures 8b, 1b, 9b)

Definition: The angle created by the posterior surface of the calcaneal tuberosity and the longitudinal axis of the calcaneus. (The angle has been used to evaluate the degree of posterosuperior prominence of the calcaneus, termed Haglund's deformity, if pronounced, on radiographs by comparing the posterosuperior surface line of the calcaneus with the plantar calcaneal line.) TAPCAL and TAPCALx are similar to the Phillip and Fowler Angle of the calcaneus as described by Gutierrez et al. (32).

Method: A line is drawn from the most superior point of the calcaneal tuberosity roughly parallel to the upper half of the posterior surface of the calcaneus tuberosity. Because of the variation in the slope of sections comprising the upper half of the posterior surface of any one bone, the parallel line may be difficult to identify. It may be parallel to either the middle section of the upper half, or a line drawn between the slope of the superior 1/3 and the slope at the border just superior to the most prominent aspect of the posterior calcaneus. The line should be roughly parallel to the posterosuperior surface of the calcaneus; whichever of the above appears most appropriate. Thus, it may be necessary to estimate the slope by visually "averaging out" the observable differences in the slopes. The angle is measured at the intersection of this parallel line and a line parallel to the longitudinal axis of the calcaneus.

Tuber Angle of the Distal Calcaneus (TADCAL and TADCALx) (Figures 8b, 1b, 9b)

Definition: The angle created by a line tangent to the most posterior point of the calcaneal tuberosity (excluding any prominent posterior projecting spur), perpendicular to the longitudinal axis of the calcaneus, and a line parallel to the posterior surface of the calcaneal tuberosity superiorly.

Method: A line is drawn from the most posterior point of the calcaneal tuberosity perpendicular to the long axis of the calcaneus. The angle is measured at the intersection of that line and the line parallel to the posterior surface of the calcaneus tuberosity (see TACALa) (TAPCAL and TAPCALx).

Chapter 3: Literature cited

1. Baron RL, Stugielski CF, Christman RA: "Positioning Techniques and Terminology", in *Foot and Ankle Radiology*. Second ed., edited by RA Christman, p 43, Wolters Kluwer, Philadelphia, 2015.
2. Elftman H, Manter J: The evolution of the human foot, with especial reference to the joints. *J Anat* **70**: 56, 1935.
3. Morton DJ: *The Human Foot: Its Evolutionary Development, Physiology and Functional Disorders*, Columbia University Press, New York, 1935.
4. Harris RI, Beath T: 1948. Hypermobility flat-foot with short tendo Achillis. *J Bone Joint Surg* **31A**: 116, 1948.
5. Hicks JH: The mechanics of the foot I. The joints. *J Anat* **87**: 345, 1953.
6. Elftman H: The transverse tarsal joint and its control. *Clin Orthop* **16**: 41, 1960.
7. Close J, Inman VT, Todd FN: The function of the subtalar joint. *Clin Orthop Relat Res* **50** :159, 1967.
8. Inman VT: *The Joints of the Ankle*, The Williams and Wilkins Company, Baltimore, 1976.
9. Root ML, Orien WP, Weed JH: *Normal and Abnormal Function of the Foot*, Clinical Biomechanics Corporation, Los Angeles, 1977.
10. DeSilva JM, Holt KG, Churchill SE, et al: The lower limb and mechanics of walking in *Australopithecus sediba*. *Science* **340**:1232999, 2013.
11. Steele DG: The estimation of sex on the basis of the talus and calcaneus. *Am J Phys Anthropol* **45**; 581, 1976.
12. Introna F, Di Vella G, Campobasso CP, et al: Sex determination by discriminant analysis of calcanei measurements. *J Forensic Sci* **42**: 728, 1997.
13. White TD, Folkens PA: "Chapter 2 Bone Biology" in *Human Osteology*, edited by TD White and PA Folkens, p 15, Academic Press, San Diego, 2000.
14. Murphy AMC: The calcaneus: sex assessment of prehistoric New Zealand Polynesian skeletal remains. *Forensic Sci Int* **129**: 205, 2002a.

15. Murphy AMC: The talus: sex assessment of prehistoric New Zealand Polynesian skeletal remains. *Forensic Sci Int* **128**: 155, 2002b.
16. Harris SM, Case DT: Sexual dimorphism in the tarsal bones: implications for sex determination. *J Forensic Sci* **57**: 295, 2012.
17. Bruckner J: Variations in the human subtalar joint. *J Orthop Sports Phys Therapy* **8**: 489, 1987.
18. Day MH, Wood BA: Functional affinities of the Olduvai hominid 8 talus. *Man* **3**: 440, 1968.
19. DeSilva JM: *Vertical climbing adaptations in the anthropoid ankle and midfoot: implications for locomotion in Miocene catarrhines and Plio-pleistocene hominins (PhD dissertation)*, University of Michigan: Ann Arbor, 2008.
20. DeSilva JM: Functional morphology of the ankle and the likelihood of climbing in early hominins. *Proc Natl Acad Sci USA* **106**: 6567, 2009.
21. DeSilva JM, Papakyrikos A: A case of valgus ankle in an early Pleistocene hominin. *Int J Osteoarchaeol* **21**: 732, 2011.
22. DeSilva JM, Throckmorton ZJ: Lucy's flat feet: the relationship between the ankle and rearfoot arching in early hominins. *PLoS One* **5**: e14432, 2010.
23. Gomberg DN: *Form and Function of the Hominoid Foot* (PhD dissertation), University of Massachusetts, Amherst, 1981.
24. Sarrafian SK, Kelikian AS: "Chapter 2 Osteology", in *Anatomy of the Foot and Ankle*, Third ed., edited by AS Kelikian, p 40, Wlters Kluwer / Lippincott Williams & Wilkins, Philadelphia, 2011.
25. Latimer B, Ohman JC, Lovejoy C: Talocrural joint in African hominoids: implications for *Australopithecus afarensis*. *Am J Phys Anthropol* **74**: 155,1987.
26. Sewell RBS: A study of the astragalus: Part III. *J Anat Physiol* **39**: 74, 1904a.
27. Sewell RBS: A study of the astragalus: Part I. *J Anat Physiol* **38**: 233, 1904b
28. Trinkaus E: *A Functional Analysis of the Neandertal Foot (PhD dissertation)*, University of Pennsylvania, Philadelphia, 1975.
29. Christman, RA: Radiographic anatomy of the foot and ankle – Part 2 The greater tarsus. *JAPMA* **104**: 503, 2014.

30. Clint SA, Morris, TP, Shaw OM, et al: The reliability and variation of measurements of the os calcis angles in children. *J Bone Joint Surg* **92-B**: 571, 2010.
31. Böhler L: Diagnosis, pathology and treatment of fractures of the os calcis. *J Bone Joint Surg (Am)* **29**: 89, 1931.
32. Gutierrez P, Navarro M, Ojeda M: Radiologic morphology of the calcaneus. *JAPMA* **103**: 32, 2013.
33. Khoshhal KI, Ibrahim AF, Al-Nakshabandi NA, et al: Böhler's and Gissane's angles of the calcaneus. *Saudi Med J* **25**: 1970, 2004.
34. Saxena A, Weddington J: New radiographic angle to assess intra-articular calcaneal fractures. *J Foot Surg* **28**: 200, 1989.
35. Didia BC, Dimkpa JN: The calcaneal angle in Nigerians. *JAPMA* **89**: 472, 1999.
36. DeSilva JM, Gill CM, Swanson Z, et al: Reconstructing foot form and function in early hominis using human models. *Am J Phys Anthropol* **153**: 104, 2014.
37. Lautzenheiser SG, Kramer PA: Linear and angular measurements of the foot of modern humans: A test of Morton's foot types. *Anat Rec* **296**: 1526, 2013.
38. Sanner WH, Whitney AK: "Foot Segment Relationships and Bone Morphology", in *Foot and Ankle Radiology*. Second ed., edited by RA Christman, p 209, Wolters Kluwer, Philadelphia, 2015.
39. Gamble, FO, Yale I: "Chapter 12 Roentgenology and Biomechanics" in *Clinical Foot Roentgenology*. Second edition, edited by FO Gamble and I Yale, p 169, Krieger Publishing, New York, 1975.
40. Riepert T, Drechsler T, Schild H, et al: Estimation of sex on the basis of radiographs of the calcaneus. *J Forensic Legal Med* **77**: 133, 1996.

Chapter 3: List of Tables

Table 1. Measurements and descriptive statistics of bone and radiographic angular measurements of the talus (n = 54, degrees of freedom = 53 for all values).

Table 2. Measurements and descriptive statistics of bone and radiographic angular measurements for the calcaneus (n = 54, degrees of freedom = 53 for all values).

Note: The regression coefficient (B) indicates the ratio of radiographic measurement to the bony measurement, i.e., the degree of change associated with measuring the radiograph.

Description	Variable	Bone			Radiologic (x)			t-test Analysis		Linear Regression Analysis	
		Mean	SEM	SD	Mean	SEM	SD	t	p	b	r ²
Angle Head of the Talus	AHTAL	86.76	0.847	6.22	86.44	0.836	6.14	0.716	0.47	1.003	0.74
Angle Head of the Talus	AHTALpl	87.31	0.880	6.47	86.44	0.836	6.14	1.987	0.05	0.993	0.75
Angle of the Neck of the Talus	ANTAL	104.23	0.771	5.67	104.86	0.792	5.82	-1.335	0.19	1.010	0.67
Angle of the Neck of the Talus	ANTALpl	105.45	0.789	5.80	104.86	0.792	5.82	1.407	0.17	1.005	0.73
Inclination Angle Neck of the Talus	IANTAL	31.43	0.505	3.71	34.63	0.479	3.52	-8.187	0.00	0.906	0.46

Table 1. Descriptive statistics and analysis of bone and radiographic angular measurements for the talus (n=54, degrees of freedom =53 for all values).

Note: The regression coefficient (b) indicates the ratio of radiographic measurement to the bony measurement, i.e., the degree of change associated with measuring on the radiograph.

Description	Variable	Bone			Radiologic (x)			t-test		Linear Regression Analysis	
		Mean	SEM	SD	Mean	SEM	SD	t	p	b	r ²
Anterior Angle AP view of the Calcaneus	AAAPCALa	91.22	0.853	6.27	91.39	0.891	6.55	-0.385	0.70	0.997	0.77
Anterior Angle AP view of the Calcaneus	AAAPCALb	91.02	0.891	6.55	91.39	0.891	6.55	-0.736	0.47	0.995	0.70
Angle of Inclination Posterior Talar Facet of the Calcaneus	AIPTFCAL	45.92	0.605	4.45	46.81	0.721	5.30	-2.053	0.05	0.977	0.64
Angle of Inclination Middle Talar Facet of the Calcaneus	AIMTFCAL	53.36	1.046	7.69	54.29	0.953	7.00	-1.483	0.14	0.981	0.64

Table 2. Descriptive statistics and analysis of bone and radiographic angular measurements for the calcaneus (n=54, degrees of freedom = 53 for all values).

Description	Variable	Bone			Radiologic (x)			t-test		Linear Regression Analysis	
		Mean	SEM	SD	Mean	SEM	SD	t	p	b	r ²
Anterior Angle Lateral view of the Calcaneus	AALCAL	105.65	0.828	6.08	105.41	0.920	6.76	0.504	0.62	0.077	0.73
Böehler's Tuber Angle of the Calcaneus	BTACAL	28.52	0.669	4.92	30.55	0.702	5.16	-6.089	0.00	0.842	0.78
Gissane's Angle of the Calcaneus	GACAL	124.26	0.714	5.25	124.18	0.787	5.78	0.121	0.90	0.543	0.35
Compression angle of the Calcaneus	CACAL	24.52	0.622	4.57	25.63	0.800	5.88	-2.497	0.02	0.648	0.69
Front Angle of the Calcaneus	FACAL	35.51	0.447	3.28	34.72	0.514	3.78	1.895	0.32	0.547	0.39
Tuber Angle of the Plantar Calcaneus	TACALa (TAPCAL)	63.82	0.843	6.19	64.39	0.869	6.39	-0.864	0.39	0.684	0.49
Tuber Angle of the Distal Calcaneus	TACALb (TADCAL)	26.15	0.836	6.147	25.56	0.873	6.42	0.876	0.39	0.661	0.47

Table 2 (continued). Descriptive statistics and analysis of bone and radiographic angular measurements for the calcaneus (n=54, degrees of freedom =53 for all values).

Note: The regression coefficient (b) indicates the ratio of radiographic measurement to the bony measurement, i.e., the degrees of change associated with measuring on the radiograph.

Chapter 3: List of Figures

Figure 1a. DP radiograph left foot.

Figure 1b. Lateral radiograph left foot.

Figure 2a. Dorsal surface measurements left talus.

Figure 2b. Plantar surface measurements left talus (photo flipped horizontally).

Figure 3a. Dorsal surface measurement left talus.

Figure 3b. DP radiographic view measurements left talus.

Figure 4a. Lateral surface measurement left talus (photo flipped horizontally).

Figure 4b. Medial surface measurement left talus.

Figure 5. Lateral radiographic view measurement left talus.

Figure 6a. Dorsal surface measurement left calcaneus.

Figure 6b. Plantar surface measurement left calcaneus (photo flipped horizontally).

Figure 7a. Plantar surface measurement left calcaneus (photo flipped horizontally).

Figure 7b. DP radiographic view measurement left foot.

Figure 8a. Lateral surface measurements left calcaneus (photo flipped horizontally).

Figure 8b. Lateral surface measurements left calcaneus (photo flipped horizontally).

Figure 9a. Lateral radiographic view measurements left calcaneus.

Figure 9b. Lateral radiographic view measurements left calcaneus.

Figure 10. Lateral plane relationship IANTAL (photographic) and IANTALx (radiographic) measurements of the talus.

Figure 11. Transverse plane relationship AAAPCALa (photographic) and AAAPCALx (radiographic) measurements (in degrees) of the calcaneus.

Figure 12. Lateral plane relationship BTACAL (photographic) and BTACALx (radiographic) measurements (in degrees) of the calcaneus.

Figure 13. Lateral plane relationship GACAL (photographic) and GACALx (radiographic) measurements (in degrees) of the calcaneus.



Figure 1a. AP radiograph view of the leg foot.
Figure 1b. Lateral radiograph of the leg foot.

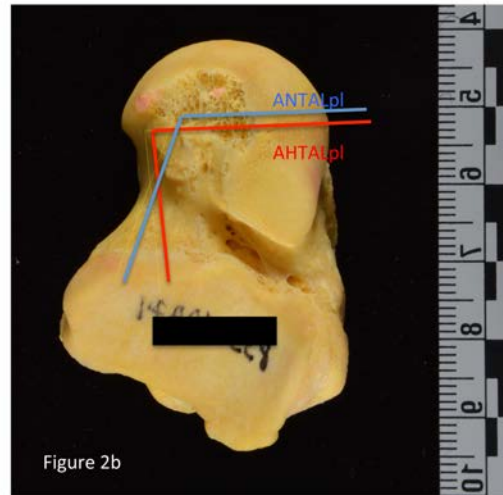
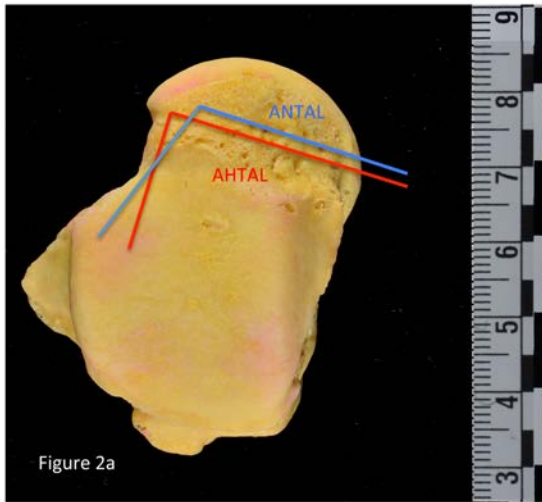


Figure 2a. Dorsal view of the leg talus.
Figure 2b. Plantar view of the leg talus (flipped horizontally).

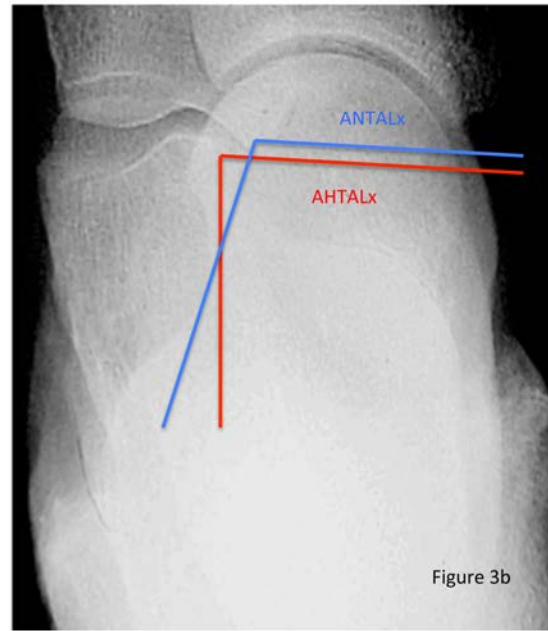
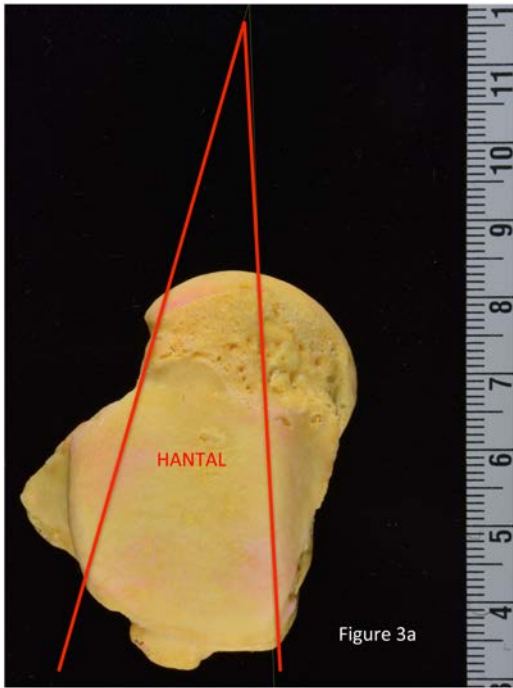


Figure 3a. Dorsal surface measurement left talus.
Figure 3b. DP radiographic view measurements left talus.

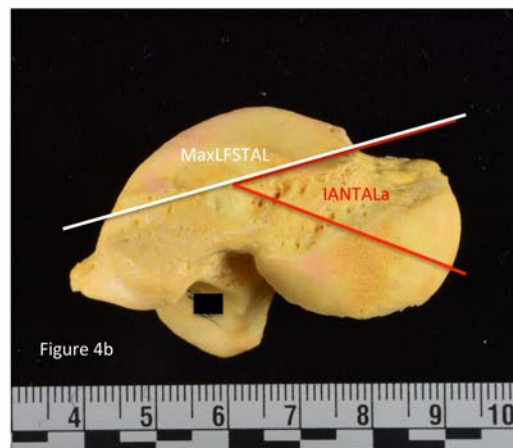
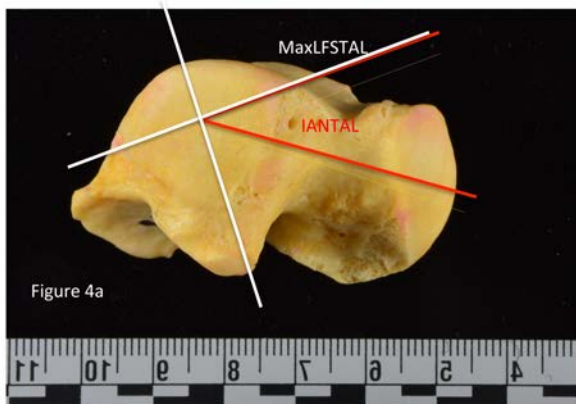


Figure 4a. Lateral surface measurements left talus (photo flipped horizontally).
Figure 4b. Medial surface measurement left talus.

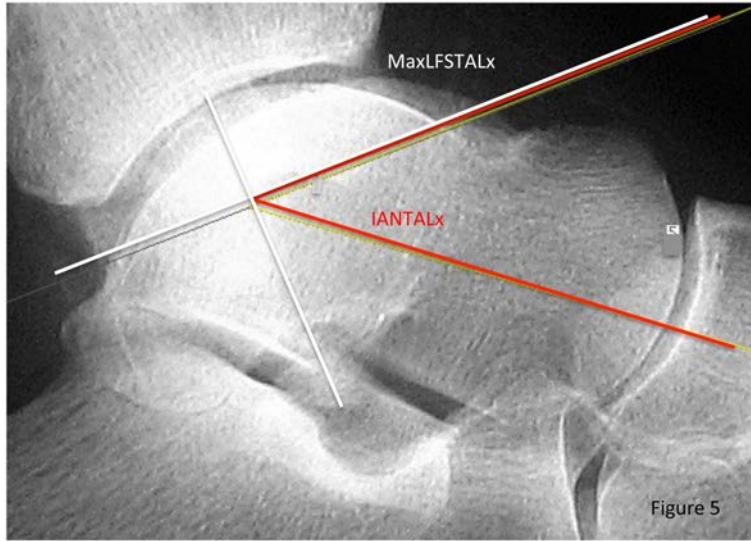


Figure 5. Lateral radiographic view measurement left talus.



Figure 6a

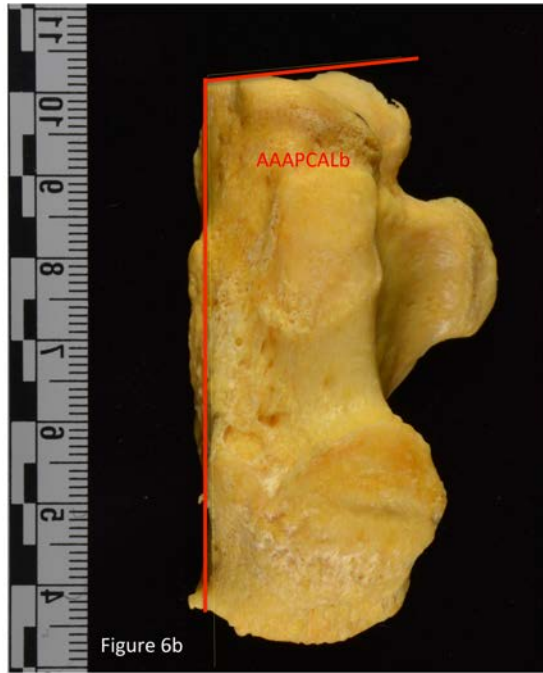


Figure 6b

Figure 6a. Dorsal surface measurement left calcaneus.
Figure 6b. Plantar surface measurement left calcaneus (photo flipped horizontally).

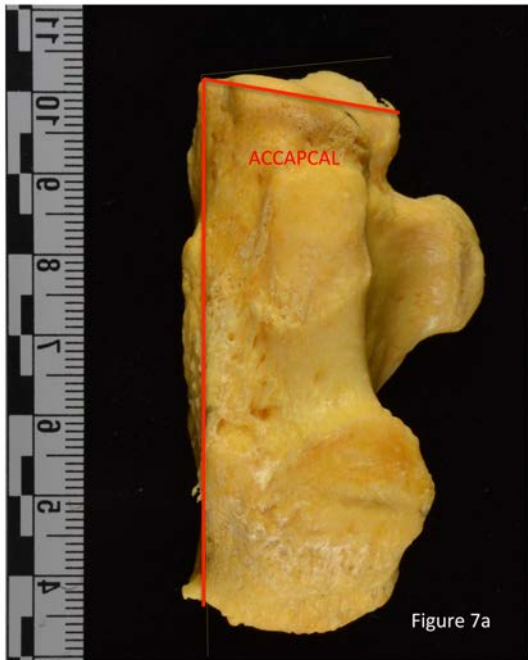
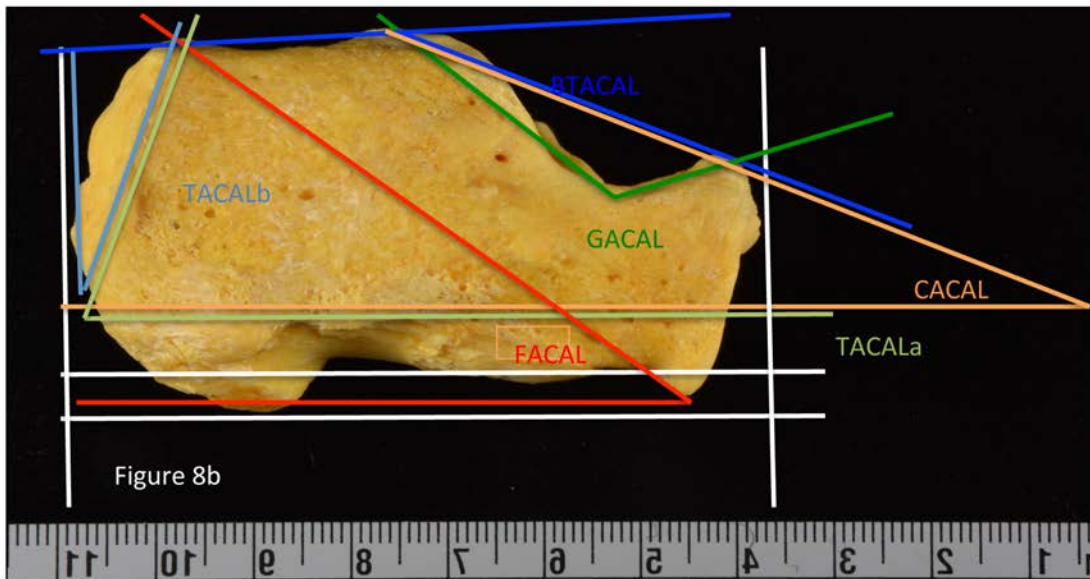
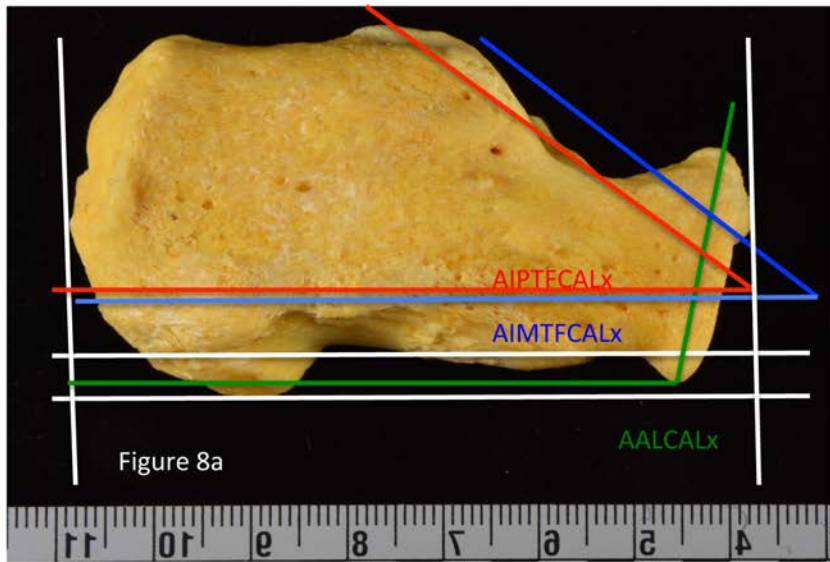


Figure 7a. Plantar surface measurement left calcaneus (photo flipped horizontally.)
Figure 7b. DP radiographic view measurement left foot.



Figures 8a. Lateral view of the left calcaneus (flipped horizontally).
 Figure 8b. Lateral view of the left calcaneus (flipped horizontally).

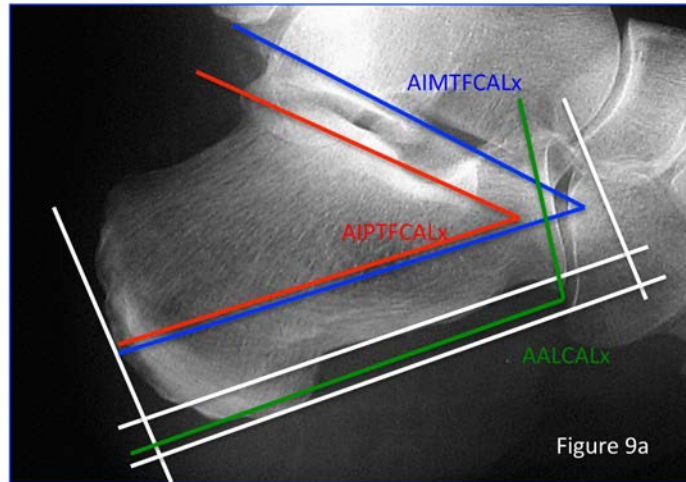


Figure 9a

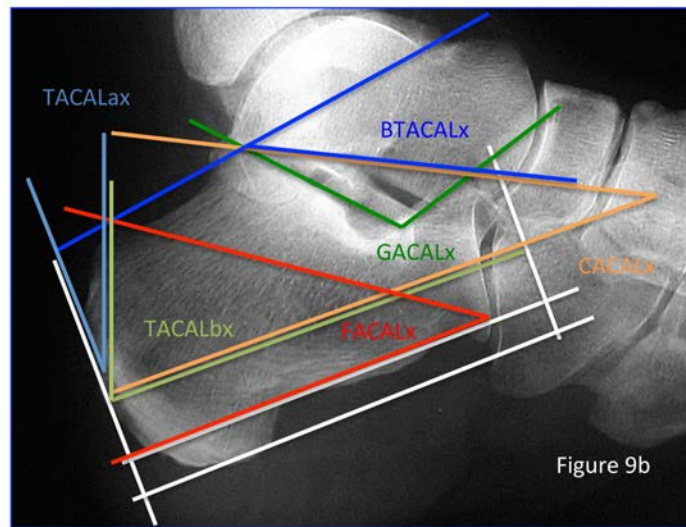


Figure 9b

Figure 9a. Lateral radiographic view measurements left calcaneus.
 Figure 9b. Lateral radiographic view measurements left calcaneus.

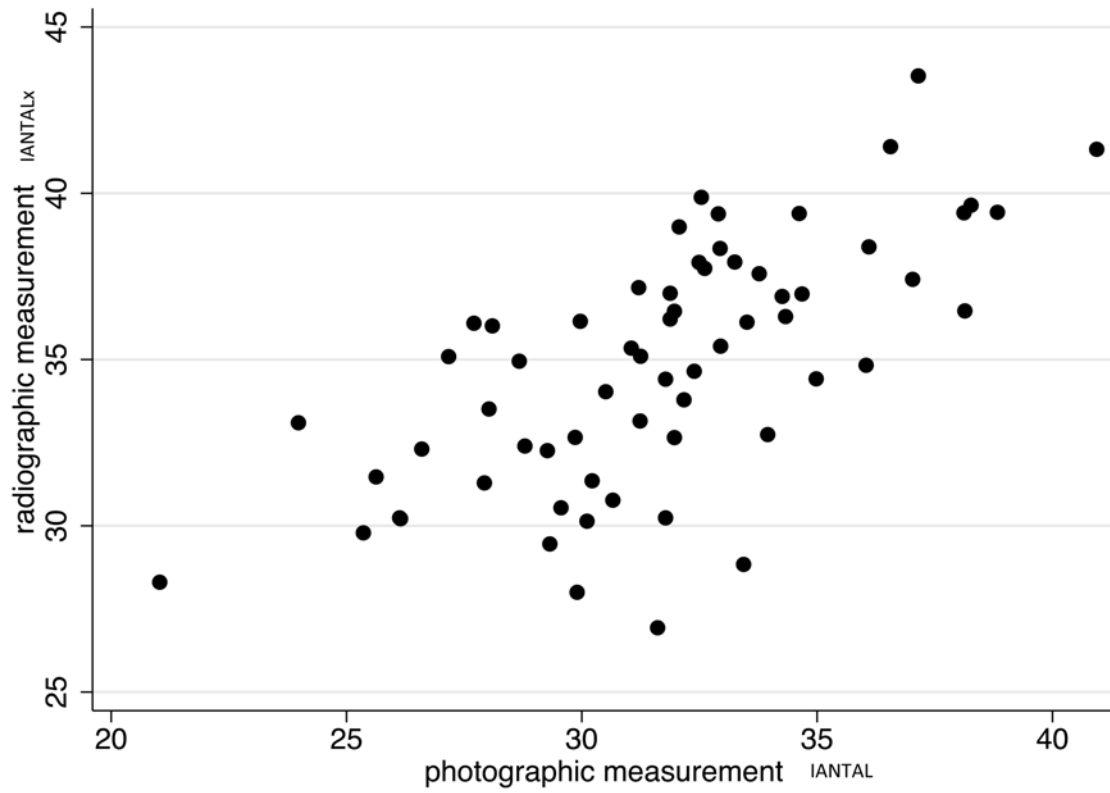


Figure 10. Sagittal plane relationship (IANTAL and IANTALx) of the talus.

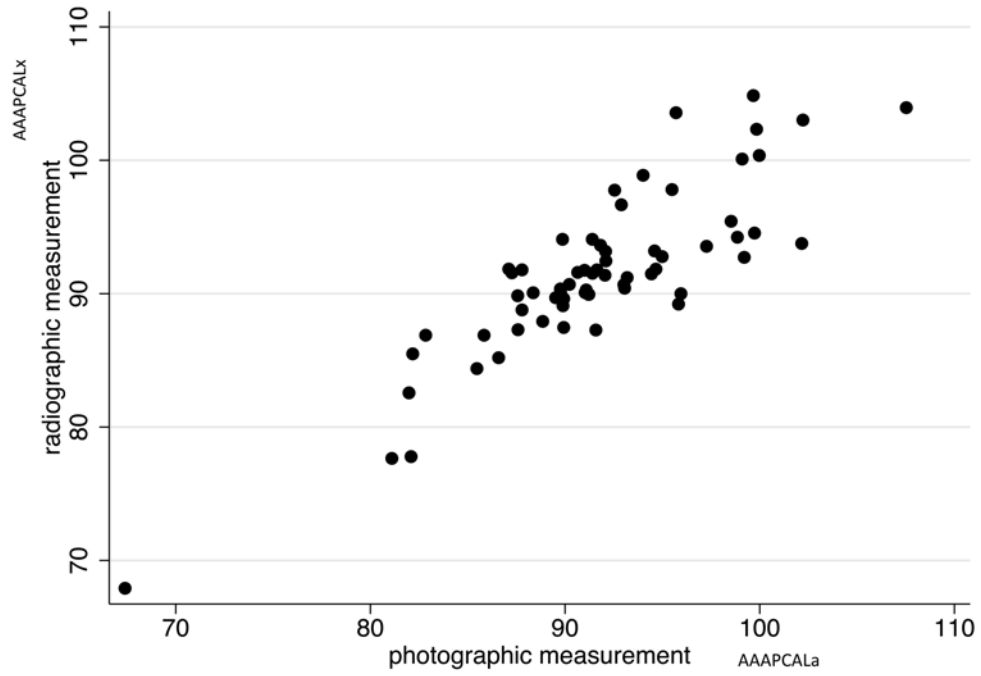


Figure 11. Transverse plane relationship (AAAPCALa and AAAPCALx) of the calcaneus.

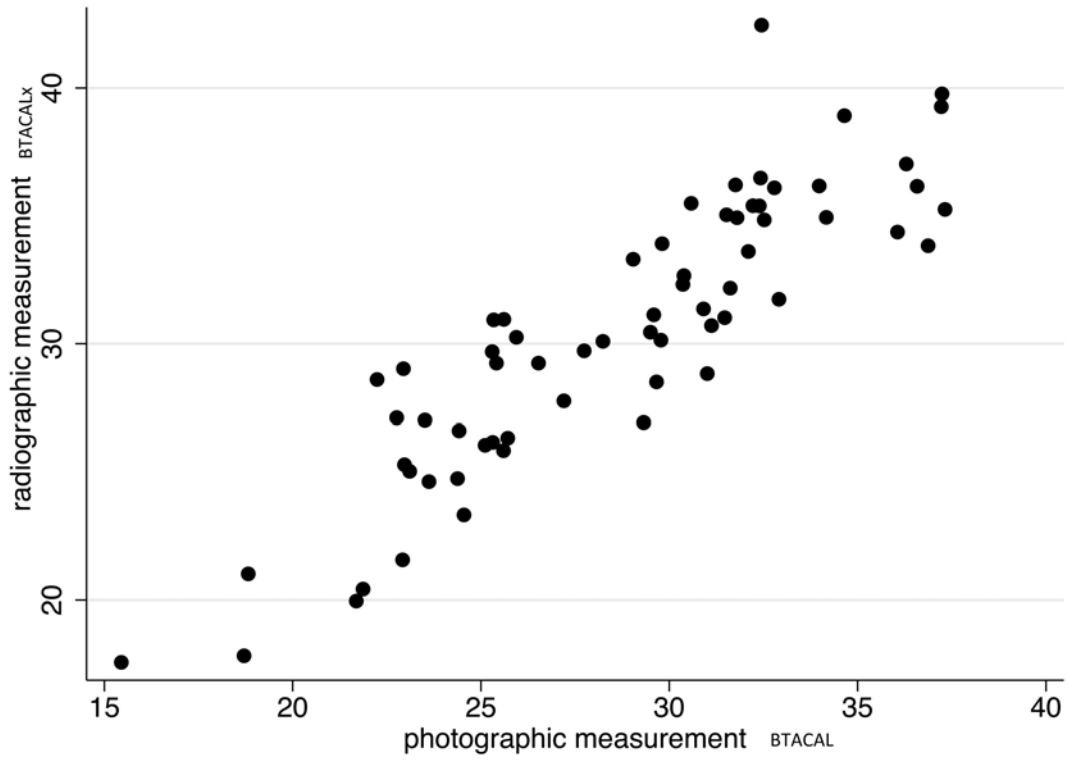


Figure 12. Sagittal plane relationship (BTACAL and BTACALx) of the calcaneus.

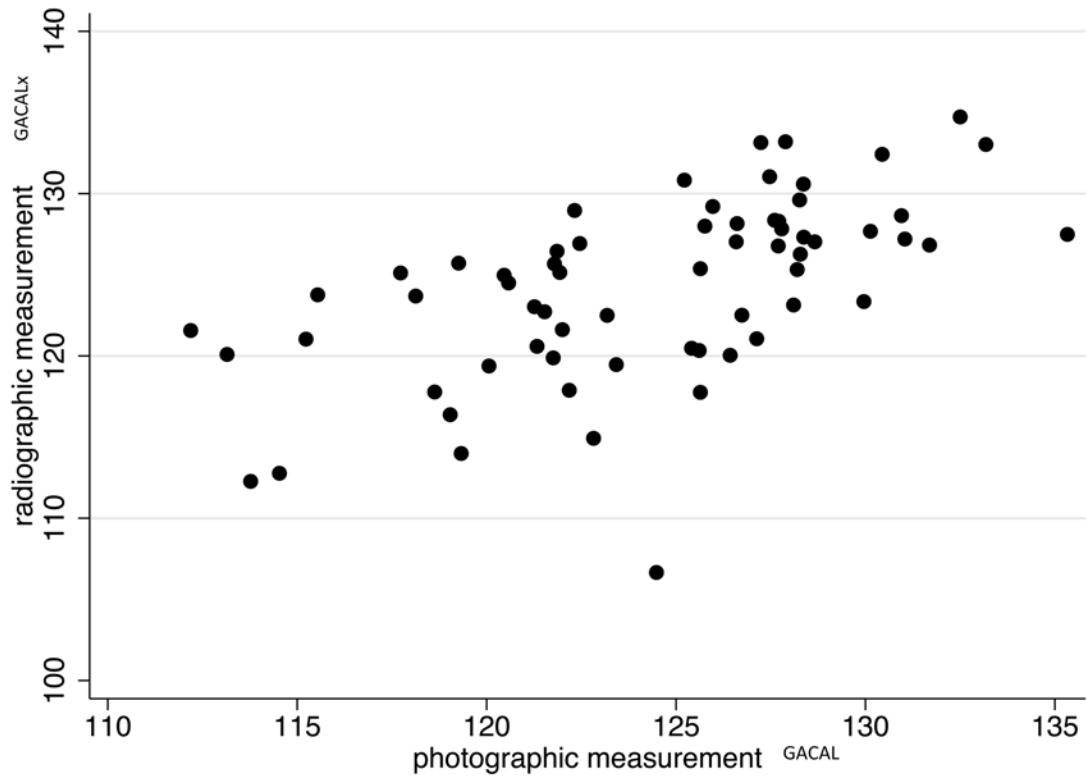


Figure 13. Sagittal plane relationship (GACAL and GACALx) of the calcaneus.

Chapter 4. Radiographic measurements of the talus and calcaneus in the adult pes planus foot type

Preface

The manuscript for this chapter, coauthored with Patricia A. Kramer, was submitted to *The American Journal of Physical Anthropology* for publication consideration on March 26, 2018. It is currently under review. Changes were made to the manuscript since submission where appropriate for context or consistency in chapter presentation. Appendix C has tables with the measurements used for statistical analysis. More detailed information concerning the statistical analyses can be found in Appendix D.

Abstract

Objective: A distinctive feature of the modern human foot is the presence of a medial longitudinal arch when weight-bearing. Foot types based on arch height range from pes planus (flatfoot) to pes cavus (high arch). The talus and calcaneus play a major role in the biomechanics of the human foot. However, the association between the morphology of these bones and foot type has not been fully investigated. A better understanding of this relationship may assist in the interpretation of pedal remains of fossil hominins, where features of the foot and ankle morphology have been described as consistent with that of pes planus seen in modern humans.

Methods: For this study weight-bearing radiographs of 103 patients from an urban US Level 1 trauma center taken as part of a clinical examination for medical evaluation were

selected. These radiographs were classified as to foot type by arch height as defined using the calcaneal inclination angle. From this group, 68 radiographs were suitable for linear and angular measurements of the talus and 74 of the calcaneus.

Results: The results demonstrate that most angular measures of the calcaneus were associated with arch height ($r^2 = 0.17 - 0.44$). However, angular measurements of the talus and linear measurements of both the talus and calcaneus were either weakly or not associated with arch height ($r^2 = 0.00 - 0.09$).

Discussion: These results indicate that the relationship between the morphologies of these bones and the biomechanics of the modern human foot in the interpretation of hominin pedal remains is complex, requiring further investigation.

Key Words: Talus, calcaneus, morphology, pes planus, radiograph

Introduction

The foot of hominins evolved from a grasping organ adapted to arboreal life to a stable platform for habitual bipedal gait on the ground. While the fossil record documents the shape of individual bony elements of the foot in the proposed hominin ancestors, the fragmentary nature of the fossil record and the problems involved in determining the functional relationship of these bony elements to each other creates problems with the interpretation of pedal remains. This necessitates the reliance on studies of the foot of the living representative of the genus *Homo* to understand the locomotor abilities of these ancestral forms. It has been postulated that the foot of our hominin ancestors was functionally similar that seen in modern individuals with a pes planus (or low medial longitudinal arch) foot type (Morton, 1935; DeSilva,

2010; DeSilva and Throckmorton, 2010; DeSilva et al., 2014; DeSilva et al., 2015). The talus and calcaneus are pivotal bones in arch formation, particularly in relation to pes planus. However, before fully testing the idea that pes planus is of particular importance in understanding the evolution of hominin foot evolution, examining the relationship of the morphology of the talus and calcaneus to arch shape is essential.

Significant differences in the height of the medial longitudinal arch in weight-bearing have been well documented in the medical literature (e.g. Menz and Munteanu, 2005; Bourdet et al., 2013; Sanner and Whitney, 2015a). Foot types based on arch height range from the pes planus (flatfoot) to pes cavus (high arch). The pes planus foot has been defined in various ways. Most commonly, the pes planus foot type has been described as a foot with the medial margin of the plantar aspect of the foot in contact with the ground. Others have described it with a more variable morphology. Staheli (1999) defined flatfoot simply as a condition in which the foot has an increased contact area with the ground, while Helfet and Lee (1980) described it as a condition in which the medial longitudinal arch is lower than “normal” when-bearing the weight of the body (Cavanagh and Rodgers, 1987). The problem with these definitions, and thus identifying a pes planus foot type, is knowing how low the arch must be for a foot to be defined as a pes planus foot type.

There has also been much debate in the medical literature regarding what is meant by the term “normal” (Phillips, 1999; Staheli, 1999; Phillips, 2000). It has been suggested that a normal arch height is any value within ± 2 standard deviations from the mean (Staheli, 1999). Others have suggested that a foot should be considered abnormally flat when it has “no reserve” available for subtalar joint pronation when weight-bearing (Phillips, 1999). The term

normal as used in this study applies to the range of measurement values described as “normal” in the medical literature. However, this is not meant to signify that any other values in arch height outside of this range are abnormal or are outside of the range of normal variation. The terms abnormal and pathologic as used in this paper are understood to signify that there are structural features of the foot that would be considered abnormal, such as a dislocated joint, a shape or features of a bone outside of the what is considered usual variation in appearance, or if there is evidence of advanced arthritis, evidence of trauma, or other destructive processes.

Pes planus is a commonly recognized human foot variation. Children generally have a pes planus appearing foot at birth; most individuals with flatfeet are said to develop arches by four to five years of age (Helfet and Lee, 1980). Prevalence of flatfoot in children has been described as being between 20-45% depending upon the population under study (Isbigbi et al., 2005; Ezema et al., 2014). While more common in children than in adults, it is unknown what percentage of children with pes planus will retain the foot type as adults. A prevalence of 20 to 33% has been reported in the literature (Harris and Beath, 1947; Stewart, 1970; Helfet and Lee, 1980). Pes planus is seen more often in certain adult population groups (Krogman, 1962); however, the variations in prevalence of pes planus as reported in the literature may be the result of differences in the accepted definition of pes planus as well as in the methodology used in determining pes planus.

Proposals for pes planus classification differ on the basis of etiology, clinical features, natural history, and potential for causing disability (Page, 1983; Lepow and Valenza, 1989; Staheli, 1999; Lee et al., 2005; Giza et al., 2007; Richie, 2007; Benedetti et al., 2010; Bubra et al., 2015). Pes planus can be classified as either physiologic or pathologic (Staheli, 1999). Certain

forms of pes planus, such as peroneal spastic flatfoot due to tarsal coalition, congenital vertical talus, talipes calcaneovalgus, peroneal spastic flatfoot, talipes calcaneovalgus, accessory navicular, ligamentous laxity, and generalized dysplasia are considered congenital pathologic conditions (Lee et al., 2005). Medial arch collapse that results from dysfunction caused by bone fracture or traumatic rupture of the posterior tibial tendon, systemic arthritis problems, and neuromuscular imbalance are examples of acquired pathologic conditions. Physiologic flatfoot is described as a benign condition that, while tending to disappear in childhood, may be retained into adulthood (Staheli, 1999). The clinical signs of this physiologic form of flatfoot, termed here as flexible pes planus (or flexible flatfoot) includes a “normal” appearing arch in non-weight-bearing with some degree of reduction of the arch height in stance (Page, 1983; Lee et al., 2005). The flexible pes planus may be considered within the range of normal variation when there are no abnormal systemic causative factors, such as ligamentous laxity. This form of pes planus may not produce significant symptomatology or disability (Staheli, 1999). Adult flexible flatfoot is thus a continuation of a pediatric condition characterized by partial or complete loss of the medial arch (Lee et al., 2005). The adult flexible flatfoot, however, may progress from an asymptomatic “physiologic” pes planus to a more rigid “pathologic” adult acquired pes planus with more limited joint motion (Richie, 2007). The result is a more rigid functioning foot with posterior tibial tendon degeneration (Giza et al., 2007; Richie, 2007; Bubra et al., 2015). Flexible pes planus and its adult form, the adult acquired flatfoot, is probably the most common form of flatfoot. Other factors can also result in excessive reduction in arch height and cause symptomatology, include any conditions that

contributes to a medial shift in weight-bearing such as genu valgum, obesity, and wide base of gait (Lee et al., 2005).

Evaluating a patient for pes planus involves clinical examination, which may include radiographic evaluation (Menz, 1998). Weight-bearing radiographs (anterior-posterior (AP), lateral, and oblique views, as well as Harris-Beath views if a tarsal coalition is suspected) may be ordered (Lee et al., 2005). The radiographic features of pes planus have been widely reviewed in the literature (Kaplan and Symonds, 1945; Bonnet and Baker, 1946; Cavanagh and Rodgers, 1987; Lepow and Valenza 1989; McCrory et al., 1997; Menz, 1998; Lee et al., 2005; Menz and Munteanu, 2005; Younger et al., 2005; Murley et al., 2009; Bourdet et al., 2013; Sanner and Whitney, 2015a). The accuracy of classifying a foot as pes planus using weight-bearing radiographs has been compared to other methods of evaluation, including weight-bearing pedal prints and clinical examination. Radiographs provide the most valid representation of skeletal foot alignment (Saltzman and Nawoczenski, 1995; Menz and Munteanu, 2005; Murley et al., 2009; Benedetti et al., 2010). The reliability of radiographic measurements has been considered the “gold standard” in the clinical assessment of foot type, demonstrating significant associations ($p < 0.01$) with measurements of the same parameters using other clinical techniques (Menz and Munteanu, 2005).

The flexible pes planus is the result of excessive subtalar joint pronation occurring during the gait cycle (Root et al., 1977). Subtalar (and midtarsal) joint pronation is associated with depression of the medial arch, producing the clinically described “flatfoot” deformity. Arch height in the flexible flatfoot is thus dependent upon the degree of pronation. The talus and calcaneus, which form the subtalar joint, play a major role in foot biomechanics and arch

formation in the modern human foot. The talus (os astragalus) occupies the central position between the leg and foot; its shape partly reflects the longitudinal arched structure of the foot, especially the medial arch (Oxnard and Lisowski, 1980). The second largest tarsal bone, it has no muscle attachments and its movement is dependent on its relationships with other pedal bones and its ligamentous attachments at the ankle, subtalar, and talocalcaneal navicular joints. It is a short bone, complex in nature, divided into a head, neck and body. The calcaneus (os calcis) is the largest tarsal bone. Its most prominent feature is the calcaneal tuberosity, which helps to form the heel of the foot. The calcaneus is located inferior to the talus and helps support it. The calcaneus is roughly rectangular in shape, with six surfaces. The long axis of the calcaneus is tilted anteriorly, superiorly, and laterally relative to the horizontal plane (Draves, 1986).

In excessive pronation, the talus adducts and plantarflexes, resulting in the reduction of the height of the longitudinal medial arch, while the calcaneus everts and plantarflexes (Lee et al., 2005). Subtalar joint pronation unlocks the midtarsal joint, making it unstable and leading to various degrees of transverse plane abduction (Root et al., 1977). Subtalar joint pronation does not, however, necessarily produce complete arch collapse. Pronation is a triplanar motion (in the sagittal, frontal, and transverse planes). As a result of variations in joint structure, usually one plane will dominate in excessive pronation. The foot configuration in midstance is, in part, determined by which plane dominates. For example, if the sagittal plane "deformity" is dominant, the talar head will plantarflex, and a characteristic pes planus foot type with significant reduction in arch height is produced. If the transverse plane motion of pronation is dominant, the talar head will adduct more than it plantarflexes, and the arch will not

necessarily appear to be significantly depressed. Thus, as a result of variations in joint structure, an excessively pronated foot can produce a footprint with a “normal appearing” arch (Root et al., 1977; Agoada, 1989). In other words, all flexible pes planus feet are the result of excessive pronation, but not all excessively pronated feet will appear as pes planus.

While the morphologic variation of the talus and calcaneus has been noted in the anatomical literature (White and Folkens, 2000; Sarrafian and Kelikian, 2011), the role of this variation in the differences seen in subtalar motion, and thus arch height, is unclear. Excessive subtalar and midtarsal joint pronation in midstance that can result in a clinical flatfoot is a complex process. The biomechanics of the foot as it relates to arch height is still not completely understood despite years of investigation which have included cadaver specimens, clinical patient examinations, and mathematic modeling (MacConaill, 1945; MacConaill, 1949; Hicks, 1953; Hicks, 1954; Hicks, 1955; Root et al., 1977; Bojsen-Moller, 1979; Van Langelaan, 1983; Demp, 1989; Volger and Bojsen-Moller, 2000; Kelikian, 2011). Relying mainly on cadaver specimens rather than the osteology of living subjects, attempts have been made to define the complicated joint axes of motion in the foot (Jones 1945; Barnett and Napier, 1952; Inman, 1976; Root et al., 1977; Phillips and Phillips, 1983). Using the postulated axes of motion, subtalar joint motion has also been described (Manter, 1941; Wright et al., 1964; Green et al., 1979).

Harris and Beath (1948) reported on one of the few studies to examine the functional relationship between variation in the bones of the subtalar joint and actual foot configuration. They looked at foot radiographs of military recruits and found that a major difference between the flexible flatfoot and normal foot was support of the talar head by the sustentaculum tali. In

the hypermobile flatfoot, the sustentaculum tali was narrow, while in normal feet it was broad, rounded, and running forward to the anterior margin of the talus. In the flatfoot, the head and neck of the talus were short and were facing medially and anteriorly. They also looked at the foot bones of collected specimens (that were not examined before the foot was skeletonized and bones disarticulated) and found some of the same features in certain bones as seen in the radiographs of the military recruits. This reinforced their belief talar morphological variation could explain the etiology of the hypermobile flatfoot seen in recruits. Other investigators have also looked at the relationship between variation of the morphology in these bones and foot function (Landry and Agoada, 1986; Bruckner, 1987; McPoil et al., 1987; Bruckner, 1997; Anderson et al., 1997; Mahato, 2011; Muthukumaravel et al., 2011; Lufler et al., 2012; Anjaneyulu et al., 2014; Heard-Booth, 2014). Few of these studies have examined the morphology of these bones in an intact, weight-bearing foot of a living individual. Thus, the relationship among this bony variation and the amount of subtalar joint pronation that can take place and the height of the longitudinal arch remains unclear.

The fossil record documents the form of the proposed hominin ancestors. The record's fragmentary nature continues to necessitate reliance on investigations of the variation in foot function of modern humans as it relates to pes planus, to postulate the reconstruction, structural relationships, biomechanics and the evolutionary steps that lead to modern human bipedalism. While the hominin fossil record for pedal remains continues to expand (Harcourt-Smith and Aiello, 2004; Kidd, 2004; Kidd and Oxnard, 2005; Trinkaus, 2005; Gebo and Schwartz, 2006; Jungers et al., 2009a; Jungers et al., 2009b; Lovejoy et al., 2009; Zipfel et al., 2009; DeSilva and Papakyrikos, 2011; Zipfel et al., 2011; DeSilva et al., 2012; Berger et al., Pablos et al., 2013;

2015; Boyle and DeSilva, 2015; Harcourt-Smith et al. 2015; Pablos, 2015), applying what is known about human foot biomechanics and pathology is still important in order to interpret the known fossil material and reconstruct the evolution of human bipedalism DeSilva, 2008; DeSilva, 2009; DeSilva, 2010; DeSilva et al., 2010; DeSilva and Gill, 2013; DeSilva et al., 2013; Lautzenheiser and Kramer, 2013; DeSilva et al., 2014; DeSilva et al., 2015;). For example, DeSilva and Throckmorton (2010) evaluated the radiographs of the tibial arch angle in modern humans and compared these images to the tibial remains of *Australopithecus afarensis* (specimen A.L. 288-1) to come to the conclusion that Lucy's ankle morphology was consistent with non-pathological "flat-footedness" seen in modern humans. The results of this study suggested that there was variation in arch development in Plio-Pleistocene hominins.

The availability of weight-bearing standardized radiographic images of the human foot taken for medical evaluation provides a large number of individuals for statistical analysis. A close relationship between measurements taken from an image of the calcaneus and talus and the physical bones has been demonstrated (Agoada, 2018; Agoada and Kramer, 2018). Thus, the ability to use images to examine the morphology of the talus and calcaneus in an intact foot has been established. What is now needed is an investigation of the morphology of the talus and calcaneus in known foot types as determined by analysis from radiographic images. The results can then be applied to the evaluation of the talus and calcaneus from modern osteological collections, as well as from the hominin pedal fossil record, to better understand the morphologies of these bones as they relate to foot form, function and the evolution of the modern human foot.

Hypothesis: Linear and angular measurements of the talus and calcaneus measured on radiographic images of the weight-bearing foot are associated with adult human foot types.

Materials and Methods

The radiographic database of a Level 1 healthcare facility for a large metropolitan area was searched for the occurrence of weight-bearing lateral and anterior–posterior (AP) digital radiographs of patients taken in the standardized fashion (see Figures 1a and 3a). Approval of this project was obtained from the Institutional Review Board. Radiographs were ordered as part of a medical examination of patients to “rule out” acute injury. Patients with chronic pain as their primary diagnosis and children were excluded. From this database 103 radiographs were identified as useable for foot type classification.

Classification of foot type. To explore the relationship between talar and calcaneal measurements and foot type, the criteria for foot type classification needs to be established. The calcaneal inclination angle (CIA) as described in the literature (Sanner and Whitney, 2015b) was used to identify foot type, as this measurement is commonly associated with excessive midstance pronation and arch height. The subject’s foot type was classified as normal arch, low arch, or high arch based on measurements for the CIA reported in the literature (Lautzenheiser and Kramer, 2013; Sanner and Whitney, 2015a):

LA (Low Arch or pes planus): 15.99° or less

Includes SF (Severe flat foot): 10.00° or less

NA (Normal Arch): 16.00 – 24.99°

HA (High Arch or pes cavus): 25.00 -29.99°

Includes SC (Severe pes cavus): 30.00 ° or more

In addition to CIA, other linear and angular measurements have also been associated with arch configuration and foot type (Sanner and Whitney, 2015a). These include the Talocalcaneal Angle (sometimes referred to as the talocalcaneal divergence) in the AP view (APTCA) (Benedetti et al., 2010; Bourdet et al., 2013; Sanner and Whitney, 2015a); Talocalcaneal angle in the lateral view (LTCA) (Benedetti et al., 2010; Sanner and Whitney, 2015a); talocuboid angle in the AP view (TCUA) (Lautzenheiser and Kramer, 2013; Sanner and Whitney, 2015a); talar-first metatarsal angle (TFMA) or Méary's angle in the lateral view (Lee et al., 2005; Younger et al., 2005; Bourdet et al., 2013). (See Tables 1a for the list of the variables, Figures. 1-3b and the Appendix for definition and description.)

Associating these measurements with foot type as determined by the CIA measurement was performed to assess whether the foot type categorization used in this study is reinforced by variables described in the literature as also associated with arch type. The values of the following arch height ratios were calculated from the linear measurements to explore the relationship between relative linear bone measurements and linear foot measurements:

normalized navicular height (NNH) (AH/FL) and truncated normalization navicular height (TNNH) (AH/FLCM) (terms used by Menz and Munteanu, 2005, to describe these ratios).

Within-bone radiographic measurements of the talus and calcaneus were selected based on the known accuracy of these measurements for linear values (Agoada, 2018) and angular values (Agoada and Kramer, 2018). (See Tables 2a and 3a for a list of these variables, Figures 4-10 and the Appendix for definitions and descriptions.) A radiograph's suitability for use in this study was based on an analysis from the radiograph of the positioning of the foot in relation to the x-ray beam and receptor plate and the ability to identify the points used in a variable's measurements. Talus and calcaneus linear ratios were also created to assess whether relative relationships exist that may correlate with foot type that could not be identified by linear measures alone (Table 3).

All linear and angular measurements were taken using Osirix (Osirix Viewer, Geneva, Switzerland) and at least 10% were randomly chosen for repeated measurement a minimum of 2 months later. Intraclass correlation coefficients (ICC) using Pearson product-moment coefficient of correlation (r) between the initial and second set of measurements ranged from 0.67 to 0.99 ($p < 0.05$).

Descriptive statistics were calculated on the measurements taken from the radiographic images of the talus and calcaneus. Student t -test comparing the CIA measurements with the radiographic measurements of the talus and calcaneus were performed to identify the presence of significant differences in measurement dimensions between bone and radiograph. The degree to which measurements are associated was established using ordinary least squares regression and confirmed with reduced major axis analysis. Regression coefficient (b) and

coefficient of determination (r^2) values were examined to assess the relationship between measurements. Statistical significance was established using an alpha of 95%. Because 65 regressions were necessary, Bonferroni correction for multiple comparisons was performed, which yields statistical significant if $p \leq 0.05/65 \approx 0.001$. Descriptive statistics and other analyses were computed using Stata (V12, Statacorp, College Station, TX).

Results

Relationship between foot type (using CIA1) and other measurements (Tables 1a, 1b, 1c).

Of the 103 radiographs selected for foot type analysis, 45 were identified as individuals having lower than normal arches (pes planus), 37 had arches within the defined normal range, and 21 had arches above the average range (pes cavus) using CIA1 to establish foot type (Sanner and Whitney, 2015a). The possible metrics of foot type that were most strongly associated with foot type were an alternative method of measuring calcaneal inclination angle (CIA2) ($r^2 = 0.77$), talocalcaneal angle in the lateral view (LTCA) ($r^2 = 0.47$), and first metatarsal declination angle (FMDA) ($r^2 = 0.24$). As expected, the linear measurement having the strongest association with foot type was AH ($r^2 = 0.41$), as were the arch height indices truncated normalized navicular height (TNNH) for AH/FLCM and normalized navicular height (NNH) for AH/FL. Other linear foot measurements were not as strongly associated with the CIA. The radiographs examined in this study were derived from the same population as those from Lautzenheiser and Kramer (2013) for their study concerning linear and angular measurements of the human foot, reporting similar results to those recorded here for some of the foot measurement variables (see Table 5).

Relationship between foot type and within bone measurements (Tables 2a, 2b, 2c; 3a, 3b, 3c).

With the demonstration of a positive relationship between the CIA and other measurements associated with foot type, the relationships between within bone measurements of the talus and calcaneus with foot type variables were examined. From the 103 radiographs, 74 were chosen as suitable for calcaneus measurements (Tables 2a and 2b) and 68 for talus measurements (Tables 3a and 3b). Sixty-seven of those radiographs were used for both talus and calcaneus measurements. While linear measurements of the calcaneus demonstrated a weak association with foot type ($r^2 < 0.01-0.09$), most angular calcaneal measurements taken from the lateral view displayed a stronger association ($r^2 = 0.17-0.44$) (Table 2c). None of the talar linear and angular measurements demonstrated a strong association to foot type ($r^2 = 0.00-0.06$) (Table 3c).

Relationship between foot type and within bone measurement indices (Tables 4a, 4b, 4c, 4d).

Indices of linear measurements of the calcaneus and talus demonstrated little relationship to foot type. Most calcaneus indices were associated with foot type displaying a coefficient of determination of $r^2 = 0.11-0.13$. The weakest association was minimum anterior width of the calcaneus/maximum length of the calcaneus (MinAWCALx/MLCALx) ($r^2 = < 0.01$). The strongest associations for talus indices were talus maximum talar length/foot length (MaxLTALx/FL) ($r^2 = 0.11$), and maximum talar length/ foot length (MaxLTALx/FLCM) ($r^2 = 0.11$).

Discussion

Linear and angular measurements of the foot (Tables 1a, 1b, 1c).

The principle goal of this study is to examine, using weight-bearing radiographic images, the possible relationship between within-bone measurements of the talus and calcaneus and foot type. First, however, categorization of foot type as defined by Calcaneal Inclination Angle (CIA) (sometimes referred to as calcaneal pitch) was necessary. CIA is a major criterion for the assessment of foot type and arch height. For example, Sanner and Whitney (2015a) describe the CIA for the “normal range” as 18-20°, Bourdet et al. (2013) 16-19°, and Menz and Munteanu (2005) 21°. In most studies (including this study), the CIA is determined as an angle between the plantar surface of the calcaneus and the supporting surface, but some studies have used a line drawn from the most inferior point of the plantar surface of the calcaneus to the plantar surface of the fifth metatarsal head instead (Sanner and Whitney, 2015a) which produces a somewhat greater angle (CIA2 variable; see the Appendix). Thus, the results of this study based on foot type designation, should be comparable with other investigations using the same CIA definition.

The average CIA reported by Lautzenheiser and Kramer (2013) in their study of foot radiographs derived from the same population base was 19.59°, close to the average of 18.53° for all three groups and 20.22° for the normal type in this study (Table 5). The CIA used to categorize foot type in this study (CIA1) produced the following values (Table 1): normal arch (NA) 20.22°; low arch (LA) 12.85° high arch (HA) 27.73°. These results compare favorably with average values for CIA1 reported by Pehlivan et al. (2008) in 32 symptomatic and 24 asymptomatic flatfeet were $10.84^\circ \pm 2.49^\circ$ (range, 6° to 15°) and $12.45^\circ \pm 3.71^\circ$ (range, 4° to

20°), respectively.

Since the CIA was the only variable used to categorize foot type in this study, examination of a relationship between the CIA and foot function was performed by comparing the CIA measurements to other angular radiographic measurements used in assessing a weight-bearing foot for excessive subtalar joint pronation (Lee et al., 2005; Sanner and Whitney, 2015a). The CIA was associated with other measurements of the foot that are related to pes planus (CIA2, LTCA, FMDA, AH) (Table 1c). While some angles that have been associated the amount of subtalar joint pronation (APTCA, TUCA, TDA, and TFMA) had low relatively r^2 values, the use of the CIA measurement for foot type designation is supported by this study. Of note is that an excessively pronated foot can, however, present with a normal CIA (Root et al., 1977; Agoada, 1989).

Bourdet et al., (2013) did find that talocalcaneal divergence did not correlate with clinically excessive pronation, as demonstrated by heel valgus (APTC $r^2 = 0.06$ using coefficient of determination in this study). The talar declination angle (TDA) is reported to normally average about 21° (Sanner and Whitney, 2015a) and was found to be 20.26 by Lautzenheiser and Kramer (2013) for a sample from the same population pool as this study (Table 5). The reason that the TDA ($r^2 = 0.08$) is greater here than reported in other studies is unclear.

Linear and angular measurements of the talus (Tables 3c and 4d).

Harris and Beath (1948) concluded that the head and neck of the talus in the flexible flatfoot is shorter than in the normal foot. In our study, using a much larger sample size based on weight-bearing radiographs, no correlation between talus linear measurements and foot

type was found. Comparing talar measurements taken from CT scans of 10 individuals with symptomatic pes planus with 10 individuals scanned for acute injuries, Anderson et al. (1997) found significant differences between ratios of talar length with talar width, talar length with talar height, and head length with head width. The tali were narrower and shorter in height with heads that were more elongated in the pes planus individuals. In this study, within-bone linear indices were not strongly associated with foot type (Table 4). Relative talar length to foot length displayed (MaxLTALx/FL, MaxLTALx/FLCM displayed the strongest association with foot type ($r^2 = 0.11$) while indices for within bone talar measurements showed a weaker association ($r^2 = <0.01-0.07$). As with linear measurements, angular measurements taken for the talus did not correlate with foot type. That variations in angular measures of the talus did not correlate with foot types was unexpected, especially with angles of the talar neck to the body. In the weight-bearing foot, the neck of the talus runs in a medial and plantar direction, although the angle made by the neck's longitudinal axis to the talar body in the transverse plane has been noted to be variable (Day and Wood, 1968; Draves, 1986; Sarrafian and Kelikian, 2011). The neck axis also deviates downward in relation to the body creating an angle of inclination in the sagittal plane, which is also variable (Day and Wood, 1968; Draves, 1986; Sarrafian and Kelikian, 2011). According to Sanner and Whitney (2015a) a more plantarflexed talar neck is associated with an excessively pronated foot, as is a more plantarflexed sustentaculum tali in relation to the plane of support. In contrast to this observation, a less plantarflexed (and thus lower value for the talar inclination angle) has been described for non-human primates, which are considered to have a more primitive foot that lacks a medial longitudinal arch with weight-bearing (Morton, 1935; Lisowski, 1967). Since in the excessively pronated foot, the talus is

adducted in the transverse plane and plantarflexed in the sagittal plane, we expected that talar neck angles would be associated with foot type. While the inclination angle of the talar neck (IANTALx-1 and IANTALx-2) value averages (29.07° and 37.55°) were similar to those reported in the literature for physical bone (31.2° -37.5° (Day and Wood, 1968; Sarrafian and Kelikian, 2011), IANTALx, AHTALx, or ANTALx displayed little association with foot type ($r^2 = 0.00 - 0.04$).

During human postnatal development, the talus neck torsion increases, a condition also associated with the development of arches of the foot (Lisowski, 1967). Forefoot varus is a frontal plane structural position where the forefoot is an inverted position relative to the rearfoot at the level of the midtarsal joint. It has been described as due to inadequate frontal plane torsion of the head and neck of the talus that should occur during normal ontogeny of the foot (Valmassy, 1996). To compensate for this position and bring the forefoot down to the weight-bearing surface, the subtalar joint will pronate. The result may be a pes planus foot. Thus, it is possible that the principle plane of functional variation is the frontal plane, specifically the torsion of the talar head, a morphological feature associated with functional variation (Lisowski, 1967; Day and Wood, 1968) that cannot be evaluated on AP and lateral radiographs.

It is also possible, based on the results of this study, that structural variation in talar morphology of the body and head-neck relationships are not related to foot type. Considering the importance of the talus in foot function and biomechanics, this would be unexpected. Nonetheless, the lack of a relationship between talar morphology and foot type could be explained in a number of ways. For example, given that the position of the talus in the foot is dependent upon the adjacent bones and capsular structures because no muscle inserts directly

into it (Grice, 1952). It is possible that the relationship of the talus to foot function in habitual bipedal gait is dependent upon soft tissue attachments and relationships to the other bones with which the talus articulates. If this is correct, then the morphology of other bones of the foot need to be investigated using radiographic imaging to understand the relationship between variation in their bony osteology to foot function and type. The morphological variation of the human talus as it related to modern human foot biomechanics requires further study.

Linear and angular measurements of the calcaneus (Tables 2c and 4c).

Linear measurements of the calcaneus, as well as indices created from the linear measurements demonstrate weak associations with foot type. In this study, calcaneal length variable (MLCAL2x) average 190.0 mm, close to the average of 189.3 mm in a study by Lautzenheiser and Kramer (2013) from the same population pool (Table 5). As noted, truncated normalized navicular height (TNNH) and normalized navicular height (NAH) were used to normalize differences in foot length vs. arch height for comparison. Both linear calcaneal measurements were positively associated with foot length ($r^2 = 0.12$), though the association was not strong and did not demonstrate a within bone relationship. Relative body height of the calcaneus to length of the calcaneus was the only within bone index that displayed a similar association ($r^2 = 0.13$).

Most calcaneus angular measurements using the lateral view were positively associated with foot type ($r^2 = 0.00-0.44$) (Table 2c). The foot angular values were greater in the low arch group for the following variables: APTCA, TCUA, and TFMA were smaller CIA1, CIA2, AALCALx,

and LTCA (Table 2b). The differences in angle measurements among foot type are in agreement with those reported previously Sanner and Whitney (2015b). The GACALx measurement (which at $r^2 = 0.03$ showed little association with foot type) displayed a greater than expected difference between this study (122.40 mm average for normal, 120.7 mm average all three categories) and that reported by Lautzenheiser and Kramer (2013) (125.51 mm average) derived from the same population as this study (Table 5).

These results can be interpreted based on an understanding of the morphology of the calcaneus. The anterior, or distal, surface of the calcaneus is wholly articular, forming the calcaneocuboid Joint (CCJ) with the cuboid bone. This joint is a concavo-convex or saddle shaped, allowing very little motion between the two articular surfaces. The facet is convex from medial to lateral and concave from superior to inferior. A shelf like projection, the beak of the calcaneus, is located at the superiomedial aspect of the articular surface, superior to the cuboid bone (Bojsen-Moller 1979; Sarrafian and Kelikian, 2011). On the lateral weight-bearing radiographs the CCJ, as reflected by the AALCALx, appears to be roughly perpendicular to the supporting surface. Thus, it would be expected that, as the calcaneus becomes more parallel to the supporting surface with increased pronation (as in the low arch foot) the closer this measurement would be to 90°. This is reflected in the measurements, where the AALCALx is smaller in the low arch and greater in the normal and high arch foot. Of note is that a “flat CCJ” is seen in pes planus; a sellar CCJ is seen in the cavus foot (Landry and Agoada, 1986; DeSilva et al., 2014). The AALCALx measurements suggest a flatter foot is associated with a flatter, less contoured CCJ in the sagittal plane, producing small measurement and functionally less stable foot.

The middle talar articular facet of the calcaneus is located on the superior surface of the sustentaculum tali, a shelf of bone projecting from the medial surface of the calcaneus. The angulation of the sustentaculum in relationship to the body in the sagittal plane may vary as well. It is oriented from a superior-posterior to an inferior-anterior direction, with an angle averaging 46°, with a range of 30° to 60° degrees (Sarrafian and Kelikian, 2011). In this study, the average range in for the AIMTFCALx, depending on foot type is between 46.62° (low arch) and 53.84° (high arch) (Table 4). Since the middle facet is located on the sustentaculum tali, the angle of this surface should reflect the slope of the sustentaculum tali. The similarity of the measurements between AIMTFCALx in this study and that reported by Sarrafian and Kelikian (2011) for the physical bone support the conclusion that AIMTFCALx represents the slope of the sustentaculum tali.

The sustentaculum tali has been described by Harris and Beath (1948) as being important in providing support for the talar head. They believed that a major difference between the flexible flatfoot and normal foot is in the support by the sustentaculum tali. As noted, our study found no association between plantarflexion of the talar neck in relationship to the talar body (IANTALx). A similar lack of a relationship was expected for AIMTFCALx since this angle should reflect that of the talar neck. However, AIMTFCALx did have an association with foot type ($r^2 = 0.17$), with a lower value (46.62°) than either the normal arch (49.52°) or high arch (53.84°) foot types. Harris and Beath (1948) believed that in the flexible flatfoot the sustentaculum tali is narrow rather than being broad, rounded, and running forward to the anterior margin of the talus as in the normal foot, thus lacking the “firm” support for the talar neck. While they did not address the slope of the sustentaculum tali in support of the talus in

their text, after reviewing the photos of the calcaneus they used in their paper (Figure 16-A, page 127), it does appear that the calcaneus they identified as providing firmer support also had a greater slope of the sustentaculum tali. Of note, the other features of the sustentaculum tali described by Harris and Beath (1948) as differentiating a flexible flatfoot from a normal foot could not be evaluated adequately on the AP and Lateral views of the foot.

The posterior articular facet for the talus is located on the middle third of the bone and is oval in shape. It is markedly convex along its longitudinal axis, which runs from a posterior medial to an anterior lateral direction. This facet articulates with the inferior surface of the body of the talus. AIPTFCALx represents the angle of the articular surface for the body of the talus and in this study, like AIMTFCALx, is smaller in the low arch (foot type 43.98° vs. 46.74° and 54.41°, for normal and high arch), suggesting that a decrease in these angle values is indicative of a more flexible foot. This may help explain why the amount of plantarflexion in the talar neck (IANTALx) was not more strongly associated with an excessively pronated foot i.e., flexibility of the talocalcaneal joint is not related to plantarflexion of the talar neck or an increase in the slope of the sustentaculum tali. Rather, it appears to be related to a decrease support for the body of the talus as represented by AIPTFCALx.

Böehler's angle (BTACALx) ($r^2 = 0.34$), compression angle of the calcaneus (CACALx) ($r^2 = 0.44$), and front angle of the calcaneus (FACALx) ($r^2 = 0.29$) were all smaller in the low arch foot than either the normal or high arch foot, suggesting perhaps a less angulated calcaneus in the low arch foot. Böehler's angle, used to assess calcaneal fractures (Böehler, 1931; Khoshhal et al., 2004), has been described as normally between 20-45° (Sanner and Whitney, 2015a). In

this study, the average of all foot types was 33.30°, close to the average of 33.5° as reported by Lautzenheiser and Kramer (2013) for their study drawn from the same population sample (Table 5). They did not, however, find a positive correlation between the “calcaneal orientation to the ground” and “angles within the calcaneus” which would include Böehler’s angle.

TACALax and TACALbx values should add up to 90°, so it is expected that their association with foot type would be similar ($r^2 = 0.09$). The measurements for both low arch and normal foot types were quite similar to each other and quite different than the high arch foot, suggesting that variation in the shape of the posterior calcaneus may be a morphologic feature that differentiates the high arch foot rather than the pes planus foot. The calcaneal angular measures related to the articular surfaces with the talus (LTCA, AIPTFCALx, AIMTFCALx) and the cuboid (AALCALx) as well those related to the shape of the calcaneus (BTACALx, CACALx, and FACALx) were more strongly associated with foot type in the sagittal plane. The talocalcaneal articulation in the AP view, as represented by AAAPCALx ($r^2 = 0.02$) was, however, not associated. The shape of the calcaneal tuberosity relates, at least in part, to the insertion of the Achilles tendon and plantar fascia (Griffin et al., 2015) and appears to have a weaker association to foot type as reflected by the TACALax and TACALbx r^2 values (0.09).

Based on the results of this study, it may be hypothesized that the shape of the talus does not play a major role in arch height and thus the pes planus foot type, in modern humans. Our results suggest that variation seen in the talus of modern humans does not significantly impact arch configuration. Measurements of the talus, including the talar neck angle measurements, both in the transverse and sagittal planes, did not appear to be strongly

associated with arch height. A more ape-like configuration (higher in the transverse plane and lower in the sagittal plane) (Lewis, 1980) is expected if the pes planus foot type of modern humans is more “primitive.” Using variation in gross talar morphology, at least the metrics measurable on the radiographs used in this study, would not appear to be especially informative about arch form in extinct hominins. Variations in the shape of the calcaneus as demonstrated by the associations between these angular measurements and foot type, however, does suggest that a relationship exists between calcaneal morphology and arch height (and thus pes planus) in modern humans. Studying calcaneal morphology might be informative in assessing the medial longitudinal arch in extinct hominin, especially as it may relate to the “locking mechanism” of the calcaneocuboid joint (Bojsen-Moller, 1979; Lewis, 1980) and the effects of the windlass mechanism on the shape of the calcaneus (Hicks, 1954; Griffin et al., 2015). The associations of within bone angles that represent articular surfaces and shape of the calcaneus with foot type suggests that this bone, rather than the talus, plays an important role in determining arch height and foot biomechanics in bipedal gait in modern humans. As with the talus, there might be other size and shape differences useful in identifying a pes planus foot type from the calcaneus that cannot be evaluated from plain radiographs.

Conclusion

The benefit of using radiographic imaging in the field of physical anthropology to investigate morphology and function is well recognized (Hinton, 2013). Because the radiographic measurements of talus and calcaneus in the transverse and sagittal planes have been demonstrated to be associated with measurement of the physical bone (Agoda, 2018;

Agoada and Kramer, 2018), it is now possible to further analyze these bony elements in ways that cannot be performed using radiographic images alone.

Analysis of the radiographs used in this study suggests that the association between certain angular measurements of the calcaneus and foot type may be useful in the identification of pes planus. What has not been demonstrated is as strong an association between angular measurements of the talus and linear measurements of both the talus and calcaneus and the pes planus foot type. These results leave unanswered questions concerning other possible relationships between the morphologic variations seen in the calcaneus and talus of humans and foot type and foot function. The morphology of the talus and (especially) the calcaneus deserves further investigation into their relationship to the pes planus foot type to assist in the understanding of foot biomechanics and the evolution of the modern foot from hominin ancestors.

Chapter 4: Appendix

All linear and angular measurements were made using Osirix (Osirix Viewer, Geneva, Switzerland). Except where noted, all within-bone variables are the same as those described by Agoada (2018) for linear measurements and by Agoada and Kramer (2018) for angular measurements.

Angular variables of the foot lateral view

Calcaneal Inclination Angle (CAI1) (Figure 1)

Method: Angle formed by a line connecting the inferior limit, distal facet of the calcaneus (the CCJ) and distoinferior limit of the calcaneal tuberosity* and the plane of support (POS), sometimes called the calcaneal pitch (Saltzman et al., 1995; Menz and Munteanu, 2005; Bourdet et al., 2013; Lautzenheiser and Kramer, 2013). (*The line connecting the inferior limit, distal facet of the calcaneus and distoinferior limit of the calcaneal tuberosity, the calcaneal inclination line (CIL), is not necessarily parallel to the longitudinal axis of the calcaneus (LAC)).

Calcaneal Inclination Angle (CAI2) (Figure 1)

Method: Angle formed by the calcaneal inclination line and a line connecting the inferior surface of the calcaneus and the most inferior point of the 5th metatarsal head (Sanner and Whitney, 2015a).

Talocalcaneal Angle in the Lateral View (LTCA) (Figure 1)

Definition: Angle formed between the calcaneal inclination line and the axis of the talar neck (Sanner and Whitney, 2015a).

Talar Declination Angle (TDA) (Figure 1)

Definition: Angle formed where the axis of the talar neck intersects the plane of support (Whitney, 1978; Sanner and Whitney, 2015a).

Talar-First Metatarsal Angle (TFMA) (Figure 1)

Definition: Angle formed by the longitudinal axis of the talus and longitudinal axis of the first metatarsal (Lee et al., 2005; Pehlivan et al., 2008; Sensiba et al., 2010). This angle is sometimes referred to as Méary's angle (Younger et al., 2005; Bourdet et al., 2013).

First Metatarsal Declination Angle (FMDA) (Figure 1)

Definition: Angle formed by the longitudinal axis of the first metatarsal and the plane of support.

Linear variables of the foot lateral view

Arch Height (AH) (Figure 2)

Definition: Height of the medial longitudinal arch in the weight-bearing foot measured as the distance between the most inferior point of the navicular and the plane of surface, perpendicular to the Foot Length line (FLL) (McCroly et al., 1997; Menz and Munteanu, 2005; Sanner and Whitney, 2015a).

Foot Length Line (FLL) (Figure 2)

Definition: Length of the foot, from the most Inferior point of the calcaneus to the most inferior point of the first metatarsal head, parallel to the plane of support (Demp, 1989). (All horizontal length distances are measured parallel to the foot length line, and thus to the plane of support.)

Foot Length (FLCM) (Figure 2)

Definition: Length of the foot from posterior calcaneus to distal first metatarsal head (Lautzenheiser and Kramer, 2013).

Foot Length (FL) (Figure 2)

Definition: Length of the foot, from the posterior aspect of the calcaneus to the most distal point of the distal phalanx of the hallux (Lautzenheiser and Kramer, 2014).

Total foot length (TFL) (Figure 2)

Definition: Length of the foot, from the posterior skin line of the heel and the distal tip of the skin line of the hallux (Lautzenheiser and Kramer, 2014). The results of the TFL measurements are not reported in this paper, since the entire foot was not included on several of the radiographs.

Cyma Line Measurement (CLAH) (Figure 2)

Definition: Distance between a vertical line representing the AH measurement and a vertical line drawn from the most anterior point of the cuboid perpendicular to the supporting surface (Agoada, 2018).

Cyma Line Measurement (AHFLCM) (Figure 2)

Definition: Distance between a vertical line drawn from the most anterior point of the anterior talus perpendicular to the supporting surface and a vertical line drawn from the most anterior point of the calcaneocuboid joint perpendicular to the supporting surface.

Cyma Line (CL) (Figure 2)

Definition: Line through CCJ and TNJ in the lateral view, creating a “Lazy S” in the normal foot (Sanner and Whitney, 2015a).

Angular variables of the foot AP view

The Talocalcaneal Angle in the AP view (APTCA) (Figures 3a and 3b)

Definition: Angle formed by a line connecting the longitudinal axis of the rearfoot (LARF) and longitudinal axis of the talar head and neck (Sanner and Whitney, 2015a).

Talocuboid Angle (TCUA) (Figure 3b)

Definition: Angle formed by a line connecting the longitudinal axis of the talar head and neck and a tangent along the lateral side of the cuboid (Sanner and Whitney, 2015a).

Linear variables of the talus lateral view

Maximum Talar Length (MaxLTALx) (Figure 4)

Definition: The distance between the most posterior point of the posterolateral tubercle and the most anterior point of the talar head. If an os trigonum is present, it is not included in the measurement.

Maximum Height of the Body of the Talus (MaxHB TALx) (Figure 4)

Definition: The distance between the most superior point of the trochlear lateral surface (either medial or lateral) and the most inferior point of the lateral process of the talar body at the apex.

Body Height of the Talus (BHTALx) (Figure 4)

Definition: The distance between the most superior point of the trochlear surface (either medial or lateral) and most inferior point of the talus.

Method: A line is drawn between the most inferior point of the talar head and the most inferior point of the posteromedial tubercle of the talus. BHTALx is the distance between the superior surface of the talus and the point perpendicular to the line.

Maximum Length Fibular Malleolar Facet of the talus (MaxLFMTALx) (Figure 4)

Definition: The distance between the most anterior point of the border of the lateral surface and the most posterior margin of the lateral surface, parallel to the body of the talus.

Method: A line is drawn roughly parallel to the longitudinal axis of the talus (LAT). The most anterior aspect is the point where the neck and body meet; the most posterior point is where this line transects the posterior border.

Maximum Length of Fibular Malleolar Facet (MaxLFMTALx) (Figure 4)

Definition: The distance between the most anterior point of the border of the lateral surface and the most posterior margin of the lateral surface.

Method: A line is drawn roughly parallel to the longitudinal axis of the talus (LAT). The most anterior aspect is the point where the neck and body meet; the most posterior point is where this line transects the posterior border.

Maximum Length Trochlear Surface of the talus (MaxLFTSTALx) (Figure 4)

Definition: The maximum distance between the most anterior point and most posterior point of the trochlear of the talus.

Method: A line is drawn between the most anterior aspect of the trochlear (the point where the neck and body meet anteriorly) and the most posterior aspect of the trochlear (the point where this line transects the posterior border at its most posterior point).

Angular variables of the talus lateral view

Inclination Angle Neck of the Talus (IANTALx-1) (Day and Wood, 1968) (Figure 5)

Definition: Angle created by the intersection of the longitudinal axis of the neck of the talus and the longitudinal axis of the body of the talus as represented by the line *MaxLFMTALx*. The angle of inclination of the talar neck represents the angle of inclination of the talar neck relative to the body in the sagittal plane.

Method: The axis of the neck is determined by a line drawn from the approximately midpoint of the articular surface of the head, through a point midway between the upper and lower borders of the neck. This axis may also be roughly parallel to the inferior border of the neck, if observable. IANTALx is formed by the intersection of these two axes. The longitudinal axis of the neck may or may not intersect the longitudinal axis of the body at the point where the vertical axis intersects the horizontal axis of the body. (This measurement for IANTALx was not compared to the physical bone measurement from Agoada and Kramer, 2018.)

Inclination Angle Neck of the Talus (IANTALx-2) (modified from Day and Wood, 1968) (Figure 5)

Definition: Angle created by the intersection of the longitudinal axis of the neck of the talus and the longitudinal axis of the body of the talus as represented by the line *MaxLFTSTALx*. (This is the definition used for IANTALx in Agoada and Kramer, 2018.)

Linear variables of the talus AP view

Maximum Length of the Head and Neck of the Talus (MaxLHNTALx) (Figure 6)

Definition: The distance between the most anterior point of the head of the talus and the point where the base of the neck is widest (flares out) at the body of the talus at the lateral border of the neck.

Method: A straight line is drawn parallel to the lateral border of the talar neck. The lateral border of the neck is parallel to the section before it flares out at its base. A second line is drawn perpendicular to the first, traversing the widest point of the talar neck at the lateral border (where it flares out to become continuous with the body). MaxLHNTALx is measured as the distance between the most anterior aspect of the head and the second line drawn, perpendicular to that line.

Maximum Width of the Head of the Talus (MaxWHTALx) (Figure 6)

Definition: The distance between the most medial and the most lateral points of the head of the talus.

Minimum Width of the Neck of the Talus (MinWNTALx) (Figure 6)

Definition: The shortest distance between the medial and lateral borders of the talar neck, perpendicular to the long axis of the lateral border.

Method: The measured line is drawn between the narrowest point on the lateral border and where it traverses the medial border.

Angular variables of the talus AP view

Angle of the Head of the Talus (AHTALx) (Figures 6)

Definition: The angle of the head of the talus in relation to the talar neck.

Method: The angle is formed by a line between the widest medial and lateral points of the head of the talus and a line parallel to the lateral border of the neck of the talus.

Angle of the Neck of the Talus (ANTALx) (Figures 6)

Definition: The angle of the head of the talus in relation to the talar neck at its base.

Method: The angle is formed by a line between the widest medial and lateral points of the head of the talus and a line parallel to the base of the lateral border of the neck of the talus as it begins to curve laterally. The line is thus parallel to the section of the lateral border of the neck where it flares out at its base.

Linear variables of the calcaneus lateral view

Maximum Length of the Calcaneus (MLCALx) (Figure 7)

Definition: The distance between the most anterior point of the calcaneus and the most posterior point of the calcaneal tuberosity, measured roughly parallel to the long axis of the calcaneus (LAC). The long axis of the calcaneus is not necessarily parallel to the calcaneal inclination line (CIL).

Maximum Length of the Calcaneus (MLCAL- 2x) (Figure 7)

Definition: The distance between the anterior border of the lateral surface of the calcaneus, at the point where it begins to curve superiorly, and the most posterior point of the calcaneal tuberosity, measured roughly parallel to the long axis of the calcaneus.

Body Height of the Calcaneus (BHCALx) (Figure 7)

Definition: The distance between the most inferior point of the calcaneal tuberosity to the most superior point of the posterior articular facet.

Method: Measurement is taken from a line extended distally from the plantar aspect of the calcaneal tuberosity, parallel to the long axis of the calcaneus. BHCALx is measured perpendicular to this line.

Minimum Body Height of the Calcaneus (MinBHCALx) (Figure 7)

Definition: The minimum distance between the superior border of the calcaneus posterior to the posterior articular facet superiorly, and the line representing the most superior point of the inferior border of the lateral surface, anterior to the calcaneal tuberosity.

Minimum Anterior Height of the Calcaneus (MinAHCALx) (Figure 7)

Definition: The distance between the most inferior point of the anterior border of the calcaneus, and the superior border of the lateral surface, just posterior to the articular face for the cuboid, and anterior to the superior prominence of the lateral surface. This measurement is roughly perpendicular to the long axis of the calcaneus.

Method: A straight line is drawn from the most inferior point of the calcaneal tuberosity distally roughly parallel to the long axis of the calcaneus. A second line is drawn perpendicular to this line, going through the most inferior point to the superior border of the distal calcaneus. MinAHCALx is measured along that line as the distance from the most inferior point of the distal aspect of the calcaneus to where it transects the superior border of the distal aspect of the calcaneus.

Angular variables of the calcaneus lateral view

Angle of Inclination Posterior Talar Facet of the Calcaneus (AIPTFCALx) (Figure 8)

Definition: The angle between the posterior talar articular surface and the longitudinal axis of the calcaneus (Modified from Bruckner, 1987).

Method: A line is drawn from the highest point of the posterior talar articular surface through an inferior point just anterior to where the surface curves into the inferior border of the sinus tarsi. A second line is drawn parallel to the longitudinal axis of the calcaneus. This is the angle where these two lines intersect.

Angle of Inclination Middle Talar Facet of the Calcaneus (AIMTFCALx) (Figure 8)

Definition: The angle between the middle talar articular surface and the longitudinal axis of the calcaneus. This measurement represents the slope of the sustentaculum tali. It is termed as the angle of inclination of the sustentaculum tali by Sanner and Whitney (2015a), described as the angle between lines drawn parallel to the surface of the middle articular facet and parallel to the inferior surface of the calcaneus).

Method: A line is drawn parallel to the surface of the middle talar articular facet. The line should be parallel to the slope of the surface at middle section of the middle talar facet that is observable (usually the lower ½ of the midsection of the slope, excluding any extreme slope at the most superior aspect, or reduced slope at the distal aspect, if visible). The angle is created where this line and the line drawn parallel to the longitudinal axis of the calcaneus intersect. If articular surface of the middle articular facet is not clearly observable on radiograph, the radiograph should not be used for this measurement.

Anterior Angle Lateral View of the Calcaneus (AALCALx) (Figure 8)

Definition: The angle between the distal anterior border and the longitudinal axis of the calcaneus (Modified from Bruckner, 1987).

Method: A line is drawn parallel to the anterior border of the lateral surface of the calcaneus. This line usually connects the most superior and inferior points of the anterior surface, though more importantly, should be roughly parallel to the anterior aspect of the calcaneus, usually at its midsection. A second line is drawn from the anterior inferior point of the calcaneus parallel to the longitudinal axis of the calcaneus. The angle is created where these two lines intersect.

Böhler's Angle of the Calcaneus (BTACALx) (Figure 9)

Definition: The angle formed by the anterior and posterior surfaces of the superior border of the calcaneus (modified from Sarrafian and Kelikian, 2011). Böhler's (sometimes written as Böhler's) angle may also be referred to as Böhler angle or Böhler's tuber angle.)

Method: An acute angle is formed anteriorly by a line drawn from the superior aspect of the calcaneal tuberosity and highest point of the calcaneus (which may or may not be the most superior point of the posterior talar articular surface) and a line drawn from the highest point of the calcaneus and the most superior point of the anterior aspect of the calcaneus (lateral or medial).

Gissane's Angle of the Calcaneus (GACALx) (Figure 9)

Definition: The angle formed by the posterior talar articular surface and the superior surface anterior to it as seen on the lateral surface of the calcaneus (modified from Lautzenheiser and Kramer, 2013).

Method: One line is drawn from the superior point of the posterior facet of the calcaneus to the inferior point on the posterior facet (Parallel to AIPTFCALx). A second line is drawn from the most inferior point of the posterior articular facet at the inferior border to the most superior point of the anterior border (or to the most superior point just proximal to the anterior border) of the calcaneus. (This line is usually parallel to the superior border). The angle is measured where these lines intersect at the inferior point of the posterior talar articular facet (see Khoshhal et al. (2004) for variations on this measurement).

Compression Angle of the Calcaneus (CACALx) (Figure 9)

Definition: This angle has been used to assess traumatic compression of the posterior subtalar joint by comparing the superior aspect anterior to the posterior border of the posterior talar facet with the longitudinal axis of the calcaneus (modified from Saxena and Weddington, 1989).

Method: The angle is created by a line connecting the superior surface of the superior point of the calcaneus and the superior aspect of the distal calcaneus (the more inferior line used to create Böehler's angle) and a line parallel to the longitudinal axis of the calcaneus. The angle is created where the two line intersect.

Front Angle of the Calcaneus (FACALx) (Figure 9)

Definition: The angle created by the superior point of the calcaneal tuberosity (Modified from Riepert et al, 1996).

Method: One line is drawn from the most superior point of the calcaneal tuberosity to the most inferior point of the distal anterior calcaneus. A second line is drawn from the inferior point of the distal anterior calcaneus parallel to the long axis of the calcaneus. The angle is measured where the two lines intersect at the inferior distal anterior aspect of the calcaneus.

Tuber Angle of the Plantar Calcaneus (TACALax) (Figure 9)

Definition: The angle created by the posterior surface of the calcaneal tuberosity and the longitudinal axis of the calcaneus (Modified from Riepert et al., 1996). The angle has been used to evaluate the degree of posterosuperior prominence of the calcaneus, termed Haglund's deformity, if pronounced, on radiographs by comparing the posterosuperior surface line of the calcaneus with the plantar calcaneal line. TACALax is similar to the Phillip and Fowler angle of the calcaneus as described by Gutierrez et al. (2013).

Method: A line is drawn from the most superior point of the calcaneal tuberosity roughly parallel to the upper half of the posterior surface of the calcaneus tuberosity. Because of the variation in the slope of sections comprising the upper half of the posterior surface of any one bone, the parallel line may be difficult to identify. It may be parallel to either the middle section of the upper half, or a line drawn between the slope of the superior 1/3 and the slope at the border just superior to the most prominent aspect of the posterior calcaneus. The line should be roughly parallel to the posterosuperior surface of the calcaneus (whichever of the above appears most appropriate). Thus, it may be necessary to estimate the slope by visually "averaging out" the observable differences in the slopes. The angle is measured at the intersection of this parallel line and a line parallel to the longitudinal axis of the calcaneus.)

Tuber Angle of the Distal Calcaneus (TACALbx) (Figure 9)

Definition: The angle created by a line tangent to the most posterior point of the calcaneal tuberosity (excluding any prominent posterior projecting spur), perpendicular to the longitudinal axis of the calcaneus, and a line parallel to the posterior surface of the calcaneal tuberosity superiorly.

Method: A line is drawn from the most posterior point of the calcaneal tuberosity perpendicular to the long axis of the calcaneus. The angle is measured at the intersection of that line and the line parallel to the posterior surface of the calcaneus tuberosity (see TACALax).

Linear variables of the calcaneus AP view

Minimum Anterior Width of the Calcaneus (MinAWCALx) (Figure 10)

Definition: The distance between the medial and lateral borders of the calcaneus, at the level of the cuboid articular facet. However, since the medial and lateral borders of the calcaneus maybe difficult to identify, this measurement is taken as the distance between the most medial (and proximal) and most lateral (and distal) points of the calcaneal articular surface on the *cuboid*.

Angular variables of the calcaneus AP view

Anterior Angle AP View of the Calcaneus (AAAPCALx) (Figure 10)

Definition: The angle created by a line drawn parallel to the distal anterior border of the calcaneus and a line parallel to the lateral border of the distal aspect of the calcaneus, exclusive of any exostosis or bony prominence protruding from the lateral border.

Method: The anterior line is drawn parallel to the anterior border, exclusive of where the surface flares anteriorly as part of the anterior articular facet medially, or where the border curves proximally. The anterior line should be parallel to the calcaneocuboid joint border centrally, before it curves proximally, which represents the anterior border of the calcaneus superiorly. However, the anterior border may be difficult to identify. In that case, the least angulated section of the most distal aspect of the border (usually at the more lateral aspect of the anterior border) may be used. If the anterior border is not clearly observable, a line connected the anterior-medial and anterior lateral borders may also be used. A line parallel to the posterior border of the cuboid may be used if the anterior border of the calcaneus is not observable. The lateral line is drawn parallel to the lateral border of the calcaneus, exclusive of any exostosis or bony prominence protruding from the lateral border. The line is usually parallel to the most proximal portion of the lateral border observable. The angle is measured where these two axes intersect.

Chapter 4: Literature cited

- Agoada D. 1989. The relationship of human footprints to actual foot configuration. *Am J Phys Anthropol* 75:181-182.
- Agoada D. 2018. The relationship between linear osteological and radiographic measurements of the human calcaneus and talus. *Anat Rec* 301:21-33.
- Agoada D, and Kramer PA. 2018. The relationship between angular osteological and radiographic measurements of the human talus and calcaneus. *J Am Podiatr Med Assoc*. In review.
- Anderson JG, Harrington R, and Ching RP. 1997. Alterations in talar morphology associated with adult flatfoot. *Foot Ankle Int* 18:705-709.
- Anjaneyulu K, Philips C, Tamang BK, and Kumar A. 2014. Patterns of talar articulating facets in adult human calcanei from North-East India and their clinical correlation. *Asian J Med Sci* 5:89-93.
- Barnett CH, and Napier JR. 1952. The axis of rotation at the ankle joint in man. Its influence upon the form of the talus and the mobility of the fibula. *J Anat* 86:1-9.
- Benedetti MG, Berti L, Straudi S, Ceccarelli FC, and Giannini S. 2010. Clinicoradiographic assessment of flexible flatfoot in children. *J Am Podiatr Med Assoc*. 100:463-471.
- Berger LR, Hawks J, de Ruiter DJ, Churchill SE, Schmid P, Delezene LK, Kivell TL, Garvin HM, Williams SA, DeSilva JM et al. . 2015. *Homo naledi*, a new species of the genus *Homo* from the Dinaledi Chamber, South Africa. *eLIFE* 4:e09560.
- Böehler L. 1931. Diagnosis, pathology, and treatment of fractures of the os calcis. *J Bone Joint Surg* 13:75-89.
- Bojsen-Moller F. 1979. Calcaneocuboid joint and stability of the longitudinal arch of the foot at high and low gear push off. *J Anat* 129:165-176.
- Bonnet WL, and Baker DR. 1946. Diagnosis of pes planus by x-ray. *Radiology* 46:36-45.
- Bourdet C, Seringe R, Adamsbaum C, Glorion C, and Wicart P. 2013. Flatfoot in children and adolescents. Analysis of imaging findings and therapeutic implications. *Orthop Trauma: Surg Res* 99:80-87.
- Boyle EK, and DeSilva JM. 2015. A Large *Homo erectus* Talus from Koobi Fora, Kenya (KNM-ER 5428), and Pleistocene Hominin Talar Evolution. *PaleoAnthropol* 1:1-13.

- Bruckner J. 1987. Variations in the human subtalar joint. *J Orthoped Sports Phys Ther* 8:489-494.
- Bruckner J. 1997. Subtalar variation and heel spurs. *Lower Extrem* 4:25-33.
- Bubra PS, Keighley G, Rateesh G, and Carmody D. 2015. A population of patient-specific adult acquired flatfoot deformity models before and after surgery. *J Fam Med Primary Care* 4:26-29.
- Cavanagh PR, and Rodgers MM. 1987. The arch index: A useful measure from footprints. *J Biomech* 20:547-551.
- Day MH, and Wood BA. 1968. Functional affinities of the Olduvai hominid 8 talus. *Man* 3:440-455.
- Demp PH. 1989. A mathematical taxonomy to evaluate the biomechanical quality of the human foot. *Int J Math Comput Model* 12:777-790.
- DeSilva JM. 2008. Vertical climbing adaptations in the anthropoid ankle and midfoot: implications for locomotion in Miocene catarrhines and Plio-pleistocene hominins. (PhD Dissertation) University of Michigan.
- DeSilva JM. 2009. Functional morphology of the ankle and the likelihood of climbing in early hominins. *Proc National Acad Sci USA* 106:6567-6572.
- DeSilva JM. 2010. Revisiting the "midtarsal break". *Amer J Phys Anthropol* 141:245-258.
- DeSilva JM, Bonneannee R, Swanson Z, Gill CM, Sobel M, Uy J, and Gill SV. 2015. Midtarsal break variation in modern humans: Functional causes, skeletal correlates, and paleontological implications. *Amer J Phys Anthropol* 156:543-552.
- DeSilva JM, Gill CM, Swanson Z, Bonneannee R, and Gill SV. 2014. Reconstructing foot form and function in early hominins using modern human models. *Amer J Phys Anthropol* 153:104-105.
- DeSilva JM, and Gill SV. 2013. Brief communication: A midtarsal (midfoot) break in the human foot. *American journal of physical anthropology* 151:495-499.
- DeSilva JM, Holt KG, Churchill SE, Carlson KJ, Walker CS, Zipfel B, and Berger LR. 2013. The lower limb and mechanics of walking in *Australopithecus sediba*. *Science* 340:1232999-1232991-1232999-1232995.
- DeSilva JM, and Papakyrikos A. 2011. A case of valgus ankle in an early Pleistocene hominin. *Int J Osteoarchaeol* 21:732-742.

- DeSilva JM, Proctor DJ, and Zipfel B. 2012. A complete second metatarsal (StW 89) from Sterkfontein Member 4, South Africa. *J Human Evol* 63:487-496.
- DeSilva JM, and Throckmorton ZJ. 2010. Lucy's flat feet: the relationship between the ankle and rearfoot arching in early hominins. *PloS one* 5(12):e14432.
- DeSilva JM, Zipfel B, Van Arsdale AP, and Tocheri MW. 2010. The Olduvai hominid 8 foot: adult or subadult? *J Human Evol* 58:41-423.
- Draves DJ. 1986. *Anatomy of the Lower Extremity*. Baltimore: Williams and Wilkins.
- Ezema CI, Abaraogu UO, and Okafor GO. 2014. Flat foot and associated factors among primary school children: A cross-sectional study. *Hong Kong Physio* 32:13-20.
- Gebo DL, and Schwartz GT. 2006. Foot bones from Omo: implications for hominid evolution. *Amer J Phys Anthropol* 129:499-511.
- Giza E, Cush G, and Schon LC. 2007. The flexible flatfoot in the adult. *Foot Ankle Clin N Am* 12:251-271.
- Green DR, Whitney AK, and Walters P. 1979. Subtalar joint motion A simplified view. *J Amer Podiatr Med Assoc* 69:83-91.
- Grice DS. 1952. An extra-articular arthrodesis of the subastraglar joint for correction of paralytic flat feet in children. *J Bone Joint Surg* 34A:927-940.
- Griffin NL, Miller CE, Schmitt D, and D'Aout K. 2015. Understanding the evolution of the windlass mechanism of the human foot from comparative anatomy: Insights, obstacles, and future directions. *Amer J Phys Anthropol* 156:1-10.
- Gutierrez P, Navarro M, and Ojeda M. 2013. Radiologic morphology of the calcaneus. *J Amer Podiatr Med Assoc* 103:32-35.
- Harcourt-Smith WE, and Aiello LC. 2004. Fossils, feet and the evolution of human bipedal locomotion. *J Anat* 204:403-416.
- Harcourt-Smith WE, Throckmorton ZJ, Congdon KA, Zipfel B, Deane AS, Drapeau MSM, Churchill SE, Berger LR, and DeSilva JM. 2015. The foot of *Homo naledi*. *Nat Commun* 6:8432. Doi: 10.1038/ncomms9432:1-8.
- Harris RI, and Beath T. 1947. *An Investigation of foot ailments and Canadian Soldiers*. Ottawa: New York Academy of Medicine.

- Harris RI, and Beath T. 1948. Hypermobility flat-foot with short tendo Achillis. *J Biomech* 31A:116-150.
- Heard-Booth AN. 2014. Using calcaneal morphology to predict medial longitudinal arch height in fossil hominins. *Amer J Phys Anthropol* 153:139.
- Helfet AJ, and Lee DG. 1980. *Disorders of the Foot*. Philadelphia: J.B. Lippincott Company.
- Hicks JH. 1953. The mechanics of the foot I The joints. *J Anat* 87:345-357.
- Hicks JH. 1954. The mechanics of the foot II the plantar aponeurosis and the arch. *J Anat* 88:25-31.
- Hicks JH. 1955. The foot as a support. *Acta anat* 25:34-45.
- Hinton J. 2013. The Significance of Conventional Radiographs in Physical Anthropology. on line Accessed 7-22-2013: Osteoware.
- Inman VT. 1976. *The Joints of the Ankle*. Baltimore: The Williams and Wilkins Company.
- Isbigbi PS, Msamati BC, and Shariff MB. 2005. Arch index as a predictor of pes planus. *J Amer Podiatr Med Assoc* 95:273-276.
- Jones RL. 1945. The functional significance of the declination of the axis of the subtalar joint. *Anat Rec* 93:151-159.
- Jungers WL, Harcourt-Smith WE, Wunderlich RE, Tocheri MW, Larson SG, Sutikna T, Due RA, and Morwood MJ. 2009a. The foot of *Homo floresiensis*. *Nature* 459(7243):81-84.
- Jungers WL, Larson SG, Harcourt-Smith WE, Morwood MJ, Sutikna T, Awe RD, and Djubiantono T. 2009b. Descriptions of the lower limb skeleton of *Homo floresiensis*. *J Human Evol* 57:538-554.
- Kaplan M, and Symonds M. 1945. Pes planus: a method of mensuration. *Radiology* 44:355-356.
- Kelikian AS. 2011. *Sarraffian's Anatomy of the Foot and Ankle*. Philadelphia: Wolters Kluwer / Lippincott Williams & Wilkins.
- Khoshhal KI, Ibrahim AF, Al-Nakshabandi NA, Zamzam MM, Al-Boukai AA, and Zamzami MM. 2004. Böhler's and Gissane's angles of the calcaneus. *Saudi Med J* 25:1967-1970.
- Kidd RS. 2004. *On the nature of morphology: Selected canonical variates analysis of the hominoid hindtarsus and their interpretation*. Cambridge, UK: Cambridge University Press.

- Kidd RS, and Oxnard CE. 2005. Little foot and big thoughts - a re-evaluation of Stw573 foot from Sterkfontein, South Africa. *J Comparative Human Biol* 55:189-212.
- Krogman WM. 1962. Man's posture: Where from? Where to? *Clin Orthop* 25:98-109.
- Landry M, and Agoada D. 1986. The significance of the calcaneocuboid joint in the evolution of human bipedality. *Amer J Phys Anthropol* 69:225.
- Lautzenheiser SG, and Kramer PA. 2013. Linear and angular measurements of the foot of modern humans: A test of Morton's foot types. *Anat Rec* 296:1526–1533.
- Lautzenheiser SG, and Kramer PA. 2014. Foot bones to footprints: Estimating skeletal and fleshy-foot lengths from isolated pedal elements. *Amer J Phys Anthropol* 153:165.
- Lee MS, Vanore JV, Thomas JL, Catanzariti AR, Kogler G, Kravitz SR, Miller SJ, and Gassen SC. 2005. Diagnosis and treatment of adult flatfoot. *J Foot Ankle Surg* 44:78-113.
- Lepow GM, and Valenza PL. 1989. Flatfoot overview. *Clin Podiatric Med Surg* 6:477-489.
- Lewis OJ. 1980. The joints of the evolving foot. Part II. The intrinsic joints. *J Anat* 130:833-857.
- Lisowski FP. 1967. Angular growth changes and comparisons in the primate talus. *Folia Primat* 7:81-97.
- Lovejoy CO, Latimer B, Suwa G, Asfaw B, and White TD. 2009. Combined prehension and propulsion: The foot of *Ardipithecus ramidus*. *Science* 326:72-79.
- Lufler RS, Hoagland TM, Niu JN, and Gross KD. 2012. Anatomical origin of forefoot varus malalignment. *J Amer Podiatr Med Assoc* 102:390-395.
- MacConaill MA. 1945. The postural mechanism of the human foot. *Proc Royal Irish Acad Sect B* 50:265-278.
- MacConaill MA. 1949. The movements of bones and joints 2. Function of the musculature. *J Bone Joint Surg* 31B:100-104.
- Mahato NK. 2011. Morphology of sustentaculum tali: Biomechanical importance and correlation with angular dimensions of the talus. *The Foot* 21:179-183.
- Manter J. 1941. Movements of the subtalar and transverse tarsal joints. *Anat Rec* 80:397-410.
- McCrary JL, Young MJ, Boulton AJM, and Cavanagh PR. 1997. Arch index as a predictor of arch height. *The Foot* 7:79-81.

- McPoil T, Cameron J, and Adrian MJ. 1987. Anatomical characteristics of the talus in relation to forefoot deformities. *J Amer Podiatr Med Assoc* 77:77-81.
- Menz HB. 1998. Alternative techniques for the clinical assessment of foot pronation. *J Amer Podiatr Med Assoc* 88:119-129.
- Menz HB, and Munteanu SE. 2005. Validity of 3 clinical techniques for the measurement of static foot posture in older people. *J Orthop Sports Phys Ther* 35:479-486.
- Morton DJ. 1935. *The Human Foot: Its Evolutionary Development, Physiology and Functional Disorders*. New York: Columbia University Press.
- Murley GS, Menz HB, and Landorf KB. 2009. A protocol for classifying normal- and flat-arched foot posture for research studies using clinical and radiographic measurements. *J Foot Ankle Res* 2:22.
- Muthukumaravel N, Ravichandran D, and Melanirajendra S. 2011. Human calcaneal facets for the talus: Patterns and clinical implications. *J Clin Diagnostic Res* 5:791-794.
- Oxnard CE, and Lisowski FP. 1980. Functional articulation of some hominoid foot bones: implication for the Olduvai (Hominid 8) foot. *Amer J Phys Anthropol* 52:107-117.
- Pablos A. 2015. The foot in the Homo fossil record. *Mitteilungen der Gesellschaft für Urgeschichte* 24:11-28.
- Pablos A, Martinez I, Lorenzo C, Gracia A, Sala N, and Arsuaga JL. 2013. Human talus bones from the Middle Pleistocene site of Sima de los Huesos (Sierra de Atapuerca, Burgos, Spain). *J Human Evol* 65:79-92.
- Page JC. 1983. Symptomatic flatfoot. Etiology and diagnosis. *J Amer Podiatr Med Assoc* 73:393-399.
- Pehlivan O, Cilli F, Mahirogullari M, Karabudak O, and Koksal O. 2008. Radiographic correlation of symptomatic and asymptomatic flexible flatfoot in young male adults. *Int Orthop (SICOT)* 33:447-450.
- Phillips RD. 1999. Planovalgus foot deformity revisited (Letter to the editor). *J Am Med Assoc* 89:265-269.
- Phillips RD. 2000. The normal foot. *J Amer Podiatr Med Assoc* 90:342-345.
- Phillips RD, and Phillips RL. 1983. Quantitative analysis of the locking position of the midtarsal joint. *J Amer Podiatr Med Assoc* 73:518-522.

- Richie HR. 2007. Biomechanics and clinical analysis of the adult acquired flatfoot. *Clin Podiatric Med Surg* 24:617-644.
- Riepert T, Drechsler T, Schild H, Nafe B, and Mattern R. 1996. Estimation of sex on the basis of radiographs of the calcaneus. *J Forensic Legal Med* 77:133-140.
- Root ML, Orien WP, and Weed JH. 1977. *Normal and Abnormal Function of the Foot*. Los Angeles: Clinical Biomechanics Corporation.
- Saltzman CL, and Nawoczenski DA. 1995. Complexities of foot architecture as a base of support. *J Orthop Sports Phys Ther* 21:354-360.
- Saltzman CL, Nawoczenski DA, and Talbot KD. 1995. Measurement of the medial longitudinal arch. *Arch Phys Med Rehabil* 76:45-49.
- Sanner WH, and Whitney KA. 2015a. Foot segment relationships and bone morphology. In: Christman RA, editor. *Foot and Ankle Radiology*. Philadelphia: Wolters Kluwer. p 209-234.
- Sanner WH, and Whitney KA. 2015b. Principles of biomechanical radiographic analysis of the foot. In: Christman RA, editor. *Foot and Ankle Radiology*. 2nd ed. Philadelphia: Wolters Kluwer. p 199-207.
- Sarrafian SK, and Kelikian AS. 2011. Osteology. In: Kelikian AS, editor. *Anatomy of the Foot and Ankle*. Third ed. Philadelphia, PA: Wolters Kluwer/Lippincott Williams & Wilkins. p 40-119.
- Saxena A, and Weddington J. 1989. New radiographic angle to assess intra-articular calcaneal fractures. *J Foot Surg* 28:200-203.
- Sensiba PR, Coffey MJ, Williams NE, Mariscalco M, and Laughlin RT. 2010. Inter- and intraobserver reliability in the radiographic evaluation of adult flatfoot deformity. *Foot Ankle Int* 31:141-145.
- Staheli LT. 1999. Planovalgus foot deformity. *J Amer Podiatr Med Assoc* 89:94-99.
- Stewart SF. 1970. Human gait and the human foot: An ethnological study of flatfoot. *Clin Orthop Relat Res*:111-132.
- Trinkaus E. 2005. Anatomical evidence for the antiquity of human footwear use. *J Archaeol Sci* 321:1515-1526.
- Valmassy RL. 1996. *Clinical Biomechanics of the Lower Extremities*. Chapter 2 Pathomechanics of lower extremity function. St. Louis: Mosby, Inc.

- Van Langelaan EJ. 1983. A kinematical analysis of the tarsal joints: An x-ray photogrammetric study. *Acta Orthop Scand Suppl* 204:1-269.
- Volger HW, and Bojsen-Moller F. 2000. Tarsal functions, movement, and stabilization mechanisms in foot, ankle, and leg performance. *J Amer Podiatr Med Assoc* 90:112-125.
- White TD, and Folkens PA. 2000. *Human Osteology*. San Diego: Academic Press.
- Whitney AK. 1978. *Radiographic Charting Technic*. Philadelphia: Pennsylvania College of Podiatric Medicine.
- Wright DG, Desai SM, and Henderson WH. 1964. Action of the subtalar and ankle-joint complex during the stance phase of walking. *J Bone Joint Surg*:361-382.
- Younger AS, Sawatzky B, and Dryden P. 2005. Radiographic assessment of adult flatfoot. *Foot Ankle Int* 26:820-825.
- Zipfel B, DeSilva JM, and Kidd RS. 2009. Earliest complete hominin fifth metatarsal-Implications for the evolution of the lateral column of the foot. *Amer J Phys Anthropol* 140:532-545.

Chapter 4: List of Tables

Table 1a. List of foot measurement abbreviations.

Table 1b. Descriptive statistics of the averaged values of the measurements of the foot.

Table 1c. Foot measurements linear regression analysis.

Table 2a. List of calcaneus measurement abbreviations.

Table 2b. Descriptive statistics of the measurements of the calcaneus.

Table 2c. Measurements of the calcaneus with CIA linear regression analysis.

Table 3a. List of talus measurement abbreviations.

Table 3b. Descriptive statistics of the measurements of the talus.

Table 3c. Measurements of the talus with CIA linear regression analysis.

Table 4a. Descriptive statistics of the calcaneus indices.

Table 4b. Descriptive statistics of the talus indices.

Table 4c. Measurements of the calcaneus indices with CIA linear regression analysis.

Table 4d. Measurements of the talus indices with CIA linear regression analysis.

Table 5. Comparisons of certain measurements with those reported by Lautzenheiser and Kramer (2013).

Variables of the Foot	Variable Abbrev
The Talocalcaneal Angle in the AP view	APTCA
Talocuboid Angle	TCUA
Calcaneal Inclination Angle	CIA1
Calcaneal Inclination Angle	CIA2
Talocalcaneal Angle in the Lateral view	LTCA
Talar Declination Angle	TDA
First Metatarsal Declination Angle	FMDA
Talar-First Metatarsal Angle	TFMA
Arch Height	AH
Foot Length Line	FLL
Foot Length	FLCM
Foot Length	FL
Cyma Line Measurement	CLAH
Truncated Normalized Navicular Height (Arch Height/Foot Length Index)	TNNH (AHFLCM)
Normalized Navicular Height (Arch Height/Foot Length Index)	NNH (AHFL)

Table 1a. List of foot measurement abbreviations.

Variable	Foot Type Units	Low Arch					Normal Arch					High Arch				
		n	Mean	SD	Min	Max	n	Mean	SD	Min	Max	n	Mean	SD	Min	Max
APTCA	Degrees	45	22.30	8.84	9.48	44.32	37	18.49	6.89	8.50	41.06	21	17.94	5.14	5.28	27.17
TCUA	Degrees	45	42.50	10.87	19.95	68.26	37	35.23	9.33	11.83	56.38	21	34.99	10.63	8.59	60.13
CIA1	Degrees	45	12.80	2.19	7.40	15.56	37	20.22	2.84	16.07	24.55	21	27.73	2.24	25.32	32.97
CIA2	Degrees	45	15.07	2.56	9.69	20.30	37	22.45	3.41	16.53	29.26	21	29.31	3.08	23.44	35.59
LTCA	Degrees	45	39.74	5.03	30.02	52.86	37	44.36	4.04	35.74	53.69	21	51.52	4.89	44.16	61.09
TDA	Degrees	45	26.90	4.94	18.20	41.20	37	24.27	3.49	18.27	33.24	21	23.75	4.85	13.99	31.86
FMDA	Degrees	45	19.23	3.22	11.37	26.95	37	22.32	2.83	14.07	27.59	21	23.36	2.91	17.69	29.77
TFMA	Degrees	45	8.01	6.60	0.19	27.87	37	3.81	3.58	0.14	14.92	21	4.26	3.16	0.36	10.77
AH	Mm	45	31.74	5.59	20.7	43.2	37	39.32	5.31	29.7	52.0	21	43.70	6.54	26.6	52.6
FLL	Mm	45	160.11	15.44	126.6	191.5	37	153.95	14.17	126.9	182.1	21	157.35	11.49	130.4	175.7
FLCM	Mm	45	191.80	16.96	159.9	226.8	37	186.62	16.49	157.2	221.5	21	192.12	11.88	166.9	209.6
FL	Mm	45	247.49	21.36	207.7	290.1	37	241.88	22.10	204.0	289.5	21	248.31	15.57	214.4	269.4
CLAH	Mm	45	10.40	4.79	0.9	23.6	37	9.62	3.88	1.9	14.9	21	11.43	3.95	5.5	19.2
TNNH (AHFLCM)	----	45	0.1664	0.2992	0.0960	0.2190	37	0.2118	0.0315	0.1470	0.2870	21	0.2287	0.0403	0.1390	0.3040
NNH (AHFL)	----	45	0.1307	0.0229	0.0740	0.1770	37	0.1617	0.0249	0.1120	0.2180	21	0.1770	0.0313	0.1080	0.2320

Table 1b. Descriptive statistics of the averaged values of the measurements of the foot.

Variable	n	t-test analysis		Regression analysis	
		t	p	b	r ²
APTCA	103	-2.26	0.03	-1.208	0.06
TCUA	103	-2.90	0.05	-2.130	0.09
CIA1	103	24.15	<0.01	3.731	0.85
CIA2	103	17.01	<0.01	3.577	0.77
LTCA	103	7.59	<0.01	2.856	0.47
TDA	103	-2.30	0.02	-0.861	0.08
FMDA	103	5.03	<0.01	1.106	0.24
TFMA	103	-2.80	<0.01	-1.102	0.10
AH	103	6.83	<0.01	3.104	0.41
FLL	103	-0.95	0.35	-1.031	0.01
FLCM	103	-0.26	0.79	-0.301	<0.01
FL	103	-0.15	0.88	-0.223	<0.01
CLAH	103	0.50	0.62	0.166	<0.01
TNNH (AHFLCM)	103	6.14	<0.01	0.017	0.37
NNH (AHFL)	103	5.89	<0.01	0.012	0.35

Table 1c. Foot measurements linear regression analysis.

<u>Variables of the calcaneus</u>	<u>Variable Abbrev</u>
Maximum Length of the Calcaneus	MLCALx
Maximum Length of the Calcaneus	MLCAL-2x
Body Height of the Calcaneus	BHCALx
Minimum Body Height of the Calcaneus	MinBHCALx
Minimum Anterior Height of the Calcaneus	MinAHCALx
Minimum Anterior Width of the Calcaneus	MinAWCALx
Anterior Angle AP View of the Calcaneus	AAAPCALx
Angle of Inclination Posterior Talar Facet of the Calcaneus	AIPTFCALx
Angle of Inclination Middle Talar Facet of the Calcaneus	AIMTFCALx
Anterior Angle Lateral View of the Calcaneus	AALCALx
Böhler's Tuber Angle of the Calcaneus	BTACALx
Gissane's Angle of the Calcaneus	GACALx
Compression Angle of the Calcaneus	CACALx
Front Angle of the Calcaneus	FACALx
Tuber Angle of the Plantar Calcaneus	TACALx
Tuber Angle of the Distal Calcaneus	TACALbx

Table 2a. List of calcaneus measurement abbreviations.

Foot Type		Low Arch					Normal Arch					High Arch				
Variable	Units	N	Mean	SD	Min	Max	N	Mean	SD	Min	Max	N	Mean	SD	Min	Max
MLCALx	Mm	34	86.14	8.94	69.9	106.4	23	82.91	7.43	69.2	102.2	17	87.99	5.44	77.1	100.4
MLCAL-2x	Mm	34	81.67	8.623	64.9	100.8	23	77.68	6.86	63.8	92.9	17	81.43	5.44	71.1	93.1
BHCALx	Mm	34	50.16	6.02	39.7	63.5	23	49.07	5.08	38.3	58.2	17	54.14	4.23	47.1	62.1
MinBHCALx	Mm	34	37.69	4.25	31.6	46.8	23	37.96	3.30	33.1	44.2	17	40.81	2.97	34.7	45.3
MinAHCALx	Mm	34	24.89	3.16	19.7	31.0	23	23.58	2.32	18.7	26.9	17	23.38	1.77	20.3	27.3
MinAWCALx	Mm	34	24.54	2.06	21.9	29.2	23	23.69	2.67	19.1	29.2	17	25.16	2.26	22.3	30.2
AAAPCALx	Degrees	34	96.14	7.30	79.13	113.69	23	98.03	6.91	86.42	112.81	17	98.56	7.14	85.82	113.13
AIPTFCALx	Degrees	34	43.98	4.69	30.86	54.06	23	46.74	5.70	34.39	57.74	17	54.41	7.02	39.08	66.97
AIMTFCALx	Degrees	34	46.62	5.47	35.00	56.25	23	49.52	6.70	38.68	62.27	17	53.84	7.19	37.41	66.86
AALCALx	Degrees	34	97.01	3.73	89.08	103.72	23	103.11	7.43	90.38	116.11	17	109.65	7.91	101.17	131.28
BTACALx	Degrees	34	29.21	4.54	18.14	40.32	23	32.44	4.94	21.16	40.59	17	38.33	5.82	29.55	48.65
GACALx	Degrees	34	117.77	7.87	102.01	133.13	23	122.40	6.90	104.64	132.77	17	120.03	7.32	109.22	132.57
CACALx	Degrees	34	19.67	3.07	12.56	26.12	23	24.12	5.14	13.40	33.54	17	30.41	7.01	18.33	47.41
FACALx	Degrees	34	29.35	3.54	22.89	35.71	23	32.40	5.19	23.55	44.37	17	36.88	5.91	26.94	51.28
TACALax	Degrees	34	67.29	6.76	50.10	78.43	23	65.83	7.78	50.53	79.39	17	61.72	5.44	51.20	71.75
TACALbx	Degrees	34	22.77	6.68	12.14	39.28	23	23.92	7.48	10.94	39.92	17	28.41	5.67	18.88	38.76

Table 2b. Descriptive statistics of the measurements of the calcaneus.

Variable	n	t-test analysis		Regression analysis	
		t	p	b	r ²
MLCALx	74	0.36	0.72	0.231	<0.01
MLCAL2x	74	-0.44	0.66	-0.275	<0.01
BHCALx	74	1.82	0.08	0.824	0.06
MinBHCALx	74	2.21	0.03	0.708	0.09
MinAHCALx	74	-1.81	0.08	-0.409	0.08
MinAWCALx	74	0.46	0.65	0.092	<0.01
AAAPCALx	74	1.03	0.31	0.643	0.02
AIPTFCALx	74	4.62	<0.01	2.469	0.33
AIMTFCALx	74	3.28	<0.01	1.764	0.17
AALCALx	74	5.16	<0.01	3.130	0.41
BTACALx	74	5.01	<0.01	2.204	0.34
GACALx	74	1.15	0.25	0.762	0.03
CACALx	74	5.24	<0.01	2.632	0.44
FACALx	74	4.41	<0.01	1.842	0.29
TACALax	74	-2.68	0.01	-1.320	0.09
TACALbx	74	2.66	0.01	1.318	0.09

Table 2c. Measurements of the calcaneus with CIA linear regression analysis.

<u>Variables of the talus</u>	<u>Variable Abbrev</u>
Maximum Talar Length	MaxLTALx
Maximum Height of the Body of the Talus	MaxHBTALx
Body Height of the Talus	BHTALx
Maximum Length of Fibular Malleolar Facet	MaxLFMTALx
Maximum Width of the Head of the Talus	MaxWHTALx
Minimum Width of the Neck of the Talus	MinWNTALx
Maximum Length of the Head and Neck of the Talus	MaxLHNTALx
Angle of the Head of the Talus	AHTALx
Angle of the Neck of the Talus	ANTALx
Inclination Angle Neck of the Talus	IANTALx-1
Inclination Angle Neck of the Talus	IANTALx-2

Table 3a. List of talus measurement abbreviations.

Foot Type		Low Arch					Normal Arch					High Arch				
Variable	Units	n	Mean	SD	Min	Max	n	Mean	SD	Min	Max	n	Mean	SD	Min	Max
MaxLTALx	Mm	28	59.58	8.41	47.5	81.2	25	59.30	5.91	50.3	69.0	15	62.29	3.94	53.0	69.3
MaxHBALx	Mm	28	32.44	4.37	26.1	43.2	25	32.69	3.26	25.9	40.5	15	34.01	2.77	28.5	37.7
BHTALx	Mm	28	30.33	4.02	23.7	39.3	25	30.83	4.35	24.6	42.8	15	32.21	2.82	25.9	35.2
MaxLFMTALx	Mm	28	28.18	3.69	22.7	35.9	25	28.86	3.11	23.1	34.1	15	30.43	3.40	24.5	37.6
MaxWHTALx	Mm	28	31.50	4.32	24.6	38.3	25	31.64	3.96	26.8	41.6	15	33.37	2.33	29.7	37.8
MinWNTALx	Mm	28	28.20	3.69	22.3	35.5	25	28.35	3.95	21.2	37.0	15	28.54	1.61	25.3	31.2
MaxLHNTALx	Mm	28	27.10	4.22	20.3	35.8	25	26.99	4.35	20.9	38.3	15	29.03	2.15	25.2	32.5
AHTALx	Degrees	28	87.51	5.45	79.64	106.68	25	86.24	6.51	73.35	96.65	15	87.88	7.65	70.56	104.60
ANTALx	Degrees	28	115.11	5.19	106.72	126.08	25	112.75	6.09	101.14	123.44	15	112.53	6.41	97.73	125.48
IANTALx-1	Degrees	28	28.65	3.00	24.55	37.20	25	29.60	4.23	19.69	36.61	15	28.98	2.40	25.01	33.19
IANTALx-2	Degrees	28	38.34	5.00	30.89	50.84	25	36.53	5.04	29.40	49.42	15	37.79	6.04	21.15	46.29

Table 3b. Descriptive statistics of the measurements of the talus.

Variable	n	T-test analysis		Regression analysis	
		t	p	b	r ²
MaxLTALx	68	0.92	0.36	0.5805	0.02
MaxHBTALx	68	1.01	0.32	0.3601	0.02
BHTALx	68	1.33	0.19	0.4426	0.03
MaxLFMTALx	68	1.6	0.12	0.5541	0.06
MaxWHTALx	68	1.26	0.21	0.4186	0.03
MinWNTALx	68	0.32	0.75	0.0837	<0.01
MaxLHNTALx	68	1.31	0.2	0.4187	0.03
AHTALx	68	0.01	0.99	0.0066	<0.01
ANTALx	68	-1.44	0.16	-0.7079	0.04
IANTALx-1	68	0.54	0.59	0.1300	<0.01
IANTALx-2	68	-0.48	0.63	-0.2301	<0.01

Table 3c. Measurements of the talus with CIA linear regression analysis.

Indices Calcaneus/Foot	Low Arch					Normal Arch					High Arch				
	n	Mean	SD	Min	Max	n	Mean	SD	Min	Max	n	Mean	SD	Min	Max
MLCALx/FL	34	0.3455	0.0152	0.3218	0.3712	23	0.3531	0.0132	0.3316	0.3800	17	0.3586	0.0167	0.3282	0.3901
MLCALx/FLCM	34	0.4469	0.0195	0.4094	0.4782	23	0.4575	0.0161	0.4277	0.4985	17	0.4631	0.0210	0.4320	0.5115
BHCALx/MLCALx	34	0.5821	0.0345	0.4969	0.6616	23	0.5918	0.0309	0.5195	0.6408	17	0.6154	0.0324	0.5490	0.6536
MinAHCALx/MLCALx	34	0.2889	0.0190	0.2533	0.3283	23	0.2848	0.0210	0.2470	0.3367	17	0.2689	0.0233	0.2204	0.3085
MinAWCALx/MLCALx	34	0.2864	0.0245	0.2431	0.3305	23	0.2861	0.0246	0.2324	0.3338	17	0.2893	0.0251	0.2582	0.3416
MinAWCALx/MinAHCALx	34	0.9957	0.1065	0.7931	1.1934	23	1.0074	0.0893	0.8197	1.1979	17	1.0806	0.0967	0.9344	1.2808

Table 4a. Descriptive statistics of the calcaneus indices.

Indices Talus/Foot	Low Arch					Normal Arch					High Arch				
	n	Mean	SD	Min	Max	n	Mean	SD	Min	Max	n	Mean	SD	Min	Max
MaxLTALx/FL	28	0.2416	0.0178	0.2130	0.2799	25	0.2492	0.0132	0.2313	0.2808	15	0.2543	0.0106	0.2383	0.2672
MaxLTALx/FLCM	28	0.3123	0.0222	0.2722	0.3580	25	0.3234	0.0168	0.3008	0.3671	15	0.3283	0.0131	0.3063	0.3482
BHTALx/MaxLTALx	28	0.5105	0.0324	0.4300	0.5878	25	0.5204	0.0540	0.4499	0.6605	15	0.5170	0.0300	0.4592	0.5607
BHTALx/MaxLFMTALx	28	1.0814	0.0804	0.9294	1.1947	25	1.0705	0.1111	0.8735	1.3162	15	1.0636	0.0849	0.9362	1.1918
MaxLFMTALx/MaxLTALx	28	0.4745	0.0457	0.4107	0.5836	25	0.4877	0.0394	0.3993	0.5898	15	0.4882	0.0405	0.4329	0.5749
MaxLHNTALx/FL	28	0.1100	0.0122	0.0853	0.1380	25	0.1133	0.0132	0.0915	0.1390	15	0.1186	0.0079	0.1020	0.1275
MaxLHNTALx/FLCM	28	0.1422	0.0155	0.1112	0.1774	25	0.1470	0.0173	0.1190	0.1832	15	0.1532	0.0109	0.1326	0.1639
MaxWHTALx/MaxLHNTALx	28	1.17	0.1053	0.9498	1.3596	25	1.1838	0.1260	1.0065	1.4394	15	1.1518	0.0735	1.0369	1.2759
MinWNTALx/MaxWHTALx	28	0.8965	0.0328	0.8212	0.9601	25	0.8953	0.0470	0.7439	0.9612	15	0.8571	0.0450	0.7839	0.9265

Table 4b. Descriptive statistics of the talus indices.

Variable	n	t-test analysis		Linear regression analysis	
		t	p	b	r ²
MLCALx/FL	74	2.41	0.02	0.0034	0.12
MLCALx/FLCM	74	2.42	0.02	0.0042	0.12
BHCALx/MLCALx	74	2.86	<0.01	0.0079	0.13
MinAHCALx/MLCALx	74	-2.37	0.02	-0.0046	0.12
MinAWCALx/MLCALx	74	0.28	0.78	0.0006	<0.01
MinAWCALx/MinAHCALx	74	2.25	0.03	0.0194	0.11

Table 4c. Measurements of the calcaneus indices with CIA linear regression analysis.

Variable	n	t-test analysis		Linear regression analysis	
		t-test	p	b	r ²
MaxLTALx/FL	68	2.45	0.02	0.0033	0.11
MaxLTALx/FLCM	68	2.56	0.01	0.0042	0.11
BHTALx/MaxLTALx	68	0.73	0.47	0.0020	0.01
BHTALx/MaxLFMTALx	68	-0.62	0.54	-0.0046	0.01
MaxLFMTALx/MaxLTALx	68	0.95	0.35	0.0038	0.02
MaxLHNTALx/FL	68	2.32	0.03	0.0021	0.07
MaxLHNTALx/FLCM	68	2.3	0.026	0.0027	0.07
MaxWHTALx/MaxLHNTALx	68	-0.41	0.684	-0.0032	<0.01
MinWNTALx/MaxWHTALx	68	-2.35	0.023	-0.0087	0.10

Table 4d. Measurements of the talus indices with CIA linear regression analysis.

Variable	Abbrev	Units	This study (all foot types)				Lautzenheiser and Kramer	
			n	Mean	r ²	p (t-test)	n	Mean
Calcaneal Inclination Angle (Pitch) - normal	CIA1	Degrees	103	18.53	0.85	<0.01	50	19.59
Talar Declination Angle (Strade)	TDA	Degrees	103	25.26	0.08	0.02	50	20.26
Foot Length	FLCM	Mm	103	190.0	0.00	0.79	50	189.3
Böhler's Tuber Angle of the Calcaneus - normal	BTACALx	Degrees	74	33.32	0.34	<0.01	50	33.45
Gissane's Angle of the Calcaneus - normal	GACALx	Degrees	74	120.07	0.03	0.25	50	125.51

Table 5. Comparisons of certain measurements with those reported by Lautzenheiser and Kramer (2013).

Chapter 4: List of Figures

- Figure 1. Angular variables of the foot lateral view.
- Figure 2. Linear variables of the foot lateral view.
- Figure 3. Angular variables of the foot AP view.
- Figure 4. Linear variables of the talus lateral view.
- Figure 5. Angular variables talus lateral view.
- Figure 6. Linear and angular variables of the talus AP view.
- Figure 7. Linear variables of the calcaneus lateral view.
- Figure 8. Angular variables of the calcaneus lateral view.
- Figure 9. Angular variables of the calcaneus lateral view.
- Figure 10. Linear and angular variables of the calcaneus AP view.

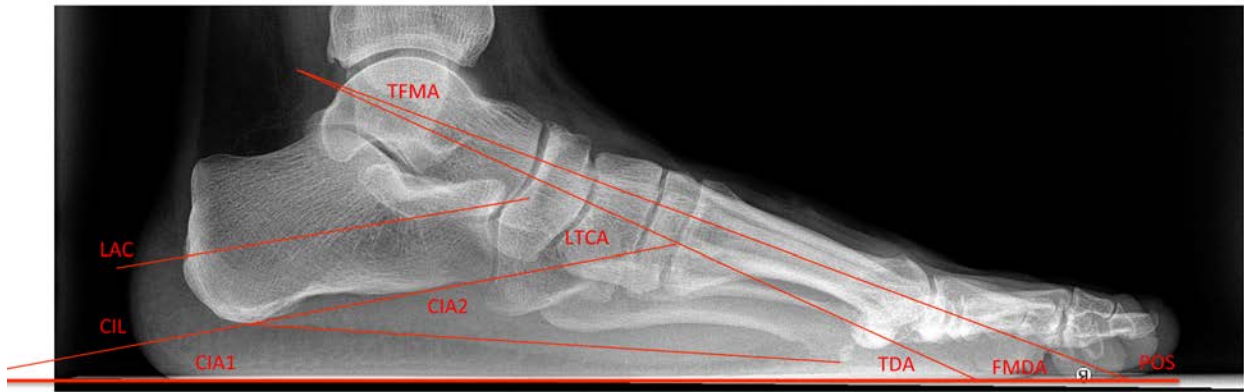


Figure 1

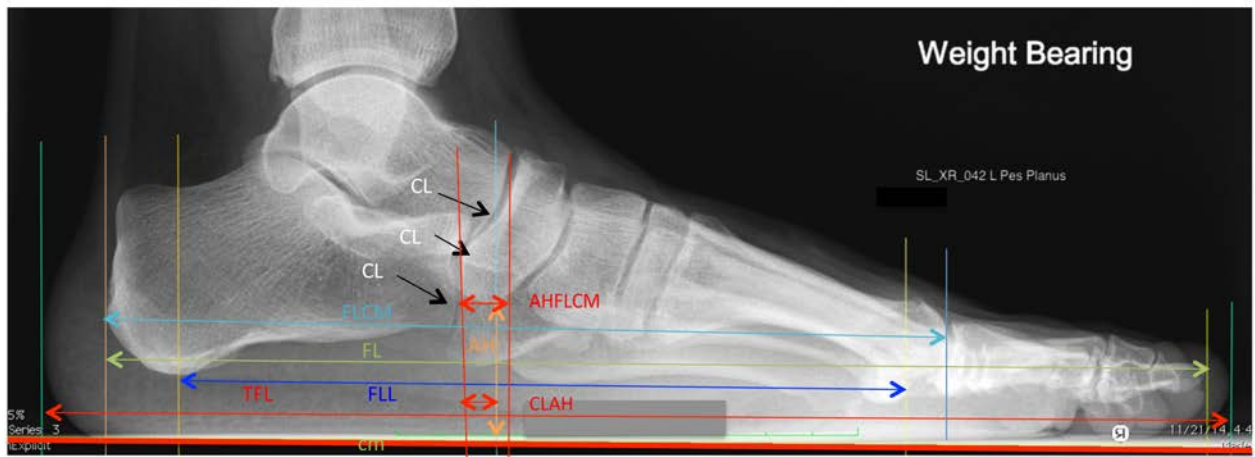


Figure 2

Figure 1. Angular variables of the foot lateral view.
 Figure 2. Linear variables of the foot lateral view.

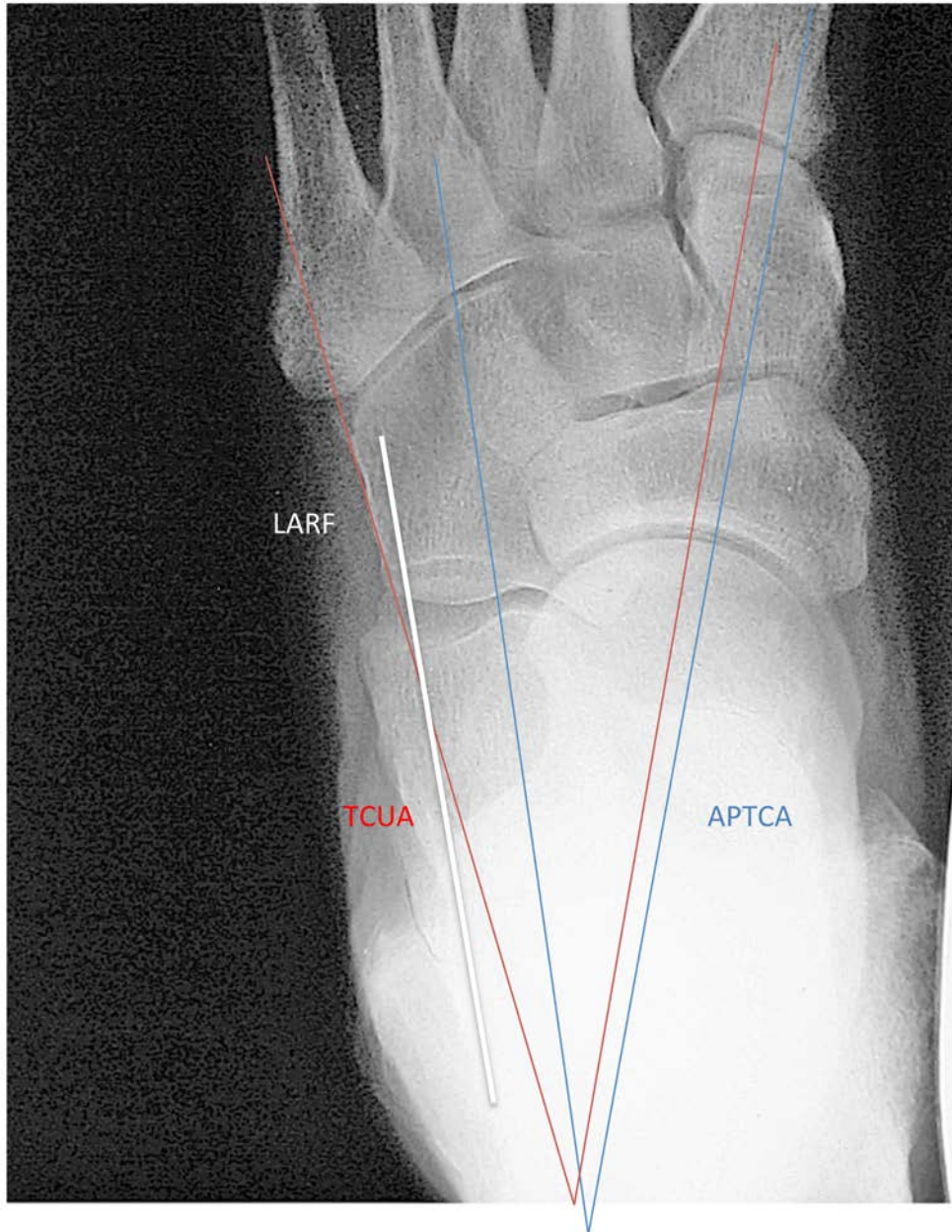


Figure 3. Angular variables of the foot AP view.

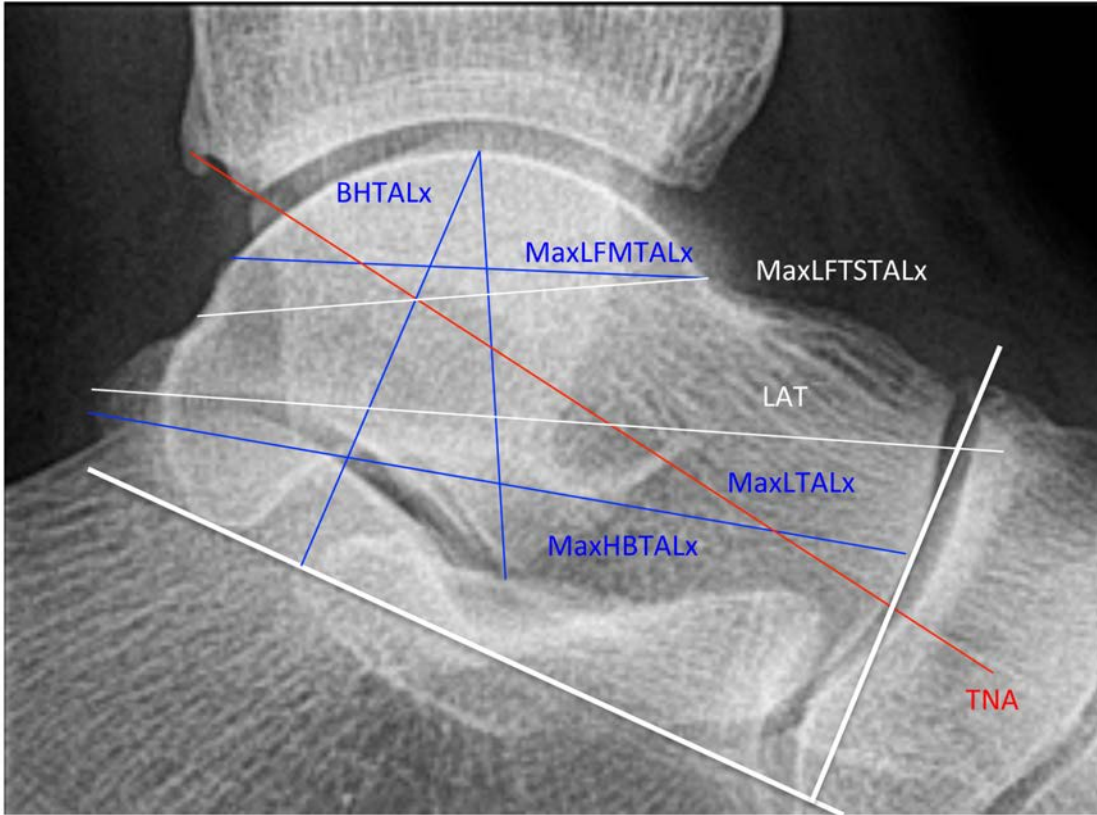


Figure 4. Linear variables of the talus lateral view.

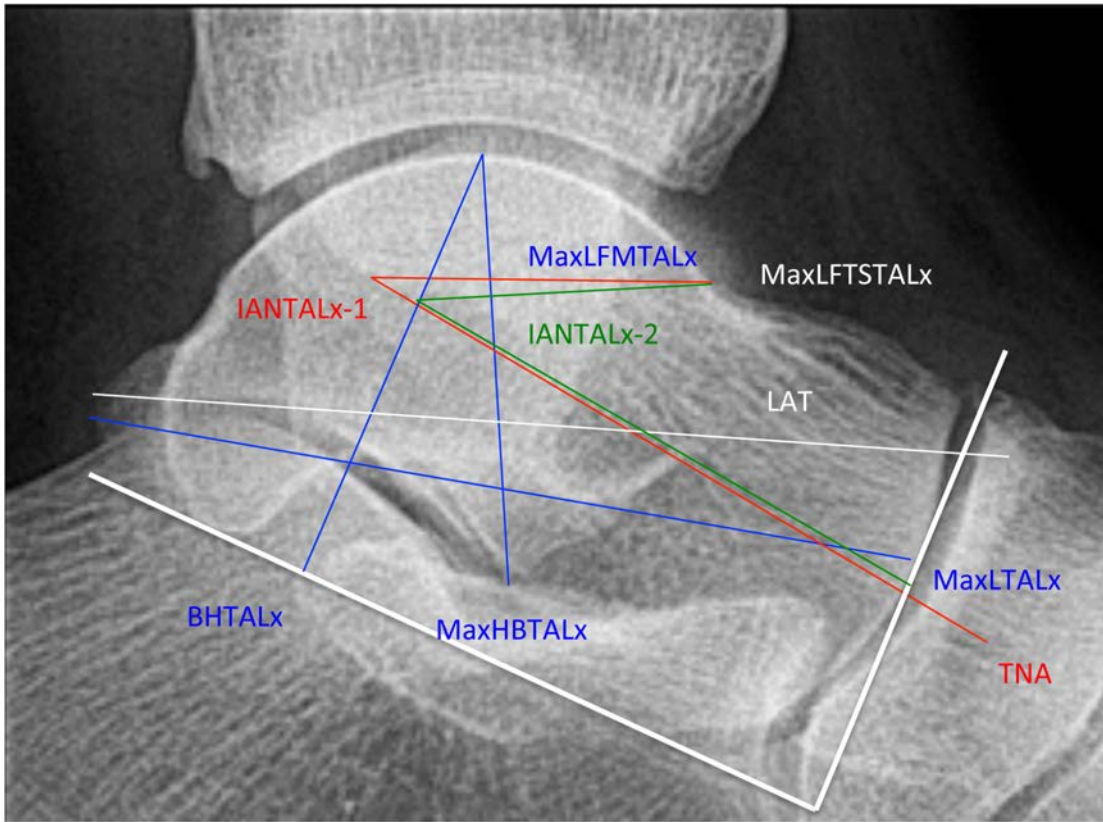


Figure 5. Angular variables talus lateral view.

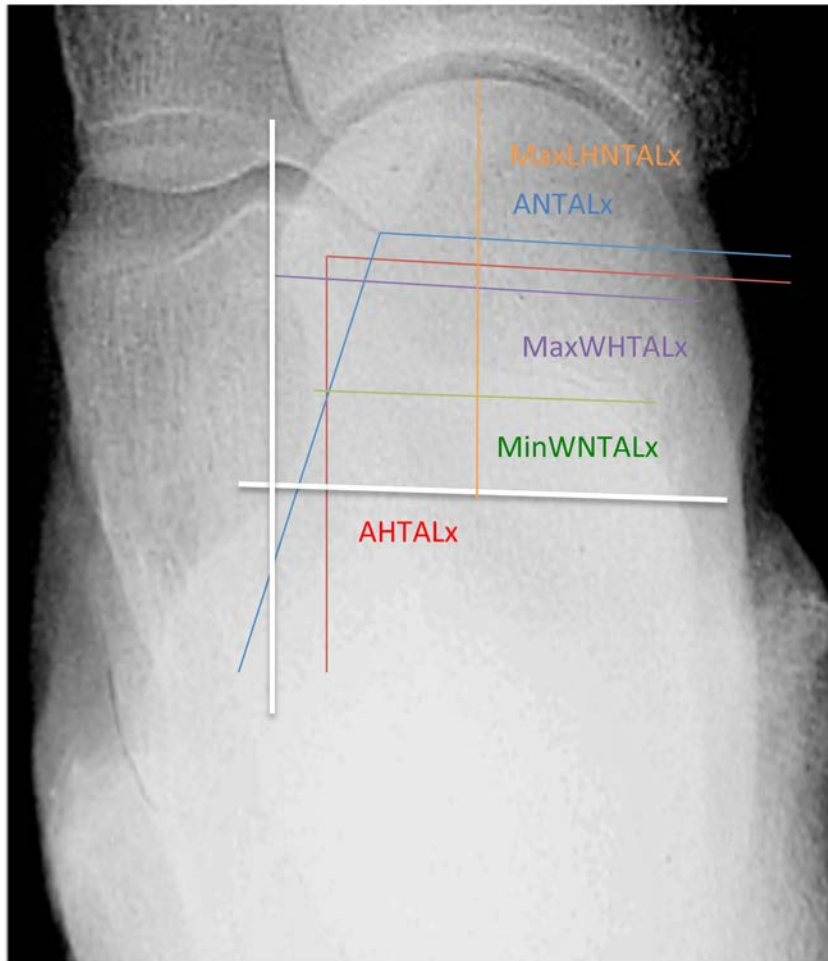


Figure 6. Linear and angular variables of the talus AP view.

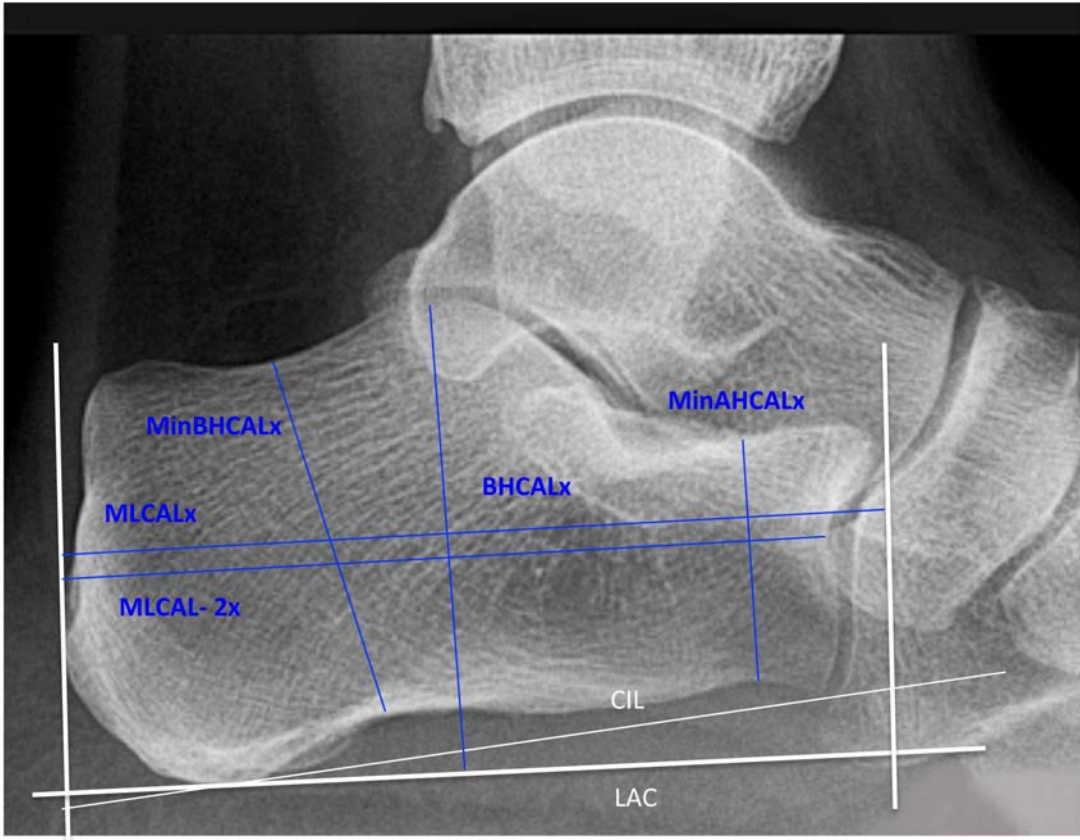


Figure 7. Linear variables of the calcaneus lateral view.

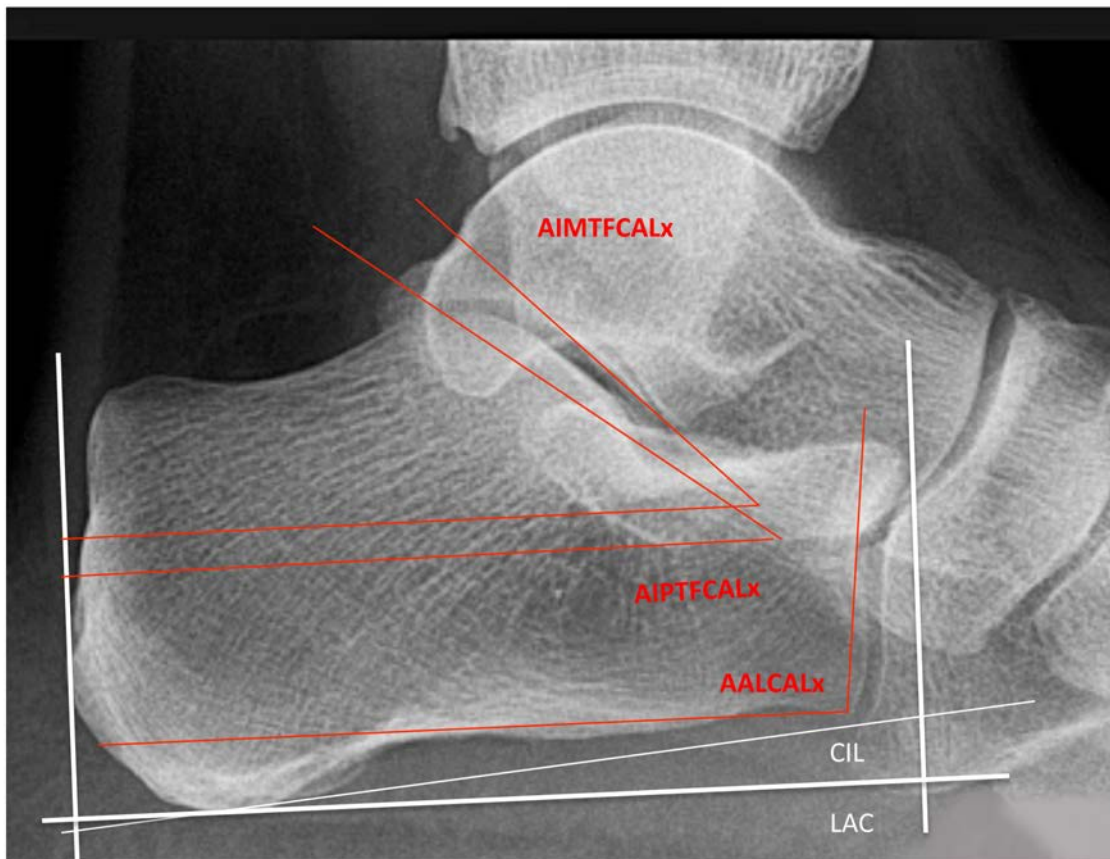


Figure 8. Angular variables of the calcaneus lateral view.

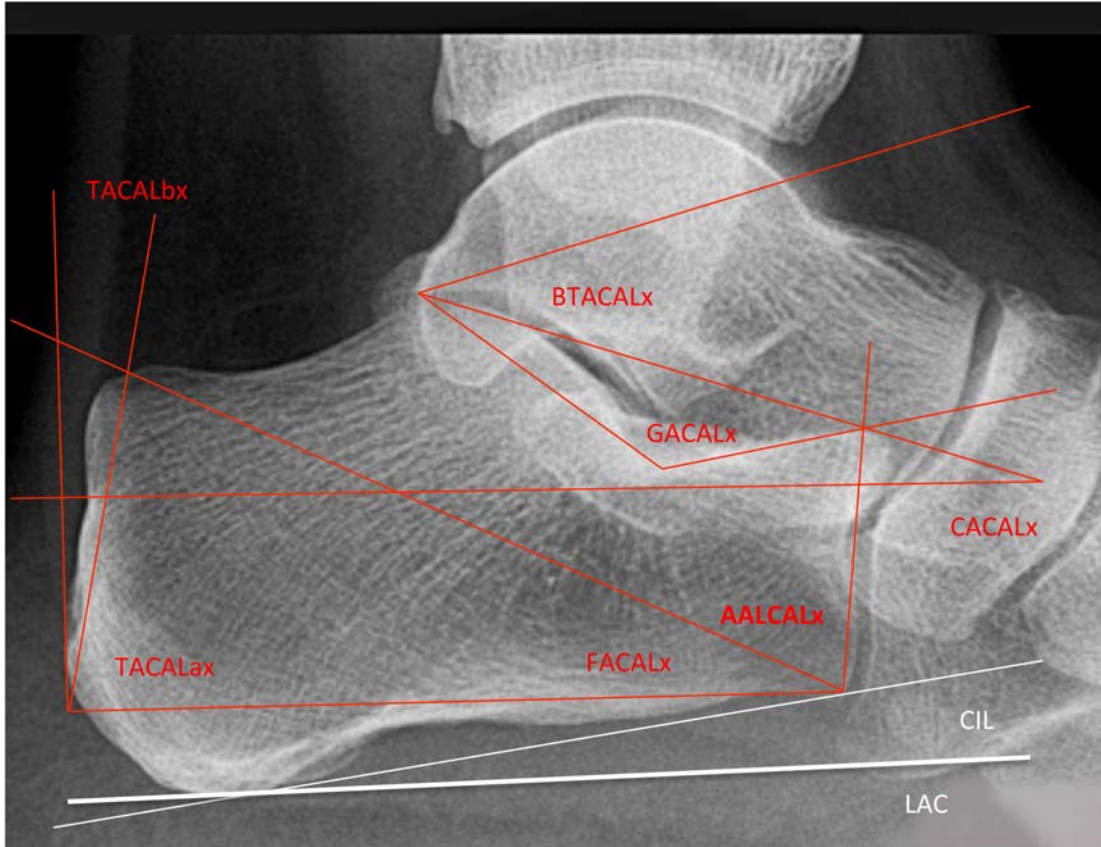


Figure 9. Angular variables of the calcaneus lateral view.

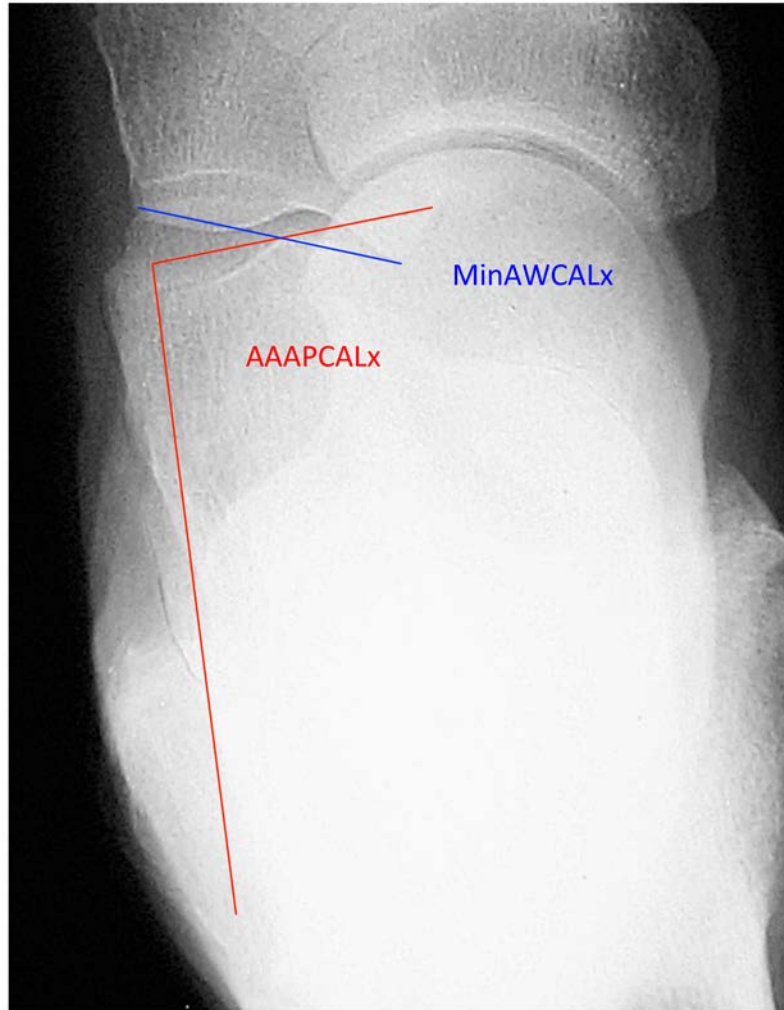


Figure 10. Linear and angular variables of the calcaneus AP view.

Chapter 5: Evolution of the human foot, areas of future investigation, and conclusions

Summary of results from Chapters 2, 3, and 4: Implications

The goal of this dissertation has been to use radiographic images to explore the relationship between the morphologies of the talus and calcaneus and the biomechanics of the modern human as expressed by arch height. The central hypothesis presented here is that there are linear and angular measurements of the talus and calcaneus in modern humans useful to help identify a foot as pes planus. However, first the relationship between radiographic image of the talus and calcaneus and the physical bone had to be established. This was achieved by demonstrating a strong relationship between linear angular measurements from the physical bone with those taken from the radiographic image. The results of this dissertation indicate a relationship between angular measurements of the calcaneus and arch height in modern humans. While a relationship between talar measurements and arch height could not be shown, the information derived from this study opens up other areas for further investigation concerning the morphology of the talus and calcaneus in the understanding of the modern human pes planus foot type that should be useful in the interpretation of both fossil and recent hominin pedal remains.

A major concern when reconstructing the osteology of a foot from its individual isolated units is the ability to properly articulate the “dry bones” to create a structure which accurately represents the intact weight-bearing foot in life along with its associated bony and soft tissue functional relationships. A review of the literature raises concerns about the accuracy of results reported in the literature. For his study of the Olduvai Hominid (OH) 8, Lewis (1980) articulated

the casts of fossil pedal elements and compared them to the articulated bones of the feet of human and great apes. Lewis (1980) stated that he could “easily” articulate the tarsal bones into their correct closed pack relationship to each other but gives no evidence that his method of restoring articular relationships was, in fact, accurate. Oxnard and Lisowski (1980) rearticulated the dry bones of a series of modern ape and human feet and found that they could rearticulate the bones producing accurate relationships when comparing their results to dissected specimens in which ligaments, articular cartilages and soft tissues were present. However, they gave no indication of how this accuracy was determined. Trinkaus (1983) believed that individual bones could be rearticulated into “best-fit” position for such structures as arch reconstruction. He did admit, however, that this method tends to place the bones in the closed packed position creating a tarsometatarsal skeleton that is in a “highly pronated” position, concluding that while “...the presence of pedal arches in Neandertals feet is best indicated by their articulated tarsometatarsal skeletons, ... it is not possible to indicate fully the original configurations of their pedal arches in these skeletal assemblies” (Trinkaus, 1983 p.384). While he believed that his method of reconstruction would create a foot with a longitudinal arch that was somewhat higher than in life, he admits, “...how much higher cannot be determined.” Griffin et al. (2015) expressed their concerns with the problems associated with establishing a standard method for measuring medial longitudinal arch height in a complete living foot when only incomplete or isolated skeletal remains are available. For example, they noted that a method for reliably identifying the presence of a plantar aponeurosis as seen in humans based on skeletal features alone has yet to be established. Finally, they concluded that, “... while the medial longitudinal arch is hallmark of the modern

human foot, setting humans apart from other living primate, the ability to identifying its presence in the fossil record based on isolated skeletal material is very difficult” (Griffin et al., 2015 p.7).

The concerns of accurately reconstructing a hominin foot from isolated bones have been addressed in this study. To investigate the relationship between tarsal morphology and the functional intact foot, measurements from an articulated, weight-bearing foot of known foot type are necessary. Since this requires the intact foot of a living individual capable of weight-bearing, such an investigation can only be performed using radiographic imaging, such as can be provided by standard weight-bearing views of the foot. The results from Chapters 2 and 3 indicate that radiographs can be studied in the same manner as the physical bone for the variables examined, allow weight-bearing radiographs to be used in the investigation of the relationship between talar and calcaneal morphology and an intact weight-bearing foot.

Areas of future investigation: Hypotheses concerning requirements for the foot in obligate bipedalism and striding gait

Based on the results presented in Chapter 4, the following hypotheses are presented:

(1) The shape of the talus does not play a major role in pes planus. Measurements of the talus, including the talar neck angle, both in the transverse and sagittal planes, did not correlate with pes planus. This suggests that the morphology of the talus has been relatively stable since the origins of modern human bipedalism, and the variation seen in modern humans evolved, and any variation seen in the talus does not impact the arch configuration.

(2) Variations in the “locking mechanism” of the calcaneocuboid joint may account for

variations in arch height in modern humans, by providing less stability in the lower arch foot than in the higher arch foot.

(3) Variations in the shape of the calcaneus are related to arch height and pes planus. The results from this investigation demonstrate that none of the linear measurements, or linear measurement indices, for the calcaneus correlates with arch height while most of the within bone angular measurements of the calcaneus in the sagittal plane do correlate with arch height to some degree (see Chapter 4). The associations between within bone angular values of the calcaneus and arch height may be explained by the relationship between the calcaneus and talus, and the effects of the windlass mechanism on the shape of the calcaneus.

These hypotheses derive from the results of the studies documented in Chapters 2, 3, and 4 and are offered to stimulate future work in understanding the impact of shape variation of the talus and calcaneus on hominin bipedalism. Evolutionary changes in these three areas have taken place to “fine-tune” the striding bipedal gait of modern humans, allowing for stability and efficiency, as well as long distance walking and sustained running. The changes in the talus evolved early and allow for a wider range of variation without affecting arch height, while variations in the calcaneus do have a role in the pes planus foot type of modern humans and can be of use in interpreting the hominin fossil record.

This categorization is based solely on pedal material and does not take into account the detailed descriptions of associated cranial, upper extremity, and lower extremity material. These hypothesis are presented to assist in the interpretation of the morphological changes of the calcaneus and talus as they relate to the evolution of bipedalism in modern humans. They are proposed with the understanding that AP and lateral radiographs provide limited

information on frontal plane morphology. Other talus and calcaneus measurement variables may exist that can be useful in determining foot type. In addition, foot type determination and the study of the evolutionary course of the human foot will require taking and analyzing linear and angular measurements of other bones of the foot besides the talus and calcaneus.

A modern human shaped-talus

When compared to humans, the tali of nonhuman primates have a greater neck angle in the transverse plane and a smaller angle in the sagittal plane (Lisowski, 1967). The horizontal angle of the neck of the talus in the transverse plane, as determined by Day and Wood (1968), is greater in pongids and Olduvai hominid (OH) 8 when compared to humans. While the relationship between abduction of the talus and pronation of the foot has been described (Root et al., 1977) and Harris and Beath (1948) found that the head and neck of the talus face more medially in the hypermobile flatfoot, a relationship between the horizontal angle of the neck of the talus and the excessively pronated pes planus has not been established. A strong association between the talar head and neck in the transverse plane (variables AHTAL, ANTAL) with a pronated foot, which would be expected if the talar neck was more abducted, was not found in this study. The angle of inclination of the talar neck (IANTAL), created by the plantarflexed position of the talar neck in relation to the talar body in the sagittal plane is variable in humans (Day and Wood, 1968; Kelikian, 2011). It tends to be greater in modern humans than in the pongid foot and OH 8 (Day and Wood, 1968). However, as in the transverse plane, there was no significant difference between the angle of inclination of the neck of the

talus and foot type in this study, suggesting that the variation seen in this angle, as in the horizontal angle, is not related to arch height or foot biomechanics in the modern human foot.

The talus of early members of the genus *Homo*, has been alternately described as ape-like (Lewis, 1980; Oxnard and Lisowski, 1980; Kidd and Oxnard, 2005) or human-like (Day and Napier, 1964; Day and Wood, 1968; Susman and Stern, 1982; Susman 1983; Harcourt-Smith et al., 2015). However, the tali of hominins associated with *Homo erectus*, early *Homo sapiens*, and Neandertals, all appear to be similar to that of modern humans in talar angles and linear measurements, with the exception of talar bodies being described as “squat” (reduced vertical heights when compared to modern humans (Pearson et al., 2008; Pablos et al., 2013; Boyle and DeSilva, 2015). The functional significance of this morphology is unclear, though it has been suggested that it signifies a lower arch height (Lu et al., 2011). Except for the vertical height and robustness, the tali of these hominins were functionally the same as modern humans (Trinkaus, 1975; Rhoads and Trinkaus, 1977; Trinkaus, 1983). A more “ape-like” talar morphology is not seen in either *Homo erectus*, early *Homo sapiens*, or modern humans with the pes planus foot type, which would be expected if the foot of these hominin groups is functionally more “primitive.”

If the interpretation of the results suggested by this study is correct, i.e., that in modern human variation in talar angles and linear measurements are not related to foot type, then I postulate the following explanations for this lack of a relationship between talar morphology and pes planus. The talus is a bone that has no tendinous insertions. It is possible that its relationship to foot function in modern humans is dependent upon its soft tissue attachments to the other bones with which it articulates, and that a range of variation can be tolerated

independent of foot type. The medial and anterior facets of the calcaneus, the navicular articular surface, the glenoid cartilage (navicular fibrocartilage), and the spring (plantar calcaneonavicular) ligament (inferior to the cartilage), create a socket for the talar head. This joint relationship has been termed the acetabulum pedis (Kelikian, 2011), coxa pedis (Pisani et al., 1994), or the calcaneopedal unit (Seringe and Wicart, 2013) (Figure 1a -1c). This socket, made up of both bone and soft tissue, provides stability for the talar head, while permitting a range of motion that allows the talus to abduct and plantarflex in relationship to the rest of the foot while the foot is weight-bearing. Medial rotation of the tibia in the transverse plane takes place as the knee flexes at the beginning of the stance phase of gait and the talus must medially rotate with it, since it is relatively fixed within the ankle joint in the transverse and frontal planes. Although the talar head appears to be only loosely approximated with the navicular on radiographic images, in life the talus is tightly held, while allowing for a range of motion in all three planes in relationship to the rest of the foot, similar to the head of the femur in the hip acetabulum. It may be, in part, variation in the structure of the acetabulum pedis, rather than the bony variation in the measurements of the talus that accounts for difference in arch height. The morphology of the other bones that make up the acetabulum needs further investigation using both radiographic imaging and examination of the physical bones and their soft tissue relationships, to better understand talus variation as it relates to foot function and arch height. The talus, as it relates to foot type, is still not completely understood, especially in its relationship to other tarsal bones.

The shape of the talus, based on this study, does not appear to play a major role in pes planus. It seems that the morphology of the talus has been relatively stable since the *Homo*

stage of bipedalism evolved, and any variation seen in the talus of modern humans does not substantially impact the arch configuration. This conclusion is presented with the understanding that the variables used here, designed to take corresponding measurements on both physical bone and the radiographic image, may not account for all the quantitative morphological features of the talus. Further investigation of the relationship between talar morphology and pes planus should be explored employing 3D analysis techniques to help to confirm this hypothesis.

A “locking” calcaneocuboid joint (CCJ)

The human calcaneocuboid joint (CCJ) is classified as a concavo-convex, saddle or sellar type of synovial joint (see Appendix A). The posterior facet of the CCJ is saddle shaped, being concave from side to side and convex from superior to inferior. The posterior and medial surfaces of the cuboid meet at the more plantar aspect of the bone, forming the calcaneal beak (or process) of the cuboid (Figures 2a-2d). When articulated, the beak of the cuboid (calcaneal process of the cuboid) sits in a corresponding groove on the calcaneus (calcaneal coronoid fossa) just anterior and inferior to the sustentaculum tali at the posteromedial end of the anterior surface of the calcaneus (Figure 3; also see Chapter 1, Appendix A, Figure 3f). Thus, the beak of the cuboid extends posteriorly from the medial part of the cuboid, “undershooting” the calcaneus, supporting it in a “bracket-like” way (Kelikian, 2011). It is held in position by the strong plantar calcaneocuboid ligament (Bojsen-Moller, 1979).

With the foot in its anatomical position, the CCJ is roughly parallel to the frontal plane (as is the talonavicular joint) and at about 90° to the longitudinal axis of the foot. It forms part

of the midtarsal functional joint of the foot along with the talonavicular part of the talocalcaneonavicular joint. Bojsen-Moller (1979) describes the articulating surface on the cuboid as being shaped, not as a saddle, but as a “sector” of one end of an hourglass shaped surface of revolution with the main CCJ axis oriented longitudinally in the foot through the calcaneal process of the cuboid. The cuboid is grooved laterally by the fibularis (peroneus) longus that results in pronatory movement along the pivot. A secondary axis to the CCJ passes through the lateral part of the calcaneus in a mediosuperior direction (Bojsen-Moller, 1979). Movement of the cuboid is stopped by the calcaneus, which overhangs the calcaneal process of the cuboid superiorly and the joint is brought into the closed packed position.

The calcaneocuboid joint has been studied in relationship to the structure of the anterior calcaneus in terms of foot type and function, using both radiographic images of the foot and the physical bones. Lewis (1980) found a flat CCJ not only in the hominin fossil pedal remains (Olduvai OH 8) and the chimpanzee, but in the human flatfoot as well. He also noted an obliquely oriented (from superior and distal to proximal and inferior) and more extreme sellar configuration to CCJ in pes cavus. Bojsen-Moller (1979) studied the CCJ in the skeleton of 25 human feet. He noted that the calcaneal process of the cuboid in the specimens he studied varied in size and that in two of the 25 specimens it was “virtually” non-existent. The recess on the calcaneus was correspondingly flat, and the joint in these individuals could be classified as plane rather than saddle-shaped. A relatively flat CCJ is seen in pes planus; a sellar CCJ is seen in the cavus foot (Landry and Agoada, 1986; DeSilva et al., 2014; Heard-booth, 2015). Variations in the calcaneocuboid joint can, at least in part, produce a functionally less stable foot as seen in the lower arch. Volger and Bojsen-Moller (2000) postulate that since the

cuboid, like the talus, has no muscle attachments, it is also dependent on its soft tissue attachments and articulations with other bones, including the anterior calcaneus with its overlapping anterior process.

The AALCALx variable measurement results from this study supports the relationship between the calcaneocuboid joint and foot type; i.e., a flatter joint produces a functionally less stable foot as seen associated with the lower arch. This study demonstrates that, in the weight-bearing foot, the anterior border of the calcaneus appears to be roughly perpendicular to the supporting surface. As expected, the more parallel the calcaneus is to the surface (as in the low arch foot) the closer this measurement should be to 90°. This is reflected in the AALCALx measurements, which were lower in the low arch and higher in the normal and high arch foot.

The term “midtarsal break” or “midfoot break” was first proposed by Elftman and Manter (1935) to describe midfoot dorsiflexion in the sagittal plane observed in nonhuman primates in stance. Since its identification, the midtarsal break has been assumed to take place at the calcaneocuboid joint. DeSilva et al. (DeSilva, 2010; DeSilva and Gill, 2013; DeSilva et al., 2015) have provided evidence that the midtarsal break occurs at both the CCJ and cuboid-metatarsal joint (CMJ), rather than solely at the CCJ. They have extensively discussed the CCJ in relation to the midtarsal break seen during the midstance phase at heel off in nonhuman primates and occasionally as a variation in modern humans with pes planus. DeSilva et al., (2013) noted that when the midtarsal break occurs in humans it usually takes place at the CMJ rather than the CCJ. DeSilva (2010) demonstrated that the midtarsal break is a complex motion, with the resulting dorsiflexion occurring at both the CCJ and CMJ. The latter joint

contributes roughly 2/3 of total midfoot dorsiflexion and former only about 1/3 of total midfoot dorsiflexion.

DeSilva et al. (2013) mentioned, without elaboration, that the midfoot break probably also involves a rotational component. This aspect of midtarsal break motion has not received as much attention as it should. As described by Bojsen-Moller (1979), the axis of motion of the CCJ is parallel to the longitudinal length of the foot. This would indicate that, in both human and non-human primate, motion at that joint would be mainly in the frontal plane and little, if any, motion would occur in the sagittal plane. However, since the axis of the MCJ is more oblique, a component of sagittal plane motion at that joint would be expected. Thus, any “midtarsal break” of the CCJ that could potentially cause lateral foot instability would occur (and thus be observed) mainly in the frontal plane. A smaller angle for the anterior aspect of the calcaneus (AALCAL and AALCALx) in the sagittal plane has been noted to be associated with the low arch foot. This smaller angulation would result in the CCJ axis being more perpendicular to the foot’s longitudinal axis and more parallel to the ground in the sagittal plane in the low arch foot. The result would be a freer rotation around the CCJ axis and less stability. In addition, while the calcaneal process of the cuboid is not easily observable on the lateral radiograph, the prominent anterior tubercle at the superior aspect of the anterior calcaneus, which represents the “overhang” that limits motion at the CCJ, is present and more prominent on the higher arch foot and can help explain the increased stability of the foot associated with a higher arch (Bojsen-Moller, 1979). In the human foot, the locking mechanism between the calcaneus and the cuboid helps stabilize the midfoot and prevents the midfoot break. This appears to be the primary source of lateral foot stability in stance. Even if the

midtarsal break involving the MCJ is correct, the locking mechanism of the CCJ and the presence of a medial longitudinal arch that tenses during hindfoot inversion is still critical in stability of the lateral foot and in preventing a midfoot break in humans (DeSilva, 2010; DeSilva and Gill, 2013). None of the feet used in the Chapter 4 study had deformities that would significantly interfere with normal locomotion; it is assumed that all subjects walked in the characteristic striding bipedal gait of modern *Homo sapiens*. Whether any of the individuals whose radiographs were used for Chapter 4 had a midtarsal break during the stance phase of gait at either the CCJ or CMJ in the sagittal plane is unknown.

The results presented in Chapter 4, and a review of the literature, supports the hypothesis that variations in the “locking mechanism” of the calcaneocuboid joint accounts for much of the variation in arch height, by providing less stability in a low arch foot. Future investigations using 3D technology to better establish the shapes and positions of the joints in weight-bearing is needed to further elucidate these issues.

The shape of the calcaneus and the windlass mechanism

In addition to the anterior aspect of the calcaneus as it relates to the CCJ, other important features of the calcaneus in its role in arch height, foot biomechanics and bipedal gait exist. There may be size and shape features, such as the articular surfaces with the talus and the sustentaculum tali, that may be associated with a pes planus foot type that could not be fully evaluated in this study. For example, Harris and Beath (1948) observed that in the hypermobile flatfoot, the sustentaculum tali is narrow, while in the normal foot it is broad, rounded, and is projected forward to the anterior margin of the talus, reinforcing their

conclusion that this type of variation helps explain the etiology of the flexible flatfoot; i.e., a narrow sustentaculum tali provides an inadequate support for the talar head. However, variations in the angulation of the sustentaculum tali in relationship to the longitudinal axis of the calcaneus in the sagittal plane may also be associated with foot type. The sustentaculum tali is oriented from a superior-posterior to an inferior-anterior direction (AIMTFCALx variable) with an angle averaging 46° , ranging between 30° and 60° (Kelikian, 2011). In Chapter 4, the average range for the AIMTFCALx, depending on foot type is between 46.62° (low arch) and 53.84° (high arch). Since the middle facet is located on the sustentaculum tali, the angle of this surface should reflect the slope of the sustentaculum tali. The similarity of the measurements between this study and that reported by (Kelikian, 2011) supports the measurement values found in Chapter 4. While Harris and Beath (1948) did not address the slope of the sustentaculum tali as important to the support of the talus in their text, it appears that, when reviewing the photo of the calcaneus in their paper pictured as an example of providing “firm support” for the head of the talus, also has a greater slope of the sustentaculum tali (Harris and Beath, 1948 p. 127 Figure 16-A). In Chapter 4, the measurement values of the angle of the middle talar articular facet (AIMTFCALx) and the posterior articular facet (AIPTFCALx) are lower (less plantarflexed) in the low arch foot type. This is interesting since a less plantarflexed talar neck as seen in the living apes is considered more “primitive” (Lewis, 1980) (Figure 4; also see Figures 10a and 10b from Appendix A). A less plantarflexed talar neck should be associated with a less plantarflexed AIMTFCALx if the neck is being supported by the sustentaculum tali, as Harris and Beath (1948) propose.

In addition to the relationship between the calcaneus and cuboid (AALCALx), calcaneus

measurements (Chapter 4) were found to be associated with certain variables (such as LTCA) that reflect its articular relationship to the talus (AIPTFCALx, AIMTFCALx). As noted, the posterior articular facet angle (AIPTFCALx) appears to be less plantarflexed (closer to being parallel with the supporting surface) in the low arch foot. Variations in the configuration of the articular facets of the subtalar joint as seen in the transverse plane have also been postulated as being related to excessive subtalar joint pronation and foot type (Harris and Beath, 1948; Bruckner, 1987); however, these are morphological features that could not be evaluated using the plain radiographs of the foot.

In Chapter 4 arch height was also found to be associated with other angle values related to the shape of the calcaneus. These variables Böehler's angle (Böehler, 1931; Khoshhal et al., 2004; Lautzenheiser and Kramer, 2013) (BTACALx), Compression Angle of the Calcaneus (Saxena and Weddington, 1989) (CACAL and CACALx) and Front Angle of the Calcaneus (Riepert et al., 1996) (FACAL and FACALx) were all found to be lower in the low arch foot type, suggesting perhaps a less angulated calcaneus in the low arch foot when compared to the normal foot.

The association of angular values of the talus with angular values for both the calcaneus (LTCA) and the supporting surface (TDA), the manner in which the talus sits on the calcaneus (AIPTFCAL, AIMTFCAL), and the absence of a close association between the linear and angular measurements of the talus, all support the hypothesis that variations in the shape of the calcaneus are related to arch height and pes planus.

The windlass mechanism was first proposed by Hicks (1954) as part of the way in which the structures of the human foot create the stability necessary for the forefoot to propel the

body forward in striding bipedal gait. There are four elements to this mechanism: the triceps surae (the two heads of the gastrocnemius muscle and the soleus muscle), plantar aponeurosis, medial longitudinal arch, and metatarsophalangeal joints.

Described simply, the plantar aponeurosis (sometimes referred to as the plantar fascia) acts as a cable, tightening with the contraction of the triceps surae at heel off during the midstance phase of gait. Tension placed on the plantar aponeurosis is further increased with the dorsiflexion of the metatarsophalangeal joints as the body weight moves forward over the supporting limb during the stance phase of gait. This tension causes compression of the bones of the midfoot, raising the medial longitudinal arch creating the rigidity in the foot necessary for propulsion by the forefoot and especially the hallux at toe off (Hicks, 1954; Griffin et al., 2015). The plantar aponeurosis is a strong layer of fibrous deep fascia. The central portion is the thickest, attaching to the medial process of the calcaneal tuberosity posterior and dividing anteriorly into five slips, one to each toe (Draves, 1986). In humans, the Achilles tendon and plantar aponeurosis are linked developmentally. Some of the insertion fibers of the Achilles tendon are continuous with the plantar fascia (Kelikian, 2011), essentially creating a single band of fibrous tissue from the triceps surae to the metatarsophalangeal joints. No other living nonhuman primate has the well-developed plantar aponeurosis seen in modern humans (Susman, 1983). Morton (1935) observed, "...nothing approaching the human plantar aponeurosis is observed in the chimp foot." As a soft tissue feature, identifying the plantar fascia on the isolated calcaneus on both human and nonhuman primates is difficult. This adds to the difficulty in identifying the presence of a windlass mechanism in early hominins, such as OH 8 and StW573 because other components of the windlass mechanism which could be

identified, such as those that would be found on the calcaneus, are either poorly preserved or missing (Griffin et al., 2015).

There also continues to be a lack of sufficient early hominin fossil material to assess the triceps surae (Achilles or calcaneal) tendon to assist in the identification of the presences of the windlass mechanism. While the tendon's attachment can be inferred by the morphology of its insertion on the calcaneal tuberosity posteriorly (Aiello and Dean, 2002), there are no preserved early *Homo* calcanei and legs that can be used to reliably estimate the Achilles tendon's length (Bramble and Lieberman, 2004). Bramble and Lieberman (2004) observed that the Achilles tendon insertion on the posterior surface of the calcaneus in three early australopithecine Hadar specimens (AL 333-8, 333-37 and 333-55) is "chimpanzee-like" in size in contrast to the wider and taller attachment area of modern humans. They speculate that the Achilles tendon as seen in modern humans was absent in *Australopithecus* and conclude that the Achilles tendon length necessary for the windlass mechanism originated less than 3 million years ago, probably with the genus *Homo*. Of note, an Achilles tendon more like that of modern humans has been postulated from the calcaneus of *Australopithecus sediba* (Zipfel et al., 2011).

The third component of the windlass mechanism is the presence of a medial longitudinal arch. The medial longitudinal arch is made up of the calcaneus, talus, navicular, medial cuneiform, and first metatarsal (see Appendix A). Of note, the plantar aponeurosis plays an important role in reinforcing and maintaining the integrity of the medial longitudinal arch throughout the stance phase (Griffin et al., 2015).

The fourth component of the windlass mechanism is the unique morphology of the metatarsophalangeal joints in humans when compared to non-human primates in its adapted for forefoot propulsion. However, Griffin et al. (2015) conclude that relying on one of the components of the windlass mechanism from fossil pedal remains may not be enough to determine its presence during the hominin's stance phase of gait.

The attachments of the triceps surae, plantar aponeurosis (and other soft tissue supportive structures, such as the long plantar ligament), are reflected in the shape of the calcaneus. The location of their attachments should affect the ability of the windlass mechanism to stabilize the foot and maintain the medial longitudinal arch. The tuber angle of the plantar calcaneus (TAPCAL and TAPCALx) and tuber angle of the distal calcaneus (TADCAL and TADCALx) averages are similar to each other in both the normal arch foot and low arch foot and are quite different than the high arch foot. This suggests that the shape of the posterior calcaneus in the high arch foot may be related to both the greater impact on the posterior calcaneus at heel strike and the increased stress placed on the posterior and plantar aspects of the heel as part of the windlass mechanism in this foot type.

The unique size of the calcaneal tuberosity seen in modern humans has been explained as related to the high stress that the posterior-plantar aspect of the calcaneus undergoes at heel strike during the gait cycle. What has received less attention, but may be just as important, is the role the calcaneus (especially the shape of the calcaneus) plays in the creation of the windlass mechanism that helps provide stability of the foot at heel off through toe off, as well as maintaining arch height during the stance phase of gait (Griffin et al., 2015). The calcaneus deserves further investigation into features that may be useful in identifying a foot as

pes plans as well as in understanding its role in the evolution of the modern human foot.

Griffin et al. (2015) concluded that establishing methods that can predict such relationships as the presence of a modern human-like Achilles tendon and plantar aponeurosis in fossil material (p.7) "...through the study of the calcaneus would increase the value of these isolated fossil pedal remains."

Areas of future investigation: Recommendations for future areas of research concerning the interpretation of fossil hominin pedal remains

The three hypotheses presented here concerning the relationship between the morphology of the talus and calcaneus and foot type may be useful in the interpretation of the fossil hominin pedal record. Such information assists in the understanding of how the fossil hominin foot functioned as well as the evolutionary steps that may have lead from a more ape-like pronograde foot to the modern human bipedal foot. Future investigations of these hypotheses would include:

1. Studying the hominin fossil pedal record to find if there is support for the hypothesis presented here that the three requirements for the obligate bipedalism and striding gait include a modern human talus, a locking calcaneocuboid joint, and the windless mechanism.
2. Using this information in the evaluation of fossil hominin material to assist in the interpretation of pedal remains as they relate to the biomechanics and evolution of the obligate striding bipedal gait.

3. Using this information to study the morphology of the talus, calcaneus and other bones of the foot for significant differences in bipedal gait, of both early and later *Homo sapiens*, to assist in the understand of how their gait may have differed from modern humans and how those differences may have affected the efficiency of their gait in such activities as long-distance walking and endurance running.

Areas of future investigation: Recommendations for further studies of the morphology of the talus, calcaneus and other bones of the modern human foot

The studies presented in Chapters 2,3 and 4 demonstrate the need for further study of the morphology of the talus, calcaneus and other bones of the modern human foot to clarify the relation of the variability of these elements to the pes planus foot. Further research is required to better define those features of the modern human foot that are related to foot biomechanics and pes planus. This information would assist in studies of the relationship between foot type, osteology, and such cultural factors as shoe gear use in collections of osteologic remains of more recent human populations. Finally, such information may be useful in postulating foot form and function at assist in the identification of unknown individuals from pedal remains.

To supplement the knowledge gained from Chapters 2 and 3 concerning the morphology of the talus and calcaneus, the following areas of future investigation are recommended:

1. Interobserver studies to test the reliability of the methodology used in measurements taken for this study.
2. Associating measurements from weight-bearing foot radiographs as used in this study (Chapter 4) with subject demographics, medical histories, and clinical examination.
3. Associating measurements taken from plane radiographs with other examinations, such as CT and MRI scans, and using the 3D techniques of geometric morphometrics to explore relationships and shape variability.
4. Perform statistical descriptions and intrapopulation comparisons on the on the calcaneus angular measurements results from Chapter 4, using Student *t*-testing, univariate discriminant function analysis, and multivariate discriminant function analysis to evaluate the dimorphism between the low arch and “non-low arch” foot types. Two-sample Student *t*-tests comparing measurements between these two categories can be performed. Univariate discriminant function analysis can then be performed on each measurement variable to determine the accuracy with which a single variable could, by itself, identify an individual’s foot type. Finally, stepwise multivariate discriminant function analysis can be performed. When all calcaneal measurement variables are used together in direct analysis, the accuracy of identifying a low arch individual between stepwise and direct analysis can be compared.
5. Using the angular calcaneus measurements derived from this study to classify foot type based on dry bone collections. This information can then be applied to identify

other variables that may be associated with foot type, from the calcaneus, talus (e.g. talar neck torsion) or other pedal elements (e.g. navicular). This type of investigation can initially be performed on the same foot specimens used in Chapters 2 and 3, where measurements of the talus and calcaneus have already been recorded.

Conclusions

The relationship between measurements of the talus and calcaneus and the pes planus foot type has been explored in this dissertation using weight-bearing radiographs, indicating a correlation between foot type and angular measurements of the calcaneus. From these investigations, hypotheses have been developed concerning the use of talar and calcaneal morphology in the interpretation of the fossil pedal material and the evolution of the human foot associated with the obligate, bipedal striding gait. In addition, demonstrating a close relationship between measurements of the physical bone and its radiographic image can also be used as a basis for further investigation into the relationship between the morphology of these bones and foot type when examining osteological collections from modern populations and archeological sites. The ultimate goal of this dissertation is the application of this knowledge when evaluating the physical bone from a hominin population, whether modern or ancient, to assist in the determination of the foot type and biomechanics of the individual under examination. To have this ability to examine the physical bone in the same manner as its radiographic image opens up access to a whole new area that can be applied to the analysis of isolated bones: the weight-bearing AP and lateral views of the modern human foot, now

digitized and potentially readily available. It is hoped that this dissertation has provided material, hypotheses and results to advance the goal of understanding the human foot, its function and evolution, as it relates to the pes planus foot type.

Chapter 5: Literature cited

- Aiello LC, and Dean D. 2002. Human Evolutionary Anatomy. Amsterdam: Elsevier Ltd.
- Bohler L. 1931. Diagnosis, pathology, and treatment of fractures of the os calcis. *J Bone Joint Surg* 13:75-89.
- Bojsen-Moller F. 1979. Calcaneocuboid joint and stability of the longitudinal arch of the foot at high and low gear push off. *J Anat* 129:165-176.
- Boyle EK, and DeSilva JM. 2015. A Large *Homo erectus* Talus from Koobi Fora, Kenya (KNM-ER 5428), and Pleistocene Hominin Talar Evolution. *PaleoAnthropol* 1:1-13.
- Bramble DM, and Lieberman DE. 2004. Endurance running and the evolution of *Homo*. *Nature* 432:345-352.
- Bruckner J. 1987. Variations in the human subtalar joint. *J Orthopedics Sports Phys Therapy* 8:489-494.
- Day MH, and Napier JR. 1964. Hominid fossils from Bed I, Tanganyika. Fossil foot bone. *Nature* 201:969-970.
- Day MH, and Wood BA. 1968. Functional affinities of the Olduvai hominid 8 talus. *Man* 3:440-455.
- DeSilva JM. 2010. Revisiting the "midtarsal break". *Am J Phys Anthropol* 141:245-258.
- DeSilva JM, Bonneanee R, Swanson Z, Gill CM, Sobel M, Uy J, and Gill SV. 2015. Midtarsal break variation in modern humans: Functional causes, skeletal correlates, and paleontological implications. *Am J Phys Anthropol* 156:543-552.
- DeSilva JM, Gill CM, Swanson Z, Bonneanee R, and Gill SV. 2014. Reconstructing foot form and function in early hominins using modern human models. *Am J Phys Anthropol* 153:104.
- DeSilva JM, and Gill SV. 2013. Brief communication: A midtarsal (midfoot) break in the human foot. *Am J Phys Anthropol* 151:495-499.
- Draves DJ. 1986. Anatomy of the Lower Extremity. Baltimore: Williams and Wilkins.
- Elftman H, and Manter J. 1935. The Evolution of the Human Foot, with Especial Reference to the Joints. *J Anat* 70:56-67.

- Griffin NL, Miller CE, Schmitt D, and D'Aout K. 2015. Understanding the evolution of the windlass mechanism of the human foot from comparative anatomy: Insights, obstacles, and future directions. *Am J Phys Anthropol* 156:1-10.
- Harris RI, and Beath T. 1948. Hypermobility flat-foot with short tendo Achillis. *J Biomech* 31A:116-150.
- Harcourt-Smith WE, Throckmorton ZJ, Congdon KA, Zipfel B, Deane AS, Drapeau MSM, Churchill SE, Berger LR, and DeSilva JM. 2015. The foot of *Homo naledi*. *Nat Commun* 6:8432. doi: 10.1038/ncomms9432:1-8.
- Hicks JH. 1954. The mechanics of the foot II the plantar aponeurosis and the arch. *J Anat* 88:25-31.
- Kelikian AS. 2011. *Sarrafiian's Anatomy of the Foot and Ankle*. Philadelphia: Wolters Kluwer / Lippincott Williams & Wilkins.
- Khoshhal KI, Ibrahim AF, Al-Nakshabandi NA, Zamzam MM, Al-Boukai AA, and Zamzami MM. 2004. Böhler's and Gissane's angles of the calcaneus. *Saudi Med J* 25:1967-1970.
- Kidd RS, and Oxnard CE. 2005. Little foot and big thoughts - a re-evaluation of Stw573 foot from Sterkfontein, South Africa. *J Comparative Human Biol* 55:189-212.
- Landry M, and Agoada D. 1986. The significance of the calcaneocuboid joint in the evolution of human bipedality. *Am J Phys Anthropol* 69:225.
- Lautzenheiser SG, and Kramer PA. 2013. Linear and angular measurements of the foot of modern humans: A test of Morton's foot types. *Anat Rec* 296:1526-1533.
- Lewis OJ. 1980. The joints of the evolving foot. Part III. The fossil evidence. *J Anat* 131:275-298.
- Lisowski FP. 1967. Angular growth changes and comparisons in the primate talus. *Folia Primat* 7:81-97.
- Lu Z, Meldrum DJ, Huang Y, He J, and Sarmiento EE. 2011. The Jinniushan hominin pedal skeleton from the late Middle Pleistocene of China. *Homo: internationale Zeitschrift für die vergleichende Forschung am Menschen*.
- Oxnard CE, and Lisowski FP. 1980. Functional articulation of some hominoid foot bones: implication for the Olduvai (Hominid 8) foot. *Am J Phys Anthropol* 52:107-117.
- Pablos A, Martinez I, Lorenzo C, Gracia A, Sala N, and Arsuaga JL. 2013. Human talus bones from the Middle Pleistocene site of Sima de los Huesos (Sierra de Atapuerca, Burgos, Spain). *J Human Evol* 65:79-92.

- Pearson OM, Royer DF, Grine FE, and Fleagle JG. 2008. A description of the Omo I postcranial skeleton, including newly discovered fossils. *J Human Evol* 55:421-437.
- Pisani G, Pisani PC, and Parino E. 1994. Degenerative Pathology of the Coxa Pedis – A New Pathological Entity. *Eur J Foot Ankle Surg* 1:67-74.
- Rhoads JG, and Trinkaus E. 1977. Morphometrics of the Neandertal talus. *Am J Phys Anthropol* 46:29-44.
- Riepert T, Drechsler T, Schild H, Nafe B, and Mattern R. 1996. Estimation of sex on the basis of radiographs of the calcaneus. *J Forensic Legal Med* 77:133-140.
- Root ML, Orien WP, and Weed JH. 1977. *Normal and Abnormal Function of the Foot*. Los Angeles: Clinical Biomechanics Corporation.
- Sanner WH, and Whitney KA. 2015. Foot segment relationships and bone morphology. In: Christman RA, editor. *Foot and Ankle Radiology*. Philadelphia: Wolters Kluwer. p 209-234.
- Saxena A, and Weddington J. 1989. New radiographic angle to assess intra-articular calcaneal fractures. *J Foot Surg* 28(No 3):200-203.
- Seringe R, and Wicart P. 2013. The talonavicular and subtalar joints: The “calcaneopedal unit” concept. *Orthop Trauma: Surg Res* 99:s345-S355.
- Susman RL. 1983. Evolution of the human foot: evidence from Plio-Pleistocene hominids. *Foot Ankle* 3:365-376.
- Susman RL, and Stern JT, Jr. 1982. Functional morphology of *Homo habilis*. *Science* 217:931-933.
- Trinkaus E. 1975. *A Functional Analysis of the Neandertal Foot*. PhD dissertation. Philadelphia, PA: University of Pennsylvania.
- Trinkaus E. 1983. Functional aspects of Neandertal pedal remains. *Foot Ankle* 3:377-390.
- Volger HW, and Bojsen-Moller F. 2000. Tarsal functions, movement, and stabilization mechanisms in foot, ankle, and leg performance. *J Am Podiatr Med Assoc* 90:112-125.
- Zipfel B, DeSilva JM, Kidd RS, Carlson KJ, Churchill SE, and Berger LR. 2011. The foot and ankle of *Australopithecus sediba*. *Science* 333:1417-1420.

Chapter 5: List of Figures

Figure 1a. Acetabulum pedis (right foot).

Figure 1b. Right calcaneus superior surface.

Figure 1c. Right talus plantar surface.

Figure 2a. Right cuboid (plantar surface).

Figure 2b. Right cuboid (superior surface).

Figure 2c. Right cuboid (posterior surface).

Figure 2d. Right cuboid (medial surface)

Figure 3. Calcaneocuboid relationship (right foot).

Figure 4. Illustration of differences in posterior and middle facet angles pes planus vs. pes cavus (in degrees).

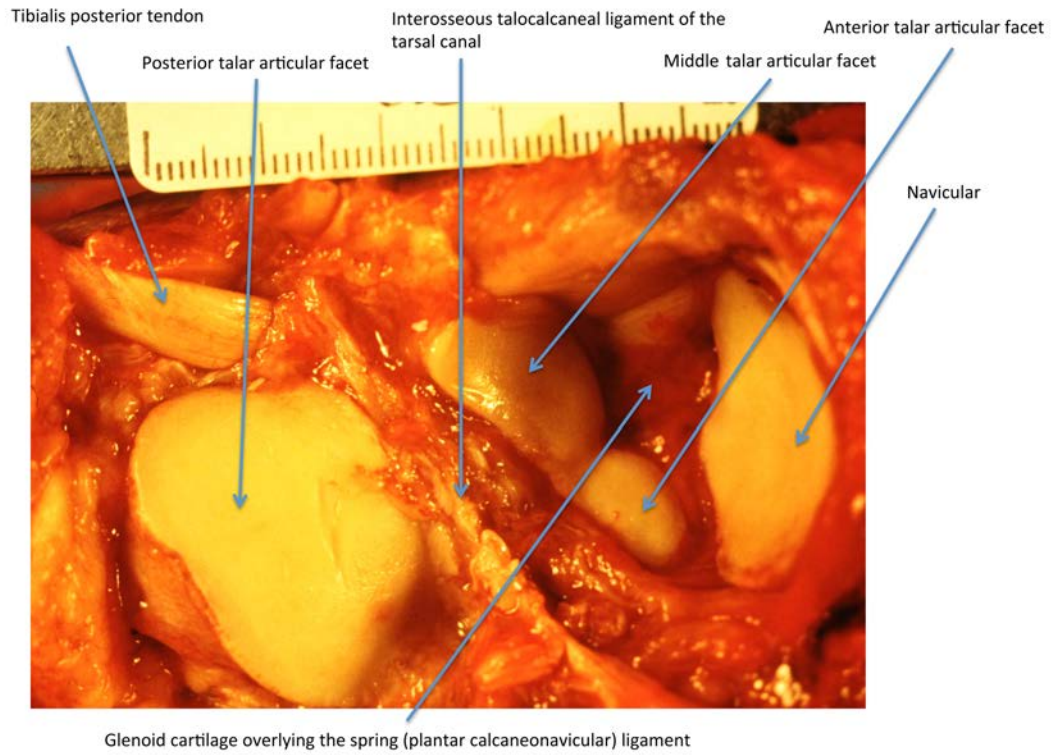


Figure 1a. Acetabulum pedis (right foot).

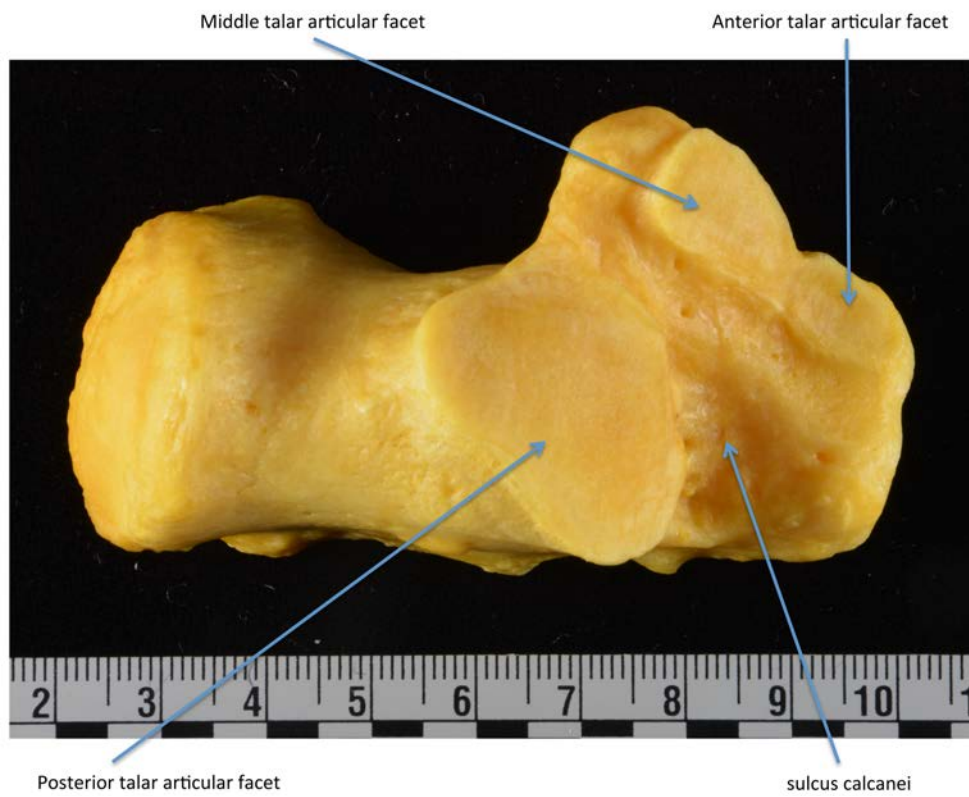


Figure 1b. Right calcaneus superior surface.

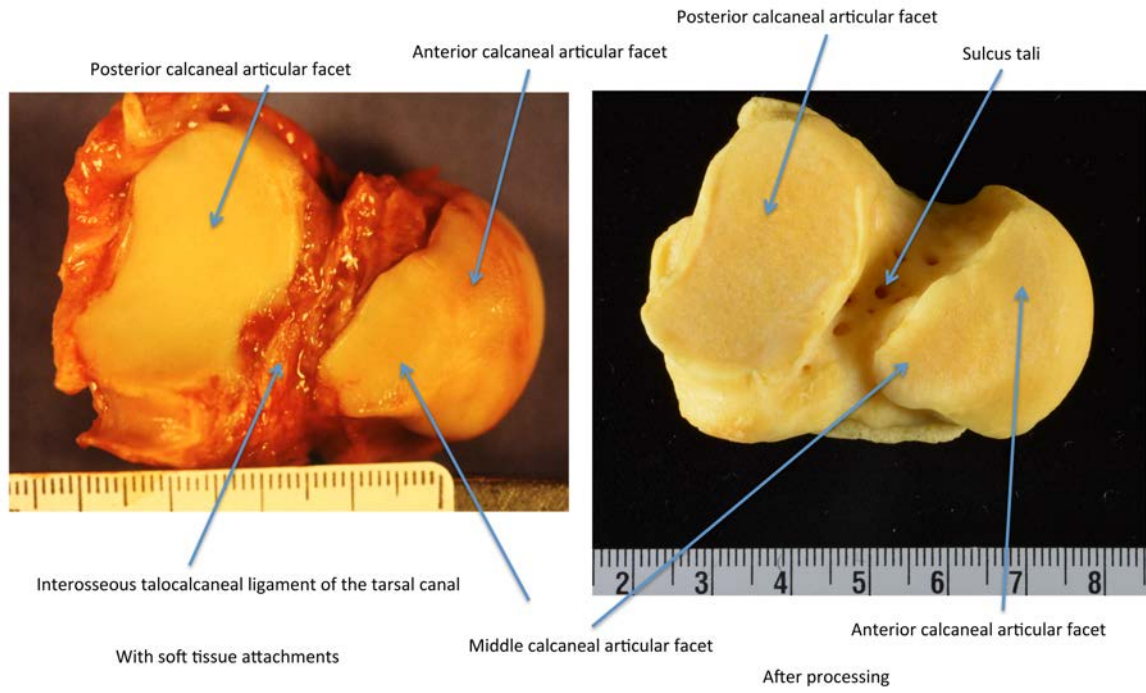


Figure 1c. Right talus plantar surface.

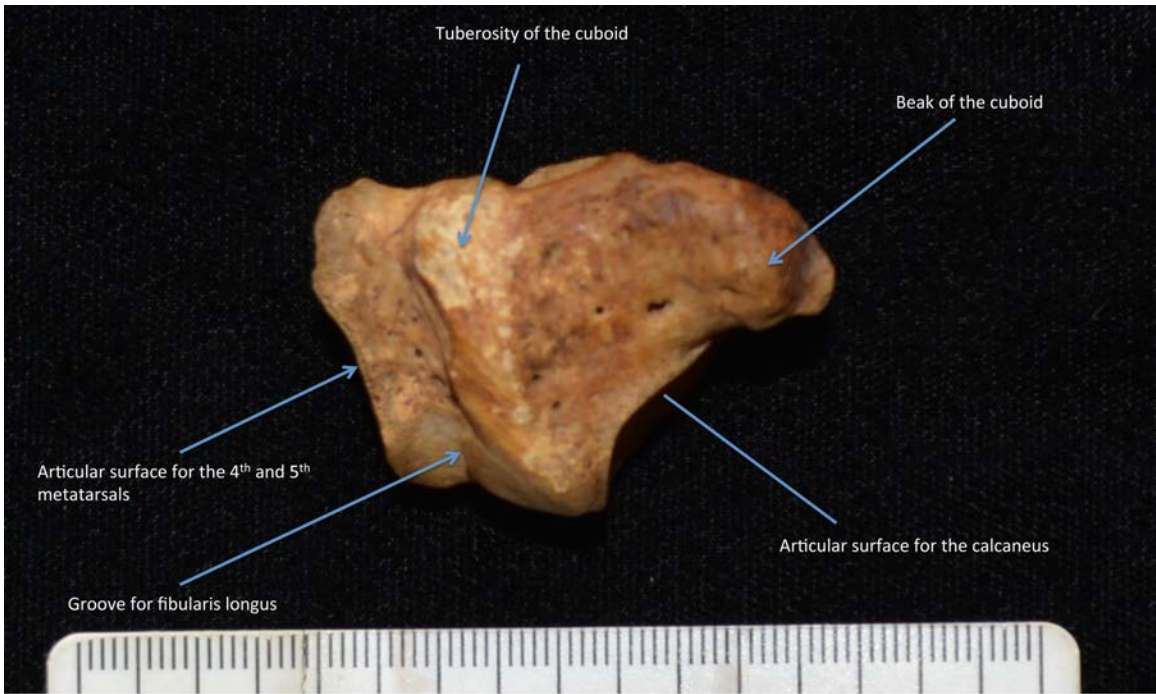


Figure 2a. Right cuboid (plantar surface).

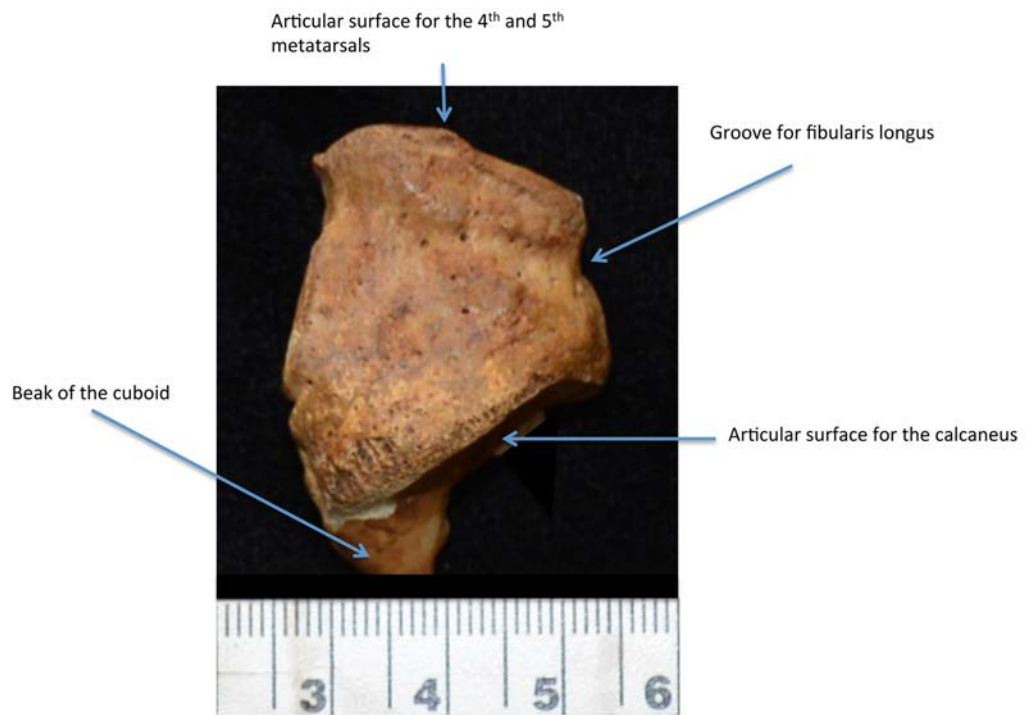


Figure 2b. Right cuboid (superior surface).



Figure 2c. Right cuboid (posterior surface).

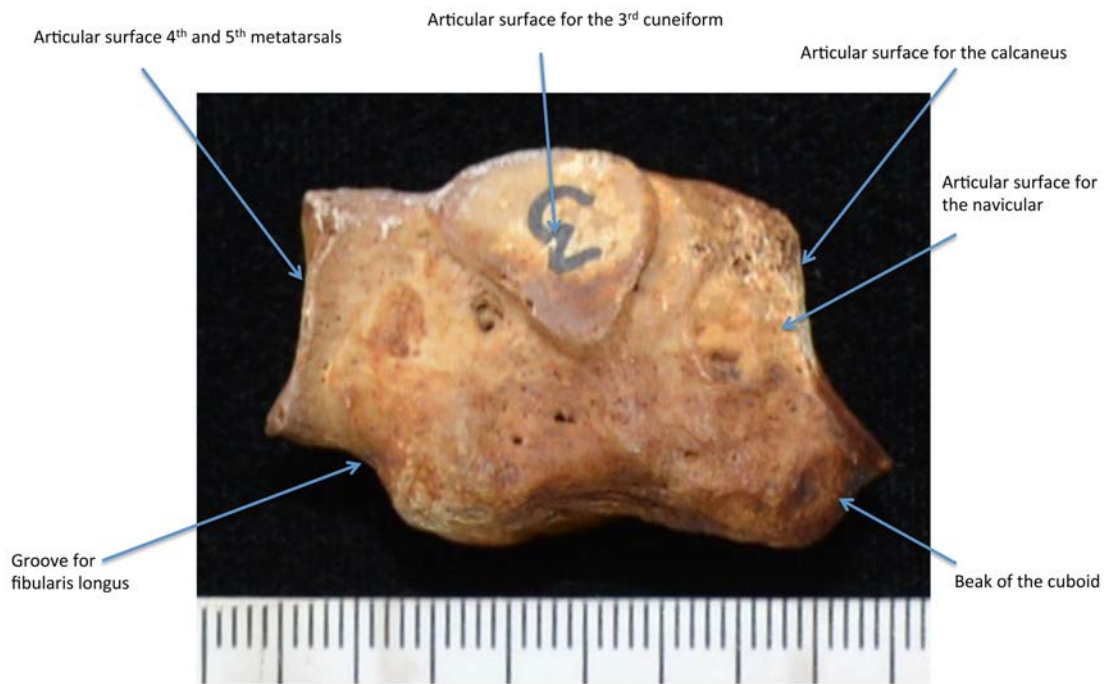


Figure 2d. Right cuboid (medial surface).

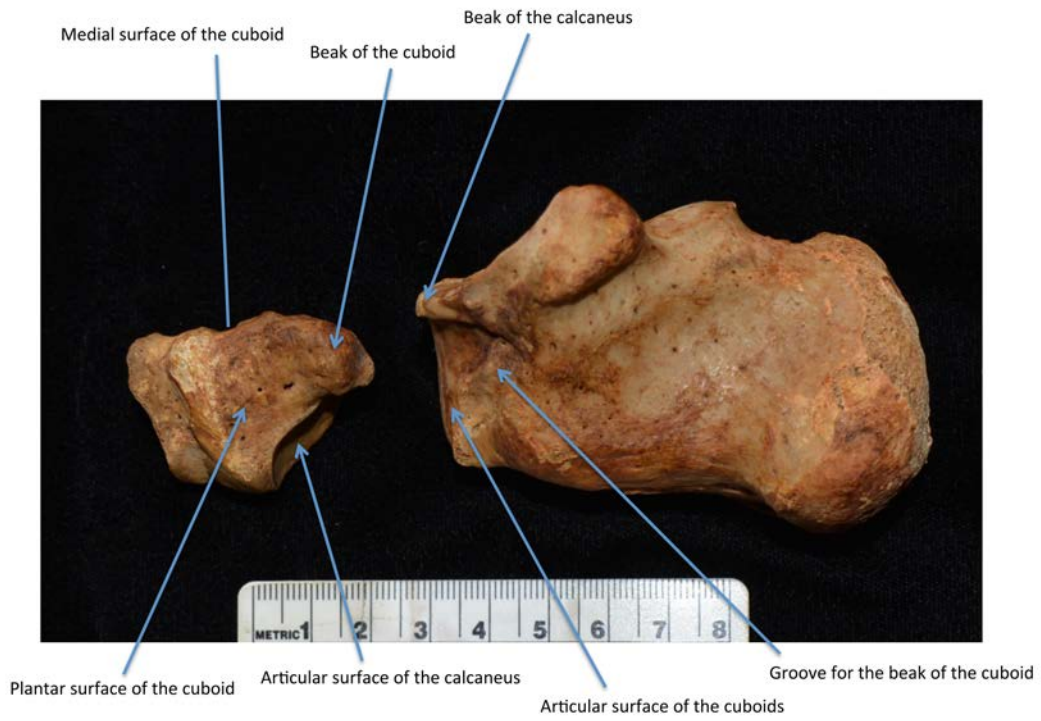


Figure 3. Calcaneocuboid relationship (right foot).

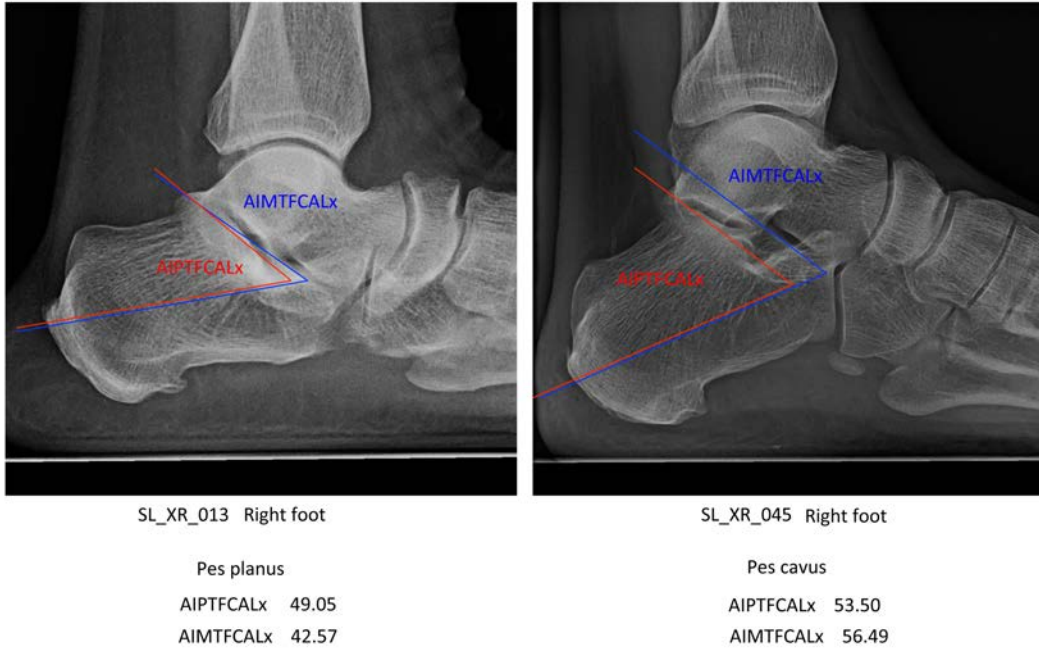


Figure 4. Illustration of differences in posterior and middle facet angles pes planus vs. pes cavus (in degrees).

Appendix A: Tarsal anatomy

The talus and calcaneus are complex bones; but appreciating their morphology is critical to understanding their role in human foot type biomechanics and classification, as well as in the process of measuring the bones and their radiologic images.

Talus (astragalus) (Chapter 1, Figures 1a-1f)

The talus is the second largest tarsal bone (Draves, 1986). It has no muscle attachments; its movements are dependent upon its relationships and soft tissue attachments, at the ankle, subtalar, and talocalcaneal navicular joints. The talus occupies a central position between the leg and foot; its shape partly reflects the longitudinal arched structure of the foot, especially the medial arch (Oxnard and Lisowski, 1980). It is a short bone, complex in nature, consisting of a head, neck and body. The body of the talus is cube shaped, made up of six surfaces.

The superior surface of the body (the trochlea) is pulley-like in shape, forming the ankle joint with the inferior surface of the tibia. The surface is convex anteroposterior and slightly concave superiorly in mediolateral direction (Kelikian, 2011). The medial border has been described as being slightly lower than the lateral border (Kelikian, 2011); however, with the bone on a flat surface, others have described the superior-most point of the superior surface as usually along its medial border (Steele, 1976). In the transverse plane, the lateral border curves medially going from anterior to posterior while the medial border is straight, thus parallel to the medial border of the talar body. The result is that the superior surface is wider anteriorly than it is posteriorly. The medial border is continuous with the coma shaped facet on the medial surface for articulation with the lateral aspect of the medial malleolus; the lateral border is continuous with the triangular shaped articular facet on the medial surface for the lateral malleolus. The anterior border of the trochlear surface may be straight, slightly concave, convex along its entire length, or in an elongated "S" shape (Kelikian, 2011).

Most of the lateral surface of the body is triangular, apex facing inferiorly, continuous superiorly with the trochlear surface. The articular surface is concave going from superior to inferior and slightly convex going anterior to posterior (Kelikian, 2011). This surface articulates with the medial articular surface of the lateral malleolus. The roughened apex of the lateral surface called the lateral process, projects laterally and may be quite prominent.

The medial surface of the body is divided into two surfaces, a smooth articular surface superiorly and a rough non-articular surface inferiorly. The articular surface is a cartilage covered comma shaped facet, widest side facing anteriorly, for articulation with the lateral surface of the medial malleolus. It is continuous with the superior surface of the body. The articular surface sometimes extends distal onto the superomedial surface of the neck of the talus. In the frontal plane, the articular surface is wider superiorly than it is inferiorly. The medial surface also has roughened areas inferior to the coma shaped articular facet for ligamentous attachments. The posterior inferior non-articular portion of the medial surface is continuous with the medial tubercle of the posterior surface (posteromedial tubercle) and may be quite prominent. The medial wall of the groove for the flexor hallucis longus marks the posterior border of this non-articular surface.

The posterior surface of the body has a posteriorly projecting prominence, the posterior process of the talus, which is divided into two smaller tubercles by the sulcus for the tendon of the flexor hallucis longus muscle. This groove may form at angle of between 132 to 175° in relation to a line drawn perpendicular to the long axis of the body, going in a superior lateral to inferior medial direction (Draves, 1986). The more lateral tubercle of the posterior process (posterolateral tubercle) is sometimes formed from a secondary center of ossification, which, if unfused, becomes a separate supernumerary bone, the os trigonum. The medial tubercle is usually less prominent than the lateral and is continuous with the posterior and inferior aspect of the medial surface of the body.

The inferior, or plantar, surface of the body is wholly articular and is covered with cartilage. It articulates with the posterior facet of the calcaneus, together forming the talocalcaneal, or anatomical subtalar, joint (Draves, 1986). It is deeply concave, its longitudinal axis running from a posteromedial to an anterolateral direction.

The anterior surface of the body is continuous with the neck of the talus. The average length of the neck is 17 mm, with a range of 12 to 23 mm (Kelikian, 2011). The medial articular surface of the body, as well as the anterior border of the superior trochlear facet of the body, sometimes extends distally onto the neck of the talus. The sulcus tali is located on the inferior aspect of the neck, separating the posterior facet of the body from the anterior and middle facet found on the head of the talus. The sulcus tali forms the sinus tarsi with the superior surface of the calcaneus. The sulcus tali is oriented in a medial posterior to lateral anterior direction. It is narrow medially and widens laterally.

The shape of the talus is determined by the medial deviation and torsion of its neck and head (Lisowski, 1967). The neck of the talus runs in a somewhat medial and plantar direction. The *angle of the neck* is formed made by the neck's longitudinal axis the talar body in the transverse plane. Towards the end of fetal life, the neck of the talus, which earlier in fetal development is widely adducted becomes less adducted and more in line with the body of the talus. Thus, the adult talus has a smaller neck angle than in the newborn tali. During human postnatal development, the talar neck angle becomes reduced, a condition that favors the development of arches of the foot (Lisowski, 1967). It is variable in the adult, averaging between 10-15 degrees, depending upon method of measurement, in the adult (Draves, 1986). The decrease in the neck angulation is necessary for the development of the arches of the foot especially in the development of the longitudinal arch. The neck is also angled in an inferior direction in the sagittal plane, creating the *angle of inclination* in relation to the body of the talus (Kelikian, 2011).

There is also torsion at the neck in the frontal plane in relation to the body, creating an angle between the long axis of the talar head and superior surface of the talar body, termed the angle of talar torsion, angle of declination of the talus, or angle of lateral rotation (Draves, 1986; Kelikian, 2011). The torsion is such that the axis of the talar head goes from a dorsal lateral to a plantar medial direction. The angle faces in a medial direction. Postnatal, the torsion of the head and neck of the talus increases (Lisowski, 1967), thus adults have a significantly greater angle of torsion than the newborn tali. During human postnatal development the talus head and neck torsion increases with age, also necessary for the development of the arches of the foot, especially in the development of the longitudinal arch (Lisowski, 1967). Depending on the study, the angle or talar torsion averages 45 to 49°.

The head of the talus is located anteriorly, medially, and inferiorly to the talar body. It has two major surfaces. Its anterior, or distal, surface is convex and wholly articular. It articulates with the navicular, forming part of the talocalcaneonavicular joint. Due to the torsion of the talar neck, the navicular articular surface of the head of the talus is more superior laterally than it is medially. The longitudinal axis of the head in the frontal plane is thus oriented superiorly and laterally (Kelikian, 2011). Inferiorly, there are anterior and middle calcaneal facets, which articulate with corresponding facets on the superior surface of the calcaneus. The anterior facet is continuous with the anterior surface of the head, forming part of the talocalcaneonavicular joint; it may either be continuous with the middle facet or separated from it by a ridge. The middle facet articulates with the superior surface of the sustentaculum tali, a bony projection from the medial surface of the calcaneus.

Radiographic anatomy of the talus (Chapter 1, Figures 2a and 2b)

On the AP weight-bearing view, only the talar head and neck are visible. The distal tibia usually obscures the anterior aspect of the talar body, including its anterior border, from view. The outline of the central aspect of the talar head can be clearly seen where it articulates with the navicular. The widest points of the head medially and laterally mark where the navicular articular surface ends and the neck begins (Christman, 2014). The point where the head joins the neck is less distinct medially. The medial margin of the neck is less distinct and appears shorter than the lateral margin as it is obscured by the anteroinferior border of the tibial malleolar articular surface and, more proximally, the oblique ridge along the medial surface of the talar body (Christman, 2014). The medial margin of the neck is also straighter than is the lateral border. The medial aspect of the anterior calcaneus may obscure the lateral margin of the neck. The lateral margin corresponds to the large ridge separating the neck's superior and inferior surfaces. The ridge flares out proximally, corresponding to the anterior border of the fibular articular surface that may extend to the neck (Christman, 2014).

The entire talus can be identified on the lateral view (Christman, 2015). The tibial malleolus is superimposed on the anterior aspect of the talus, and the fibular malleolus on the posterior portion. These structures may obscure, to some degree, the viewing of parts of the talus with which they overlap (Christman 2014). The overlapping anterior process of the calcaneus may obscure this angulation and the inferior aspect of the head of the talus.

The anterior margin of the talus corresponds to the navicular articular surface of the talar head. This margin continues plantarly superimposed on the anterior process of the calcaneus. A rather indistinct angulation separates the plantar margin of the head from the medial calcaneal articular surface on the neck. The dorsal margin of the neck is located between the dorsolateral corner of the navicular articular surface and the trochlear surface for the tibia. The dorsal margin of the neck, as well as the points where the neck can be distinguished from the talar head and trochlear surface may not be distinct, depending upon the amount of pronation and supination, as well as the position of the talus relative to the x-ray beam and image receptor (Christman, 2014). The dorsal margin of the neck continues proximally as two convex dorsal margins that may or may not be collinear or nearly collinear to each other. These margins represent the medial and lateral margins of the trochlear articular surface for the tibia (Christman, 2014). The margin that continues posteriorly from the neck's

dorsal margin corresponds to the medial border of the trochlear surface. The dorsal margin that continues posteriorly from the sclerotic concavity of the neck, as an abrupt line, forms a more acute angle as it continues into the lateral border of the trochlear surface. The margin corresponding to the medial trochlear border is usually superior to the margin of the lateral trochlear border anteriorly, though this may vary depending on the position of the talus in relation to the x-ray beam and the receptor surface. The two margins may cross each other near the center of the joint (Christman, 2014).

Posteriorly, the margin corresponding to the medial trochlear border is plantar to the margin corresponding to the lateral trochlear border. The medial and lateral margins continue posteriorly, the most posterior of the two corresponds to the posterolateral tubercle of the talar posterior process (Christman, 2014). The medial tubercle of the posterior process (posteromedial tubercle) can be identified anterior and parallel to the lateral tubercle of the posterior process (posterolateral tubercle); it appears as a well-defined, crescentic increased density. The posterior inferior margin representing the posterior calcaneal articular surface is seen beginning slightly inferior and parallel to this margin continuing posteriorly. However, the radiographic appearance of the superior and inferior margins of the talus can vary a great deal, depending upon its relationship to the x-ray beam and receptor, which can be affected by the position of the ankle joint axis, talus, and foot (Christman, 2014). The talar lateral process appears as the letter "V," the apex facing plantarly between the middle and posterior calcaneal articular surfaces (Christman, 2014).

The plantar margin of the neck corresponds to the medial articular surface for the calcaneus. The plantar margin of the medial articular surface ends posteriorly; however, another plantar margin slightly inferior and parallel to the former continues as the posterior calcaneal articular surface and continues as the inferior aspect of the posterolateral tubercle of the posterior process (Christman, 2014).

Calcaneus (os calcis) (Chapter 1, Figures 3a-3f)

The calcaneus is the largest tarsal bone. Its most prominent feature is the calcaneal tuberosity, which helps to form the heel of the foot. The calcaneus is located inferior to the talus and is roughly rectangular in shape, with six surfaces. The long axis of the calcaneus when weight-bearing is tilted anteriorly, superiorly, and laterally relative to the horizontal plane, normally at a 30 to 35° angle in the sagittal plane (Draves, 1986).

The anterior, or distal, surface is wholly articular, forming the calcaneocuboid joint with the cuboid. This joint is a concavo-convex, saddle, or sellar shaped joint allowing very little motion between the two articular surfaces. The facet is convex from medial to lateral and concave from superior to inferior. A shelf like projection, the beak of the calcaneus, is located at the superomedial aspect of the articular surface, superior to the cuboid (Kelikian, 2011).

The superior surface can be divided into three regions of approximately equal areas: posterior, middle and anterior (Draves, 1986). The posterior third is non-articular. The medial border of the superior surface is concave in shape in an anterior to posterior direction. The lateral border has been described as being mildly convex though it can be straight to mildly convex (Kelikian, 2011). The posterior articular facet for the talus is located on the middle third and is oval in shape. It is markedly convex on its longitudinal axis, which runs from a posterior

medial to an anterior lateral direction. This facet articulates with the inferior surface of the body of the talus. The middle one-third is separated from the anterior one-third by a groove, the calcaneal sulcus, or sulcus calcanei, which runs from a posterolateral to anteromedial direction. The sulcus calcanei, along with the sulcus tali on the inferior surface of the body of the talus, forms the sinus tarsi. The two more distal superior facets, which articulate with the inferior surface of the talar head, are located on the anterior third portion of the superior surface of the calcaneus. The middle talar articular facet of the calcaneus is located on the superior surface of the sustentaculum tali. The anterior talar facet of the calcaneus is more anterior and lateral. It articulates with the anterior calcaneal facet of the talus, contributing to the formation of the talocalcaneonavicular joint. There is noted variability in the relationship of the articular facets on the superior surface of the calcaneus (Bunning, 1964; Bunning and Barnett, 1965; Jha and Singh, 1972; Naskashima and Hojo, 1986; Kelikian, 2011). The anterior facet may be distinct, absent, or continuous with the middle facet. Rarely, the anterior, middle and posterior facets are fused together (Bunning, 1964; Bunning and Barnett, 1965). The anterior one-third of the superior surface of the calcaneus is non-articular and roughened by ligamentous and tendinous attachments. The anterior border of the superior surface projects distally to varying degrees, depending upon the depth of the convexity of the anterior surface of the calcaneus, and whether there is any spurring present.

The axis of the lateral surface of the calcaneus is parallel to the long axis of the body and rough in nature. It has been described as relatively flat, with a mild convexity in the superior segment of the posterior one third of the bone in the frontal plane. There may be a lateral projection present, the peroneal tubercle (also called the peroneal trochlear, or process trochlearis) that can vary in size and shape (Oliver, 1969; Draves, 1986). The peroneal tubercle may present as an elongated ridge in shape, oriented in a superior posterior to inferior anterior direction at a 45° angle (Kelikian, 2011). The peroneal tubercle can also be round and slightly raised. There may be a groove superior to the peroneal tubercle for the tendon of fibularis brevis. In one study, this groove was present in 2.6% of the bones studied (Kelikian, 2011). More commonly, there is a groove present inferior to the peroneal tubercle for the tendon of the fibularis longus. This groove has been noted in 85% of the bones studied. The peroneal tubercle itself is present 36 to 44% of the time and absent 56-64% of the time (Draves, 1986). Superiorly and posterior to the peroneal tubercle (at about one o'clock) a smaller projection is sometimes present, the tubercle for the calcaneofibular ligament (peroneal spine) (Draves, 1986). A third tubercle, the retrotrochlear eminence, is found posterior to the peroneal tubercle and groove for the fibularis longus. As with the peroneal tubercle and the surrounding grooves, the peroneal spine and retrotrochlear eminence are not always present; when they are, they can be variable in size. The retrotrochlear eminence, however, is usually present 98%, though it can be prominent and pointed, or broad, rounded and relatively flat (Kelikian, 2011). In addition, an anterior facet for articulation with the os peroneum may be found on the lateral surface, when this variable sesamoid bone is present.

The posterior surface is rough and triangular in shape, apex facing superiorly. The surface can be divided into thirds. The superior surface is smooth and may have a bursa between it and the Achilles tendon in life. The Achilles tendon inserts into the middle one-third of the posterior surface of the calcaneal tuberosity. The posterior one third may be enlarged and may or may not have a large spur projecting superiorly and sometimes also posteriorly.

The inferior one-third area of the posterior surface is rough and striated, covered with the fat pad of the heel in life. The inferior border is continuous with the plantar surface of the calcaneal tuberosity.

The inferior or plantar surface is triangular in shape, apex facing distally. The lateral border is oblique, directed in an anterior and medial direction, and usually more distinct than the lateral border (Kelikian, 2011). The medial border is more concave in a posterior to anterior direction. The prominent calcaneal tuberosity is located on the inferior surface of the calcaneus. It may be considered as being continuous with the inferior one-third of the posterior surface. The calcaneal tuberosity is the major weight-bearing surface of the calcaneus. Plantarily it is divided into a larger medial process and a smaller lateral process. The two processes may be confluent or separated by a groove. The lateral process may be absent (Kelikian, 2011). At its distal aspect is the attachment for the proximal attachment of the plantar aponeurosis or fascia. There may be calcification of the ligament at its attachment, creating a shelf of bone, which appears as a spur on the lateral radiographic view. In one study of 50 calcanei, a plantar calcaneal spur was noted projecting from the medial tubercle in 36% of the sample (Kelikian, 2011). The tuberosity may be enlarged by the presence of spurs; the size of the tuberosity can vary in size in relationship to the body depending upon the individual (Kelikian, 2011). The area anterior to the tuberosity is triangular in shape. Distally, the anterior tubercle is found on the plantar surface of the calcaneus near the apex of the triangle (Kelikian, 2011).

The medial surface of the calcaneus is concave in both an anterior to posterior and superior to inferior direction. The length and width of the sustentaculum tali varies; in one study, the width averaged 13 mm, with a range between 8 and 18 mm (Kelikian, 2011). The angulation of the sustentaculum in relationship to the body in the sagittal plane may vary as well. It is oriented from a superior-posterior to an inferior-anterior direction, with an angle averaging 46°, with a range of 30 to 60° (Kelikian, 2011). The tendon of the flexor hallucis longus muscle grooves the sustentaculum tali inferiorly. The middle talar facet of the calcaneus is located on its superior surface. The articular surface is concave along its longitudinal axis, running from a posterior medial to anterior lateral direction. The medial surface of the sustentaculum tali is rough for attachment of the medial collateral ligament of the ankle; prominent spurring may be present at the ligamentous attachment.

Radiographic anatomy of the calcaneus (Chapter 1 Figures 4a and 4b)

In the AP view, lateral and anterior aspects of the distal calcaneus are the only regions clearly visible (from Christman, 2015). The overlapping lateral aspect of the neck of the talus obscures the medial border of the anterior aspect of the calcaneus, though, depending upon the density of the talus, it may be visible. Most of the calcaneus, including the sustentaculum tali, cannot usually be observed in a standard AP radiographic view. Two anterior margins can usually be observed, a distal one superimposed on the cuboid, and a more proximal one. The distal margin, representing the inferior aspect of the anterior articular surface, is not clearly visible because this joint is oblique relative to the x-ray beam and because it's obscured by the cuboid (Christman, 2014). The more proximal margin is curvilinear and well defined, corresponding to the superior aspect of the anterior articular surface of the calcaneus. Because

the superior portion of the calcaneocuboid articulation is parallel to the central beam, it is clearly observable and separated from the posterior articular surface of the cuboid (Christman, 2014). The lateral margin represents the lateral surface of the calcaneal surface. The lateral surface may not appear flat depending upon the prominence of the tubercles along the lateral surface. The retrotrochlear eminence may be observable depending on the soft tissues and whether the more proximal portion of the calcaneus is included in the view (Christman, 2014). The lateral margin of the entire lateral calcaneal surface is sometimes visible on the AP view. Bony prominences located on the lateral surface may be seen, if present, depending upon the angulation of the calcaneus to the x-ray beam and receptor (Christman, 2014).

On the lateral view the entire calcaneus, including the sustentaculum tali and the middle and posterior talar articular surfaces, as well as the calcaneal tuberosity, can be seen (Christman, 2014). Four radiographic margins are observable representing the anterior, inferior, posterior, and superior surfaces. The medial calcaneal tuberosity makes up the posterior portion of its inferior margin. The lateral calcaneal tuberosity is usually seen as an irregular increase in density superior to the medial tuberosity (Christman, 2014). The posterior margin represents the lateral aspect of the posterior surface of the calcaneus.

The anterior margin of the calcaneus, representing the calcaneocuboid joint in the sagittal plane ranges from straight to lazy "S" line, paralleling the cuboid's posterior margin. The plantar half corresponds to the lateral aspect of the anterior articular surface (Christman, 2014). The anterior process of the calcaneus is present at the superior portion of the anterior border; it is partly superimposed on the talar head. A small protuberance may be noted projecting off the anterior process representing the calcaneal beak.

The plantar margin represents the inferior surface of the calcaneus. The calcaneal tuberosity is present posteriorly. The medial process is located inferiorly and anteriorly to the larger lateral process. The lateral process is seen as an irregular increased density superior to the medial tuberosity.

The posterior margin represents the lateral aspect of the posterior surface. The three segments of this surface can usually be identified. A distinct separation is observable between the middle and lower section, sometimes as a small step-off, other times as a smooth transition as the border goes in more anterior direction. The division between the upper and middle sections may or may be distinct.

The superior margin represents the superior surface of the calcaneus. The margin can be divided into the three sections of this surface. The posterior one-third is non-articular and concave to varying degrees. The posterior talar articular facet surface can be identified along the middle one-third section of the superior margin; it is superimposed, to some degree, by the posteromedial process of the talus. It slopes in an anterior plantar direction to varying degrees. It is nearly flat to mildly convex. It ends anteriorly at a concavity presenting the lateral entrance of the tarsal canal.

The middle articular surface for the talus is noticeable along this margin representing the superior surface of the sustentaculum tali. The sustentaculum tali itself appears rectangular in shape; it may be difficult to identify just inferior to the middle talar articular surface. The sinus tarsi is located anterior to the middle talar articular surface; it may be obscured by the talus in the rectus and pronated foot. The anterior talar articular surface is not visible.

Appendix A: Literature cited

- Bunning PSC. 1964. Some observations on the West African calcaneus and the associated talocalcaneal interosseous ligamentous apparatus. *Am J Phys Anthropol* 22:467-472.
- Bunning PSC, and Barnett CH. 1965. A comparison of adult and foetal talocalcaneal articulations. *J Anat Lond* 99:71-76.
- Christman RA. 2014. Radiographic Anatomy of the Foot and Ankle—Part 2 The Greater Tarsus. *J Am Podiatr Med Assoc* 104:493-503.
- Christman RA. 2015. *Foot and Ankle Radiology*. Second edition. Philadelphia: Wolters Kluwer.
- Draves DJ. 1986. *Anatomy of the Lower Extremity*. Baltimore: Williams and Wilkins.
- Jha MR, and Singh DR. 1972. Variations in the articular facets on the superior surface of calcaneus. *J Anat Soc India* 21:40-44.
- Kelikian AS. 2011. *Sarrafian's Anatomy of the Foot and Ankle*. Philadelphia: Wolters Kluwer / Lippincott Williams & Wilkins.
- Lisowski FP. 1967. Angular growth changes and comparisons in the primate talus. *Folia Primat* 7:81-97.
- Nakashima T, and Hojo T. 1986. Variations in the talar articular facets of Japanese calcanei. *Fukuoka Acta Med* 77(No 10):544-548.
- Oliver G. 1969. *Practical Anthropology*. Springfield: Charles C. Thomas.
- Oxnard CE, and Lisowski FP. 1980. Functional articulation of some hominoid foot bones: implication for the Olduvai (Hominid 8) foot. *Am J Phys Anthropol* 52:107-117.

Appendix B: Further Details Materials and Methods Chapters 2 and 3

The specimens used for this study were collected between 1986 and 1988 from lower extremity amputations performed at the (then) New England Deaconess Hospital (NEDH) in Boston, MA. The specimens and associated patient information were collected with the written approval of the NEDH Institutional Review Board on Human Studies. These individuals underwent below or above knee amputations for infection or acute ischemia. Information concerning their age, ancestry, sex, stature, and medical condition in most cases was recorded (Table 1). The New England Deaconess Hospital was (and now as part of the Beth Israel Deaconess Hospital network continues to be) a medical center specializing in the treatment of individuals with diabetes mellitus (DM) and/or peripheral vascular disease (PVD). At the time period that these amputations were performed, surgical methods were being developed to restore circulation to limbs where blood supply was reduced or totally blocked secondary to arterial vascular disease. Among the surgical techniques used to restore circulation when the blockage was in the femoral artery was a “fem-pop bypass graft” (FPBG) where, using a harvested vein or artificial vessel, the blockage was bypassed with the connection of the graft proximal to the blocked portion of the femoral artery to the patent popliteal artery distally. However, if the blockage was distal to the popliteal artery, the FPBG technique could not be used, since the diameter of the tibial artery was too narrow. In the event that circulation could not be restored to the dysvascular limb, a below-knee or above-knee amputation was performed proximal to the area of blockage, depending upon the level of the blockage. However, by 1989, techniques for bypassing a blockage distal to the popliteal artery were being perfected. As a result, many more limbs were saved and the number of amputated feet suitable for study became few and far between.

The individuals in this study range between 36 and 89 years of age at the time of their amputation, with most being born in the first one-third of the twentieth century. This information is important in studying the size of the bony elements for demographic and forensic purposes, where populations of individuals in the United States born later in the twentieth century tend to be larger. Since the complications from medical conditions that necessitate an amputation increase with age, most of the limbs used in this study were from older adults. Demographic information was taken from their pathology and hospital medical records where available; none of the individual’s height or weight was measured directly as part of this study. In some instances, recorded heights and weights were taken from the information provided by previous hospital admissions. It should be noted that height will decrease somewhat as an individual ages and weight will vary depending upon the medical condition and patient’s health. A total of 32 limbs from male patients and 22 from female patients were collected for these studies. (With further examination of the hospital records, the sex of the 3 individuals mentioned in Chapters 2 and 3 as of unknown sex was later identified as female).

The limbs were placed in cold storage after examination by a pathologist. The processing of the amputated limb began with sectioning the limb above the ankle, retaining the distal portion of the tibia and fibular. The foot was x-rayed in the standardized non-weight-bearing fashion for obtaining anterior-posterior (AP) (also referred to as dorso-plantar or DP) and lateral views (Gamble and Yale, 1975; Christman, 2015). In the AP view the foot is flat on

the image receptor and the x-ray tube angulation is 15° from the vertical, directed posteriorly toward the second metatarsocuneiform joint. In the lateral view the medial aspect of the foot is placed against the image receptor and the x-ray tube angulation is set at 0° toward the lateral cuboid-cuneiform region. AP views were taken with a setting of 200 mA for 0.012 seconds (2.4 mAs) at 60 kVp, and a second AP image was taken to over expose the resultant image and better identify areas where the talus and calcaneus overlap, with a setting of 200 mA for 0.018 seconds (3.6 mAs) at 66 kVp. The lateral view was taken with a setting of 200 mA for 0.012 seconds (2.4 mAs) at 60 kVp.

After taking the AP and lateral radiographic views, each foot was skeletonized. Maceration and preparation of the skeletal material took place at the NEDH mortuary. Toxic chemicals could not be employed in this setting to process the specimens. An enzyme-based laundry detergent “pre-soaker” method as described by Ossian (1970) was used instead (also see (Fenton et al., 2003)). In this method, the skeletal material, after sharp dissection with the removal of as much soft tissue as possible, is placed in water with the addition of an enzyme detergent (in this case Axion^R was used). Because heat increases the speed of the breakdown process while boiling would denature the protein, the water must be kept at a constant temperature (Ossian recommends between 50° and 70°C). A slow cooker (Crock-Pot[®]) was used to consistently heat the solution until the fully immersed bones were clean. After a few days of soaking any remaining tissue that did not fall off of the bone was easily removed. The bones were then soaked in acetone overnight, dried, labeled and boxed. This method worked well with essentially no grease and minimal damage to the bone. Only bones affected by osteopenia were somewhat brittle. After over 25 years of storage the bones continued to be in excellent condition for examination and measurement, without grease, odor, or destruction. The lower tibia and fibula, talus, calcaneus, navicular, cuboid, medial, intermediate, and lateral cuneiforms, all five metatarsals, and the proximal and distal phalanges of the hallux were retained.

Appendix B: Literature cited

Christman RA. 2015. Film-Screen Radiology. In: Christman RA, editor. Foot and Ankle Radiology. Second ed. Philadelphia, PA: Wolters Kluwer. p 15-35.

Fenton TW, Birkby WH, and Cornelison J. 2003. A fast and non-bleaching method for forensic skeletal preparation. J Forensic Sci 48(2):274-276.

Gamble FO, and Yale I. 1975. Clinical Foot Roentgenology, 2nd edition. New York: Krieger Publishing.

Ossian CR. 1970. Preparation of disarticulated skeletons using enzyme-based laundry "pre-soaks". Copeia 1970:199-200.

Schmitt DM. 1966. How to Prepare Skeletons. Rochester NY: Ward's Natural Science Establishment, Inc.

Appendix B: List of Tables

Table 1. Demographics and medical histories for subjects Chapters 2 and 3.

Table 2. Demographics and medical histories for subjects Chapters 2 and 3 abbreviations.

SN	Sex	Side	DOB (D/M/Y)	Age (yrs.)	Ethnicity	Height (cm)	Weight (kg)	Medical history	Reason for amputation
1	M	R	5/9/25	66	Caucasian	170	67	CAD, s/p DJD	Chronic osteomyelitis R femur
2	F	L	3/1/13	74	Caucasian	173	82	DM, PVD, s/p FPBG	L leg gangrene, ischemia
3	M	L	*0/0/14	73	Caucasian	U	61	CAD, COPD, hyperparathyroidism,	Acute ischemia
4	M	R	U	72	Caucasian	U	U	PVD	Ischemia
5	M	R	4/2/09	76	Caucasian	172	75	PVD, COPD, ARF	Acute ischemia
6	F	L	12/19/15	69	Caucasian	157	52	DM, PVD, neuropathy, CHF, s/p R AKA	Gangrene R hallux, cellulitis
7	F	R	8/19/06	80	U	168	71	PVD, ASO	Acute ischemia
8	M	R	1/19/24	63	U	165	78	IDDM, PVD, CHF, CAD	Ischemia
9	F	R	5/17/13	73	Caucasian	157	47	PVD	Gangrene
10	F	L	5/11/51	35	Caucasian	168	105	PVD	Infection; acute ischemia
11	M	R	9/29/45	42	Caucasian	185	79	DM, CRF, neuropathy	Gangrene
12	F	L	U	69	U	U	U	U	U
13	M	R	5/22/43	44	Caucasian	183	68	Hodgkin's Disease, cutaneous leg ulcers	S/P hallux amp w infection
14	M	R	8/26/10	76	Caucasian	U	70	NIDDM, CHF	Acute ischemia; dry gangrene, **
15	M	R	10/5/17	69	Caucasian	168	64	DM, neuropathy, s/p MI	Gangrenous toes, acute ischemia
16	M	L	8/26/10	76	Caucasian	U	70	NIDDM, CHF	Acute ischemia, **
17	M	R	10/15/21	65	Caucasian	170	56	IDDM, s/p FTBG s/p amp 1st, 2nd toes	Advanced ischemia, dry gangrene
18	M	R	10/11/09	75	Caucasian	170	79	DM, PVD, HT, CHF	Gangrene R hallux; ischemia
19	F	L	U	76	U	U	U	U	U
20	F	L	12/14/31	55	Caucasian	180	85	DM, CRF, neuropathy, CHF, CAD, s/p MI	Acute ischemia s/p renal transplant,
21	F	L	11/13/19	67	Caucasian	168	81	CHF	gangrene (s/p trauma posterior calf)

Table 1. Demographics and medical histories for subjects Chapters 2 and 3.

SN	Sex	Side	DOB (D/M/Y)	Age (yrs.)	Ethnicity	Height (cm)	Weight (kg)	Medical history	Reason for amputation
22	M	R	2/19/31	55	Caucasian	183	98	PVD, s/p L FPBG,	Ischemia
23	F	R	4/10/16	71	Caucasian	160	46	Raynaud's. COPD	Ischemia
24	F	R	4/20/44	43	Caucasian	U	71	DM, CRF, neuropathy	Ulceration, acute ischemia
25	M	L	3/18/29	53	Caucasian	160	60	PVD, HT, s/p L FPBG	Infected lower leg fasciotomy
26	F	R	8/14/11	75	Caucasian	168	60	Unknown	Hip infection
27	M	L	8/21/19	68	Caucasian	178	77	DM, PVD, s/p R BKA	Gangrenous toes, acute ischemia
28	M	L	8/7/32	55	U	180	U	PVD, COPD, HT	Ischemia
29	F	R	5/25/41	46	Caucasian	155	70	DM, CRF, CHF, neuropathy	Ischemia
30	M	R	6/23/30	57	Caucasian	188	96	Buerger's Disease (PVD) s/p FPBG	Ischemia
31	M	R	7/23/05	82	Caucasian	160	61	AODM, CAD	Ischemia
32	F	L	9/6/34	53	Caucasian	155	74	DM, PVD	Acute ischemia, ***
33	F	R	9/6/34	53	Caucasian	155	74	DM, PVD	Acute ischemia, ***
34	M	R	4/24/19	68	Caucasian	183	117	DM, PVD, neuropathy, CAD	Infection, ischemia
35	M	L	U	76	U	U	U	U	U
36	F	L	4/28/32	55	Caucasian	150	80	DM, CRF, s/p R BKA	Gangrene, infection
37	M	R	5/2/34	53	Caucasian	175	88	DM, CRF, neuropathy, PVD, s/p MI	Multiple ulceration ankle, toe, calf; gangrene
38	M	R	3/10/16	71	Caucasian	191	106	DM, CHF, CAD	Foot infection
39	M	R	12/15/59	28	Black	193	109	Unremarkable	Popliteal artery w acute ischemia
40	F	L	3/28/98	89	Black	152	42	PVD, COPD, s/p R AKA	Non healing ulcer L hallux
41	M	L	7/27/08	79	Caucasian	175	71	DM, CAD, s/p CVA	Ulceration, ischemia
42	F	R	8/20/00	87	Caucasian	152	54	PVD, s/p CVA w R hemiplegia	Acute ischemia

Table 1. Demographics and medical histories for subjects Chapters 2 and 3 (continued).

SN	Sex	Side	DOB (D/M/Y)	Age (yrs.)	Ethnicity	Height (cm)	Weight (kg)	Medical history	Reason for amputation
43	M	L	7/5/36	51	Caucasian	173	74	DM, HT, s/p MI, CHF, CAD	Acute ischemia (s/p axillo-fem BG)
44	F	R	2/14/03	85	Caucasian	158	45	PVD, COPD, CAD	Acute ischemia
45	F	L	3/27/18	70	Black	150	50	PVD	Gangrene R hallux, cellulitis
46	M	L	4/16/52	36	Caucasian	175	109	PVD	Ischemia
47	M	R	6/12/05	82	Caucasian	173	66	IDDM, PVD, s/p MI, s/p L BKA	Gangrene
48	F	L	7/18/40	48	Caucasian	173	81	DM, neuropathy, PVD	Non healing ulcer L foot
49	M	L	4/21/29	59	Caucasian	175	68	DM, PVD, neuropathy, s/p FPBG, CAD	Acute ischemia, gangrenous toes
50	M	R	3/11/28	60	Caucasian	175	104	DM, CRF, s/p L BKA	Infection; ischemia
51	M	L	12/21/10	77	Caucasian	U	71	DM, PVD, neuropathy	Ulcer L hallux; acute ischemia
52	M	R	12/1/07	80	Caucasian	170	74	NIDM, PVD, CAD, neuropathy	Ischemia
53	M	L	2/27/09	81	Caucasian	178	73	IDDM, s/p polio	Gangrene, ischemia
54	F	R	1/28/22	66	Caucasian	175	60	Paget's disease	Osteosarcoma R femur

Legend

- *Estimated
- ** Same individual: Bilateral BKA; Amputations took place within 6 weeks of each other
- *** Same individual: Bilateral BKA; Amputations took place within 3 weeks of each other

Table 1. Demographics and medical histories for subjects Chapters 2 and 3 (continued).

Legend

Abbreviation

AODM	Adult onset diabetes mellitus
AKA	Above knee amputation
BKA	Below knee amputation
CAD	Coronary artery disease
CHF	Congestive heart failure
COPD	Chronic obstructive pulmonary disease
CRF	Chronic renal failure
CVA	Cerebral vascular accident
DM	Diabetes mellitus
FPBG	Femoral-popliteal bypass graft
HT	Hypertension
IDDM	Insulin dependent diabetes mellitus
MI	Myocardial infarction
NIDDM	Non-insulin dependent diabetes mellitus
PVD	Peripheral vascular disease
U	Unknown or not recorded

Table 2. Demographics and medical histories for subjects Chapters 2 and 3 abbreviations.

Appendix C: Raw data

Note: Linear measurements are in millimeters (mm) and angular measurements are in degrees.

Chapter 2: (Tables 1a-2)

Sn	MaxLTAL	MaxLTALx	MaxHBTAL	MaxHBTALx	BHTAL (a)	BHTAL (b)	BHTALx	MaxLFMTAL	MaxLFMTALx
1	59.85	62.31	34.83	34.51	33.81	35	34.08	29.55	29.77
2	57.83	55.73	30.68	30.09	32.96	33	32.78	32.01	32.88
3	64.99	63.89	34.73	35.6	36.67	37	38.45	31.28	30.87
4	68.82	72.12	36.56	36.61	34.67	36.5	32.8	36.99	37.13
5	63.42	66.48	33.95	32.88	34.63	35.2	36.89	31.32	31.86
6	54.73	57.98	29.22	30.77	29.45	29.5	29.8	30.83	29.79
7	63.74	60.82	33.15	36.38	32.65	32.2	32.61	34.75	33.45
8	60.41	62.29	34.64	37.56	36.31	36.2	35.62	33.84	39.69
9	57.22	58.9	31.81	33.27	30.96	32	30.73	31.31	33.32
10	58.81	61.67	30.43	31.35	31.65	32.1	32.65	30.06	30.61
11	66.82	71.72	36.23	37.31	36.36	36.1	36.75	36.42	34.49
12	63.98	62.91	31.25	34.77	33.31	34.1	33.19	29.27	32.26
13	61.69	67.45	37.49	36.11	35.69	37.1	38.65	33.64	32.27
14	71.48	75.98	37.28	40.54	40.55	39.9	41.52	33.73	36.44
15	55.21	56	30.06	32.37	31.29	31.1	31.74	29.22	29.27
16	72.44	78.07	37.56	39.58	39.69	40.1	41.08	31.95	31.42
17	60.56	61.52	33.12	35.51	34.11	34.6	33.41	37.46	37.15
18	60.61	66.98	34.07	36.93	34.08	34.1	37.14	34.75	34.14
19	55.42	57.88	29.84	32.27	29.88	30.5	27.53	28.14	29.17
20	65.08	69.29	36.77	38.33	38.87	39.1	39.46	34.12	35.13
21	61.93	64.56	31.78	32.75	31.47	31.1	32.25	32.16	31.38
22	65.77	65.56	36.05	40.23	32.98	35.1	35.36	31.75	31.96
23	56.46	59.44	31.77	31.6	32.41	32.2	30.93	29.21	30.87
24	53.33	56.97	29.38	31.57	28.56	29.5	28.18	29.79	29.35
25	54.27	56.63	31.82	29.41	33.86	33.5	33.48	31.51	31.26
26	52.92	55.01	30.01	28.02	28.45	29	29.46	29.61	26.62
27	63.86	65	33.31	34.29	34.51	35.51	35.92	36.72	37.11
28	60.41	64.54	36.68	36.45	34.95	35.51	36.37	35.59	39.29
29	50.61	53.43	31.02	30.72	29.76	30.01	31.69	28.82	28.76
30	61.87	60.58	33.83	29.52	30.82	32.11	32.79	33.41	33.22
31	66.72	66.63	35.66	33.33	36.38	36.11	37.9	36.06	35.9
32	51.72	53.25	28.67	28.38	27.74	29.01	29.36	26.84	30.01
33	51.43	52.28	29.56	29.62	27.28	29.11	30.6	26.13	28.91
34	59.73	63.57	34.03	34.5	32.18	33.11	33.95	35.04	36.39
35	59.09	60.82	33.67	33.96	34.52	34.61	34.48	34.88	34.69
36	55.48	57.54	28.71	27.48	29.61	29.49	30.13	28.48	29.66
37	62.82	66.6	35.24	31.89	34.12	43.11	36.63	37.61	34.17
38	63.18	65.75	36.14	37.08	38.06	38.11	38.58	34.75	34.46
39	69.52	73.62	35.88	33.32	35.38	35.11	36.37	34.91	35.84
40	56.47	57.9	28.04	29.75	31.59	31.11	30.46	28.93	29.6
41	56.95	59.17	33.68	32.59	33.01	33.11	33.29	31.55	34.74
42	49.37	49.42	27.71	27.16	27.03	27.11	29.24	28.88	31.06
43	61.15	64.09	31.73	32.61	33.18	33.01	33.11	33.88	32.89
44	53.04	55.14	29.97	30.21	30.49	30.51	30.84	29.96	29.96
45	53.49	56.49	27.86	28.24	29.39	29.25	29.76	30.15	30.85
46	61.73	65	33.37	32.32	32.21	32.12	32.93	34.83	33.41
47	60.27	62.67	34.91	35.36	34.07	35.02	36.92	35.96	33.05
48	60.48	60.91	31.89	32.48	32.33	31.81	31.9	33.48	35.25
49	62.66	65.85	33.64	31.81	33.88	34.01	37.17	29.84	34.43
50	64.66	67.9	32.51	34.1	32.12	32.33	32.33	32.85	33.71
51	60.92	64.33	34.64	29.56	34.24	34.01	33.87	32.16	33.96
52	60.96	62.54	32.83	31.87	34.12	34.11	34.54	35.15	34.31
53	58.54	66.14	33.89	35.84	33.33	33.21	34.9	34.21	34.1
54	60.35	63.08	33.64	29.69	33.18	33.11	32.95	33.61	30.57

Table 1a. Talus linear measurement (Chapter 2).

Sn	MaxWHTAL	MaxWHTALx	MinWNTALa	MinWNTALb	MinWNTALx	MaxLHTAL	MaxLHTALx
1	28.43	33.43	26.66	24.21	27.68	26.74	27.96
2	33.25	30.32	28.31	28.07	24.64	24.65	26.56
3	34.84	37.51	31.55	31.82	32.61	25.34	26.6
4	33.48	36.53	30.79	30.78	28.53	26.91	26.41
5	31.58	30.25	29.87	29.56	32.27	26.56	27.24
6	30.93	31.69	24.09	24.03	25.51	20.95	20.31
7	28.75	28.5	26.23	26.11	25.77	24.14	21.95
8	33.07	30.3	32.41	31.67	27.96	23.67	26.67
9	25.13	31.05	25.44	24.95	28.45	22.28	24.74
10	28.38	31.53	26.51	26.64	29.58	24.42	25.16
11	35.53	37.79	30.76	31.27	32.27	32.01	33.65
12	33.05	32.38	27.58	27.07	31.94	26.71	26.63
13	29.21	34.3	26.78	27.42	30.5	28.57	27.68
14	34.26	37.75	32.19	32.83	32.62	30.77	30.39
15	30.63	33.26	28.42	28.23	27.96	23.93	23.27
16	34.53	39.91	31.53	32.18	37.06	30.14	28.84
17	32.48	34.57	27.61	28.32	29.69	28.86	28.89
18	33.91	31.01	26.21	26.43	28.31	27.87	25.49
19	30.03	26.33	25.42	26.06	26.25	22.09	19.7
20	31.96	32.85	27.27	27.53	28.7	24.6	25.68
21	30.64	29.52	26.82	27.32	21.87	23.76	22.81
22	31.63	35.75	28.48	28.25	30.83	26.64	26.33
23	30.56	30.94	26.92	26.61	30.11	23.34	25.83
24	27.71	26.23	23.52	23.82	23.84	25.25	23.41
25	30.97	33.11	25.46	25.48	29.17	21.64	22.97
26	29.31	29.82	25.72	26.48	26.93	22.59	25.65
27	32.79	33.79	27.51	28.14	30.03	25.03	24.23
28	32.51	29.94	30.12	29.71	25.50	26.71	25.38
29	25.21	28.56	23.79	22.58	25.00	23.43	23.09
30	28.73	29.93	25.61	24.44	27.29	28.51	28.53
31	35.92	28.11	29.34	28.94	27.08	31.31	25.14
32	27.84	29.95	21.84	20.87	21.83	19.34	19.22
33	26.33	26.04	20.19	20.71	22.48	22.75	23.14
34	35.17	33.73	27.32	27.88	28.37	23.09	19.79
35	33.06	36.28	29.05	28.78	28.13	21.56	21.36
36	30.79	29.08	28.35	26.57	25.78	23.29	21.77
37	32.28	30.82	30.46	30.25	28.82	25.85	22.11
38	34.95	37.04	27.19	28.59	31.27	31.61	27.23
39	34.03	37.41	29.84	29.93	31.6	30.63	31.32
40	30.01	31.4	26.27	26.68	26.16	25.41	24.85
41	33.98	27.23	27.99	26.36	22.19	19.66	17.21
42	26.09	34.22	24.71	24.12	27.3	21.63	21.57
43	35.61	38.34	30.08	30.51	30.00	23.55	23.29
44	29.25	29.81	25.11	25.62	24.68	23.6	23.98
45	27.58	26.36	22.36	22.48	20.59	22.9	18.94
46	32.26	33.58	25.79	26.09	27.99	20.75	21.03
47	32.01	27.50	26.77	24.75	22.7	26.01	25.56
48	30.63	27.50	27.42	27.03	23.05	24.64	19.14
49	32.33	28.23	28.31	28.24	25.53	26.46	26.64
50	31.94	34.86	27.82	28.12	30.78	27.79	24.17
51	38.03	31.51	29.97	29.68	27.49	22.92	18.12
52	35.69	30.57	29.28	29.28	27.82	26.46	25.01
53	33.73	33.79	29.37	28.71	29.97	26.93	28.36
54	33.51	31.56	26.71	26.96	27.83	25.83	24.24

Table 1b. Talus linear measurements (continued) (Chapter 2).

Sn	MLCAL	MLCALx	MLCAL-2	MLCAL-2x	BHCAL	BHCALx	MinBHCAL	MinBHCALx	MinAHCAL	MinAHCALx	MinAWCAL	MinAWCALx
1	83.43	82.74	80.98	80.26	46.65	49.21	39.42	37.33	23.93	21.59	22.31	22.36
2	82.81	84.16	81.91	83.41	50.38	48.22	40.72	42.44	23.71	23.81	20.67	20.66
3	87.08	84.14	86.67	87.46	52.15	48.8	43.48	38.41	28.29	26.61	21.94	22.21
4	91.81	95.15	89.79	89.51	54.5	56.15	41.52	44.6	25.64	25.77	26.51	25.99
5	83.14	84.71	80.36	81.13	54.17	55.27	43.67	42.86	28.43	28.41	22.17	19.44
6	72.01	74.04	69.92	71.99	44.46	44.68	34.24	33.66	26.69	24.61	21.28	22.45
7	84.69	84.62	82.07	82.44	49.89	49.03	40.04	40.66	25.51	25.46	23.22	25.12
8	85.64	87.5	84.06	83.32	54.96	54.72	41.52	43.13	27.34	25.5	24.01	23.38
9	80.12	81.77	78.95	77.17	48.38	47.22	38.94	39.22	22.89	21.26	21.58	23.39
10	88.61	86.01	83.62	80.23	47.13	31.74	39.66	37.96	24.91	22.92	22.38	21.64
11	92.22	95.56	90.24	93.61	54.61	57.41	45.97	47.53	25.26	26.71	26.42	22.3
12	85.35	88.39	83.73	84.86	52.21	51.83	40.31	41.35	23.47	24.16	23.58	23.07
13	85.23	88.32	85.54	85.51	53.92	58.75	46.15	45.39	25.13	25.82	23.75	25.85
14	97.52	103.36	96.21	96.35	57.62	55.79	45.22	47.25	26.89	27.86	23.09	23.41
15	77.07	82.07	75.58	76.43	47.46	46.89	36.16	37.27	22.52	22.86	23.67	21.71
16	96.81	100.97	95.67	94.76	56.63	58.56	45.79	44.28	26.91	26.15	23.91	25.12
17	83.51	87.8	81.73	83.62	52.11	49.78	39.11	40.18	27.36	25.62	24.27	26.56
18	77.25	81.73	77.11	79.81	48.71	49.42	37.47	38.19	25.52	24.34	19.67	22.75
19	78.16	79.98	77.21	78.277	44.39	44.43	32.24	33.71	25.81	23.87	21.25	21.43
20	93.12	92.1	92.49	90.84	53.58	55.13	42.29	41.77	27.32	24.88	24.89	24.13
21	87.54	90.41	85.76	84.57	49.15	57.36	39.64	39.71	25.09	24.8	22.01	23.38
22	89.01	89.23	87.05	86.58	52.91	55.63	40.71	43.21	25.75	26.48	22.21	26.74
23	79.04	86.29	75.97	78.31	45.43	47.61	34.06	36.8	28.04	25.13	20.36	22.21
24	76.57	80.08	73.86	73.02	45.02	45.29	33.78	33.29	23.79	21.52	19.34	19.26
25	76.38	80.01	74.43	77.42	43.81	43.41	35.47	34.87	24.06	25.09	21.64	23.02
26	79.21	83.18	77.09	76.7	46.24	45.64	39.37	38.54	21.76	21.58	22.37	26.36
27	85.45	88.49	84.94	87.16	48.03	50.17	40.65	39.73	25.99	25.51	23.92	24.37
28	86.59	89.25	86.06	87.13	51.62	51.73	42.63	40.05	27.59	28.11	22.55	25.26
29	77.71	79.56	75.93	78.55	42.55	42.06	35.51	33.94	24.82	23.01	21.46	19.58
30	86.56	90.59	83.35	87.1	50.81	53.86	41.14	40.64	23.33	21.57	21.97	22.97
31	80.16	86.29	80.51	85.31	51.64	54.29	40.31	39.9	27.16	27.13	24.41	23.52
32	71.41	74.57	70.33	72.26	42.84	43.78	34.45	33.04	21.39	21.86	20.21	24.73
33	72.13	74.79	71.19	72.09	43.65	45.59	33.14	32.74	20.68	20.68	21.49	21.59
34	87.63	93.88	86.22	91.75	48.02	49.61	39.38	38.93	25.71	26.53	25.79	24.96
35	86.55	89.89	86.14	88.55	49.69	51.87	40.27	39.83	22.12	23.5	26.47	25.72
36	75.97	79.52	75.98	77.41	45.38	47.29	35.59	36.57	24.06	23.38	21.15	21.44
37	92.21	98.59	91.65	97.63	56.27	57.03	41.44	40.35	30.24	30.58	23.57	22.04
38	97.43	101.03	95.01	96.09	57.03	58.81	44.71	44.65	27.04	27.95	24.07	22.37
39	95.11	95.49	94.96	94.9	60.81	62.27	45.83	43.95	27.59	29.01	26.62	22.35
40	80.89	82.54	76.78	77.88	44.24	45.88	36.32	34.98	21.71	25.07	20.06	19.1
41	83.67	84.5	80.65	79.34	49.63	56.45	41.21	39.5	24.25	24.63	25.09	25.81
42	73.21	78.2	71.46	75.16	42.92	41.55	34.31	33.54	23.39	25.57	20.89	22.52
43	88.43	92.76	83.82	90.71	49.12	52.46	37.28	37.55	23.24	27.67	20.49	22.76
44	78.13	80.53	76.75	77.87	45.44	44.45	35.71	36.21	24.05	23.78	21.54	19.65
45	79.03	82.07	74.31	75.3	44.83	43.32	32.94	33.53	22.95	22.38	19.16	22.59
46	86.63	89.16	85.65	86.24	51.48	53.74	39.68	39.51	27.61	26.15	24.66	25.71
47	73.74	76.67	71.22	72.68	51.36	51.73	42.41	39.12	25.44	27.87	23.31	21.05
48	85.82	89.05	81.41	84.01	48.95	48.69	36.99	36.57	21.42	24.74	21.95	21.49
49	87.68	89.93	86.29	84.45	52.11	53.17	40.71	39.91	26.07	27.47	20.48	19
50	86.22	93.58	85.45	87.85	49.67	49.36	37.71	33.51	26.51	27.43	22.52	22.94
51	88.51	89.95	87.91	84.85	52.62	57.19	39.01	35.76	22.55	23.9	27.13	25.1
52	81.25	83.96	78.65	81.07	48.54	49.44	38.06	37.79	23.97	23.95	24.18	20.3
53	86.21	89.85	84.99	87.23	53.81	55.71	39.54	43.57	26.48	27.16	25.08	26.13
54	81.58	85.71	80.69	81.24	47.21	47.64	35.28	35.99	24.41	24.9	24.17	23.37

Table 2. Calcaneus linear measurements (Chapter 2).

Chapter 3 (Tables 3-4b)

Sn	AHTAL	AHTALx	ANTAL	ANTALx	AHTAL (pl)	AHTALx	ANTAL(pl)	ANTALx	IANTAL	IANTALx
1	73.02	71.91	104.44	104.4	70.3	71.91	104.21	104.4	30.11	30.14
2	85.21	83.31	105.01	105.88	84.29	83.31	106.88	105.88	38.27	39.64
3	96.88	91.64	111.23	112.31	96.73	91.64	113.59	112.31	32.17	33.79
4	80.56	82.82	104.97	111.32	82.2	82.82	102.41	111.32	31.05	35.34
5	94.59	93.18	98.52	100.98	93.69	93.18	99.14	100.98	27.71	36.09
6	85.69	88.87	117.86	114.69	82.64	88.87	117.76	114.69	29.27	32.26
7	90.33	90.51	117.98	122.26	96.61	90.51	119.61	122.26	26.6	32.31
8	92.82	95.01	118.61	116.29	93.89	95.01	117.08	116.29	32.94	38.34
9	90.52	85.79	101.16	103.29	89.89	85.79	101.63	103.29	33.44	28.84
10	88.9	86.79	103.5	106.55	89.68	86.79	110.4	106.55	31.78	34.41
11	96.46	99.81	111.52	111.23	101	99.81	114.15	111.23	37.03	37.41
12	82.65	80.7	101.31	104.55	87.12	80.7	101.06	104.55	34.98	34.42
13	92.73	93.1	104.41	107.1	89.99	93.1	107.62	107.1	38.12	39.41
14	86.74	81.93	103.84	103.08	88.09	81.93	108.32	103.08	31.97	32.65
15	92.62	92.7	113.2	111.83	92.81	92.7	114.32	111.83	32.49	37.92
16	77.56	83.98	102.84	102.51	84.89	83.98	101.91	102.51	36.1	38.39
17	91.95	95.83	96.32	98.67	95.39	95.83	96.07	98.67	29.9	28
18	89.24	87.12	101.67	100.52	86.37	87.12	104.62	100.52	25.63	31.47
19	86.39	87.73	108.64	103.79	88.71	87.73	102.68	103.79	26.15	30.21
20	81.03	84.69	101.75	101.33	81.44	84.69	105.23	101.33	36.04	34.83
21	85.68	87.46	100.8	101.48	88.33	87.46	102.46	101.48	31.78	30.24
22	81.39	82.29	98.33	99.76	80.11	82.29	101.07	99.76	28.79	32.4
23	83.05	83.38	101.94	100.63	80.33	83.38	101.9	100.63	37.15	43.53
24	91.72	93.11	103.5	107.46	91.05	93.11	109.64	107.46	26.13	30.24
25	87.63	84.24	103.89	106.06	89.37	84.24	106.45	106.06	38.83	39.43
26	92.78	90.01	105.86	107.57	93.31	90.01	106.85	107.57	23.98	33.1
27	83.26	84.5	98.92	98.28	84.79	84.5	101.88	98.28	33.77	37.58
28	85.04	86.26	103.83	100.72	85.11	86.26	105.77	100.72	32.39	34.65
29	81.98	82.23	88.67	89.37	82.95	82.23	87.57	89.37	27.17	35.09
30	97.5	96.2	108.86	109.38	98.83	96.2	107.71	109.38	29.32	29.45
31	86.67	92.69	100.29	101.92	91.47	92.69	98.82	101.92	29.86	32.66
32	74.37	75.01	93.92	89.82	76.84	75.01	95.98	89.82	33.25	37.93
33	81.83	76.33	98.62	94.38	81.8	76.33	102.79	94.38	31.88	36.99
34	84.42	90.57	105.9	107.33	86.94	90.57	109.51	107.33	31.21	37.16
35	76	75.5	95.25	111.54	75.53	75.5	114.21	111.54	31.25	35.1
36	84.03	83.74	105.38	106.37	84.86	83.74	104.56	106.37	34.68	36.97
37	82.95	82.25	100.9	108.3	85.6	82.25	102.53	108.3	27.93	31.29
38	92.17	91.38	109.57	106.36	92.05	91.38	104.96	106.36	32.9	39.38
39	92.13	91.08	110.56	113.26	88.04	91.08	115.7	113.26	21.03	28.3
40	90.12	90.81	108.86	107.07	88.06	90.81	105.31	107.07	29.97	36.15
41	75.13	74.58	106.54	107.14	75.29	74.58	107.05	107.14	33.95	32.74
42	94.62	88.26	104.34	101.67	89.31	88.26	104.49	101.67	32.54	39.88
43	88.47	83.43	103.59	103.57	83.6	83.43	105.16	103.57	34.62	39.39
44	84.13	83.86	103.52	102.43	85.24	83.86	101.61	102.43	31.88	36.22
45	96.16	85.05	101.21	101.96	97.58	85.05	102.45	101.96	28.03	33.51
46	76.6	74.02	102.42	102.11	76.51	74.02	101.69	102.11	32.61	37.74
47	79.51	81.05	97.58	102.77	80.89	81.05	101.92	102.77	25.36	29.79
48	83.74	85.6	103.45	101.53	88.61	85.6	103.49	101.53	33.51	36.12
49	86.51	88.61	104.38	102.18	86.06	88.61	103.46	102.18	34.33	36.29
50	91.29	88.37	106.67	104.29	90.07	88.37	106.68	104.29	30.51	34.03
51	90.59	89.04	103.82	102.21	90.05	89.04	105.7	102.21	30.22	31.35
52	96.08	94.17	109.85	107.02	98.3	94.17	109.99	107.02	30.66	30.77
53	89.2	92.77	103.73	104.52	90.7	92.77	103.01	104.52	31.24	33.15
54	82.18	82.42	104.94	109.36	81.28	82.42	103.41	109.36	32.95	35.4

Table 3. Talus angular measurements (Chapter 3).

Sn	AAAPCALa	AAAPCALx	AAAPCALb	AAAPCALx	AIPTFCAL	AIPTFCALx	AIMTFCAL	AIMTFCALx	AALCAL	AALCALx	BTACAL
1	87.27	91.56	88.07	91.56	44.29	44.26	54.61	58.25	103.66	105.68	25.71
2	67.39	67.91	66.35	67.91	48.19	47.81	68.52	62.1	117.62	114.31	25.34
3	92.05	91.39	90.19	91.39	45.85	49.86	59.99	57.63	111.89	113.78	36.29
4	92.1	92.45	85.12	92.45	45.78	43.78	59.91	53.19	120.81	123.65	31.47
5	91.58	87.27	93.94	87.27	45.85	50.47	47.68	48.02	111.37	113.83	34.65
6	97.27	93.55	93.25	93.55	44.14	39.66	37.03	46.08	99.28	104.44	25.94
7	81.1	77.65	85.77	77.65	46.53	47.42	49.69	64.14	119.87	111.99	24.42
8	94.67	91.84	93.24	91.84	55.69	52.75	53.46	60.29	106.4	109.16	25.3
9	87.58	87.3	86.3	87.3	47.02	47.36	35.68	43.01	100.28	101.14	18.82
10	82.17	85.49	79.53	85.49	49.3	53.32	54.87	61.98	115.85	114.11	23.51
11	99.73	94.54	98.3	94.54	43.69	47.63	45.43	48.98	111.43	114.76	31.76
12	95.49	97.8	94.56	97.8	46.5	52.35	50.23	51.98	103.07	104.43	32.91
13	85.47	84.38	88.62	84.38	50.87	57.7	57.95	52.37	105.53	104.91	36.58
14	90.22	90.69	90.74	90.69	48.83	48.29	59.12	58.05	105.84	103.66	25.61
15	93.06	90.41	90.27	90.41	50.31	53.95	67.13	69.89	109.57	115.12	37.22
16	87.79	91.78	89.51	91.78	48.04	45.41	56.11	55.94	101	103.67	34.17
17	89.93	89.62	92.62	89.62	45.27	47.73	57.23	59.8	106.68	104.27	28.24
18	91.4	94.08	92.32	94.08	46.53	47.54	48.99	45.25	101.04	105.35	30.58
19	92.08	93.17	94.36	93.17	41.14	38.62	43.69	39.37	98.53	93.06	22.24
20	91.21	89.94	88.8	89.94	40.2	45.39	44.01	48.99	101.24	103.11	22.92
21	99.2	92.72	86.78	92.72	46.01	44.21	40.92	45.33	102.52	102.31	32.39
22	99.84	102.33	99.1	102.33	52.25	50.03	59.52	51.69	109.33	107.05	32.45
23	107.53	103.94	109.49	103.94	44.54	40.16	66.83	65.85	106.1	105.91	29.5
24	102.22	103.02	103.38	103.02	55.5	54.43	57.36	53.12	112.69	115.34	33.98
25	99.1	100.1	100.87	100.1	42.23	41.75	52.85	55.64	103.59	106.32	29.81
26	92.55	97.76	95.45	97.76	48.5	53.26	59.14	59.21	102.09	106.93	31.52
27	88.36	90.07	89.87	90.07	48.52	51.13	56.22	56.94	109.61	107.65	32.52
28	89.89	89.09	90.33	89.09	45.27	41.25	51.89	50.56	108.88	99.23	25.6
29	82.84	86.88	81.32	86.88	48.37	48.92	58.27	56.97	106.78	108.96	24.55
30	94.44	91.48	91.05	91.48	45.7	50.31	48.22	55.35	111.52	118.27	32.22
31	98.53	95.43	94.13	95.43	43.01	40.45	59.11	59.49	91.07	89.45	36.06
32	91.22	89.94	91.86	89.94	47.54	48.19	56.31	53.23	109.51	107.04	24.38
33	89.93	87.46	88.53	87.46	50.75	52.56	60.8	65.93	104.78	108.39	29.04
34	89.78	90.05	89.44	90.05	38.13	46.27	59.91	58.75	110.23	106.12	22.97
35	87.57	89.84	90.81	89.84	49.66	49.53	42.61	41.69	111.01	110.52	29.32
36	82.09	77.78	80.15	77.78	41.54	45.06	51.61	47.04	99.99	100.26	23.62
37	92.89	96.67	88.03	96.67	35.24	34.83	46.16	51.27	103.27	100.09	22.94
38	81.98	82.56	86.76	82.56	45.54	49.27	60	56.76	101.91	104.96	30.39
39	86.59	85.2	83.06	85.2	40.52	40.82	44.46	42.61	108.85	107.09	25.31
40	95.7	103.57	96.02	103.57	40.98	43.67	60.42	62.9	98.35	96.94	29.59
41	91.03	90.08	91.11	90.08	46.7	50.06	47.77	54.6	93.77	95.56	31.12
42	91.41	91.53	89.22	91.53	39.09	38.82	38.47	43.82	100.69	96.77	15.45
43	94.01	98.88	95.16	98.88	44.25	48.41	53.97	53.64	100.6	100.49	37.32
44	94.6	93.2	96.12	93.2	39.45	43.89	50.1	49.05	102.01	96.62	25.41
45	91	91.75	91.08	91.75	42.06	41.45	57.04	57.76	107.74	101.9	21.69
46	91.09	90.28	92.2	90.28	44.52	43.78	60.41	60.78	110.9	110.98	31.8
47	87.11	91.84	89.81	91.84	49.34	47.64	47.85	52.31	101.31	97.46	23.11
48	87.79	88.78	96.58	88.78	49.7	49.16	63.3	59.39	106.97	107.42	22.76
49	89.76	90.36	84.94	90.36	53.04	52.81	44.04	42.4	103.58	104.6	29.78
50	91.64	91.79	91.4	91.79	40.07	39.55	50.99	48.59	102.53	98.27	27.2
51	95.83	89.22	94.8	89.22	46.49	42.93	63.6	60.49	110.61	106.58	27.74
52	99.67	104.85	103.25	104.85	38.24	35.5	54.37	52.96	95.31	94.64	30.91
53	89.87	94.08	91.28	94.08	52.94	58.92	49.4	56.55	105.09	109.08	31.62
54	89.52	89.7	89.81	89.7	50.19	47.15	56.04	63.59	101.2	98.73	32.1

Table 4a. Calcaneal angular measurements (Chapter 3).

Sn	BTACALx	GACAL	GACALx	CACAL	CACALx	FACAL	FACALx	TACALa	TACALax	TACALb	TACALbx
1	26.33	127.71	128.29	26.83	26.79	37.25	34.63	66.86	68.16	21.56	22.84
2	30.93	114.53	112.77	28.37	32.1	35.54	36.74	66.64	65.79	22.19	23.16
3	37.03	130.95	128.64	28.08	31.35	37.59	37.93	53.28	55.09	35.37	34.25
4	31.02	133.18	133.03	28.58	24.65	38.6	36.31	59.26	63.68	31.15	27.79
5	38.92	123.18	122.5	27	29.25	40.83	37.67	60.28	61.18	31.16	27.54
6	30.25	118.63	117.78	18.42	19.91	34.09	32.64	74.29	63.04	16.53	27.92
7	26.61	126.59	127.03	24.53	22.88	37.95	34.88	59.73	64.01	30.9	25.3
8	29.69	113.77	112.27	28.24	30.65	39.46	38.27	60.51	49.67	28.93	41.32
9	21.02	125.41	120.47	19.51	22.44	33.01	36.76	54.72	55.71	35.59	34.28
10	27.02	119.04	116.38	20.36	22.85	36.97	34.32	65.41	63.68	25.09	26.11
11	36.21	135.33	127.49	28.17	30.12	36.46	34.15	64.7	63.29	25.74	28.42
12	31.74	125.64	125.38	27.83	31.05	33.29	36.53	63.56	65.95	25.64	24.48
13	36.16	131.04	127.2	29.32	37.99	36.16	40.99	70.52	66.91	19.5	22.71
14	30.95	130.44	132.42	30.25	27.62	39.52	34	63.12	65.81	26.77	24.03
15	39.27	127.79	127.83	29.38	32.39	34.64	38.74	68.85	65.83	21.25	23.25
16	34.94	132.5	134.73	31.62	28.69	34.08	32.29	60.82	64.19	27.87	25
17	30.09	126.61	128.16	25.97	27.77	38.45	36.01	65.92	66.67	24.11	23.46
18	35.49	120.58	124.49	25.36	28.45	33.91	33.67	69.76	73.15	19.16	16.6
19	28.6	121.26	123.03	16.84	18.24	30.24	27.81	78.29	80.62	12.02	8.62
20	21.57	125.64	117.76	19.62	17.04	32.6	33.64	60.32	65.84	29.99	24.03
21	35.39	127.89	133.2	24	24.1	32.03	29.89	61.59	64.68	28.31	25.98
22	42.46	128.36	130.59	29.3	34.67	34.87	34.01	68.05	61.37	20.9	28.87
23	30.45	121.79	125.67	25.35	20.43	36.89	32.85	68.78	73.71	20.82	15.84
24	36.17	121.86	126.45	31.16	30.73	37	36.12	69.13	70.76	21.22	19.02
25	33.91	125.22	130.83	24.06	27.09	33.46	36.22	67.75	66.73	22.59	23.65
26	35.04	129.96	123.35	27.89	31.27	35.1	37.9	63.47	64.38	26.15	25.26
27	34.84	127.7	126.78	28.23	30.68	37.62	38.23	63.43	65.08	26.47	24.28
28	25.84	128.26	129.61	26.74	20.78	40.79	33.29	59.82	65.66	30.33	24.06
29	23.33	120.06	119.38	25.41	26.36	39.31	39.2	57.84	62.48	32.42	27.15
30	35.4	125.97	129.2	26.6	34.57	38.42	40.02	65.38	62.93	24.51	26.89
31	34.37	122	121.62	21.64	18.72	30.04	28.78	72.08	73.32	17.74	16.31
32	24.75	119.33	113.99	28.43	27.96	40.84	39.92	51.96	55.62	37.71	33.01
33	33.3	125.61	120.34	23.7	31.51	33.65	39.44	52.82	49.39	36.92	39.8
34	25.29	127.13	121.06	21.11	18.92	37.69	30.66	62.85	55.35	27.18	34.59
35	26.93	128.2	125.32	27.07	25.31	35.95	34.5	61.57	63.99	28.52	26.56
36	24.63	122.82	114.92	17.91	19.27	31.79	34.02	67.58	66.65	23.04	23.39
37	29.02	118.13	123.69	12.05	12.76	31.74	26.17	71.42	53.85	18.61	35.9
38	32.66	127.24	133.14	27.02	29.09	36.21	34.99	64.55	59.39	25.43	31.16
39	26.16	128.66	127.03	19.96	17.29	31.27	30.53	71.21	73.07	19.2	17.04
40	31.13	125.76	128	20.37	24.53	31.12	33.79	64.42	59.73	26.02	30.47
41	30.71	121.53	122.72	27.38	30.74	38.45	38.03	66.27	69.26	24.47	21.15
42	17.56	119.26	125.71	13.53	15.39	33.36	30.18	61.12	65.8	28.64	24.38
43	35.25	128.1	123.14	24.31	25.92	27.87	32.36	65.73	68.03	24.5	21.24
44	29.24	128.28	126.27	18.67	23.79	32.06	32.58	53.35	54.85	36.54	34.8
45	19.96	115.54	123.76	16.98	17.17	34.95	33.23	64	64.31	25.75	25.25
46	34.93	128.37	127.32	26.45	29.15	37.4	38.45	54.7	63.1	35.04	27.68
47	25.03	121.76	119.88	27.19	22.72	41.71	37.17	75.58	75.66	14.79	14.59
48	27.11	112.19	121.57	23.51	26.21	37.62	38.64	56.69	61.36	33.67	28.7
49	30.14	113.15	120.09	22.22	23.05	33.32	34.04	63.51	62.71	27.51	27.16
50	27.77	121.93	125.14	18.85	16.22	30.43	27.62	62.76	66.89	26.84	23.26
51	29.72	117.73	125.11	23.69	21.3	34.26	28.21	63.12	70.9	26.96	18.88
52	31.36	122.46	126.93	21.94	20.56	31.73	30.63	63.56	69.67	27.17	20.89
53	32.17	124.48	106.65	31.79	38.46	41.41	44.28	49.76	54.28	39.64	35.71
54	33.61	123.42	119.46	25.15	24.94	36.56	30.88	73.82	73.94	15.76	15.99

Table 4d. Calcaneal angular measurements (continued) (Chapter 3).

Chapter 4 (Tables 5a-10b)

Sn	Side	TCUA	CIA1	CIA2	LTCA	TDA	FMDA	TFMA
19571225	R	31.16	23.01	27.36	46.59	24.07	25.51	1.97
19470409	L	50.82	15.11	17.27	36.37	21.43	22.02	0.61
19650810	L	40.13	12.21	15.06	40.07	27.85	20.33	7.7
19650810	R	24.39	14.05	17.28	42.8	28.95	17.82	11.05
19590729	L	37.74	13.54	19.27	40.13	26.46	26.95	0.23
19590729	R	34.77	12.8	18.88	32.95	20.14	19.67	0.19
19540718	R	47.07	16.11	18.16	46.26	30.26	23.4	6.87
19650309	L	37.79	16.78	19.03	39.64	28.8	22.99	5.84
19600315	L	21.58	17.96	20.73	41.75	23.73	23.89	0.18
19511231	L	56.38	22.72	25.36	45.46	23.11	24.22	1.15
19511231	R	29.97	22.86	26.41	51.29	28.54	22.85	5.82
19510401	L	43.93	26.74	28.15	49.68	22.76	21.01	2
19561204	L	24.19	14.8	17.14	46.09	31.23	22.3	9.23
19561204	R	37.51	8.15	10.89	40.72	32.19	23.23	9.13
19600315	L	31.77	17.55	20.89	41.55	23	19.85	4.28
19640420	L	36.88	22.35	25.2	43.58	21.24	22.11	0.81
19640420	R	32.81	21.49	25.09	44.33	23.1	22.92	0.14
19710208	L	33.11	27.08	26.76	45.94	18.74	22.49	3.79
19710208	R	27.77	27.22	27.22	47.13	20.07	21.64	1.93
19630731	L	42.83	29.31	30.05	61.09	31.86	25.72	5.92
19630731	R	46.58	28.6	30.97	59.25	30.92	24.53	6.74
19920821	L	35.41	20.06	22.54	45.89	25.75	22.46	3.28
19840828	L	34.67	23.01	23.31	46.26	23.26	27.59	4.14
19860124	L	29.87	19.47	20.38	44.59	25.12	24.54	0.8
19580925	L	30.9	25.56	25.78	48.03	22.55	29.77	7.34
19540718	R	38.39	16.68	19.04	49.97	33.24	22.81	10.55
19530319	R	36.18	15.27	16.63	38.78	23.55	20.49	3.14
19530319	L	30.12	13.67	15.8	37.09	23.65	21.18	2.15
19360507	L	43.58	26.71	28.72	48.09	21.46	21.29	0.36
19360507	R	52.23	24.55	25.33	49.36	25.01	23.45	0.39
19940112	R	26.12	19.24	20.53	40.15	20.74	20.4	0.44
19700612	L	11.83	24.4	28.24	44.57	19.83	26.69	6.6
19530922	L	32.31	27.24	29.99	44.16	16.38	27.24	10.77
19530922	R	33.21	24.29	27.03	44.99	20.35	23.15	2.83
19590523	L	29.28	19.95	25.18	44.48	24.44	23.03	1.3
19590523	R	25.15	25.46	30.31	52.57	27.32	21.63	5.63
19351111	L	55.53	16.39	19.17	38.06	21.76	21.96	0.17
19351111	R	56.07	11.68	16.32	37.8	25.92	21.18	4.48
19891222	L	31.35	18.22	19.07	44.95	26.62	14.07	12.72
19891222	R	32.08	15.14	16.67	41.93	26.86	16.86	10.08
19640919	L	40.98	19.79	19.68	40.34	20.55	18.01	2.66
19640919	R	46.23	15.37	17.01	42.77	27.4	15.35	11.94
19870101	R	36.09	13.95	15.26	35.16	21.16	18.48	2.9
19640808	L	45.33	8.93	11.57	37.53	25.58	19.66	8.86
19600915	L	21.85	31.82	34.52	57.78	26.17	27.45	1.25
19600915	R	40.35	26.69	29.88	46.38	18.56	23.53	4.93
19590429	L	36.66	18.52	21.31	45.01	26.58	20.86	5.68
19690101	L	33.58	23.41	26.27	41.82	18.27	26.69	8.52
19411227	L	35.39	25.95	28.32	50.72	24.87	22.46	1.78
19481029	L	36.79	22.44	23.37	45.98	23.23	21.14	2.04
19500214	R	36.86	20.46	22.07	46.48	26.11	24.08	2.17
19491003	L	27.36	14.22	17.69	39.69	25.38	23.83	1.65
19611020	L	20.92	20.75	24.91	45.81	25.05	25.59	0.32

Table 5a. Angular measurements of the foot (Chapter 4).

Sn	Side	TCUA	CIA1	CIA2	LTCa	TDA	FMDA	TFMA
19480805	L	45.11	15.16	15.31	39.05	23.81	19.59	4.24
19480805	R	42.58	13.66	14.15	44.82	31.18	17.36	13.71
19441208	L	22.85	24.2	29.26	48.88	24.74	24.34	0.37
19441208	R	26.12	23.99	26.04	49.52	25.61	21.62	4.26
19821001	L	46.79	11.63	9.69	52.86	41.2	12.98	27.87
19821001	R	46.79	11.63	9.69	52.86	41.2	12.98	27.87
19470319	L	40.34	10.9	13.58	37.33	26.42	20.43	5.95
19460128	R	54.81	10.98	13.98	46.64	35.74	13.79	21.99
19930625	L	58.54	13.34	14.4	45.51	32.14	18.76	13.42
19550225	R	38.84	22.11	25.53	53.69	31.51	16.57	14.92
19510517	L	36.61	16.07	18.28	40.47	24.48	19.08	5.37
19710701	L	35.53	10.26	14.25	33	22.65	23.37	0.75
19820225	L	43.41	16.84	18.5	37.62	20.55	22.91	2.67
19820225	R	53.55	14.42	15.71	37.73	23.29	22.29	0.94
19810901	L	42.82	13.88	15.26	36.48	22.65	24.75	1.5
19810901	R	59.82	15.02	16.6	41.65	26.63	22.52	4.33
19907719	L	50.92	13.4	13.46	39.41	28.14	16.12	12.01
19907719	R	53.15	14.53	14.97	45.5	30.65	16.55	14.27
19571223	L	60.13	25.32	23.44	49.12	23.73	17.69	6.1
19760603	L	68.26	9.01	10.95	36.89	27.9	11.37	16.42
19760603	R	55.86	10.6	12.99	38.1	27.35	17.48	9.86
19490806	L	49.09	15.56	18.78	45.98	30.5	17.4	12.9
19490806	R	37.26	14.29	18.2	41.02	26.8	18.9	7.9
19500424	L	31.33	26.22	29.96	47.97	21.36	21.92	0.66
19500424	R	32.24	28.5	31.43	52.59	24.11	21.48	2.5
19850627	L	44.32	22.78	23	45.26	22.31	20.5	1.87
19850627	R	31.57	21.3	21.26	47.78	26.42	23.12	3.46
19960516	R	42.73	13.13	14.15	38.03	25.2	18.46	6.82
19600315	L	29.85	17.29	19.91	39.83	22.46	23.72	1.2
19781018	R	41.78	16.33	16.53	44.88	28.67	20.77	7.95
19781018	L	32.77	17.41	18.18	35.74	18.5	21.81	3.58
19550614	L	46.24	17.4	18.6	38.36	20.81	17.24	3.76
9265897	R	43.24	13.78	15.42	39.54	25.75	17.86	8
19520930	L	40.61	7.4	10.49	30.02	22.51	18.59	4.08
19520930	R	55.75	9.96	10.43	32.97	23.04	17.8	5.13
19470910	L	32.48	12.96	16.62	32.42	19.5	17.49	2
19470910	R	44.24	14.22	16.96	34.96	20.46	17.02	3.59
19361003	L	33.22	13.56	20.3	43.85	30.4	23.23	7.3
19810101	L	19.95	12.3	14.65	30.54	18.2	20.77	2.5
19850525	R	24.39	25.96	25.97	56.26	30.46	28.22	2.31
19510901	L	55.76	13.17	15.16	43.73	30.45	18.9	11.74
19510901	R	50.98	9.06	15.54	40.29	31.14	18.5	12.84
19560709	R	34.79	25.95	24.79	57.19	31.26	22.5	8.67
19470726	R	35.42	9.37	13.29	37.45	27.86	18.25	9.61
19870711	L	39.45	28.83	31.01	53.56	24.81	22.72	2.09
19870711	R	40.46	32.14	33.59	56.78	24.88	21.69	2.95
19540426	L	39.54	28.11	29	50.73	22.59	21.05	1.36
19540426	R	8.59	32.97	35.59	46.91	13.99	24.52	10.46
19921011	L	26.58	14.96	14.76	38.42	23.46	21.61	1.93
19921011	R	31.41	14.82	15.86	41.16	26.36	20.91	5.62

Table 5b. Angular measurements of the foot (Chapter 4).

Sn	Side	AH	FLL	FLCM	FL	CL	CLAH	AHFLCM	AHFL	Sn
19571225	R	38.7	168.5	178.8	235	Anterior	11.8	0.216	0.165	19571225
19470409	L	27	142.6	171.8	223	Anterior	7.9	0.157	0.121	19470409
19650810	L	31.9	160.8	186.4	232.6	Anterior	11.2	0.171	0.137	19650810
19650810	R	33.4	162.3	190.1	241	Anterior	13.6	0.176	0.139	19650810
19590729	L	37.5	153.5	188.4	245.5	Anterior	15.4	0.199	0.153	19590729
19590729	R	37.8	152.2	184	243.7	Anterior	12.4	0.205	0.155	19590729
19540718	R	29.7	143.7	178.1	232.3	Anterior	6.5	0.167	0.128	19540718
19650309	L	48.8	182.1	221.5	289.5	Posterior	14.3	0.22	0.169	19650309
19600315	L	39.1	161.5	199.2	258.9	Anterior	13.7	0.196	0.151	19600315
19511231	L	43.9	144	173.5	225.2	Posterior	8.6	0.253	0.195	19511231
19511231	R	39.8	145.5	178.9	231.3	Anterior	11.2	0.222	0.172	19511231
19510401	L	44.3	163.2	196.9	255.9	Anterior	7.4	0.225	0.173	19510401
19561204	L	29.4	141.7	169.7	220.5	Anterior	3.2	0.173	0.133	19561204
19561204	R	23.7	143.3	171.5	223.8	Posterior	7.2	0.138	0.106	19561204
19600315	L	38.4	161.9	198.6	258.6	Anterior	14.6	0.193	0.148	19600315
19640420	L	38.5	133.7	159.1	204	Anterior	4	0.242	0.127	19640420
19640420	R	41.9	136.5	161.7	207.6	Posterior	5.2	0.259	0.201	19640420
19710208	L	44.2	153.9	191.7	246.5	Anterior	10.5	0.231	0.179	19710208
19710208	R	48	158.1	185.5	241.8	Posterior	8.5	0.259	0.199	19710208
19630731	L	37.3	175.7	209.6	269.1	Anterior	13.4	0.178	0.139	19630731
19630731	R	41.6	169.6	205.7	262.6	Anterior	13.4	0.202	0.158	19630731
19920821	L	41.7	146.5	179.4	230.4	Posterior	5.3	0.232	0.174	19920821
19840828	L	41.3	141.4	171.1	224.5	Posterior	3.5	0.241	0.184	19840828
19860124	L	37.6	152.7	183.2	236.2	Anterior	12.2	0.205	0.159	19860124
19580925	L	52.6	141	173.2	227.1	Posterior	7.4	0.304	0.232	19580925
19540718	R	31.3	146.8	177.6	231.7	Anterior	5.8	0.176	0.135	19540718
19530319	R	37.3	148.5	176.7	230.1	Posterior	4	0.211	0.162	19530319
19530319	L	31.1	148.2	178.6	231.8	Posterior	3.2	0.174	0.134	19530319
19360507	L	40	141.5	170.8	222.4	Anterior	5.5	0.234	0.18	19360507
19360507	R	36.4	148.2	179.5	228.8	Anterior	11.9	0.203	0.159	19360507
19940112	R	38.4	161.7	190.7	251.2	Anterior	5.2	0.201	0.153	19940112
19700612	L	52	151.2	181.4	238	Anterior	11	0.287	0.218	19700612
19530922	L	49.3	130.4	166.9	214.4	Posterior	9.2	0.295	0.23	19530922
19530922	R	45.7	136.2	173	218.2	Posterior	7.8	0.264	0.209	19530922
19590523	L	41.6	152.2	184.4	238	Anterior	13.9	0.226	0.175	19590523
19590523	R	41.1	153.2	184.7	237	Anterior	16.6	0.223	0.173	19590523
19351111	L	35.1	129.5	161.8	208.7	Anterior	9.4	0.217	0.168	19351111
19351111	R	31	126.6	165.1	212.5	Anterior	12.1	0.188	0.146	19351111
19891222	L	31.7	163.9	203.9	261.7	Anterior	14.4	0.155	0.121	19891222
19891222	R	33	165.7	201.2	256.2	Anterior	21.3	0.164	0.129	19891222
19640919	L	33.2	126.9	157.2	205.5	Anterior	8.8	0.211	0.162	19640919
19640919	R	29.5	132.1	161.6	211.7	Anterior	9.1	0.183	0.139	19640919
19870101	R	30.7	161.8	203	261.2	Anterior	6.7	0.151	0.177	19870101
19640808	L	28.2	156.8	182.5	237.9	Anterior	6.8	0.155	0.118	19640808
19600915	L	48.8	145.4	185	236.9	Anterior	11.9	0.264	0.206	19600915
19600915	R	52.2	143.8	183.9	234.5	Anterior	10.7	0.283	0.223	19600915
19590429	L	40.8	156.5	194.5	247.5	Anterior	13.7	0.21	0.165	19590429
19690101	L	38.4	147	176.7	229.5	Anterior	6.5	0.217	0.167	19690101
19411227	L	44	162.4	192.4	245.2	Anterior	16.1	0.229	0.179	19411227
19481029	L	36.3	163.7	192.6	247	Anterior	8.7	0.188	0.147	19481029
19500214	R	36.8	136	173	221.5	Anterior	8.3	0.213	0.166	19500214
19491003	L	39.5	161.8	204.5	266.1	Anterior	12.1	0.193	0.148	19491003
19611020	L	46.3	152.8	185.2	242.2	Anterior	7.6	0.25	0.191	19611020

Table 6a. Linear measurements of the foot (Chapter 4).

Sn	Side	AH	FLL	FLCM	FL	CL	CLAH	AHFLCM	AHFL
19480805	L	28.8	149.4	180.6	231.9	Anterior	8.4	0.159	0.124
19480805	R	26.6	150.9	182.1	235.6	Anterior	6.2	0.146	0.113
19441208	L	48.7	154.6	189.8	243.4	Anterior	11.1	0.257	0.2
19441208	R	43.1	158.5	188.8	242.9	Anterior	14	0.228	0.177
19821001	L	20.7	155.1	188.1	238.4	Anterior	12.5	0.11	0.087
19821001	R	31.2	161.7	192.5	246	Anterior	12.1	0.162	0.127
19470319	L	31.5	175.1	208.1	264.8	Anterior	12.5	0.151	0.119
19460128	R	25	158.4	188.4	242.5	Anterior	16.5	0.133	0.103
19930625	L	22.1	156.9	181.7	234.2	Anterior	9.8	0.122	0.094
19550225	R	38	155	194.4	253.6	Anterior	12.7	0.195	0.15
19510517	L	36	155.9	185.9	246.2	Posterior	8	0.194	0.146
19710701	L	35.5	147.4	171	222.8	Anterior	9.2	0.208	0.159
19820225	L	33.2	142.6	172.9	221.7	Anterior	6.2	0.192	0.15
19820225	R	34.4	157.3	177.6	228.3	Anterior	6.5	0.194	0.151
19810901	L	32.2	152.2	186.1	239.8	Anterior	10.6	0.173	0.134
19810901	R	28.7	154.8	191.3	249	Anterior	10.5	0.15	0.115
19907719	L	23.4	191.5	223	277.7	Anterior	13.4	0.105	0.105
19900719	R	26.6	187.4	216	288	Anterior	5.2	0.123	0.096
19571223	L	26.6	153.8	191.8	246.4	Anterior	7.7	0.139	0.108
19760603	L	20.9	189.1	216.9	281.6	Anterior	9.9	0.096	0.074
19760603	R	34.4	191.3	218.8	283.3	Anterior	12.1	0.157	0.121
19490806	L	27.3	148.6	186.2	238.5	Anterior	16	0.147	0.114
19490806	R	34.3	149.9	187	238.2	Anterior	16.5	0.184	0.144
19500424	L	52.4	170.7	206.4	269.4	Anterior	18.8	0.254	0.195
19500424	R	51.7	169.2	204.4	267.6	Posterior	19.2	0.251	0.193
19850627	L	30.6	173.6	207.7	274.2	Posterior	2.8	0.147	0.112
19850627	R	35.1	173.2	209.1	275.5	Posterior	1.9	0.168	0.127
19960516	R	34.3	169.4	197.9	256.4	Anterior	4.3	0.173	0.134
19600315	L	39.4	163.4	198.4	257.9	Anterior	13.2	0.199	0.152
19781018	R	41.4	181.2	218.8	281.4	Anterior	14.4	0.189	0.147
19781018	L	48	175	211.8	273	Anterior	13	0.227	0.176
19550614	L	37.9	172.4	212.6	276.8	Posterior	14.9	0.178	0.137
9265897	R	33.2	171.7	209.4	272.8	Posterior	12.6	0.159	0.123
19520930	L	35.4	170.4	207.5	265.7	Anterior	12.9	0.171	0.133
19520930	R	23.9	164	199.9	257	Posterior	0.9	0.12	0.093
19470910	L	41.7	166.2	197.4	259.1	Posterior	9.6	0.211	0.161
19470910	R	39.2	161.1	194.5	256.7	Anterior	8.4	0.202	0.153
19361003	L	39.5	168.1	195.6	252.7	Anterior	12.7	0.202	0.156
19810101	L	32.4	155.7	180	234.1	Anterior	7.4	0.18	0.138
19850525	R	47.7	163	204.8	261	Anterior	8.7	0.233	0.183
19510901	L	34.7	163.2	201.1	255.9	Anterior	19.9	0.172	0.136
19510901	R	31	167.4	204.7	261.3	Anterior	23.6	0.151	0.119
19560709	R	36.9	163.4	198.3	255.5	Anterior	11.1	0.186	0.144
19470726	R	34.9	136	159.9	207.7	Posterior	5.1	0.219	0.168
19870711	L	39.3	162.8	198.6	261.4	Anterior	12.6	0.198	0.15
19870711	R	39.3	160.5	198.8	261.5	Anterior	12.9	0.198	0.15
19540426	L	38.9	164.5	194.1	249.5	Anterior	12	0.2	0.156
19540426	R	41.5	158.3	191.1	248.9	Posterior	6.5	0.217	0.167
19921011	L	40.4	188.7	225.9	289.3	Anterior	8.4	0.179	0.14
19921011	R	43.2	188.1	226.8	290.1	Anterior	8.1	0.19	0.149

Table 6b. Linear measurements of the foot (continued) (Chapter 4).

Sn	Side	Age	Talus	Calcaneus	Foottype	MLCALx	MLCAL2x	BHCALx	MinBHCALx	MinAHCALx	MinAWCALx	AAAPCALx
19571225	R	57	X	X	NA	82	76	47.4	35	22.2	22.6	96.53
19470409	L	70			LA							
19650810	L	52			LA							
19650810	R	52			LA							
19590729	L	58	X	X	LA	80.6	76	51.4	38.5	24.4	23.3	87.82
19590729	R	58	X	X	LA	80.4	76.5	47.1	37.7	26.2	23.7	91.66
19540718	R	63	X	X	NA	81	76.8	47.4	37.2	23.9	22.7	98.18
19650309	L	52	X	X	NA	102.2	92.1	58.2	44.2	25.3	29.2	95.8
19600315	L	57	X	X	NA	87.9	80.2	54.1	40.9	26.6	29	86.45
19511231	L	65	X	X	NA	82.2	77.8	47.9	36.5	23.3	19.1	102.33
19511231	R	65	X	X	NA	79.7	75.3	45.8	35.3	22.2	22.1	100.79
19510401	L	66	X	X	HA	89.8	84.8	57.4	40.2	22.9	25.4	97.33
19561204	L	60	X	X	LA	77.1	73.4	44.1	33.4	21.9	24.1	83.41
19561204	R	60	X	X	SF	80.7	79.9	44.7	33.6	23	23.7	85.85
19600315	L	57			NA							
19640420	L	53	X	X	NA	75.7	69.9	42	34.2	18.7	19.2	97.55
19640420	R	53	X	X	NA	75.5	70.8	43.5	34.1	19.8	19.1	102.38
19710208	L	46	X	X	HA	88.4	82	57	44.2	24.9	30.2	94.67
19710208	R	46	X	X	HA	88.5	82.9	57.1	44.3	27.3	27.7	92.87
19630731	L	54	X	X	HA	92.2	88.8	56.3	41.2	23.4	25.2	113.13
19630731	R	54	X	X	HA	94.5	87.8	59.1	41.7	23.7	24.4	102.63
19920821	L	25			NA							
19840828	L	33	X	X	NA	85.3	80.3	49.7	39.4	26.4	26.3	89.73
19860124	L	31	X	X	NA	83.9	78.7	46.8	40.2	24	24.9	93.31
19580925	L	59	X	X	HA	88.6	84.6	52.5	38.3	25.5	25.7	104.71
19540718	R	63	X	X	NA	77.9	75.8	48.8	37.2	23.1	24.1	95.16
19530319	R	64			LA							
19530319	L	64	X	X	LA	83.7	80.2	43.6	34.2	21.2	25.3	98.91
19360507	L	81	X	X	HA	81.2	77.1	48.1	34.7	21.7	22.3	105.16
19360507	R	81	X	X	NA	81.4	75.8	47.5	35.7	24.3	22.6	112.81
19940112	R	23	X	X	NA	87.4	83.9	45.4	36.9	23.7	24.8	102.97
19700612	L	47			NA							
19530922	L	64	X	X	HA	77.1	71.1	50	39.7	22.3	23.7	100.86
19530922	R	64	X	X	NA	78.5	71.9	48.4	39	21.8	24.1	100.18
19590523	L	58	X	X	NA							
19590523	R	58	X	X	HA	81.4	74.5	51.2	38.8	22.7	24.2	102.44
19351111	L	82	X	X	NA	69.2	63.8	43.8	34	23.3	23.1	103.6
19351111	R	82		X	LA	69.9	64.9	44	33	22.1	23.1	104.64
19891222	L	27			NA							
19891222	R	27			LA							
19640919	L	53	X	X	NA	69.6	65.6	38.3	33.1	18.7	22.4	86.42
19640919	R	53	X	X	LA	70	67.1	39.9	31.8	19.7	23	94.84
19870101	R	30	X	X	LA	92.3	89	52.4	41.9	30.3	28.8	92.56
19640808	L	53	X	X	SF	79.9	75.2	39.7	35.3	23.1	22.5	93.46
19600915	L	57	X	X	SC	85.7	77.4	53.5	41.7	25	26.6	103.71
19600915	R	57	X	X	HA	86.6	77.7	56.6	40.3	23.9	29.2	101.27
19590429	L	58			NA							
19690101	L	48			NA							
19411227	L	75	X	X	HA	86.1	79.4	54.4	35.7	24.4	22.8	103.42
19481029	L	69			NA							
19500214	R	67	X	X	NA	80.5	77.1	49.5	36.9	23.2	23	103.29
19491003	L	68			LA							
19611020	L	56	X	X	NA	85.4	78.9	53.4	43.4	24	23.1	101.29

Table 7a. Calcaneus measurements and demographics (Chapter 4).

Sn	Side	Age	Talus	Calcaneus	MLCALx	MLCAL2x	BHCALx	MinBHCALx	MinAHCALx	MinAWCALx
19480805	L	69	X	X	76.6	70.4	44.8	31.7	21	22.5
19480805	R	69	X	X	77.9	73.3	44.7	32.7	20.4	22.8
19441208	L	72	X	X						
19441208	R	72			88.1	82.7	53.4	41.8	23.1	26.1
19821001	L	35	X	X						
19821001	R	35			88	81.4	52	34.2	24.3	24
19470319	L	70	X	X	85.2	83.2	52.3	39.2	22.8	26.7
19460128	R	71								
19930625	L	24	X	X	78.3	75.4	49	33	24.8	24.4
19550225	R	62	X	X	86.3	80.3	55.3	37.1	26.3	23.3
19510517	L	66								
19710701	L	46	X		75.3	73.8	41.7	32.6	20.7	23.9
19820225	L	35	X	X	83.6	79.2	49	36.1	25.6	23.6
19820225	R	35	X	X	83.9	79.3	47.8	34.9	24.9	21.9
19810901	L	36	X	X	89	82.1	49.4	37.3	25.8	22.8
19810901	R	36	X	X	91.3	83.9	51.7	37.6	25.7	22.8
19907719	L	27	X	X	94.6	90.9	56	45.8	30.4	29.2
19900719	R	27	X	X	93.8	91.3	57.7	46.8	29	27.5
19571223	L	59								
19760603	L	41			92.5	89.3	57.2	41.8	27.1	26.8
19760603	R	41			94.4	89.1	53.3	43.5	25.1	28.4
19490806	L	68								
19490806	R	68								
19500424	L	67								
19500424	R	67								
19850627	L	32	X	X						
19850627	R	32	X	X						
19960516	R	21	X	X	91.8	87.3	51.5	39	24	26.1
19600315	L	57	X	X	87	80.9	54.9	41.9	25.9	23.4
19781018	R	39								
19781018	L	39								
19550614	L	62	X	X	96.7	92.9	58.2	42.9	26.9	27.1
9265897	R	62		X	95.5	89	57.3	42.4	27.4	27.3
19520930	L	65	X	X	94.6	89.7	54.2	38.3	29	23
19520930	R	65	X	X	95.4	91.7	52.8	38.5	28.8	24.1
19470910	L	70	X	X	88.1	82.3	50.6	38.6	25.1	23.6
19470910	R	70		X	88.8	82.7	51.1	40.1	25.4	22.4
19361003	L	81								
19810101	L	36	X	X	81	75.5	43.8	36.8	22.8	22.4
19850525	R	32	X	X	100.4	93.1	62.1	45.3	22.8	22.4
19510901	L	66	X	X	86.5	80.4	55.3	38.9	23.5	24.7
19510901	R	66	X	X	86	81.2	56.9	40.8	23.4	25.1
19560709	R	61								
19470726	R	70	X	X	74	70.2	43.3	31.6	21.8	22.2
19870711	L	30	X	X	85.8	81.2	47.1	40.3	23.2	24.2
19870711	R	30	X	X	86.2	82.3	49.2	39.9	23.1	23.1
19540426	L	63			92.1	78.4	51.2	44.8	20.3	24.7
19540426	R	63			91.3	81.2	57.6	42.6	20.3	26
19921011	L	25	X	X	106.4	100.8	60.5	42.1	30.1	26.3
19921011	R	25		X	105.2	100.1	63.5	43.7	31	25.8

Table 7b. Calcaneus measurements and demographics (continued) (Chapter 4).

Sn	Side	AIPTFCALx	AIMTFCALx	AALCALx	BTACALx	GACALx	CACALx	FACALx	TACALx	TACALbx
19571225	R	45.54	56.4	111.86	30.99	123.03	22.67	31.4	65.96	21.78
19470409	L									
19650810	L									
19650810	R									
19590729	L	45.13	52.63	93.72	35.59	115.64	24.35	33.56	56.91	31.51
19590729	R	47.65	52.02	95.28	34.36	119.42	23.63	34.89	58.24	31.09
19540718	R	43.47	49.71	99.7	30.79	118.78	22.27	31.82	69.28	20.4
19650309	L	54.71	44.13	111.38	40.59	119.6	30.62	31.55	71.91	20.27
19600315	L	42.07	40.9	94.27	36.19	128.76	21.9	27.05	79.39	10.94
19511231	L	47.76	47.34	100.36	34.34	125.73	25.02	31.15	53.89	35.64
19511231	R	49.08	50.28	97.16	37.37	125.28	27.32	30.76	54.76	35.95
19510401	L	53.83	50.8	113.21	48.65	125.51	34.54	33	61.69	29.07
19561204	L	49.05	42.57	97.53	28.68	111.1	17.71	26.21	68.78	20.46
19561204	R	45.52	45.93	97.78	31.37	109.32	20.31	29.29	59.51	30.29
19600315	L									
19640420	L	55.58	61.48	111.07	30.69	114.65	30.43	40.68	50.53	39.92
19640420	R	49.89	62.27	106.75	31.32	116.5	26.62	36.24	55.11	33.09
19710208	L	53.23	53.38	107.64	42.28	122.41	31.33	37.19	60.23	30.7
19710208	R	62.28	49.8	104.58	42.54	114.11	33.3	40.48	59.34	30.9
19630731	L	56.27	59.83	105.94	32.61	114.07	26.58	32.4	59.53	28.71
19630731	R	50.35	60.77	108.41	32.21	114.18	24.01	33.33	60.84	29.32
19920821	L									
19840828	L	48.54	51.69	95.78	35.81	123.73	24.26	32.54	62.64	21.93
19860124	L	57.74	56.53	116.11	33.57	124.98	33.54	44.01	58.1	32.49
19580925	L	39.08	48.68	101.17	30.98	132.57	21.36	32.62	70.45	19.21
19540718	R	40.99	59.26	97.81	29.81	119.33	16.92	28.89	73.27	17.18
19530319	R									
19530319	L	42.6	56.25	100.84	25.39	125.94	22.86	35.71	57.44	33.62
19360507	L	51.92	47.87	103.21	36.19	113.77	26.25	28.55	69.17	20.59
19360507	R	49.52	46.22	95.13	30.62	104.64	21.68	27.28	64.88	25.27
19940112	R	43.08	48.55	107.13	21.16	128.76	20.89	31.93	59.51	30.59
19700612	L									
19530922	L	47.37	37.41	108.6	29.55	131.1	27.24	40.07	69.03	21.04
19530922	R	53.96	44.51	113.6	32.25	124.59	33.21	44.37	59.18	27.63
19590523	L									
19590523	R	53.55	56.25	108.18	40.93	121.56	32.32	37.96	71.75	18.88
19351111	L	37.43	40.34	90.38	22.11	107.99	13.4	29.54	69.61	20.51
19351111	R	41.47	38.08	91.77	22.99	115.19	17.63	32.22	73.23	16.06
19891222	L									
19891222	R									
19640919	L	47.21	47.36	109.56	29.39	123.89	24.9	34.56	69.28	20.71
19640919	R	44.53	45.88	103.5	29.28	123.37	20.46	31.1	70.27	20.25
19870101	R	42.92	40.68	94.88	18.14	115.42	15.59	33.77	55.93	33.97
19640808	L	37.03	45.97	94.81	29.73	133.13	19.9	26.96	78.43	12.14
19600915	L	53.5	56.49	107.8	38.87	116.94	29.01	38.06	61.14	28.34
19600915	R	51.97	52.03	104.38	42.11	123.11	27.57	33.47	61.27	28.91
19590429	L									
19690101	L									
19411227	L	50.02	45.75	106.21	37.31	114.29	18.33	26.94	59.63	27.26
19481029	L									
19500214	R	43.08	47.85	96.45	32.75	121.48	24.32	32.01	65.29	25.03
19491003	L									
19611020	L	49.83	56.48	101.8	37.77	123.32	29.01	36.44	69.77	20.17

Table 7c. Calcaneus measurements (continued) (Chapter 4).

Sn	Side	AIPTFCALx	AIMTFCALx	AALCALx	BTACALx	GACALx	CACALx	FACALx	TACALax	TACALbx
19480805	L	45.45	50.58	96.02	30.19	119.84	20.98	27.08	62.95	26.86
19480805	R	45.22	51.78	97.55	31.23	120.67	21.14	25.79	50.1	39.28
19441208	L									
19441208	R	48.19	48.85	113.17	30.36	132.7	26.22	33.92	73.83	17.03
19821001	L									
19821001	R	43.18	46.63	96.77	40.32	116.89	23.23	24.18	60.37	29.72
19470319	L	45.99	48.24	89.08	26.9	109.23	19.57	28.39	70.3	19.52
19460128	R									
19930625	L	48.71	48.21	92.54	35.34	108.35	18.77	25.37	76.57	13.12
19550225	R	46.89	52.79	105.06	34.52	119.52	22.01	28.19	74.63	15.67
19510517	L									
19710701	L	39.33	44.27	92.35	25.87	114.2	16.84	24.72	72.12	17.94
19820225	L	43.39	42.4	101.29	26.47	125.9	17.56	29.62	68.96	21.67
19820225	R	41.89	42.06	100.59	25.94	129.66	16.11	28.43	65.48	25.13
19810901	L	45.33	46.23	103.47	33.36	116.3	18.56	30.73	64.55	25.94
19810901	R	49.6	47.17	103.72	34.34	120.88	21.75	29.6	66	24.32
19907719	L	50.81	55.14	94.94	27.87	102.01	23.01	30.53	77.28	12.32
19900719	R	54.06	51.47	94.82	27.38	103.16	23.42	30.78	75.19	16.17
19571223	L									
19760603	L	43.28	50.56	95.96	29.57	111.67	20.89	31.58	72.67	17.59
19760603	R	47.7	49.13	94.23	29.68	113.39	26.12	34.01	71.71	18.98
19490806	L									
19490806	R									
19500424	L									
19500424	R									
19850627	L									
19850627	R									
19960516	R	46.41	53.76	102.66	29.03	112.89	21.09	32.86	70.54	19.63
19600315	L	42.74	44.92	96.25	37.34	129.24	21.6	27.74	71.58	18.89
19781018	R									
19781018	L									
19550614	L	34.39	38.68	99.44	39.9	132.77	18.32	23.55	72.65	17.41
9265897	R	37.15	35	98.67	36.24	130.5	19.3	25.17	72.46	17.46
19520930	L	30.86	48.17	94.99	31.43	128.72	14.04	22.89	71.43	17.68
19520930	R	39.13	41.34	92.94	25.62	120.21	12.56	23.05	61.21	30.56
19470910	L	36.78	44.44	98.01	23.44	128.8	17.01	27.76	69.95	20.73
19470910	R	39.94	39.98	95.85	21.87	121.58	16.39	27.33	66.58	22.55
19361003	L									
19810101	L	44.93	47.59	101.05	25.74	118.02	19.98	31.57	67.79	22.27
19850525	R	47.89	50.97	109.61	31.7	128.34	26.92	36.33	51.2	38.76
19510901	L	43.62	53.96	96.41	30.88	120.25	20.56	32.98	67.13	22.77
19510901	R	45.47	50.21	103.72	29.82	117.04	22.22	34.26	65.33	24.64
19560709	R									
19470726	R	39.56	39.79	96.43	27.92	128.62	17.39	28.97	74.1	16.25
19870711	L	61.15	56.98	109.46	34.36	109.69	35.2	41.98	56.06	34.08
19870711	R	63.8	66.86	107.18	39.85	109.22	36.32	39.62	58.24	31.5
19540426	L	66.97	64.06	127.25	44.44	126.28	47.41	51.28	57.93	36.1
19540426	R	61.76	57.33	131.28	46.98	123.39	39.2	43.7	61.67	29.62
19921011	L	49.57	43.98	99.13	25.9	105.93	16.33	28.16	67.51	22.31
19921011	R	45.48	35.44	98.6	31.81	116.71	19.05	28.08	69.9	20.93

Table 7d. Calcaneus measurements (continued) (Chapter 4).

Sn	Side	MaxHBTALx	BHTALx	MaxLFMTALx	MaxWHTALx	MinWNTALx	MaxLHNTALx	AHTALx	ANTALx	IANTALx	IANTALxJ
19571225	R	29.3	32	30.4	31.1	27.2	30.4	83.01	116.41	28.3	36.97
19470409	L										
19650810	L										
19650810	R										
19590729	L	32.8	31.2	33.4	31.2	28	25.1	87.16	115.34	25.28	39.53
19590729	R	33.6	33.4	34.2	30.2	28.2	25.2	89.15	120.58	24.97	41.04
19540718	R	31.4	32.4	31.5	28.5	25.8	24.2	83.58	107.78	33.89	49.42
19650309	L	40.5	34.3	32.7	41.6	34.9	28.9	86.66	112.46	28.68	32.74
19600315	L	31.8	28.6	31.7	30.8	29	23.7	89.25	107.51	27.02	33.16
19511231	L	30.8	28.1	26	28.5	21.2	23.2	89.32	113.14	30.57	39.33
19511231	R	30.9	28.9	25.6	30.1	25.7	24.5	93.82	115.32	35.97	42.03
19510401	L	32	28.6	29.2	33.3	29.4	26.1	104.6	125.48	26.55	36.04
19561204	L	27	26.8	24.1	26.7	24.5	20.5	86.76	112.96	33.53	41.23
19561204	R	28.4	27.6	25	26	24.4	20.3	80.26	114.07	29.4	50.84
19600315	L										
19640420	L	31.4	24.6	25.5	26.8	22.3	20.9	77.9	107.42	24.65	35.6
19640420	R	29.6	25.4	26.3	26.9	22.9	25.3	91.52	114.8	25.78	37.42
19710208	L	36.8	35.2	37.6	37.8	31.2	30.3	96.13	115.83	25.66	34.5
19710208	R	37.7	33	34.4	36.1	30.3	30.3	89.75	112.82	28.54	36.07
19630731	L	35.7	34.2	31.4	34.7	27.2	28.9	81.82	106.18	27.76	46.29
19630731	R	35.6	35	30	34.9	28.9	29.2	81.56	106.87	29.31	42.03
19920821	L										
19840828	L	32.3	30.9	29.8	29.8	26.9	21.5	73.35	101.14	33.09	36.64
19860124	L	32.3	28.8	27.1	30	26.6	26	79.52	104.98	34.88	40.25
19580925	L	32.6	31	29.7	29.7	26.9	28.1	89.6	115.09	31.14	38.36
19540718	R	30.3	30.3	28	28.4	26.4	24.4	85.1	120.06	28.13	46.76
19530319	R										
19530319	L	31.8	28.2	26.7	26.1	23	25.1	86.85	107.45	30.84	39.2
19360507	L	28.5	28.5	24.5	30.8	25.3	28	70.56	97.73	30.7	36.97
19360507	R	29.1	28.7	25.6	31.9	28.7	28.9	74.74	102.14	26.01	32.81
19940112	R	32.5	30.3	30.1	29.3	25.5	28.8	96.65	116.95	27.71	33.34
19700612	L										
19530922	L	31	25.9	26.2	31.3	27.9	25.2	90.64	116.75	25.01	21.15
19530922	R	32.1	26.6	25.9	30.2	28	25.8	89.5	121.13	25.92	29.52
19590523	L										
19590523	R	32.7	31.2	26.3	31.3	29	27.2	87.67	117.93	33.19	46.13
19351111	L	31.9	28.9	30.2	31.1	28.2	21.8	90.74	117.33	28.62	35.21
19351111	R										
19891222	L										
19891222	R										
19640919	L	25.9	25.7	23.1	27.2	24.9	25	88.7	117.65	26.99	29.4
19640919	R	26.5	24.4	23.1	26.7	24.3	24.6	81.45	110.95	30.01	31.39
19870101	R	35.3	30.8	30.6	34.8	29.9	29.7	88.4	120.33	26.57	30.89
19640808	L	28.9	26.6	24.1	27.6	26.5	20.3	79.64	113.07	32.2	35.32
19600915	L	31.8	35.1	31.9	33.2	29.6	29.9	85.62	115.18	32.07	41.65
19600915	R	31.7	33.7	32.5	33.9	29.2	29.5	86.33	116.6	31.43	36.61
19590429	L										
19690101	L										
19411227	L	33.7	30.8	28.5	30.1	27.7	26.9	85.01	110.59	27.5	33
19481029	L										
19500214	R	32.6	34	28.3	30.9	29.7	25	90.4	123.44	34.44	39.54
19491003	L										

Table 8a. Talus measurements (Chapter 4).

Sn	Side	MaxHBTALx	BHTALx	MaxLFMTALx	MaxWHTALx	MinWNTALx	MaxLHNTALx	AHTALx	ANTALx	IANTALx	IANTALxJ
19480805	L	26.9	26.9	22.7	25.9	22.7	24.8	88.69	109.12	29.23	40.81
19480805	R	27.9	25.5	25.2	25.2	22.6	22.8	91.25	121.66	29.77	43.74
19441208	L										
19441208	R	35.4	33.7	29.9	35.1	31.5	28.6	88.93	113.93	34.91	33.84
19821001	L										
19821001	R	31.6	30.8	28.6	30.2	26.1	23.2	84.3	121.32	33.07	45.91
19470319	L	29.3	31.6	27.1	35.4	32.8	28.6	95.6	115.35	28.19	32.98
19460128	R										
19930625	L	29.9	27.2	27.7	32.2	28.2	24.2	82.35	114.04	37.2	48.24
19550225	R	32.9	30.3	27.7	32.5	28.6	25.1	74.73	104.56	36.61	43.16
19510517	L										
19710701	L	26.1	23.7	25.5	27.3	24.9	22.1	86.49	114.08	27.49	35.47
19820225	L	34.5	30.8	23.4	31.3	29.7	29.3	84.83	105.71	29.45	36.27
19820225	R	32.7	29.6	25.4	32.1	30.6	31.5	83.78	107.51	27.64	33.41
19810901	L	35.6	30.9	27.3	36.1	31.1	28.5	82.32	106.85	24.55	35.2
19810901	R	33.3	31.3	26.2	32.9	30.1	30.7	83.55	106.72	26.85	36.78
19907719	L										
19907719	R	36.1	34.4	31.4	37.8	35.5	35.8	106.68	121.95	31.43	40.31
19571223	L										
19760603	L										
19760603	R										
19490806	L										
19490806	R										
19500424	L										
19500424	R										
19850627	L	38.6	42.8	34.1	39.4	36.1	38	94.32	112.98	32.63	34.16
19850627	R	38.5	42	32.3	40.4	37	38.3	81.68	115.95	32.11	38.74
19960516	R	34.7	29.2	30.1	32.8	29.7	29.6	87.91	117.54	26.5	39.12
19600315	L	32.3	28.3	32.4	31	29.6	30.8	95.79	111.17	19.69	30.64
19781018	R										
19781018	L										
19550614	L	36.5	32.7	31.9	34.8	32.4	28	86.34	118.52	24.52	31.67
9265897	R										
19520930	L	33.8	34.6	29.7	34.6	29.7	27.5	88.51	114.9	29.73	43.32
19520930	R	34.6	36	30.5	34.8	30.5	30.7	84.51	126.08	29.2	32
19470910	L	34.7	30.3	26.8	33.5	29.4	29.7	93.07	117.07	25.1	32.73
19470910	R										
19361003	L										
19810101	L	30.1	29.1	24.4	33	27.1	26.1	93.16	114	26.62	38.95
19850525	R	36.8	34.8	29.2	35.4	30.7	30.9	83.63	109.26	29.42	41.26
19510901	L	35	32.3	31.2	31.5	28.6	27.8	86.37	108.06	26.59	40.08
19510901	R	36.3	34.1	30.3	34.7	30.8	30.7	91.64	119.59	25.23	37.66
19560709	R										
19470726	R	29.4	25.1	25.1	24.6	22.3	25.9	85.66	117.87	26.26	35.21
19870711	L	36.5	33.1	31.9	34.3	27.6	32.5	92.85	108.94	27.27	36.93
19870711	R	37.1	33	33.2	33.7	27.2	32.5	92.5	112.67	29.17	39.8
19540426	L										
19540426	R										
19921011	L	42.9	38.4	35	38.9	34.4	34.4	89.94	118.33	29.51	36.079
19921011	R	43.2	39.3	35.9	39.3	33.7	33.5	84.96	116.21	29.13	36.21

Table 8b. Talus measurements (Chapter 4).

Sn	Side	MLCALxFL	MLCALxFLCM	BHCALxMLCALx	MinAHCALxMLCALx	MinAWCALxMLCALx	MinAWCALxMinAHCALx
19571225	R	0.34893617	0.458612975	0.57804878	0.270731707	0.275609756	1.018018018
19470409	L						
19650810	L						
19650810	R						
19590729	L	0.328309572	0.427813163	0.637717122	0.302729529	0.289081886	0.954918033
19590729	R	0.329913828	0.436956522	0.585820896	0.325870647	0.294776119	0.904580153
19540718	R	0.348687043	0.454800674	0.585185185	0.295061728	0.280246914	1.949790795
19650309	L	0.353022453	0.461399549	0.569471624	0.247553816	0.285714286	1.154150198
19600315	L	0.339513326	0.44126506	0.615472127	0.30261661	0.329920364	1.090225564
19511231	L	0.365008881	0.473775216	0.582725061	0.283454988	0.232360097	0.819742489
19511231	R	0.344574146	0.445500279	0.574654956	0.278544542	0.277289837	0.995495495
19510401	L	0.350918327	0.456069071	0.639198218	0.255011136	0.28285078	1.109170306
19561204	L	0.349659864	0.454331173	0.571984436	0.284046693	0.312581064	1.100456621
19561204	R	0.360589812	0.470553936	0.553903346	0.285006196	0.293680297	1.030434783
19600315	L						
19640420	L	0.371078431	0.475801383	0.554821664	0.247027741	0.253632761	1.026737968
19640420	R	0.363680154	0.466914038	0.57615894	0.262251656	0.252980132	0.964646465
19710208	L	0.35862069	0.461137194	0.64479638	0.281674208	0.341628959	1.212851406
19710208	R	0.366004963	0.477088949	0.64519774	0.308474576	0.31299435	1.014652015
19630731	L	0.34262356	0.439885496	0.610629067	0.253796095	0.273318872	1.076923077
19630731	R	0.359862909	0.459406903	0.625396825	0.250793651	0.258201058	1.029535865
19920821	L						
19840828	L	0.379955457	0.498538866	0.582649472	0.309495897	0.308323564	0.996212121
19860124	L	0.355207451	0.457969432	0.557806913	0.286054827	0.296781883	1.0375
19580925	L	0.390136504	0.511547344	0.59255079	0.287810384	0.29006772	1.007843137
19540718	R	0.336210617	0.438626126	0.626444159	0.296534018	0.309370988	1.043290043
19530319	R						
19530319	L	0.3611	0.4686	0.5209	0.2533	0.3023	1.1934
19360507	L	0.365107914	0.475409836	0.592364532	0.267241379	0.274630542	1.02764977
19360507	R	0.355769231	0.453481894	0.583538084	0.298525799	0.277641278	0.930041152
19940112	R	0.347929936	0.458311484	0.519450801	0.271167048	0.28375286	1.046413502
19700612	L						
19530922	L	0.359608209	0.461953265	0.648508431	0.28923476	0.307392996	1.062780269
19530922	R	0.359761687	0.453757225	0.61656051	0.277707006	0.307006369	1.105504587
19590523	L						
19590523	R	0.343459916	0.440714672	0.628992629	0.278869779	0.297297297	1.066079295
19351111	L	0.331576425	0.427688504	0.632947977	0.336705202	0.333815029	0.991416309
19351111	R	0.328941176	0.42337977	0.629470672	0.316165951	0.330472103	1.045248869
19891222	L						
19891222	R						
19640919	L	0.338686131	0.442748092	0.550287356	0.268678161	0.32183908	1.197860963
19640919	R	0.33065659	0.433168317	0.57	0.281428571	0.328571429	1.16751269
19870101	R	0.353369066	0.454679803	0.567713976	0.328277356	0.312026002	0.95049505
19640808	L	0.335855401	0.437808219	0.496871089	0.28911389	0.281602003	0.974025974
19600915	L	0.361756015	0.463243243	0.624270712	0.291715286	0.310385064	1.064
19600915	R	0.369296375	0.470908102	0.653579677	0.275981524	0.337182448	1.221757322
19590429	L						
19690101	L						
19411227	L	0.351141925	0.447505198	0.631823461	0.283391405	0.264808362	0.93442623
19481029	L						
19500214	R	0.363431151	0.465317919	0.614906832	0.288198758	0.285714286	0.99137931
19491003	L						
19611020	L	0.352601156	0.46112311	0.62529274	0.281030445	0.270491803	0.9625

Table 9a. Calcaneus indices (Chapter 4).

Sn	Side	MLCALxFL	MLCALxFLCM	BHCALxMLCALx	MinAHCALxMLCALx	MinAWCALxMLCALx	MinAWCALxMinAHCALx
19480805	L	0.330314791	0.42414175	0.584856397	0.274151436	0.293733681	1.071428571
19480805	R	0.330645161	0.42778693	0.57381258	0.261874198	0.292682927	1.117647059
19441208	L						
19441208	R	0.3627007	0.466631356	0.606129398	0.262202043	0.296254257	1.12987013
19821001	L						
19821001	R	0.357723577	0.457142857	0.590909091	0.276136364	0.272727273	0.987654321
19470319	L	0.321752266	0.409418549	0.613849765	0.267605634	0.313380282	1.171052632
19460128	R						
19930625	L	0.334329633	0.430930105	0.625798212	0.316730524	0.311621967	0.983870968
19550225	R	0.340299685	0.443930041	0.640787949	0.304750869	0.269988413	0.885931559
19510517	L						
19710701	L	0.337971275	0.440350877	0.553784861	0.274900398	0.317397078	1.154589372
19820225	L	0.377086152	0.483516484	0.586124402	0.306220096	0.282296651	0.921875
19820225	R	0.367498905	0.47240991	0.569725864	0.296781883	0.26102503	0.879518072
19810901	L	0.371142619	0.478237507	0.55505618	0.28988764	0.256179775	0.88372093
19810901	R	0.366666667	0.477260847	0.56626506	0.281489595	0.249726177	0.887159533
19907719	L	0.328472222	0.424215247	0.591966173	0.321353066	0.308668076	0.960526316
19900719	R	0.337774577	0.434259259	0.615138593	0.309168443	0.293176972	0.948275862
19571223	L						
19760603	L	0.328480114	0.426463808	0.618378378	0.292972973	0.28972973	0.988929889
19760603	R	0.333215672	0.431444241	0.564618644	0.265889831	0.300847458	1.131474104
19490806	L						
19490806	R						
19500424	L						
19500424	R						
19850627	L						
19850627	R						
19960516	R	0.358034321	0.463870642	0.561002179	0.261437908	0.284313725	1.0875
19600315	L	0.337340054	0.438508065	0.631034483	0.297701149	0.268965517	0.903474903
19781018	R						
19781018	L						
19550614	L	0.349349711	0.454844779	0.601861427	0.278179938	0.28024819	1.007434944
9265897	R	0.350073314	0.456064947	0.6	0.286910995	0.285863874	0.996350365
19520930	L	0.356040647	0.455903614	0.572938689	0.306553911	0.243128964	0.793103448
19520930	R	0.371206226	0.477238619	0.553459119	0.301886792	0.252620545	0.836805556
19470910	L	0.340023157	0.446301925	0.574347333	0.284903519	0.267877412	0.940239044
19470910	R	0.3459291	0.45655527	0.57545045	0.286036036	0.252252252	0.881889764
19361003	L						
19810101	L	0.34600598	0.45	0.540740741	0.281481481	0.27654321	0.98245614
19850525	R	0.38467433	0.490234375	0.618525896	0.266932271	0.264940239	0.992537313
19510901	L	0.338022665	0.430134262	0.639306358	0.271676301	0.285549133	1.05106383
19510901	R	0.329123613	0.420127015	0.661627907	0.272093023	0.291860465	1.072649573
19560709	R						
19470726	R	0.356283101	0.462789243	0.585135135	0.294594595	0.3	1.018348624
19870711	L	0.328232594	0.432024169	0.548951049	0.27039627	0.282051282	1.043103448
19870711	R	0.329636711	0.43360161	0.570765661	0.267981439	0.267981439	1
19540426	L	0.369138277	0.474497682	0.555917481	0.220412595	0.268186754	1.216748768
19540426	R	0.366813982	0.477760335	0.630887185	0.222343921	0.284775465	1.280788177
19921011	L	0.367784307	0.471004869	0.568609023	0.282894737	0.247180451	0.873754153
19921011	R	0.362633575	0.463844797	0.603612167	0.294676806	0.245247148	0.832258065

Table 9b. Calcaneus indices (Chapter 4).

Sn	Foot type	MaxLTALx /FL	MaxLTALx /FLCM	BHTALx /MaxLTALx	BHTALx /MaxLFMTALx	MaxLFMTALx /MaxLTALx	MaxLHNTALx /FL	MaxLHNTALx /FLCM	MaxWHTALx /MaxLHNTALx	MinWNTALx /MaxWHTALx
19571225	NA	0.245957447	0.323266219	0.553633218	1.052631579	0.525951557	0.129361702	0.170022371	1.023026316	0.874598071
19470409	LA									
19650810	LA									
19650810	LA									
19590729	LA	0.23910387	0.311571125	0.531516184	0.934131737	0.568994889	0.102240326	0.133227176	1.243027888	0.897435897
19590729	LA	0.240459581	0.318478261	0.56996587	0.976608187	0.583617747	0.103405827	0.136956522	1.198412698	0.933774834
19540718	NA	0.248816186	0.324536777	0.560553633	1.028571429	0.544982699	0.104175635	0.13587872	1.17768595	0.905263158
19650309	NA	0.236614853	0.309255079	0.500729927	1.048929664	0.477372263	0.099827288	0.130474041	1.439446367	0.838942308
19600315	NA	0.242564697	0.315261044	0.455414013	0.902208202	0.50477707	0.091541136	0.118975904	1.299578059	0.941558442
19511231	NA	0.239786856	0.311239193	0.52037037	1.080769231	0.481481481	0.103019538	0.133717579	1.228448276	0.743859649
19511231	NA	0.233030696	0.301285634	0.536178108	1.12890625	0.474953618	0.105923044	0.136948016	1.228571429	0.853820598
19510401	HA	0.243063697	0.315896394	0.459807074	0.979452055	0.469453376	0.101992966	0.132554596	1.275862069	0.882882883
19561204	LA	0.236734694	0.30760165	0.513409962	1.112033195	0.461685824	0.092970522	0.120801414	1.302439024	0.917602996
19561204	SF	0.246648794	0.321865889	0.5	1.104	0.452898551	0.090705987	0.118367347	1.280788177	0.938461538
19600315	NA									
19640420	NA	0.250490196	0.321181647	0.481409002	0.964705882	0.499021526	0.10245098	0.131363922	1.282296651	0.832089552
19640420	NA	0.243256262	0.312306741	0.502970297	0.965779468	0.520792079	0.121868979	0.156462585	1.063241107	0.851301115
19710208	HA	0.265314402	0.341158059	0.5382263	0.936170213	0.574923547	0.122920892	0.158059468	1.247524752	0.825396825
19710208	HA	0.267162945	0.348247978	0.510835913	0.959302326	0.53250774	0.125310174	0.163342318	1.191419142	0.83933518
19630731	HA	0.238573021	0.30629771	0.53271028	1.089171975	0.489096573	0.10739502	0.137881679	1.200692042	0.783861671
19630731	HA	0.263899467	0.336898396	0.505050505	1.166666667	0.432900433	0.111195735	0.141954302	1.195205479	0.828802229
19920821	NA									
19840828	NA	0.275278396	0.361192285	0.5	1.036912752	0.482200647	0.095768374	0.12565751	1.386046512	0.902684564
19860124	NA	0.251481795	0.324235808	0.484848485	1.062730627	0.456228956	0.110076207	0.141921397	1.153846154	0.886666667
19580925	HA	0.263760458	0.345842956	0.517529215	1.043771044	0.495826377	0.123734038	0.162240185	1.056939502	0.905723906
19540718	NA	0.249028917	0.324887387	0.525129983	1.082142857	0.485268631	0.105308589	0.137387387	1.163934426	0.929577465
19530319	LA									
19530319	LA	0.2291	0.2973	0.5311	1.0562	0.5028	0.1083	0.1405	1.0398	0.8812
19360507	HA	0.238309353	0.31030445	0.537735849	1.163265306	0.462264151	0.125899281	0.163934426	1.1	0.821428571
19360507	NA	0.236013986	0.300835655	0.531481481	1.12109375	0.474074074	0.126311189	0.161002786	1.103806228	0.89968652
19940112	NA	0.231289809	0.304667016	0.52151463	1.006644518	0.518072289	0.114649682	0.151022549	1.017361111	0.870307167
19700612	NA									
19530922	HA	0.263059701	0.337926902	0.459219858	0.988549618	0.464539007	0.117537313	0.150988616	1.242063492	0.891373802
19530922	NA	0.261686526	0.330057803	0.465849387	1.027027027	0.453590193	0.118240147	0.149132948	1.170542636	0.927152318
19590523	NA									
19590523	HA	0.251898734	0.323226854	0.522613065	1.186311787	0.440536013	0.114767932	0.147265836	1.150735294	0.926517572
19351111	NA	0.245328222	0.316440049	0.564453125	0.956953642	0.58984375	0.104456157	0.13473424	1.426605505	0.906752412
19351111	LA									
19891222	NA									
19891222	LA									
19640919	NA	0.244768856	0.319974555	0.510934394	1.112554113	0.459244533	0.121654501	0.159033079	1.088	0.915441176
19640919	LA	0.231931979	0.303836634	0.49694501	1.056277056	0.470468432	0.116202173	0.152227723	1.085365854	0.91011236
19870101	LA	0.243108729	0.312807882	0.48503937	1.006535948	0.481889764	0.113705972	0.146305419	1.171717172	0.859195402
19640808	SF	0.240437158	0.313424658	0.465034965	1.10373444	0.421328671	0.085329971	0.111232877	1.359605911	0.960144928
19600915	SC	0.266950959	0.340402393	0.560702875	1.10031348	0.509584665	0.12750533	0.162588363	1.110367893	0.891566265
19600915	HA	0.256648375	0.328648649	0.554276316	1.036923077	0.534539474	0.124525116	0.159459459	1.149152542	0.861356932
19590429	NA									
19690101	NA									
19411227	HA	0.258564437	0.32952183	0.485804416	1.080701754	0.449526814	0.109706362	0.13981289	1.118959108	0.920265781
19481029	NA									
19500214	NA	0.253724605	0.324855491	0.604982206	1.201413428	0.503558719	0.112866817	0.144508671	1.236	0.961165049
19491003	LA									
19611020	NA	0.280759703	0.367170626	0.464705882	0.990595611	0.469117647	0.116845582	0.152807775	1.176678445	0.897897898

Table 10a. Talus indices (Chapter 4).

Sn	Foot type	MaxLTALx /FL	MaxLTALx /FLCM	BHTALx /MaxLTALx	BHTALx /MaxLFMTALx	MaxLFMTALx /MaxLTALx	MaxLHNTALx /FL	MaxLHNTALx /FLCM	MaxWHTALx /MaxLHNTALx	MinWNTALx /MaxWHTALx
19480805	LA	0.222509702	0.285714286	0.521317829	1.185022026	0.439922481	0.106942648	0.137320044	1.044354839	0.876447876
19480805	LA	0.216044143	0.279516749	0.500982318	1.011904762	0.495088409	0.096774194	0.125205931	1.105263158	0.896825397
19441208	NA									
19441208	NA	0.273775216	0.352224576	0.506766917	1.127090301	0.44962406	0.117743928	0.151483051	1.227272727	0.897435897
19821001	LA									
19821001	LA	0.21300813	0.272207792	0.58778626	1.076923077	0.545801527	0.094308943	0.120519481	1.301724138	0.864238411
19470319	LA	0.227719033	0.289764536	0.524046434	1.166051661	0.449419569	0.108006042	0.137433926	1.237762238	0.926553672
19460128	LA									
19930625	LA	0.221605465	0.285635663	0.524084778	0.981949458	0.53371869	0.103330487	0.133186571	1.330578512	0.875776398
19550225	NA	0.254731861	0.332304527	0.469040248	1.093862816	0.42879257	0.098974763	0.129115226	1.294820717	0.88
19510517	NA									
19710701	LA	0.217235189	0.283040936	0.489669421	0.929411765	0.526859504	0.099192101	0.129239766	1.235294118	0.912087912
19820225	NA	0.264321155	0.338924234	0.52559727	1.316239316	0.399317406	0.132160577	0.169462117	1.068259386	0.948881789
19820225	LA	0.257555848	0.331081081	0.503401361	1.165354331	0.431972789	0.137976347	0.177364865	1.019047619	0.953271028
19810901	LA	0.266889074	0.343901128	0.4828125	1.131868132	0.4265625	0.118849041	0.153143471	1.266666667	0.861495845
19810901	LA	0.2562249	0.33350758	0.490595611	1.194656489	0.410658307	0.123293173	0.16048092	1.071661238	0.914893617
19907719	NA									
19900719	LA	0.231544833	0.297685185	0.534992224	1.095541401	0.488335925	0.128916097	0.165740741	1.055865922	0.939153439
19571223	HA									
19760603	SF									
19760603	LA									
19490806	LA									
19490806	LA									
19500424	HA									
19500424	HA									
19850627	NA	0.236323851	0.311988445	0.660493827	1.255131965	0.526234568	0.138584974	0.182956187	1.036842105	0.916243655
19850627	NA	0.238838475	0.31468197	0.638297872	1.300309598	0.490881459	0.139019964	0.183165949	1.054830287	0.915841584
19960516	LA	0.264820593	0.343102577	0.430044183	0.970099668	0.443298969	0.115444618	0.14957049	1.108108108	0.905487805
19600315	NA	0.243892982	0.31703629	0.449920509	0.87345679	0.515103339	0.119426134	0.155241935	1.006493506	0.95483871
19781018	NA									
19781018	NA									
19550614	NA	0.249277457	0.324553151	0.473913043	1.02507837	0.462318841	0.101156069	0.131702728	1.242857143	0.931034483
9265897	LA									
19520930	SF	0.25780956	0.330120482	0.505109489	1.164983165	0.433576642	0.103500188	0.13253012	1.258181818	0.858381503
19520930	SF	0.246692607	0.317158579	0.567823344	1.180327869	0.481072555	0.119455253	0.153576788	1.133550489	0.876436782
19470910	LA	0.228483211	0.299898683	0.511824324	1.130597015	0.452702703	0.114627557	0.150455927	1.127946128	0.87761194
19470910	LA									
19361003	LA									
19810101	LA	0.236651004	0.307777778	0.525270758	1.192622951	0.440433213	0.111490816	0.145	1.264367816	0.821212121
19850525	HA	0.248659004	0.316894531	0.536209553	1.191780822	0.449922958	0.118390805	0.150878906	1.145631068	0.867231638
19510901	LA	0.262211801	0.333664843	0.481371088	1.03525641	0.464977645	0.108636186	0.138239682	1.133093525	0.907936508
19510901	SF	0.253348641	0.323400098	0.51510574	1.125412541	0.457703927	0.117489476	0.149975574	1.13029316	0.887608069
19560709	HA									
19470726	SF	0.228695234	0.297060663	0.528421053	1	0.528421053	0.124699085	0.161976235	0.94980695	0.906504065
19870711	HA	0.243305279	0.320241692	0.520440252	1.037617555	0.501572327	0.124330528	0.163645519	1.055384615	0.804664723
19870711	SC	0.245889101	0.323440644	0.513219285	0.993975904	0.516329705	0.124282983	0.163480885	1.036923077	0.807121662
19540426	HA									
19540426	SC									
19921011	LA	0.268924991	0.344400177	0.493573265	1.097142857	0.449871465	0.118907708	0.15227977	1.130813953	0.884318766
19921011	LA	0.279903482	0.358024691	0.483990148	1.094707521	0.442118227	0.115477422	0.147707231	1.173134328	0.857506361

Table 10b. Talus indices (continued) (Chapter 4).


```

diff |      54   -.7475926   .4190438   3.07933   -1.588088   .0929028
-----
mean(diff) = mean(BHCAL - BHCALx)          t = -1.7840
Ho: mean(diff) = 0                          degrees of freedom = 53

Ha: mean(diff) < 0          Ha: mean(diff) != 0          Ha: mean(diff) > 0
Pr(T < t) = 0.0401         Pr(|T| > |t|) = 0.0801         Pr(T > t) = 0.9599

. ttest MinBHCAL == MinBHCALx if reading==1

Paired t test
-----
Variable |      Obs      Mean   Std. Err.   Std. Dev.   [95% Conf. Interval]
-----+-----
MinBHCAL |      54   39.2437   .4972786   3.654236   38.24629   40.24112
MinBHC-x |      54   38.98093   .5202879   3.82332   37.93736   40.02449
-----+-----
diff |      54   .2627778   .2348768   1.725985   -.2083254   .733881
-----
mean(diff) = mean(MinBHCAL - MinBHCALx)          t = 1.1188
Ho: mean(diff) = 0                          degrees of freedom = 53

Ha: mean(diff) < 0          Ha: mean(diff) != 0          Ha: mean(diff) > 0
Pr(T < t) = 0.8659         Pr(|T| > |t|) = 0.2683         Pr(T > t) = 0.1341

. ttest MinAHCAL == MinAHCALx if reading==1

Paired t test
-----
Variable |      Obs      Mean   Std. Err.   Std. Dev.   [95% Conf. Interval]
-----+-----
MinAHCAL |      54   25.07019   .2888777   2.122809   24.49077   25.6496
MinAHC-x |      54   25.07963   .3010694   2.212399   24.47576   25.6835
-----+-----
diff |      54   -.0094444   .2135395   1.569188   -.4377505   .4188616
-----
mean(diff) = mean(MinAHCAL - MinAHCALx)          t = -0.0442
Ho: mean(diff) = 0                          degrees of freedom = 53

Ha: mean(diff) < 0          Ha: mean(diff) != 0          Ha: mean(diff) > 0
Pr(T < t) = 0.4824         Pr(|T| > |t|) = 0.9649         Pr(T > t) = 0.5176

. ttest MinAWCAL == MinAWCALx if reading==1

Paired t test
-----
Variable |      Obs      Mean   Std. Err.   Std. Dev.   [95% Conf. Interval]
-----+-----
MinAWCAL |      54   22.8313   .2721894   2.000176   22.28535   23.37724
MinAWC-x |      54   23.00667   .2845398   2.090932   22.43595   23.57738
-----+-----
diff |      54   -.1753704   .2733107   2.008415   -.7235622   .3728214
-----
mean(diff) = mean(MinAWCAL - MinAWCALx)          t = -0.6417
Ho: mean(diff) = 0                          degrees of freedom = 53

```

Ha: mean(diff) < 0 Ha: mean(diff) != 0 Ha: mean(diff) > 0
 Pr(T < t) = 0.2619 Pr(|T| > |t|) = 0.5239 Pr(T > t) = 0.7381

Regression analysis with constant

. reg MLCAL MLCALx if reading==1

Source	SS	df	MS	Number of obs =	54
Model	2058.44471	1	2058.44471	F(1, 52) =	473.02
Residual	226.287833	52	4.3516891	Prob > F =	0.0000
				R-squared =	0.9010
				Adj R-squared =	0.8991
Total	2284.73255	53	43.1081613	Root MSE =	2.0861

MLCAL	Coef.	Std. Err.	t	P> t	[95% Conf. Interval]	
MLCALx	.9273056	.0426366	21.75	0.000	.8417491	1.012862
_cons	3.427275	3.709773	0.92	0.360	-4.016929	10.87148

. reg MLCAL2 MLCAL2x if reading==1

Source	SS	df	MS	Number of obs =	54
Model	2183.4573	1	2183.4573	F(1, 52) =	503.65
Residual	225.432363	52	4.33523775	Prob > F =	0.0000
				R-squared =	0.9064
				Adj R-squared =	0.9046
Total	2408.88966	53	45.4507483	Root MSE =	2.0821

MLCAL2	Coef.	Std. Err.	t	P> t	[95% Conf. Interval]	
MLCAL2x	.9519591	.0424182	22.44	0.000	.8668407	1.037077
_cons	2.834411	3.545717	0.80	0.428	-4.28059	9.949412

. reg BHCAL BHCALx if reading==1

Source	SS	df	MS	Number of obs =	54
Model	703.128338	1	703.128338	F(1, 52) =	129.77
Residual	281.750195	52	5.41827299	Prob > F =	0.0000
				R-squared =	0.7139
				Adj R-squared =	0.7084
Total	984.878533	53	18.5826138	Root MSE =	2.3277

BHCAL	Coef.	Std. Err.	t	P> t	[95% Conf. Interval]	
BHCALx	.6408643	.0562573	11.39	0.000	.5279757	.7537529
_cons	17.38949	2.858714	6.08	0.000	11.65306	23.12592

```
. reg MinBHCAL MinBHCALx if reading==1
```

Source	SS	df	MS		Number of obs =	54
Model	566.165433	1	566.165433		F(1, 52) =	207.96
Residual	141.567027	52	2.72244282		Prob > F =	0.0000
					R-squared =	0.8000
					Adj R-squared =	0.7961
Total	707.732459	53	13.3534426		Root MSE =	1.65

MinBHCAL	Coef.	Std. Err.	t	P> t	[95% Conf. Interval]	
MinBHCALx	.8548563	.059279	14.42	0.000	.7359043	.9738083
_cons	5.920614	2.321633	2.55	0.014	1.261916	10.57931

```
. reg MinAHCAL MinAHCALx if reading==1
```

Source	SS	df	MS		Number of obs =	54
Model	130.329324	1	130.329324		F(1, 52) =	62.46
Residual	108.505574	52	2.08664565		Prob > F =	0.0000
					R-squared =	0.5457
					Adj R-squared =	0.5370
Total	238.834898	53	4.50631883		Root MSE =	1.4445

MinAHCAL	Coef.	Std. Err.	t	P> t	[95% Conf. Interval]	
MinAHCALx	.7087934	.0896857	7.90	0.000	.528826	.8887609
_cons	7.293908	2.257856	3.23	0.002	2.763188	11.82463

```
. reg MinAWCAL MinAWCALx if reading==1
```

Source	SS	df	MS		Number of obs =	54
Model	57.0569895	1	57.0569895		F(1, 52) =	19.14
Residual	154.98022	52	2.98038884		Prob > F =	0.0001
					R-squared =	0.2691
					Adj R-squared =	0.2550
Total	212.037209	53	4.00070206		Root MSE =	1.7264

MinAWCAL	Coef.	Std. Err.	t	P> t	[95% Conf. Interval]	
MinAWCALx	.4962227	.1134119	4.38	0.000	.268645	.7238003
_cons	11.41487	2.619785	4.36	0.000	6.157884	16.67185

```
.
.
. pwcrr MLCAL MLCALx MLCAL2 MLCAL2x BHCAL BHCALx MinBHCAL MinBHCALx MinAHCAL
MinAHCALx MinAWCAL if reading==1,
> sig
```

	MLCAL	MLCALx	MLCAL2	MLCAL2x	BHCAL	BHCALx	MinBHCAL
MLCAL	1.0000						
MLCALx	0.9492 0.0000	1.0000					
MLCAL2	0.9822 0.0000	0.9407 0.0000	1.0000				
MLCAL2x	0.9329 0.0000	0.9504 0.0000	0.9521 0.0000	1.0000			
BHCAL	0.8266 0.0000	0.7967 0.0000	0.8545 0.0000	0.8109 0.0000	1.0000		
BHCALx	0.6722 0.0000	0.6939 0.0000	0.7182 0.0000	0.7088 0.0000	0.8449 0.0000	1.0000	
MinBHCAL	0.7681 0.0000	0.6937 0.0000	0.7918 0.0000	0.7353 0.0000	0.8809 0.0000	0.7365 0.0000	1.0000
MinBHCALx	0.7486 0.0000	0.7141 0.0000	0.7647 0.0000	0.7241 0.0000	0.8675 0.0000	0.7412 0.0000	0.8944 0.0000
MinAHCAL	0.4565 0.0005	0.4589 0.0005	0.5006 0.0001	0.5211 0.0001	0.5849 0.0000	0.4303 0.0012	0.4823 0.0002
MinAHCALx	0.5433 0.0000	0.5957 0.0000	0.5634 0.0000	0.6529 0.0000	0.6704 0.0000	0.5792 0.0000	0.5613 0.0000
MinAWCAL	0.5565 0.0000	0.5394 0.0000	0.6040 0.0000	0.5773 0.0000	0.6140 0.0000	0.5910 0.0000	0.5760 0.0000
			MinBHC-x	MinAHCAL	MinAHC-x	MinAWCAL	
MinBHCALx	1.0000						
MinAHCAL	0.4605 0.0005	1.0000					
MinAHCALx	0.5077 0.0001	0.7387 0.0000	1.0000				
MinAWCAL	0.5544 0.0000	0.2543 0.0635	0.3412 0.0116	1.0000			

Regression analysis no constant

reg MLCAL MLCALx if reading==1, noconstant

Source	SS	df	MS	Number of obs =	54
Model	381943.897	1	381943.897	F(1, 53) =	88012.39
Residual	230.001998	53	4.33966034	Prob > F =	0.0000
				R-squared =	0.9994
				Adj R-squared =	0.9994
Total	382173.899	54	7077.29442	Root MSE =	2.0832

MLCAL	Coef.	Std. Err.	t	P> t	[95% Conf. Interval]
MLCALx	.9665799	.0032581	296.67	0.000	.960045 .9731149

. reg MLCAL2 MLCAL2x if reading==1, noconstant

Source	SS	df	MS	Number of obs =	54
Model	366639.163	1	366639.163	F(1, 53) =	85151.83
Residual	228.202687	53	4.30571107	Prob > F =	0.0000
				R-squared =	0.9994
				Adj R-squared =	0.9994
Total	366867.365	54	6793.8401	Root MSE =	2.075

MLCAL2	Coef.	Std. Err.	t	P> t	[95% Conf. Interval]
MLCAL2x	.9857593	.0033781	291.81	0.000	.9789837 .992535

. reg BHCAL BHCALx if reading==1, noconstant

Source	SS	df	MS	Number of obs =	54
Model	134179.894	1	134179.894	F(1, 53) =	14746.87
Residual	482.240368	53	9.09887487	Prob > F =	0.0000
				R-squared =	0.9964
				Adj R-squared =	0.9964
Total	134662.135	54	2493.74323	Root MSE =	3.0164

BHCAL	Coef.	Std. Err.	t	P> t	[95% Conf. Interval]
BHCALx	.9809691	.008078	121.44	0.000	.9647666 .9971716

. reg MinBHCAL MinBHCALx if reading==1, noconstant

Source	SS	df	MS	Number of obs =	54
Model	83712.1472	1	83712.1472	F(1, 53) =	27856.33
Residual	159.272397	53	3.00513957	Prob > F =	0.0000
				R-squared =	0.9981
				Adj R-squared =	0.9981
Total	83871.4196	54	1553.17444	Root MSE =	1.7335

MinBHCAL	Coef.	Std. Err.	t	P> t	[95% Conf. Interval]	
MinBHCALx	1.005321	.0060234	166.90	0.000	.9932391	1.017402

. reg MinAHCAL MinAHCALx if reading==1, noconstant

Source	SS	df	MS	Number of obs = 54		
Model	34048.3194	1	34048.3194	F(1, 53) =	13851.24	
Residual	130.281504	53	2.45814158	Prob > F	= 0.0000	
				R-squared	= 0.9962	
				Adj R-squared	= 0.9961	
Total	34178.6009	54	632.937054	Root MSE	= 1.5678	

MinAHCAL	Coef.	Std. Err.	t	P> t	[95% Conf. Interval]	
MinAHCALx	.997419	.0084749	117.69	0.000	.9804205	1.014417

. reg MinAWCAL MinAWCALx if reading==1, noconstant

Source	SS	df	MS	Number of obs = 54		
Model	28148.9512	1	28148.9512	F(1, 53) =	7051.78	
Residual	211.562879	53	3.99175243	Prob > F	= 0.0000	
				R-squared	= 0.9925	
				Adj R-squared	= 0.9924	
Total	28360.5141	54	525.194706	Root MSE	= 1.9979	

MinAWCAL	Coef.	Std. Err.	t	P> t	[95% Conf. Interval]	
MinAWCALx	.9883875	.01177	83.97	0.000	.9647798	1.011995

end of do-file


```

diff |      54  -.7540741  .1752278  1.287656  -1.105537  -.4026116
-----+-----
mean(diff) = mean(BHTALa - BHTALx)          t = -4.3034
Ho: mean(diff) = 0                          degrees of freedom = 53

Ha: mean(diff) < 0          Ha: mean(diff) != 0          Ha: mean(diff) > 0
Pr(T < t) = 0.0000        Pr(|T| > |t|) = 0.0001        Pr(T > t) = 1.0000

```

. ttest BHTALb ==BHTALx if reading==1

Paired t test

Variable	Obs	Mean	Std. Err.	Std. Dev.	[95% Conf. Interval]	
BHTALb	54	33.52852	.4343484	3.191796	32.65733	34.39971
BHTALx	54	33.80593	.4435564	3.25946	32.91626	34.69559
diff	54	-.2774074	.2110652	1.551006	-.7007505	.1459357

```

mean(diff) = mean(BHTALb - BHTALx)          t = -1.3143
Ho: mean(diff) = 0                          degrees of freedom = 53

Ha: mean(diff) < 0          Ha: mean(diff) != 0          Ha: mean(diff) > 0
Pr(T < t) = 0.0972        Pr(|T| > |t|) = 0.1944        Pr(T > t) = 0.9028

```

. ttest MaxLFMTAL== MaxLFMTALx if reading==1

Paired t test

Variable	Obs	Mean	Std. Err.	Std. Dev.	[95% Conf. Interval]	
MaxLFM-L	54	32.39537	.3908966	2.872492	31.61133	33.17941
MaxLFM-x	54	32.83056	.3843682	2.824518	32.05961	33.6015
diff	54	-.4351852	.2528023	1.85771	-.9422424	.071872

```

mean(diff) = mean(MaxLFMTAL - MaxLFMTALx)    t = -1.7214
Ho: mean(diff) = 0                          degrees of freedom = 53

Ha: mean(diff) < 0          Ha: mean(diff) != 0          Ha: mean(diff) > 0
Pr(T < t) = 0.0455        Pr(|T| > |t|) = 0.0910        Pr(T > t) = 0.9545

```

. ttest MaxWHTAL ==MaxWHTALx if reading==1

Paired t test

Variable	Obs	Mean	Std. Err.	Std. Dev.	[95% Conf. Interval]	
MaxWHTAL	54	31.60204	.3969148	2.916717	30.80593	32.39815
MaxWHT-x	54	31.92167	.4774153	3.508271	30.96409	32.87924
diff	54	-.3196296	.4591651	3.37416	-1.240598	.6013389

```

mean(diff) = mean(MaxWHTAL - MaxWHTALx)    t = -0.6961
Ho: mean(diff) = 0                          degrees of freedom = 53

```

Ha: mean(diff) < 0 Ha: mean(diff) != 0 Ha: mean(diff) > 0
 Pr(T < t) = 0.2447 Pr(|T| > |t|) = 0.4894 Pr(T > t) = 0.7553

. ttest MinWNTALa== MinWNTALx if reading==1

Paired t test

Variable	Obs	Mean	Std. Err.	Std. Dev.	[95% Conf. Interval]	
MinWNT-a	54	27.42815	.3517979	2.585176	26.72253	28.13377
MinWNT-x	54	27.74648	.4494789	3.302982	26.84494	28.64802
diff	54	-.3183333	.3636835	2.672517	-1.04779	.4111233

mean(diff) = mean(MinWNTALa - MinWNTALx) t = -0.8753
 Ho: mean(diff) = 0 degrees of freedom = 53

Ha: mean(diff) < 0 Ha: mean(diff) != 0 Ha: mean(diff) > 0
 Pr(T < t) = 0.1927 Pr(|T| > |t|) = 0.3854 Pr(T > t) = 0.8073

. ttest MinWNTALb == MinWNTALx if reading==1

Paired t test

Variable	Obs	Mean	Std. Err.	Std. Dev.	[95% Conf. Interval]	
MinWNT-b	54	27.31778	.3694707	2.715044	26.57671	28.05884
MinWNT-x	54	27.74648	.4494789	3.302982	26.84494	28.64802
diff	54	-.4287037	.3381099	2.48459	-1.106866	.2494589

mean(diff) = mean(MinWNTALb - MinWNTALx) t = -1.2679
 Ho: mean(diff) = 0 degrees of freedom = 53

Ha: mean(diff) < 0 Ha: mean(diff) != 0 Ha: mean(diff) > 0
 Pr(T < t) = 0.1052 Pr(|T| > |t|) = 0.2104 Pr(T > t) = 0.8948

. ttest MaxLHNTAL ==MaxLHNTALx if reading==1

Paired t test

Variable	Obs	Mean	Std. Err.	Std. Dev.	[95% Conf. Interval]	
MaxLHN-L	54	25.2237	.4148363	3.048412	24.39165	26.05576
MaxLHN-x	54	24.54148	.4644124	3.41272	23.60999	25.47297
diff	54	.6822222	.2812399	2.066682	.1181265	1.246318

mean(diff) = mean(MaxLHNTAL - MaxLHNTALx) t = 2.4258
 Ho: mean(diff) = 0 degrees of freedom = 53

Ha: mean(diff) < 0 Ha: mean(diff) != 0 Ha: mean(diff) > 0
 Pr(T < t) = 0.9906 Pr(|T| > |t|) = 0.0187 Pr(T > t) = 0.0094

. Regress analysis with constant

. reg MaxLTAL MaxLTALx if reading==1

Source	SS	df	MS	Number of obs =	54
Model	1288.12296	1	1288.12296	F(1, 52) =	399.52
Residual	167.658227	52	3.22419667	Prob > F =	0.0000
				R-squared =	0.8848
				Adj R-squared =	0.8826
Total	1455.78119	53	27.4675696	Root MSE =	1.7956

MaxLTAL	Coef.	Std. Err.	t	P> t	[95% Conf. Interval]	
MaxLTALx	.835121	.0417813	19.99	0.000	.7512808	.9189612
_cons	7.942741	2.620733	3.03	0.004	2.683855	13.20163

. reg MaxHBTAL MaxHBTALx if reading==1

Source	SS	df	MS	Number of obs =	54
Model	243.450757	1	243.450757	F(1, 52) =	85.66
Residual	147.792097	52	2.84215571	Prob > F =	0.0000
				R-squared =	0.6222
				Adj R-squared =	0.6150
Total	391.242854	53	7.38194064	Root MSE =	1.6859

MaxHBTAL	Coef.	Std. Err.	t	P> t	[95% Conf. Interval]	
MaxHBTALx	.6491487	.0701395	9.26	0.000	.5084036	.7898939
_cons	11.38744	2.336867	4.87	0.000	6.698171	16.0767

. reg BHTALa BHTALx if reading==1

Source	SS	df	MS	Number of obs =	54
Model	393.867448	1	393.867448	F(1, 52) =	281.34
Residual	72.7983672	52	1.3999686	Prob > F =	0.0000
				R-squared =	0.8440
				Adj R-squared =	0.8410
Total	466.665815	53	8.80501537	Root MSE =	1.1832

BHTALa	Coef.	Std. Err.	t	P> t	[95% Conf. Interval]	
BHTALx	.8363565	.0498627	16.77	0.000	.7362997	.9364132
_cons	4.778047	1.693326	2.82	0.007	1.380139	8.175955

. reg BHTALb BHTALx if reading==1

Source	SS	df	MS	Number of obs =	54
Model	422.517162	1	422.517162	F(1, 52) =	187.11
				Prob > F =	0.0000

Residual	117.423519	52	2.2581446	R-squared	=	0.7825
Total	539.940681	53	10.18756	Adj R-squared	=	0.7783
				Root MSE	=	1.5027

BHTALb	Coef.	Std. Err.	t	P> t	[95% Conf. Interval]	
BHTALx	.8662406	.0633275	13.68	0.000	.7391647	.9933165
_cons	4.244452	2.150589	1.97	0.054	-.0710202	8.559924

. reg MaxLFMTAL MaxLFMTALx if reading==1

Source	SS	df	MS	Number of obs = 54		
Model	271.178162	1	271.178162	F(1, 52)	=	84.88
Residual	166.13598	52	3.1949227	Prob > F	=	0.0000
Total	437.314143	53	8.25121024	R-squared	=	0.6201
				Adj R-squared	=	0.6128
				Root MSE	=	1.7874

MaxLFMTAL	Coef.	Std. Err.	t	P> t	[95% Conf. Interval]	
MaxLFMTALx	.8008389	.0869257	9.21	0.000	.6264098	.9752679
_cons	6.103386	2.864165	2.13	0.038	.3560189	11.85075

. reg MaxWHTAL MaxWHTALx if reading==1

Source	SS	df	MS	Number of obs = 54		
Model	95.7360545	1	95.7360545	F(1, 52)	=	14.02
Residual	355.147421	52	6.8297581	Prob > F	=	0.0005
Total	450.883476	53	8.50723539	R-squared	=	0.2123
				Adj R-squared	=	0.1972
				Root MSE	=	2.6134

MaxWHTAL	Coef.	Std. Err.	t	P> t	[95% Conf. Interval]	
MaxWHTALx	.3830951	.1023226	3.74	0.000	.1777698	.5884204
_cons	19.373	3.285611	5.90	0.000	12.77994	25.96606

. reg MinWNTALa MinWNTALx if reading==1

Source	SS	df	MS	Number of obs = 54		
Model	132.6404	1	132.6404	F(1, 52)	=	31.13
Residual	221.565815	52	4.26088105	Prob > F	=	0.0000
Total	354.206215	53	6.68313613	R-squared	=	0.3745
				Adj R-squared	=	0.3624
				Root MSE	=	2.0642

MinWNTALa	Coef.	Std. Err.	t	P> t	[95% Conf. Interval]	

MinWNTALx	.478954	.0858431	5.58	0.000	.3066971	.6512109
_cons	14.13886	2.398352	5.90	0.000	9.326214	18.9515

. reg MinWNTALb MinWNTALx if reading==1

Source	SS	df	MS	Number of obs = 54		
Model	178.051497	1	178.051497	F(1, 52) =	43.54	
Residual	212.636036	52	4.08915454	Prob > F =	0.0000	
				R-squared =	0.4557	
				Adj R-squared =	0.4453	
Total	390.687533	53	7.37146289	Root MSE =	2.0222	

MinWNTALb	Coef.	Std. Err.	t	P> t	[95% Conf. Interval]	
MinWNTALx	.5549179	.0840955	6.60	0.000	.386168	.7236678
_cons	11.92076	2.349524	5.07	0.000	7.206093	16.63542

. reg MaxLHNTAL MaxLHNTALx if reading==1

Source	SS	df	MS	Number of obs = 54		
Model	316.080043	1	316.080043	F(1, 52) =	93.15	
Residual	176.439216	52	3.39306185	Prob > F =	0.0000	
				R-squared =	0.6418	
				Adj R-squared =	0.6349	
Total	492.519259	53	9.29281621	Root MSE =	1.842	

MaxLHNTAL	Coef.	Std. Err.	t	P> t	[95% Conf. Interval]	
MaxLHNTALx	.7155829	.0741408	9.65	0.000	.5668085	.8643573
_cons	7.66224	1.836711	4.17	0.000	3.97661	11.34787

How well the variables correlate with each other? What is pwcorr?

. pwcorr MaxLTAL MaxLTALx MaxHBTAL MaxHBTALx BHTALa BHTALb BHTALx MaxLFMTAL
 MaxLFMTALx MaxWHTAL MaxWHTALx MinWN
 > TALA MinWNTALb MinWNTALx MaxLHNTAL MaxLHNTALx

	MaxLTAL	MaxLTALx	MaxHBTAL	MaxHBT-x	BHTALa	BHTALb	BHTALx
MaxLTAL	1.0000						
MaxLTALx	0.9463	1.0000					
MaxHBTAL	0.8130	0.8203	1.0000				
MaxHBTALx	0.7532	0.7558	0.7830	1.0000			
BHTALa	0.8077	0.8056	0.8623	0.7669	1.0000		
BHTALb	0.7761	0.7722	0.8727	0.7241	0.9132	1.0000	
BHTALx	0.7595	0.7701	0.8679	0.7314	0.9093	0.8802	1.0000
MaxLFMTAL	0.6530	0.6500	0.6967	0.5718	0.6284	0.6525	0.5818
MaxLFMTALx	0.5643	0.5476	0.6127	0.5650	0.6037	0.5676	0.5278
MaxWHTAL	0.6679	0.6613	0.5993	0.4634	0.6832	0.5979	0.6148
MaxWHTALx	0.5696	0.5739	0.5152	0.5218	0.5876	0.5302	0.5112
MinWNTALa	0.7529	0.7328	0.6911	0.5987	0.7673	0.7135	0.6779

MinWNTALb	0.7648	0.7527	0.6720	0.6199	0.7818	0.7216	0.6706
MinWNTALx	0.6460	0.6500	0.5667	0.5555	0.6425	0.6167	0.5894
MaxLHNTAL	0.7115	0.7178	0.6107	0.5661	0.6130	0.5746	0.6500
MaxLHNTALx	0.5452	0.5434	0.5298	0.5071	0.5248	0.4805	0.5532

	MaxLFM-L	MaxLFM-x	MaxWHTAL	MaxWHT-x	MinWNT-a	MinWNT-b	MinWNT-x
MaxLFMTAL	1.0000						
MaxLFMTALx	0.7744	1.0000					
MaxWHTAL	0.5954	0.5014	1.0000				
MaxWHTALx	0.3860	0.2562	0.4581	1.0000			
MinWNTALa	0.5750	0.5611	0.7519	0.5569	1.0000		
MinWNTALb	0.5963	0.5567	0.7563	0.6178	0.9494	1.0000	
MinWNTALx	0.3370	0.2424	0.4184	0.7980	0.5998	0.6664	1.0000
MaxLHNTAL	0.4964	0.3294	0.4374	0.4274	0.5259	0.5250	0.5550
MaxLHNTALx	0.3142	0.1647	0.2397	0.5292	0.4574	0.4654	0.6127

	MaxLHN-L	MaxLHN-x
MaxLHNTAL	1.0000	
MaxLHNTALx	0.7961	1.0000

. reg MaxLTAL MaxLTALx if reading==1, noconstant

Source	SS	df	MS	Number of obs =	54
Model	196291.422	1	196291.422	F(1, 53) =	52736.13
Residual	197.273566	53	3.72214275	Prob > F =	0.0000
Total	196488.696	54	3638.67955	R-squared =	0.9990
				Adj R-squared =	0.9990
				Root MSE =	1.9293

MaxLTAL	Coef.	Std. Err.	t	P> t	[95% Conf. Interval]
MaxLTALx	.9611972	.0041856	229.64	0.000	.9528019 .9695925

Regression analysis no constant

. reg MaxHBTAL MaxHBTALx if reading==1, noconstant

Source	SS	df	MS	Number of obs =	54
Model	58664.9304	1	58664.9304	F(1, 53) =	14442.72
Residual	215.280914	53	4.06190404	Prob > F =	0.0000
Total	58880.2113	54	1090.37428	R-squared =	0.9963
				Adj R-squared =	0.9963
				Root MSE =	2.0154

MaxHBTAL	Coef.	Std. Err.	t	P> t	[95% Conf. Interval]
MaxHBTALx	.9892839	.0082318	120.18	0.000	.972773 1.005795

. reg BHTALa BHTALx if reading==1, noconstant

Source	SS	df	MS	Number of obs =	54
Model	59373.6661	1	59373.6661	F(1, 53) =	37486.57
Residual	83.9448507	53	1.58386511	Prob > F =	0.0000
				R-squared =	0.9986
				Adj R-squared =	0.9986
Total	59457.611	54	1101.06687	Root MSE =	1.2585

BHTALa	Coef.	Std. Err.	t	P> t	[95% Conf. Interval]
BHTALx	.9764161	.0050431	193.61	0.000	.9663009 .9865313

. reg BHTALb BHTALx if reading==1, noconstant

Source	SS	df	MS	Number of obs =	54
Model	61118.4452	1	61118.4452	F(1, 53) =	25663.86
Residual	126.219418	53	2.38149845	Prob > F =	0.0000
				R-squared =	0.9979
				Adj R-squared =	0.9979
Total	61244.6646	54	1134.16046	Root MSE =	1.5432

BHTALb	Coef.	Std. Err.	t	P> t	[95% Conf. Interval]
BHTALx	.9906589	.0061839	160.20	0.000	.9782556 1.003062

. reg MaxLFMTAL MaxLFMTALx if reading==1, noconstant

Source	SS	df	MS	Number of obs =	54
Model	56927.5114	1	56927.5114	F(1, 53) =	16702.24
Residual	180.64393	53	3.40837603	Prob > F =	0.0000
				R-squared =	0.9968
				Adj R-squared =	0.9968
Total	57108.1553	54	1057.55843	Root MSE =	1.8462

MaxLFMTAL	Coef.	Std. Err.	t	P> t	[95% Conf. Interval]
MaxLFMTALx	.9854037	.0076248	129.24	0.000	.9701104 1.000697

. reg MaxWHTAL MaxWHTALx if reading==1, noconstant

Source	SS	df	MS	Number of obs =	54
Model	53787.4812	1	53787.4812	F(1, 53) =	4810.60
Residual	592.594457	53	11.1810275	Prob > F =	0.0000
				R-squared =	0.9891
				Adj R-squared =	0.9889
Total	54380.0757	54	1007.03844	Root MSE =	3.3438

MaxWHTAL	Coef.	Std. Err.	t	P> t	[95% Conf. Interval]	
MaxWHTALx	.9828767	.014171	69.36	0.000	.9544534	1.0113

. reg MinWNTALa MinWNTALx if reading==1, noconstant

Source	SS	df	MS	Number of obs = 54		
Model	40608.9372	1	40608.9372	F(1, 53) = 5822.50		
Residual	369.647839	53	6.97448752	Prob > F = 0.0000		
Total	40978.585	54	758.862685	R-squared = 0.9910		
				Adj R-squared = 0.9908		
				Root MSE = 2.6409		

MinWNTALa	Coef.	Std. Err.	t	P> t	[95% Conf. Interval]	
MinWNTALx	.9815369	.0128633	76.31	0.000	.9557364	1.007337

. reg MinWNTALb MinWNTALx if reading==1, noconstant

Source	SS	df	MS	Number of obs = 54		
Model	40370.8802	1	40370.8802	F(1, 53) = 6730.59		
Residual	317.900407	53	5.9981209	Prob > F = 0.0000		
Total	40688.7806	54	753.495937	R-squared = 0.9922		
				Adj R-squared = 0.9920		
				Root MSE = 2.4491		

MinWNTALb	Coef.	Std. Err.	t	P> t	[95% Conf. Interval]	
MinWNTALx	.9786557	.011929	82.04	0.000	.9547292	1.002582

. reg MaxLHNTAL MaxLHNTALx if reading==1, noconstant

Source	SS	df	MS	Number of obs = 54		
Model	34613.7321	1	34613.7321	F(1, 53) = 7790.28		
Residual	235.489465	53	4.44319745	Prob > F = 0.0000		
Total	34849.2216	54	645.355956	R-squared = 0.9932		
				Adj R-squared = 0.9931		
				Root MSE = 2.1079		

MaxLHNTAL	Coef.	Std. Err.	t	P> t	[95% Conf. Interval]	
MaxLHNTALx	1.021983	.0115789	88.26	0.000	.9987591	1.045208

.
.
end of do-file

Chapter 3 Statistical analysis calcaneus

```
. ttest AAAPCALa == AAAPCALx if reading==1
```

```
Paired t test
```

Variable	Obs	Mean	Std. Err.	Std. Dev.	[95% Conf. Interval]	
AAAPCALa	54	91.22481	.8533339	6.270698	89.51324	92.93639
AAAPCALx	54	91.38981	.8910916	6.548159	89.60251	93.17712
diff	54	-.165	.4286541	3.149952	-1.024771	.6947713

```
mean(diff) = mean(AAAPCALa - AAAPCALx)          t = -0.3849
Ho: mean(diff) = 0                               degrees of freedom = 53
```

```
Ha: mean(diff) < 0          Ha: mean(diff) != 0          Ha: mean(diff) > 0
Pr(T < t) = 0.3509          Pr(|T| > |t|) = 0.7018          Pr(T > t) = 0.6491
```

```
. ttest AAAPCALb == AAAPCALx if reading==1
```

```
Paired t test
```

Variable	Obs	Mean	Std. Err.	Std. Dev.	[95% Conf. Interval]	
AAAPCALb	54	91.01944	.8911309	6.548448	89.23206	92.80683
AAAPCALx	54	91.38981	.8910916	6.548159	89.60251	93.17712
diff	54	-.3703704	.503476	3.699778	-1.380215	.6394745

```
mean(diff) = mean(AAAPCALb - AAAPCALx)          t = -0.7356
Ho: mean(diff) = 0                               degrees of freedom = 53
```

```
Ha: mean(diff) < 0          Ha: mean(diff) != 0          Ha: mean(diff) > 0
Pr(T < t) = 0.2326          Pr(|T| > |t|) = 0.4652          Pr(T > t) = 0.7674
```

```
. ttest AIPTEFCAL == AIPTEFCALx if reading==1
```

```
Paired t test
```

Variable	Obs	Mean	Std. Err.	Std. Dev.	[95% Conf. Interval]	
AIPTEFCAL	54	45.92407	.605032	4.446059	44.71053	47.13761
AIPTEFC~x	54	46.805	.72077	5.296556	45.35932	48.25068

```

diff |      54  -.8809259  .4290654  3.152974  -1.741522  -.0203296
-----
mean(diff) = mean(AIPTFCAL - AIPTFCALx)          t = -2.0531
Ho: mean(diff) = 0                               degrees of freedom = 53

Ha: mean(diff) < 0          Ha: mean(diff) != 0          Ha: mean(diff) > 0
Pr(T < t) = 0.0225         Pr(|T| > |t|) = 0.0450         Pr(T > t) = 0.9775

```

. ttest AIMTFCAL == AIMTFCALx if reading==1

Paired t test

```

-----
Variable |      Obs      Mean   Std. Err.   Std. Dev.   [95% Conf. Interval]
-----+-----
AIMTFCAL |      54   53.35722   1.04586    7.685472    51.25949    55.45495
AIMTFC~x |      54   54.28833   .9532556    7.004969    52.37634    56.20032
-----+-----
diff |      54  -.9311111   .6277516    4.613013   -2.190221    .3279992
-----
mean(diff) = mean(AIMTFCAL - AIMTFCALx)          t = -1.4832
Ho: mean(diff) = 0                               degrees of freedom = 53

Ha: mean(diff) < 0          Ha: mean(diff) != 0          Ha: mean(diff) > 0
Pr(T < t) = 0.0720         Pr(|T| > |t|) = 0.1439         Pr(T > t) = 0.9280

```

. ttest AALCAL == AALCALx if reading==1

Paired t test

```

-----
Variable |      Obs      Mean   Std. Err.   Std. Dev.   [95% Conf. Interval]
-----+-----
AALCAL  |      54  105.6546   .8280083    6.084593   103.9939   107.3154
AALCALx |      54  105.4141   .9199338    6.760105   103.5689   107.2592
-----+-----
diff |      54   .2405556   .4773364    3.507692   -.7168599   1.197971
-----
mean(diff) = mean(AALCAL - AALCALx)              t = 0.5040
Ho: mean(diff) = 0                               degrees of freedom = 53

Ha: mean(diff) < 0          Ha: mean(diff) != 0          Ha: mean(diff) > 0
Pr(T < t) = 0.6918         Pr(|T| > |t|) = 0.6164         Pr(T > t) = 0.3082

```

. ttest BTACAL == BTACALx if reading==1

Paired t test

```

-----
Variable |      Obs      Mean   Std. Err.   Std. Dev.   [95% Conf. Interval]
-----+-----
BTACAL  |      54   28.51574   .6692501    4.917964    27.1734    29.85809
BTACALx |      54   30.54574   .7017292    5.156635    29.13825    31.95323
-----+-----
diff |      54    -2.03   .3333826    2.449852   -2.698681   -1.361319
-----
mean(diff) = mean(BTACAL - BTACALx)              t = -6.0891

```

Ho: mean(diff) = 0 degrees of freedom = 53

Ha: mean(diff) < 0 Ha: mean(diff) != 0 Ha: mean(diff) > 0
Pr(T < t) = 0.0000 Pr(|T| > |t|) = 0.0000 Pr(T > t) = 1.0000

. ttest GACAL == GACALx if reading==1

Paired t test

Variable	Obs	Mean	Std. Err.	Std. Dev.	[95% Conf. Interval]	
GACAL	54	124.2587	.714053	5.247196	122.8265	125.6909
GACALx	54	124.1772	.786738	5.78132	122.5992	125.7552
diff	54	.0814815	.6753592	4.962857	-1.273118	1.436081

mean(diff) = mean(GACAL - GACALx) t = 0.1206
Ho: mean(diff) = 0 degrees of freedom = 53

Ha: mean(diff) < 0 Ha: mean(diff) != 0 Ha: mean(diff) > 0
Pr(T < t) = 0.5478 Pr(|T| > |t|) = 0.9044 Pr(T > t) = 0.4522

. ttest CACAL == CACALx if reading==1

Paired t test

Variable	Obs	Mean	Std. Err.	Std. Dev.	[95% Conf. Interval]	
CACAL	54	24.51741	.6222097	4.572289	23.26941	25.7654
CACALx	54	25.62759	.7995939	5.875791	24.02381	27.23137
diff	54	-1.110185	.4446319	3.267364	-2.002004	-.2183666

mean(diff) = mean(CACAL - CACALx) t = -2.4969
Ho: mean(diff) = 0 degrees of freedom = 53

Ha: mean(diff) < 0 Ha: mean(diff) != 0 Ha: mean(diff) > 0
Pr(T < t) = 0.0078 Pr(|T| > |t|) = 0.0157 Pr(T > t) = 0.9922

. ttest FACAL == FACALx if reading==1

Paired t test

Variable	Obs	Mean	Std. Err.	Std. Dev.	[95% Conf. Interval]	
FACAL	54	35.51037	.4467451	3.282893	34.61431	36.40643
FACALx	54	34.7187	.514233	3.778825	33.68728	35.75012
diff	54	.7916667	.4177027	3.069475	-.0461388	1.629472

mean(diff) = mean(FACAL - FACALx) t = 1.8953
Ho: mean(diff) = 0 degrees of freedom = 53

Ha: mean(diff) < 0 Ha: mean(diff) != 0 Ha: mean(diff) > 0

Pr(T < t) = 0.9682 Pr(|T| > |t|) = 0.0635 Pr(T > t) = 0.0318

. ttest TACALa == TACALax if reading==1

Paired t test

Variable	Obs	Mean	Std. Err.	Std. Dev.	[95% Conf. Interval]	
TACALa	54	63.82426	.8428874	6.193932	62.13364	65.51488
TACALax	54	64.39204	.8691263	6.386748	62.64879	66.13528
diff	54	-.5677778	.6571806	4.829271	-1.885915	.7503596

mean(diff) = mean(TACALa - TACALax) t = -0.8640
 Ho: mean(diff) = 0 degrees of freedom = 53

Ha: mean(diff) < 0 Ha: mean(diff) != 0 Ha: mean(diff) > 0
 Pr(T < t) = 0.1958 Pr(|T| > |t|) = 0.3915 Pr(T > t) = 0.8042

. ttest TACALb == TACALbx if reading==1

Paired t test

Variable	Obs	Mean	Std. Err.	Std. Dev.	[95% Conf. Interval]	
TACALb	54	26.14611	.8364487	6.146617	24.46841	27.82381
TACALbx	54	25.55593	.8732196	6.416827	23.80447	27.30738
diff	54	.5901852	.6740056	4.952909	-.7616988	1.942069

mean(diff) = mean(TACALb - TACALbx) t = 0.8756
 Ho: mean(diff) = 0 degrees of freedom = 53

Ha: mean(diff) < 0 Ha: mean(diff) != 0 Ha: mean(diff) > 0
 Pr(T < t) = 0.8074 Pr(|T| > |t|) = 0.3852 Pr(T > t) = 0.1926

. reg AAAPCALa AAAPCALx if reading==1

Source	SS	df	MS	Number of obs = 54	
Model	1614.31308	1	1614.31308	F(1, 52) = 178.71	
Residual	469.734266	52	9.03335126	Prob > F = 0.0000	
Total	2084.04735	53	39.3216481	R-squared = 0.7746	
				Adj R-squared = 0.7703	
				Root MSE = 3.0056	

AAAPCALa	Coef.	Std. Err.	t	P> t	[95% Conf. Interval]	
AAAPCALx	.8428237	.0630474	13.37	0.000	.7163098	.9693376
_cons	14.19931	5.77639	2.46	0.017	2.60814	25.79049

. reg AAAPCALb AAAPCALx if reading==1

Source	SS	df	MS	Number of obs =	54
Model	1605.14046	1	1605.14046	F(1, 52) =	125.02
Residual	667.614623	52	12.8387427	Prob > F =	0.0000
				R-squared =	0.7063
				Adj R-squared =	0.7006
Total	2272.75508	53	42.8821714	Root MSE =	3.5831

AAAPCALb	Coef.	Std. Err.	t	P> t	[95% Conf. Interval]
AAAPCALx	.8404258	.075163	11.18	0.000	.6896002 .9912514
_cons	14.21309	6.886417	2.06	0.044	.3944816 28.03169

. reg AIPTFCAL AIPTFCALx if reading==1

Source	SS	df	MS	Number of obs =	54
Model	677.706823	1	677.706823	F(1, 52) =	95.25
Residual	369.967681	52	7.11476309	Prob > F =	0.0000
				R-squared =	0.6469
				Adj R-squared =	0.6401
Total	1047.6745	53	19.7674435	Root MSE =	2.6674

AIPTFCAL	Coef.	Std. Err.	t	P> t	[95% Conf. Interval]
AIPTFCALx	.6751331	.0691749	9.76	0.000	.5363235 .8139428
_cons	14.32447	3.258016	4.40	0.000	7.78678 20.86215

. reg AIMTFCAL AIMTFCALx if reading==1

Source	SS	df	MS	Number of obs =	54
Model	2037.06498	1	2037.06498	F(1, 52) =	96.87
Residual	1093.45851	52	21.0280482	Prob > F =	0.0000
				R-squared =	0.6507
				Adj R-squared =	0.6440
Total	3130.52348	53	59.0664808	Root MSE =	4.5856

AIMTFCAL	Coef.	Std. Err.	t	P> t	[95% Conf. Interval]
AIMTFCALx	.8850306	.0899198	9.84	0.000	.7045933 1.065468
_cons	5.310388	4.92132	1.08	0.286	-4.564962 15.18574

. reg AALCAL AALCALx if reading==1

Source	SS	df	MS	Number of obs =	54
Model	1437.70211	1	1437.70211	F(1, 52) =	142.54
Residual	524.478431	52	10.0861237	Prob > F =	0.0000
				R-squared =	0.7327
				Adj R-squared =	0.7276

Total | 1962.18054 53 37.0222744 Root MSE = 3.1759

AALCAL	Coef.	Std. Err.	t	P> t	[95% Conf. Interval]	
AALCALx	.7704475	.0645313	11.94	0.000	.6409559	.8999391
_cons	24.43862	6.816227	3.59	0.001	10.76086	38.11638

. reg BTACAL BTACALx if reading==1

Source	SS	df	MS	Number of obs = 54		
Model	998.995616	1	998.995616	F(1, 52)	=	183.64
Residual	282.881904	52	5.44003662	Prob > F	=	0.0000
Total	1281.87752	53	24.1863683	R-squared	=	0.7793
				Adj R-squared	=	0.7751
				Root MSE	=	2.3324

BTACAL	Coef.	Std. Err.	t	P> t	[95% Conf. Interval]	
BTACALx	.8419329	.0621293	13.55	0.000	.7172613	.9666045
_cons	2.798278	1.924145	1.45	0.152	-1.062801	6.659357

. reg GACAL GACALx if reading==1

Source	SS	df	MS	Number of obs = 54		
Model	523.13736	1	523.13736	F(1, 52)	=	29.06
Residual	936.115249	52	18.0022163	Prob > F	=	0.0000
Total	1459.25261	53	27.5330681	R-squared	=	0.3585
				Adj R-squared	=	0.3462
				Root MSE	=	4.2429

GACAL	Coef.	Std. Err.	t	P> t	[95% Conf. Interval]	
GACALx	.5434292	.1008087	5.39	0.000	.3411417	.7457166
_cons	56.77718	12.53145	4.53	0.000	31.63098	81.92338

. reg CACAL CACALx if reading==1

Source	SS	df	MS	Number of obs = 54		
Model	768.7195	1	768.7195	F(1, 52)	=	117.82
Residual	339.289337	52	6.52479494	Prob > F	=	0.0000
Total	1108.00884	53	20.9058271	R-squared	=	0.6938
				Adj R-squared	=	0.6879
				Root MSE	=	2.5544

CACAL	Coef.	Std. Err.	t	P> t	[95% Conf. Interval]	
CACALx	.6481562	.0597144	10.85	0.000	.5283305	.7679819

```

      _cons |   7.906725   1.569318   5.04   0.000   4.757657   11.05579
-----+-----

```

```

. reg FACAL FACALx if reading==1

```

```

      Source |         SS      df      MS                Number of obs =      54
-----+-----+-----+-----+-----+-----
      Model |   226.835302    1   226.835302            F( 1, 52) =    34.25
      Residual |   344.36609   52   6.62242481            Prob > F      =    0.0000
-----+-----+-----+-----+-----+-----
      Total |   571.201393   53  10.7773848            R-squared     =    0.3971
                                           Adj R-squared =    0.3855
                                           Root MSE     =    2.5734

```

```

      FACAL |         Coef.   Std. Err.      t    P>|t|   [95% Conf. Interval]
-----+-----+-----+-----+-----+-----
      FACALx |    .5474703   .0935435     5.85   0.000   .3597615   .7351791
      _cons |   16.50291   3.266536     5.05   0.000   9.948127  23.0577

```

```

. reg TACALa TACALax if reading==1

```

```

      Source |         SS      df      MS                Number of obs =      54
-----+-----+-----+-----+-----+-----
      Model |   1012.61831    1  1012.61831            F( 1, 52) =   51.59
      Residual |   1020.71602   52  19.6291541            Prob > F      =    0.0000
-----+-----+-----+-----+-----+-----
      Total |   2033.33432   53  38.3647985            R-squared     =    0.4980
                                           Adj R-squared =    0.4884
                                           Root MSE     =    4.4305

```

```

      TACALa |         Coef.   Std. Err.      t    P>|t|   [95% Conf. Interval]
-----+-----+-----+-----+-----+-----
      TACALax |    .6843924   .0952869     7.18   0.000   .4931853   .8755995
      _cons |   19.75484   6.165267     3.20   0.002   7.383323  32.12635

```

```

. reg TACALb TACALbx if reading==1

```

```

      Source |         SS      df      MS                Number of obs =      54
-----+-----+-----+-----+-----+-----
      Model |    953.182944    1   953.182944            F( 1, 52) =   47.24
      Residual |   1049.20494   52  20.1770181            Prob > F      =    0.0000
-----+-----+-----+-----+-----+-----
      Total |   2002.38788   53  37.7809035            R-squared     =    0.4760
                                           Adj R-squared =    0.4659
                                           Root MSE     =    4.4919

```

```

      TACALb |         Coef.   Std. Err.      t    P>|t|   [95% Conf. Interval]
-----+-----+-----+-----+-----+-----
      TACALbx |    .660891   .0961546     6.87   0.000   .4679426   .8538394
      _cons |    9.256429   2.532207     3.66   0.001   4.175183  14.33767

```

```

. pcorr AAAPCALa AAAPCALb AIPTFCAL AIMTFCAL AALCAL BTACAL GACAL CACAL FACAL
TACALa TACALb AAAPCALx AIP

```

> TFCALx AIMTFCALx AALCALx BTACALx GACALx CACALx FACALx TACALax TACALbx

	AAAPCALa	AAAPCALb	AIPTFCAL	AIMTFCAL	AALCAL	BTACAL	GACAL
AAAPCALa	1.0000						
AAAPCALb	0.8442	1.0000					
AIPTFCAL	-0.2001	-0.1317	1.0000				
AIMTFCAL	-0.0846	0.0877	0.1263	1.0000			
AALCAL	-0.2770	-0.2352	0.2876	0.2135	1.0000		
BTACAL	0.3097	0.2701	0.3258	0.2991	-0.0455	1.0000	
GACAL	0.1274	0.1068	-0.0144	-0.1189	0.1566	0.4238	1.0000
CACAL	-0.0364	0.0808	0.7259	0.2743	0.3207	0.6363	0.4113
FACAL	-0.2369	-0.0637	0.5294	0.1771	0.4996	-0.0080	0.0209
TACALa	0.1039	0.0886	-0.0360	0.1293	-0.2283	0.2512	-0.1346
TACALb	-0.0993	-0.0826	0.0240	-0.1523	0.2235	-0.2609	0.1275
AAAPCALx	0.8574	0.8346	-0.1799	0.0183	-0.3122	0.2311	0.0691
AIPTFCALx	-0.3065	-0.1863	0.7990	0.0946	0.3074	0.3975	0.2333
AIMTFCALx	-0.0439	0.0737	0.1880	0.8105	0.1589	0.2482	-0.1217
AALCALx	-0.1197	-0.1301	0.4124	0.1225	0.8563	0.1632	0.2742
BTACALx	0.3312	0.2872	0.3144	0.2824	0.0583	0.8891	0.4234
GACALx	0.3099	0.2844	-0.2061	0.0341	0.1034	0.2917	0.5699
CACALx	-0.0921	0.0389	0.6630	0.1955	0.2499	0.5840	0.4009
FACALx	-0.2876	-0.0961	0.6095	0.1305	0.2859	0.1871	0.1592
TACALax	0.1072	0.1374	-0.0455	0.1182	-0.2287	0.2339	-0.1013
TACALbx	-0.0873	-0.1329	0.0568	-0.1444	0.2349	-0.2261	0.1170

	CACAL	FACAL	TACALa	TACALb	AAAPCALx	AIPTFC~x	AIMTFC~x
CACAL	1.0000						
FACAL	0.6101	1.0000					
TACALa	-0.0085	-0.1745	1.0000				
TACALb	-0.0128	0.1749	-0.9958	1.0000			
AAAPCALx	-0.0409	-0.2122	0.1275	-0.1314	1.0000		
AIPTFCALx	0.7092	0.5008	-0.1339	0.1289	-0.2765	1.0000	
AIMTFCALx	0.2882	0.2996	0.0725	-0.0913	0.0042	0.1626	1.0000
AALCALx	0.4942	0.5045	-0.2258	0.2209	-0.1851	0.4747	0.1552
BTACALx	0.5993	0.0079	0.2696	-0.2824	0.2339	0.3746	0.2415
GACALx	0.1324	-0.1422	0.0619	-0.0701	0.2790	-0.1818	-0.0687
CACALx	0.8380	0.4792	-0.0945	0.0749	-0.0873	0.8318	0.2447
FACALx	0.6163	0.6497	-0.3019	0.3016	-0.2157	0.7746	0.2511
TACALax	0.0648	-0.1404	0.7446	-0.7409	0.1143	-0.2130	0.0031
TACALbx	-0.0469	0.1534	-0.7255	0.7220	-0.0950	0.2108	-0.0183

	AALCALx	BTACALx	GACALx	CACALx	FACALx	TACALax	TACALbx
AALCALx	1.0000						
BTACALx	0.2733	1.0000					
GACALx	0.1160	0.3466	1.0000				
CACALx	0.4984	0.6425	0.0960	1.0000			
FACALx	0.4972	0.1746	-0.1640	0.7954	1.0000		
TACALax	-0.2895	0.1124	0.1167	-0.1782	-0.3185	1.0000	
TACALbx	0.3031	-0.1013	-0.1082	0.1796	0.3101	-0.9909	1.0000

. reg AAAPCALa AAAPCALx if reading==1, noconstant

Source	SS	df	MS	Number of obs =	54
Model	450945.938	1	450945.938	F(1, 53)	=45583.20
Residual	524.318932	53	9.89281004	Prob > F	= 0.0000
				R-squared	= 0.9988
				Adj R-squared	= 0.9988
Total	451470.257	54	8360.56031	Root MSE	= 3.1453

AAAPCALa	Coef.	Std. Err.	t	P> t	[95% Conf. Interval]
AAAPCALx	.9974156	.0046717	213.50	0.000	.9880454 1.006786

. reg AAAPCALb AAAPCALx if reading==1, noconstant

Source	SS	df	MS	Number of obs =	54
Model	448915.57	1	448915.57	F(1, 53)	=32939.71
Residual	722.305233	53	13.6284006	Prob > F	= 0.0000
				R-squared	= 0.9984
				Adj R-squared	= 0.9984
Total	449637.876	54	8326.62732	Root MSE	= 3.6917

AAAPCALb	Coef.	Std. Err.	t	P> t	[95% Conf. Interval]
AAAPCALx	.9951676	.0054832	181.49	0.000	.9841697 1.006166

. reg AIPTFCAL AIPTFCALx if reading==1, noconstant

Source	SS	df	MS	Number of obs =	54
Model	114427.284	1	114427.284	F(1, 53)	=11949.99
Residual	507.501979	53	9.57550904	Prob > F	= 0.0000
				R-squared	= 0.9956
				Adj R-squared	= 0.9955
Total	114934.786	54	2128.42196	Root MSE	= 3.0944

AIPTFCAL	Coef.	Std. Err.	t	P> t	[95% Conf. Interval]
AIPTFCALx	.97738	.0089409	109.32	0.000	.9594469 .9953131

. reg AIMTFCAL AIMTFCALx if reading==1, noconstant

Source	SS	df	MS	Number of obs =	54
Model	155750.211	1	155750.211	F(1, 53)	= 7383.88
Residual	1117.94284	53	21.0932612	Prob > F	= 0.0000
				R-squared	= 0.9929
				Adj R-squared	= 0.9927
Total	156868.154	54	2904.96582	Root MSE	= 4.5927

AIMTFCAL	Coef.	Std. Err.	t	P> t	[95% Conf. Interval]
AIMTFCALx	.981276	.0114195	85.93	0.000	.9583713 1.004181

. reg AALCAL AALCALx if reading==1, noconstant

Source	SS	df	MS	Number of obs =	54
Model	604104.688	1	604104.688	F(1, 53)	=48946.51
Residual	654.133492	53	12.3421414	Prob > F	= 0.0000
Total	604758.822	54	11199.2374	R-squared	= 0.9989
				Adj R-squared	= 0.9989
				Root MSE	= 3.5131

AALCAL	Coef.	Std. Err.	t	P> t	[95% Conf. Interval]
AALCALx	1.00135	.0045261	221.24	0.000	.9922718 1.010428

. reg BTACAL BTACALx if reading==1, noconstant

Source	SS	df	MS	Number of obs =	54
Model	44897.4534	1	44897.4534	F(1, 53)	= 8083.11
Residual	294.387471	53	5.55448059	Prob > F	= 0.0000
Total	45191.8409	54	836.885943	R-squared	= 0.9935
				Adj R-squared	= 0.9934
				Root MSE	= 2.3568

BTACAL	Coef.	Std. Err.	t	P> t	[95% Conf. Interval]
BTACALx	.9310496	.0103558	89.91	0.000	.9102785 .9518207

. reg GACAL GACALx if reading==1, noconstant

Source	SS	df	MS	Number of obs =	54
Model	833925.764	1	833925.764	F(1, 53)	=33851.05
Residual	1305.66308	53	24.6351524	Prob > F	= 0.0000
Total	835231.427	54	15467.2486	R-squared	= 0.9984
				Adj R-squared	= 0.9984
				Root MSE	= 4.9634

GACAL	Coef.	Std. Err.	t	P> t	[95% Conf. Interval]
GACALx	.9996855	.0054335	183.99	0.000	.9887874 1.010584

. reg CACAL CACALx if reading==1, noconstant

Source	SS	df	MS	Number of obs =	54
--------	----	----	----	-----------------	----

```

-----+-----
Model | 33062.6662   1 33062.6662
Residual | 504.918983  53 9.52677327
-----+-----
Total | 33567.5852  54 621.621948
-----+-----
F( 1, 53) = 3470.50
Prob > F   = 0.0000
R-squared  = 0.9850
Adj R-squared = 0.9847
Root MSE   = 3.0865

```

```

-----+-----
CACAL |      Coef.  Std. Err.    t    P>|t|    [95% Conf. Interval]
-----+-----
CACALx | .9415431   .0159825   58.91  0.000   .9094863   .9735999
-----+-----

```

. reg FACAL FACALx if reading==1, noconstant

```

-----+-----
Source |      SS      df      MS
-----+-----
Model | 68151.0713   1 68151.0713
Residual | 513.395858  53 9.68671431
-----+-----
Total | 68664.4672  54 1271.56421
-----+-----
Number of obs = 54
F( 1, 53) = 7035.52
Prob > F     = 0.0000
R-squared    = 0.9925
Adj R-squared = 0.9924
Root MSE    = 3.1123

```

```

-----+-----
FACAL |      Coef.  Std. Err.    t    P>|t|    [95% Conf. Interval]
-----+-----
FACALx | 1.017339   .0121288   83.88  0.000   .9930119   1.041666
-----+-----

```

. reg TACALa TACALax if reading==1, noconstant

```

-----+-----
Source |      SS      df      MS
-----+-----
Model | 220782.034   1 220782.034
Residual | 1222.24832  53 23.0612891
-----+-----
Total | 222004.282  54 4111.19041
-----+-----
Number of obs = 54
F( 1, 53) = 9573.71
Prob > F     = 0.0000
R-squared    = 0.9945
Adj R-squared = 0.9944
Root MSE    = 4.8022

```

```

-----+-----
TACALa |      Coef.  Std. Err.    t    P>|t|    [95% Conf. Interval]
-----+-----
TACALax | .9882486   .0101001   97.85  0.000   .9679903   1.008507
-----+-----

```

. reg TACALb TACALbx if reading==1, noconstant

```

-----+-----
Source |      SS      df      MS
-----+-----
Model | 37598.9999   1 37598.9999
Residual | 1318.82079  53 24.8834111
-----+-----
Total | 38917.8207  54 720.700383
-----+-----
Number of obs = 54
F( 1, 53) = 1511.01
Prob > F     = 0.0000
R-squared    = 0.9661
Adj R-squared = 0.9655
Root MSE    = 4.9883

```

```

-----+-----
TACALb |      Coef.  Std. Err.    t    P>|t|    [95% Conf. Interval]
-----+-----

```

TACALbx | 1.001987 .0257768 38.87 0.000 .9502856 1.053689

.
.
end of do-file


```

diff |      54      .8685185      .437111      3.212097      -.0082152      1.745252
-----+-----
mean(diff) = mean(AHTALpl - AHTALx)          t =      1.9870
Ho: mean(diff) = 0                          degrees of freedom =      53

Ha: mean(diff) < 0          Ha: mean(diff) != 0          Ha: mean(diff) > 0
Pr(T < t) = 0.9739          Pr(|T| > |t|) = 0.0521          Pr(T > t) = 0.0261

```

. ttest ANTALpl == ANTALx if reading==1

Paired t test

```

Variable |      Obs      Mean      Std. Err.      Std. Dev.      [95% Conf. Interval]
-----+-----
ANTALpl |      54     105.4531     .7891395     5.798967     103.8703     107.036
ANTALx  |      54     104.8593     .792045     5.820319     103.2706     106.4479
-----+-----
diff    |      54     .5938889     .4222097     3.102595     -.2529565     1.440734
-----+-----
mean(diff) = mean(ANTALpl - ANTALx)          t =      1.4066
Ho: mean(diff) = 0                          degrees of freedom =      53

Ha: mean(diff) < 0          Ha: mean(diff) != 0          Ha: mean(diff) > 0
Pr(T < t) = 0.9173          Pr(|T| > |t|) = 0.1654          Pr(T > t) = 0.0827

```

. ttest IANTAL== IANTALx if reading==1

Paired t test

```

Variable |      Obs      Mean      Std. Err.      Std. Dev.      [95% Conf. Interval]
-----+-----
IANTAL  |      54     31.43389     .5046185     3.708173     30.42175     32.44603
IANTALx |      54     34.62759     .4790505     3.520288     33.66674     35.58845
-----+-----
diff    |      54    -3.193704     .3901016     2.86665     -3.976148     -2.411259
-----+-----
mean(diff) = mean(IANTAL - IANTALx)          t =     -8.1869
Ho: mean(diff) = 0                          degrees of freedom =      53

Ha: mean(diff) < 0          Ha: mean(diff) != 0          Ha: mean(diff) > 0
Pr(T < t) = 0.0000          Pr(|T| > |t|) = 0.0000          Pr(T > t) = 1.0000

```

. Regression analysis with constant

reg AHTAL AHTALx if reading==1

```

Source |      SS      df      MS          Number of obs =      54
-----+-----
Model  |  1523.4558      1  1523.4558      F( 1, 52) = 149.67
Residual |  529.289907     52  10.1786521      Prob > F = 0.0000
-----+-----
Total  |  2052.7457     53  38.731051      R-squared = 0.7422
                          Adj R-squared = 0.7372
                          Root MSE = 3.1904
-----+-----

```

AHTAL	Coef.	Std. Err.	t	P> t	[95% Conf. Interval]	
AHTALx	.8728194	.0713435	12.23	0.000	.7296581	1.015981
_cons	11.31055	6.182106	1.83	0.073	-1.094754	23.71585

. reg ANTAL ANTALx if reading==1

Source	SS	df	MS	Number of obs = 54		
Model	1147.08547	1	1147.08547	F(1, 52) =	107.59	
Residual	554.424275	52	10.6620053	Prob > F =	0.0000	
Total	1701.50974	53	32.1039574	R-squared =	0.6742	
				Adj R-squared =	0.6679	
				Root MSE =	3.2653	

ANTAL	Coef.	Std. Err.	t	P> t	[95% Conf. Interval]	
ANTALx	.7993062	.077061	10.37	0.000	.644672	.9539405
_cons	20.41997	8.092769	2.52	0.015	4.180641	36.6593

. reg AHTALpl AHTALx if reading==1

Source	SS	df	MS	Number of obs = 54		
Model	1682.93508	1	1682.93508	F(1, 52) =	164.13	
Residual	533.176208	52	10.2533886	Prob > F =	0.0000	
Total	2216.11128	53	41.8134204	R-squared =	0.7594	
				Adj R-squared =	0.7548	
				Root MSE =	3.2021	

AHTALpl	Coef.	Std. Err.	t	P> t	[95% Conf. Interval]	
AHTALx	.917367	.071605	12.81	0.000	.7736812	1.061053
_cons	8.011204	6.204761	1.29	0.202	-4.439559	20.46197

. reg ANTALpl ANTALx if reading==1

Source	SS	df	MS	Number of obs = 54		
Model	1310.23716	1	1310.23716	F(1, 52) =	144.33	
Residual	472.048001	52	9.07784618	Prob > F =	0.0000	
Total	1782.28516	53	33.628022	R-squared =	0.7351	
				Adj R-squared =	0.7301	
				Root MSE =	3.0129	

ANTALpl	Coef.	Std. Err.	t	P> t	[95% Conf. Interval]	
ANTALx	.8542604	.0711061	12.01	0.000	.7115756	.9969452
_cons	15.87604	7.467395	2.13	0.038	.8916134	30.86046

. reg IANTAL IANTALx if reading==1

Source	SS	df	MS	Number of obs =	54
Model	343.55173	1	343.55173	F(1, 52) =	46.37
Residual	385.227354	52	7.40821834	Prob > F =	0.0000
				R-squared =	0.4714
				Adj R-squared =	0.4612
Total	728.779083	53	13.7505487	Root MSE =	2.7218

IANTAL	Coef.	Std. Err.	t	P> t	[95% Conf. Interval]
IANTALx	.7232359	.106204	6.81	0.000	.510122 .9363498
_cons	6.389971	3.696193	1.73	0.090	-1.026983 13.80693

. pwcorr AHTAL AHTALx AN TAL AN TALx AHTALpl IANTAL IANTALx

	AHTAL	AHTALx	AN TAL	AN TALx	AHTALpl	IAN TAL	IAN TALx
AHTAL	1.0000						
AHTALx	0.8458	1.0000					
AN TAL	0.4363	0.4576	1.0000				
AN TALx	0.2826	0.3339	0.7985	1.0000			
AHTALpl	0.9170	0.8476	0.3939	0.2981	1.0000		
IAN TAL	-0.0859	-0.0864	0.0650	0.0031	-0.0566	1.0000	
IAN TALx	-0.0790	-0.0745	0.0790	-0.0317	-0.1272	0.6704	1.0000

.Regression analysis No constant

reg AHTAL AHTALx if reading==1, noconstant

Source	SS	df	MS	Number of obs =	54
Model	407925.282	1	407925.282	F(1, 53) =	38376.89
Residual	563.360901	53	10.629451	Prob > F =	0.0000
				R-squared =	0.9986
				Adj R-squared =	0.9986
Total	408488.643	54	7564.60449	Root MSE =	3.2603

AHTAL	Coef.	Std. Err.	t	P> t	[95% Conf. Interval]
AHTALx	1.003025	.0051201	195.90	0.000	.992755 1.013294

. reg AN TAL AN TALx if reading==1, noconstant

Source	SS	df	MS	Number of obs =	54
Model	587781.536	1	587781.536	F(1, 53) =	50059.63
Residual	622.306302	53	11.7416283	Prob > F =	0.0000
				R-squared =	0.9989
				Adj R-squared =	0.9989
Total	588403.842	54	10896.3675	Root MSE =	3.4266

ANTAL	Coef.	Std. Err.	t	P> t	[95% Conf. Interval]	
ANTALx	.9934561	.0044402	223.74	0.000	.9845501	1.002362

. reg AHTALpl AHTALx if reading==1, noconstant

Source	SS	df	MS	Number of obs =	54
Model	413283.599	1	413283.599	F(1, 53) =	39806.04
Residual	550.268998	53	10.3824339	Prob > F	= 0.0000
Total	413833.868	54	7663.59015	R-squared	= 0.9987
				Adj R-squared	= 0.9986
				Root MSE	= 3.2222

AHTALpl	Coef.	Std. Err.	t	P> t	[95% Conf. Interval]	
AHTALx	1.009591	.0050602	199.51	0.000	.9994411	1.01974

. reg ANTALpl ANTALx if reading==1, noconstant

Source	SS	df	MS	Number of obs =	54
Model	601768.993	1	601768.993	F(1, 53) =	62161.30
Residual	513.08058	53	9.68076566	Prob > F	= 0.0000
Total	602282.074	54	11153.3717	R-squared	= 0.9991
				Adj R-squared	= 0.9991
				Root MSE	= 3.1114

ANTALpl	Coef.	Std. Err.	t	P> t	[95% Conf. Interval]	
ANTALx	1.005207	.0040318	249.32	0.000	.9971205	1.013294

. reg IANTAL IANTALx if reading==1, noconstant

Source	SS	df	MS	Number of obs =	54
Model	53678.2365	1	53678.2365	F(1, 53) =	6983.72
Residual	407.368612	53	7.68620023	Prob > F	= 0.0000
Total	54085.6051	54	1001.58528	R-squared	= 0.9925
				Adj R-squared	= 0.9923
				Root MSE	= 2.7724

IAANTAL	Coef.	Std. Err.	t	P> t	[95% Conf. Interval]	
IAANTALx	.9059169	.0108404	83.57	0.000	.8841738	.92766

.
.
end of do-file

Chapter 4 Descriptive statistical analysis

 -> foottype3 = 1 (Low arch)Calcaneus

Variable	Obs	Mean	Std. Dev.	Min	Max
MLCALx	34	86.13824	8.941867	69.9	106.4
MLCAL2x	34	81.66176	8.622698	64.9	100.8
BHCALx	34	50.15588	6.024706	39.7	63.5
MinBHCALx	34	37.68529	4.245292	31.6	46.8
MinAHCALx	34	24.88824	3.155732	19.7	31
MinAWCALx	34	24.53529	2.057637	21.9	29.2
AAAPCALx	34	96.14176	7.297418	79.13	113.69
AIPTFCALx	34	43.98088	4.691038	30.86	54.06
AIMTFCALx	34	46.62176	5.470833	35	56.25
AALCALx	34	97.07676	3.726565	89.08	103.72
BTACALx	34	29.21235	4.537932	18.14	40.32
GACALx	34	117.7662	7.866995	102.01	133.13
CACALx	34	19.66912	3.073751	12.56	26.12
FACALx	34	29.35235	3.542722	22.89	35.71
TACALax	34	67.29294	6.757546	50.1	78.43
TACALbx	34	22.76647	6.675026	12.14	39.28

foottype3 = 1 (Low arch)Talus

MaxLTALx	28	59.57857	8.411252	47.5	81.2
MaxHBTALx	28	32.44286	4.365643	26.1	43.2
BHTALx	28	30.33214	4.023915	23.7	39.3
MaxLFMTALx	28	28.11786	3.691236	22.7	35.9

MaxWHTALx	28	31.50357	4.322678	24.6	39.3
MinWNTALx	28	28.2	3.692836	22.3	35.5
MaxLHNTALx	28	27.10357	4.223171	20.3	35.8
AHTALx	28	87.51464	5.463091	79.64	106.68
ANTALx	28	115.1071	5.186081	106.72	126.08
IANTALx	28	28.64607	2.999214	24.55	37.2
IANTALxJ	28	38.34461	5.001401	30.89	50.84

foottype3 = 1 (Low arch)

APTCA	45	22.30289	8.839249	9.48	44.32
TCUA	45	42.50222	10.87195	19.95	68.26
CIAL	45	12.79667	2.192711	7.4	15.56
CIA2	45	15.07422	2.559781	9.69	20.3
LTCA	45	39.73533	5.027333	30.02	52.86
TDA	45	26.89622	4.944037	18.2	41.2
FMDA	45	19.23067	3.216524	11.37	26.95
TFMA	45	8.009556	6.599898	.19	27.87
AH	45	31.74222	5.590962	20.7	43.2
PLL	45	160.1089	15.43669	126.6	191.5
FLCM	45	191.8022	16.95979	159.9	226.8
FL	45	247.4889	21.36286	207.7	290.1
CLAH	45	10.4	4.787911	.9	23.6
AHFLCM	45	.1663778	.0299206	.096	.219
AHFL	45	.1306667	.0228742	.074	.177

foottype3 = 1 (Low arch) ratios

MLCALxFL	34	.3454571	.0151886	.3217523	.3712062
MLCALxFLCM	34	.4469173	.0195443	.4094185	.4782375
BHCALxMLCALx	34	.5821991	.0344506	.4968711	.6616279
MinAHCALxM~x	34	.2888242	.01897	.2533	.3282774
MinAWC~LCALx	34	.2864243	.0245008	.243129	.3304721
MinAWC~HCALx	34	.9956864	.1065034	.7931034	1.1934
MaxLTALxFL	28	.2416215	.0177513	.2130081	.2799035
MaxLTALxFLCM	28	.3122696	.0222163	.2722078	.3580247
BHTALx~LTALx	28	.5105441	.0324345	.4300442	.5877863
BHTALx~MTALx	28	1.081405	.08049	.9294118	1.194656
MaxLFMTALx~x	28	.4745071	.0456974	.4106583	.5836177
MaxLHNTALxFL	28	.1100064	.0121552	.08533	.1379763
MaxLHNTALx~M	28	.1421631	.0154738	.1112329	.1773649
MaxWHTALxM~x	28	1.169953	.1053035	.9498069	1.359606
MinWNTALxM~x	28	.8964884	.032786	.8212121	.9601449

->

foottype3 = Normal Arch Calcaneus

Variable	Obs	Mean	Std. Dev.	Min	Max
MLCALx	23	82.91304	7.433909	69.2	102.2
MLCAL2x	23	77.68261	6.85994	63.8	92.9
BHCALx	23	49.07391	5.076346	38.3	58.2
MinBHCALx	23	37.95652	3.296255	33.1	44.2
MinAHCALx	23	23.57826	2.321433	18.7	26.9
MinAWCALx	23	23.6913	2.672233	19.1	29.2
AAAPCALx	23	98.03217	6.910451	86.42	112.81
AIPTFCALx	23	46.74261	5.698135	34.39	57.74
AIMTFCALx	23	49.51913	6.701353	38.68	62.27
AALCALx	23	103.1091	7.427159	90.38	116.11
BTACALx	23	32.43957	4.936649	21.16	40.59
GACALx	23	122.3987	6.898874	104.64	132.77
CACALx	23	24.11696	5.13807	13.4	33.54
FACALx	23	32.40174	5.188297	23.55	44.37
TACALax	23	65.82652	7.77538	50.53	79.39
TACALbx	23	23.92043	7.475275	10.94	39.92

foottype3 = Normal Arch Talus

MaxLTALx	25	59.296	5.910406	50.3	69
MaxHBTALx	25	32.692	3.25601	25.9	40.5
BHTALx	25	30.828	4.352157	24.6	42.8
MaxLFMTALx	25	28.856	3.111013	23.1	34.1
MaxWHTALx	25	31.636	3.957364	26.8	41.6
MinWNTALx	25	28.348	3.946213	21.2	37
MaxLHNTALx	25	26.988	4.346006	20.9	38.3
AHTALx	25	86.2436	6.512367	73.35	96.65
ANTALx	25	112.748	6.08776	101.14	123.44
IANTALx	25	29.596	4.225697	19.69	36.61
IANTALxJ	25	36.532	5.035734	29.4	49.42

foottype3 = Normal Arch Foot

APTCA	37	18.49108	6.888239	8.5	41.06
TCUA	37	35.22838	9.326414	11.83	56.38
CIA1	37	20.22108	2.836192	16.07	24.55
CIA2	37	22.4527	3.414353	16.53	29.26
LTCA	37	44.35649	4.036738	35.74	53.69
TDA	37	24.26541	3.487033	18.27	33.24
FMDA	37	22.3227	2.832871	14.07	27.59
TFMA	37	3.812973	3.580681	.14	14.92
AH	37	39.31892	5.306539	29.7	52
FLL	37	153.9459	14.16929	126.9	182.1

FLCM	37	186.6162	16.49447	157.2	221.5
FL	37	241.8811	22.10224	204	289.5
CLAH	37	9.624324	3.876597	1.9	14.9

AHFLCM	37	.2118378	.0315273	.147	.287
AHFL	37	.1617027	.0249164	.112	.218

foottype3 = Normal Arch Ratios

MLCALxFL	23	.3531481	.0131978	.3315764	.3799555
MLCALxFLCM	23	.4575245	.0160735	.4276885	.4985389
BHCALxMLCALx	23	.5918418	.030885	.5194508	.6407879

MinAHCALxM~x	23	.2847997	.0210145	.2470277	.3367052
MinAWC~LCALx	23	.2860976	.0246316	.2323601	.333815
MinAWC~HCALx	23	1.00737	.0893177	.8197425	1.197861
MaxLTALxFL	25	.2492416	.0131523	.2312898	.2807597
MaxLTALxFLCM	25	.3233745	.0167649	.3008357	.3671706

BHTALx~LTALx	25	.5203675	.0540037	.4499205	.6604938
BHTALx~MTALx	25	1.07047	.1111497	.8734568	1.316239
MaxLFMTALx~x	25	.4877122	.0394371	.3993174	.5898438
MaxLHNTALxFL	25	.1132565	.0131527	.0915411	.13902
MaxLHNTALx~M	25	.1469671	.0173164	.1189759	.1831659

MaxWHTALxM~x	25	1.18386	.1259926	1.006494	1.439446
MinWNTALxM~x	25	.8953216	.0470223	.7438596	.961165

-> foottype3 = 5 High Arch Calcaneus

Variable	Obs	Mean	Std. Dev.	Min	Max

MLCALx	17	87.99412	5.43662	77.1	100.4
MLCAL2x	17	81.42941	5.435849	71.1	93.1
BHCALx	17	54.14118	4.229814	47.1	62.1
MinBHCALx	17	40.80588	2.973102	34.7	45.3
MinAHCALx	17	23.37647	1.773249	20.3	27.3

MinAWCALx	17	25.16471	2.259408	22.3	30.2
AAAPCALx	17	98.56059	7.139291	85.82	113.13
AIPTFCALx	17	54.40824	7.022549	39.08	66.97
AIMTFCALx	17	53.83882	7.192406	37.41	66.86
AALCALx	17	109.6535	7.910246	101.17	131.28

BTACALx	17	38.32706	5.821594	29.55	48.65
GACALx	17	120.0318	7.318522	109.22	132.57
CACALx	17	30.40529	7.013636	18.33	47.41
FACALx	17	36.88118	5.911741	26.94	51.28
TACALax	17	61.71588	5.438853	51.2	71.75

TACALbx	17	28.41118	5.671889	18.88	38.76

foottype3 = 5 High Arch Talus

MaxLTALx		15	62.28667	3.940063	53	69.3
MaxHBTALx		15	34.01333	2.774853	28.5	37.7
BHTALx		15	32.20667	2.816905	25.9	35.2
MaxLFMTALx		15	30.43333	3.4014	24.5	37.6

MaxWHTALx		15	33.36667	2.328907	29.7	37.8
MinWNTALx		15	28.54	1.609259	25.3	31.2
MaxLHNTALx		15	29.03333	2.15296	25.2	32.5
AHTALx		15	87.88467	7.644983	70.56	104.6
ANTALx		15	112.528	6.406181	97.73	125.48

IANTALx		15	28.98133	2.40122	25.01	33.19
IANTALxJ		15	37.786	6.03899	21.15	46.29

foottype3 = 5 High Arch Foot

APTCA		21	17.93714	5.144715	5.28	27.17
TCUA		21	34.98429	10.63086	8.59	60.13
CIAI		21	27.73238	2.239183	25.32	32.97

CIA2		21	29.30714	3.08174	23.44	35.59
LTCA		21	51.52048	4.890938	44.16	61.09
TDA		21	23.75476	4.852143	13.99	31.86
FMDA		21	23.35952	2.908263	17.69	29.77
TFMA		21	4.26381	3.164212	.36	10.77

AH		21	43.7	6.537507	26.6	52.6
FLL		21	157.3524	11.48667	130.4	175.7
FLCM		21	192.1238	11.88305	166.9	209.6
FL		21	248.3143	15.57181	214.4	269.4
CLAH		21	11.43333	3.895168	5.5	19.2

AHFLCM		21	.2287143	.0402569	.139	.304
AHFL		21	.177	.0313002	.108	.232

foottype3 = 5 High Arch Ratios

MLCALxFL		17	.358649	.0166531	.3282326	.3901365
MLCALxFLCM		17	.4631169	.020952	.4320242	.5115473
BHCALxMLCALx		17	.6154327	.0323809	.548951	.6535797

MinAHCALxM~x		17	.2689447	.0232615	.2204126	.3084746
MinAWC~LCALx		17	.2893349	.0250933	.2582011	.341629
MinAWC~HCALx		17	1.08005	.0967388	.9344262	1.280788
MaxLTALxFL		15	.2543373	.0106482	.2383094	.2671629
MaxLTALxFLCM		15	.32833	.0130708	.3062977	.348248

BHTALx~LTALx		15	.5169587	.0300205	.4592199	.5607029
BHTALx~MTALx		15	1.063598	.0848511	.9361702	1.191781
MaxLFMTALx~x		15	.4882349	.0405255	.4329004	.5749235
MaxLHNTALxFL		15	.118633	.0079011	.101993	.1275053
MaxLHNTALx~M		15	.1532058	.0109467	.1325546	.1639344

```
-----+-----
MaxWHTALxM~x |      15   1.151791   .0734662   1.036923   1.275862
MinWNTALxM~x |      15   .8571205   .0450139   .7838617   .9265176
```

. Linear Regressions Talus

```
. reg MaxLTALx foottype3, cluster(SpecimenNumber)
```

```
Linear regression              Number of obs   =          68
                               F(1, 49)       =           0.84
                               Prob > F             =          0.3639
                               R-squared            =          0.0178
                               Root MSE         =          6.7496
```

(Std. Err. adjusted for 50 clusters in SpecimenNumber)

```
-----+-----
MaxLTALx |              Robust
          |      Coef.   Std. Err.   t    P>|t|   [95% Conf. Interval]
-----+-----
foottype3 |   .58049   .6334028   0.92  0.364   - .6923807   1.853361
   _cons |  58.55254  2.400805  24.39  0.000   53.72794   63.37714
-----+-----
```

```
. reg MaxHTALx foottype3, cluster(SpecimenNumber)
```

```
Linear regression              Number of obs   =          68
                               F(1, 49)       =           1.01
                               Prob > F             =          0.3196
                               R-squared            =          0.0234
                               Root MSE         =          3.654
```

(Std. Err. adjusted for 50 clusters in SpecimenNumber)

```
-----+-----
MaxHTALx |              Robust
          |      Coef.   Std. Err.   t    P>|t|   [95% Conf. Interval]
-----+-----
foottype3 |   .3609982  .3590088   1.01  0.320   - .360457   1.082453
   _cons |  31.93592  1.28427   24.87  0.000   29.35508   34.51675
-----+-----
```

```
. reg BHTALx foottype3, cluster(SpecimenNumber)
```

```
Linear regression              Number of obs   =          68
                               F(1, 49)       =           1.76
                               Prob > F             =          0.1909
                               R-squared            =          0.0306
                               Root MSE         =          3.9038
```

(Std. Err. adjusted for 50 clusters in SpecimenNumber)

```
-----+-----
BHTALx |              Robust
        |      Coef.   Std. Err.   t    P>|t|   [95% Conf. Interval]
-----+-----
```

Chapter 4 Linear regression analysis

```

-----+-----
MaxWHTALxM-x |      15      1.151791      .0734662      1.036923      1.275862
MinWNTALxM-x |      15      .8571205      .0450139      .7838617      .9265176

. Linear Regressions Talus
.
. reg MaxLTALx foottype3, cluster(SpecimenNumber)

Linear regression                               Number of obs   =          68
                                                F(1, 49)       =           0.84
                                                Prob > F       =          0.3639
                                                R-squared     =          0.0178
                                                Root MSE     =          6.7496

                               (Std. Err. adjusted for 50 clusters in SpecimenNumber)
-----+-----
MaxLTALx |      Coef.      Robust      t      P>|t|      [95% Conf. Interval]
          |      Std. Err.
-----+-----
foottype3 |      .58049      .6334028      0.92      0.364      -.6923807      1.853361
_cons     |      58.55254      2.400805      24.39      0.000      53.72794      63.37714
-----+-----

. reg MaxHBOTALx foottype3, cluster(SpecimenNumber)

Linear regression                               Number of obs   =          68
                                                F(1, 49)       =           1.01
                                                Prob > F       =          0.3196
                                                R-squared     =          0.0234
                                                Root MSE     =          3.654

                               (Std. Err. adjusted for 50 clusters in SpecimenNumber)
-----+-----
MaxHBOTALx |      Coef.      Robust      t      P>|t|      [95% Conf. Interval]
          |      Std. Err.
-----+-----
foottype3 |      .3609982      .3590088      1.01      0.320      -.360457      1.082453
_cons     |      31.93592      1.28427      24.87      0.000      29.35508      34.51675
-----+-----

. reg BOTALx foottype3, cluster(SpecimenNumber)

Linear regression                               Number of obs   =          68
                                                F(1, 49)       =           1.76
                                                Prob > F       =          0.1909
                                                R-squared     =          0.0306
                                                Root MSE     =          3.9038

                               (Std. Err. adjusted for 50 clusters in SpecimenNumber)
-----+-----
BOTALx |      Coef.      Robust      t      P>|t|      [95% Conf. Interval]
        |      Std. Err.
-----+-----

```

```

footype3 | .4425953 .3336861 1.33 0.191 -.2279721 1.113163
_cons | 29.76938 1.17456 25.35 0.000 27.40902 32.12975
-----

```

```
. reg MaxLFMTALx fotype3, cluster(SpecimenNumber)
```

```

Linear regression      Number of obs   =      68
                      F(1, 49)         =      2.55
                      Prob > F         =     0.1169
                      R-squared        =     0.0611
                      Root MSE      =     3.4041

```

(Std. Err. adjusted for 50 clusters in SpecimenNumber)

```

-----+-----
MaxLFMTALx |          Robust
           |      Coef.   Std. Err.      t    P>|t|     [95% Conf. Interval]
-----+-----
footype3 |   .5541198   .3471299     1.60  0.117   - .1434638   1.251703
_cons |  27.44951   1.123135    24.44  0.000   25.19249   29.70653
-----+-----

```

```
. reg MaxWHTALx fotype3, cluster(SpecimenNumber)
```

```

Linear regression      Number of obs   =      68
                      F(1, 49)         =      1.60
                      Prob > F         =     0.2121
                      R-squared        =     0.0286
                      Root MSE      =     3.8258

```

(Std. Err. adjusted for 50 clusters in SpecimenNumber)

```

-----+-----
MaxWHTALx |          Robust
           |      Coef.   Std. Err.      t    P>|t|     [95% Conf. Interval]
-----+-----
footype3 |   .4186388   .3311444     1.26  0.212   - .2468208   1.084098
_cons |  30.86739   1.215694    25.39  0.000   28.42436   33.31041
-----+-----

```

```
. reg MinWNTALx fotype3, cluster(SpecimenNumber)
```

```

Linear regression      Number of obs   =      68
                      F(1, 49)         =      0.10
                      Prob > F         =     0.7529
                      R-squared        =     0.0015
                      Root MSE      =     3.4338

```

(Std. Err. adjusted for 50 clusters in SpecimenNumber)

```

-----+-----
MinWNTALx |          Robust
           |      Coef.   Std. Err.      t    P>|t|     [95% Conf. Interval]
-----+-----
footype3 |   .0837024   .2644059     0.32  0.753   - .4476412   .6150459
_cons |  28.11031   1.015091    27.69  0.000   26.07041   30.15021
-----+-----

```

```
. reg MaxLHNTALx foottype3, cluster(SpecimenNumber)
```

```
Linear regression      Number of obs   =      68
                      F(1, 49)         =      1.70
                      Prob > F         =     0.1979
                      R-squared        =     0.0272
                      Root MSE      =     3.9265
```

(Std. Err. adjusted for 50 clusters in SpecimenNumber)

		Robust				
MaxLHNTALx	Coef.	Std. Err.	t	P> t	[95% Conf. Interval]	
foottype3	.4187114	.3207557	1.31	0.198	-.2258713	1.063294
_cons	26.39073	1.168328	22.59	0.000	24.04288	28.73857

```
. reg AHTALx foottype3, cluster(SpecimenNumber)
```

```
Linear regression      Number of obs   =      68
                      F(1, 49)         =      0.00
                      Prob > F         =     0.9908
                      R-squared        =     0.0000
                      Root MSE      =     6.3654
```

(Std. Err. adjusted for 50 clusters in SpecimenNumber)

		Robust				
AHTALx	Coef.	Std. Err.	t	P> t	[95% Conf. Interval]	
foottype3	.0066225	.5744645	0.01	0.991	-1.147807	1.161052
_cons	87.11164	1.416217	61.51	0.000	84.26564	89.95763

```
. reg ANTALx foottype3, cluster(SpecimenNumber)
```

```
Linear regression      Number of obs   =      68
                      F(1, 49)         =      2.06
                      Prob > F         =     0.1576
                      R-squared        =     0.0355
                      Root MSE      =     5.7835
```

(Std. Err. adjusted for 50 clusters in SpecimenNumber)

		Robust				
ANTALx	Coef.	Std. Err.	t	P> t	[95% Conf. Interval]	
foottype3	-.707873	.4931957	-1.44	0.158	-1.698987	.2832409
_cons	115.5238	1.294222	89.26	0.000	112.923	118.1247

```
. reg IANTALx foottype3, cluster(SpecimenNumber)
```

```

Linear regression              Number of obs   =       68
                              F(1, 49)       =       0.29
                              Prob > F             =     0.5942
                              R-squared            =     0.0036
                              Root MSE         =     3.3967

```

(Std. Err. adjusted for 50 clusters in SpecimenNumber)

		Robust				
IANTALx	Coef.	Std. Err.	t	P> t	[95% Conf. Interval]	
footype3	.1299583	.2423292	0.54	0.594	-.3570206	.6169371
_cons	28.72908	.7943212	36.17	0.000	27.13283	30.32533

```
. reg IANTALxJ fotype3, cluster(SpecimenNumber)
```

```

Linear regression              Number of obs   =       68
                              F(1, 49)       =       0.23
                              Prob > F             =     0.6300
                              R-squared            =     0.0047
                              Root MSE         =     5.2662

```

(Std. Err. adjusted for 50 clusters in SpecimenNumber)

		Robust				
IANTALxJ	Coef.	Std. Err.	t	P> t	[95% Conf. Interval]	
footype3	-.2300917	.4747048	-0.48	0.630	-1.184047	.7238634
_cons	38.15728	1.305058	29.24	0.000	35.53467	40.7799

```
Linear regressions Calcaneus
```

```
. reg MLCALx fotype3, cluster(SpecimenNumber)
```

```

Linear regression              Number of obs   =       74
                              F(1, 50)       =       0.13
                              Prob > F             =     0.7209
                              R-squared            =     0.0022
                              Root MSE         =     7.9848

```

(Std. Err. adjusted for 51 clusters in SpecimenNumber)

		Robust				
MLCALx	Coef.	Std. Err.	t	P> t	[95% Conf. Interval]	
footype3	.23099	.6428396	0.36	0.721	-1.060191	1.522171
_cons	84.97532	2.431368	34.95	0.000	80.09178	89.85887

```
. reg MLCAL2x fotype3, cluster(SpecimenNumber)
```

```

Linear regression              Number of obs   =       74
                              F(1, 50)       =       0.19
                              Prob > F             =       0.6627
                              R-squared            =       0.0034
                              Root MSE         =       7.6279

```

(Std. Err. adjusted for 51 clusters in SpecimenNumber)

	Coef.	Robust Std. Err.	t	P> t	[95% Conf. Interval]	
MLCAL2x						
footype3	-.274792	.6262994	-0.44	0.663	-1.532751	.9831673
_cons	81.06974	2.34922	34.51	0.000	76.35119	85.78829

```
. reg BHCALx fotype3, cluster(SpecimenNumber)
```

```

Linear regression              Number of obs   =       74
                              F(1, 50)       =       3.31
                              Prob > F             =       0.0748
                              R-squared            =       0.0550
                              Root MSE         =       5.5217

```

(Std. Err. adjusted for 51 clusters in SpecimenNumber)

	Coef.	Robust Std. Err.	t	P> t	[95% Conf. Interval]	
BHCALx						
footype3	.8238451	.4526948	1.82	0.075	-.0854193	1.733109
_cons	48.64212	1.623312	29.96	0.000	45.38161	51.90264

```
. reg MinBHCALx fotype3, cluster(SpecimenNumber)
```

```

Linear regression              Number of obs   =       74
                              F(1, 50)       =       4.87
                              Prob > F             =       0.0320
                              R-squared            =       0.0862
                              Root MSE         =       3.7278

```

(Std. Err. adjusted for 51 clusters in SpecimenNumber)

	Coef.	Robust Std. Err.	t	P> t	[95% Conf. Interval]	
MinBHCALx						
footype3	.7078336	.3208938	2.21	0.032	.0632995	1.352368
_cons	36.68821	1.147825	31.96	0.000	34.38273	38.99368

```
. reg MinAHCALx fotype3, cluster(SpecimenNumber)
```

```

Linear regression              Number of obs   =       74
                              F(1, 50)       =       3.27
                              Prob > F             =       0.0764

```



```

      _cons | 27.34981 1.060819 25.78 0.000 25.2191 29.48053
-----+-----

```

```
. reg TACALax foottype3, cluster(SpecimenNumber)
```

```

Linear regression              Number of obs   =      74
                               F(1, 50)         =      7.18
                               Prob > F           =     0.0100
                               R-squared           =     0.0896
                               Root MSE        =     6.8078

```

(Std. Err. adjusted for 51 clusters in SpecimenNumber)

```

-----+-----
      |               Robust
TACALax |               Coef.   Std. Err.      t    P>|t|     [95% Conf. Interval]
-----+-----
foottype3 | -1.320098   .492799   -2.68   0.010   -2.309913   -.3302817
_cons | 68.90971   1.674426   41.15   0.000   65.54652    72.27289
-----+-----

```

```
. reg TACALbx foottype3, cluster(SpecimenNumber)
```

```

Linear regression              Number of obs   =      74
                               F(1, 50)         =      7.06
                               Prob > F           =     0.0106
                               R-squared           =     0.0912
                               Root MSE        =     6.7257

```

(Std. Err. adjusted for 51 clusters in SpecimenNumber)

```

-----+-----
      |               Robust
TACALbx |               Coef.   Std. Err.      t    P>|t|     [95% Conf. Interval]
-----+-----
foottype3 | 1.317584   .4959187   2.66   0.011   .3215019    2.313666
_cons | 21.07452   1.624186   12.98   0.000   17.81224    24.33679
-----+-----

```

Regression analysis: Table 1 Foot type (CIA1 variable) Results with Constant

```
reg APTCA foottype3, cluster(SpecimenNumber)
```

```

Linear regression              Number of obs   =     103
                               F(1, 71)         =      5.11
                               Prob > F           =     0.0268
                               R-squared           =     0.0579
                               Root MSE        =     7.5354

```

(Std. Err. adjusted for 72 clusters in SpecimenNumber)

```

-----+-----
      |               Robust
APTCA |               Coef.   Std. Err.      t    P>|t|     [95% Conf. Interval]
-----+-----
foottype3 | -1.207677   .5341445   -2.26   0.027   -2.272731   -.1426229
-----+-----

```

```

      _cons | 23.10372  1.872341  12.34  0.000  19.37038  26.83707
-----+-----

```

```

. reg TCUA foottype3, cluster(SpecimenNumber)

```

```

Linear regression              Number of obs   =      103
                              F(1, 71)       =       8.41
                              Prob > F         =     0.0050
                              R-squared        =     0.0916
                              Root MSE      =    10.374

```

(Std. Err. adjusted for 72 clusters in SpecimenNumber)

```

-----+-----
      TCUA |          Coef.   Robust
            |          Std. Err.   t   P>|t|   [95% Conf. Interval]
-----+-----
foottype3 | -2.130305   .7345132   -2.90  0.005   -3.594882   -.6657269
_cons     |  43.75466   2.362769   18.52  0.000   39.04343   48.46588
-----+-----

```

```

. reg CIA1 foottype3, cluster(SpecimenNumber)

```

```

Linear regression              Number of obs   =      103
                              F(1, 71)       =     583.37
                              Prob > F         =     0.0000
                              R-squared        =     0.8483
                              Root MSE      =     2.4403

```

(Std. Err. adjusted for 72 clusters in SpecimenNumber)

```

-----+-----
      CIA1 |          Coef.   Robust
            |          Std. Err.   t   P>|t|   [95% Conf. Interval]
-----+-----
foottype3 |  3.730829   .1544666   24.15  0.000    3.422831    4.038826
_cons     |  9.054988   .4683986   19.33  0.000    8.121028    9.988948
-----+-----

```

```

. reg CIA2 foottype3, cluster(SpecimenNumber)

```

```

Linear regression              Number of obs   =      103
                              F(1, 71)       =     289.19
                              Prob > F         =     0.0000
                              R-squared        =     0.7746
                              Root MSE      =     2.9842

```

(Std. Err. adjusted for 72 clusters in SpecimenNumber)

```

-----+-----
      CIA2 |          Coef.   Robust
            |          Std. Err.   t   P>|t|   [95% Conf. Interval]
-----+-----
foottype3 |  3.576928   .2103383   17.01  0.000    3.157525    3.996331
_cons     | 11.56274   .6108909   18.93  0.000   10.34465   12.78082
-----+-----

```

```
. reg LTCA foottype3, cluster(SpecimenNumber)
```

```
Linear regression      Number of obs   =      103
                      F(1, 71)           =      57.53
                      Prob > F          =      0.0000
                      R-squared         =      0.4709
                      Root MSE        =      4.6814
```

(Std. Err. adjusted for 72 clusters in SpecimenNumber)

	Coef.	Robust Std. Err.	t	P> t	[95% Conf. Interval]	
LTCA						
foottype3	2.855558	.3764654	7.59	0.000	2.104907	3.606208
_cons	36.56223	1.160575	31.50	0.000	34.24811	38.87635

```
. reg TDA foottype3, cluster(SpecimenNumber)
```

```
Linear regression      Number of obs   =      103
                      F(1, 71)           =      5.29
                      Prob > F          =      0.0244
                      R-squared         =      0.0819
                      Root MSE        =      4.4604
```

(Std. Err. adjusted for 72 clusters in SpecimenNumber)

	Coef.	Robust Std. Err.	t	P> t	[95% Conf. Interval]	
TDA						
foottype3	-.8610125	.3744943	-2.30	0.024	-1.607733	-.114292
_cons	27.49247	1.162846	23.64	0.000	25.17382	29.81112

```
. reg FMDA foottype3, cluster(SpecimenNumber)
```

```
Linear regression      Number of obs   =      103
                      F(1, 71)           =      25.32
                      Prob > F          =      0.0000
                      R-squared         =      0.2396
                      Root MSE        =      3.0459
```

(Std. Err. adjusted for 72 clusters in SpecimenNumber)

	Coef.	Robust Std. Err.	t	P> t	[95% Conf. Interval]	
FMDA						
foottype3	1.105544	.2197287	5.03	0.000	.6674174	1.543671
_cons	18.38178	.7281377	25.24	0.000	16.92991	19.83364

```
. reg TFMA foottype3, cluster(SpecimenNumber)
```

```
Linear regression      Number of obs   =      103
```

```

F(1, 71) = 7.85
Prob > F = 0.0065
R-squared = 0.0981
Root MSE = 5.1701

```

(Std. Err. adjusted for 72 clusters in SpecimenNumber)

		Coef.	Robust Std. Err.	t	P> t	[95% Conf. Interval]	
TFMA							
foottype3		-1.102256	.3934249	-2.80	0.007	-1.886723	-.3177888
_cons		8.531444	1.495832	5.70	0.000	5.54884	11.51405

```
. reg AH foottype3, cluster(SpecimenNumber)
```

```

Linear regression      Number of obs   =      103
                      F(1, 71)             =      46.69
                      Prob > F           =      0.0000
                      R-squared          =      0.4135
                      Root MSE        =      5.7172

```

(Std. Err. adjusted for 72 clusters in SpecimenNumber)

		Coef.	Robust Std. Err.	t	P> t	[95% Conf. Interval]	
AH							
foottype3		3.103464	.454165	6.83	0.000	2.197884	4.009043
_cons		29.03783	1.255306	23.13	0.000	26.53482	31.54083

```
. reg FLL foottype3, cluster(SpecimenNumber)
```

```

Linear regression      Number of obs   =      103
                      F(1, 71)             =      0.90
                      Prob > F           =      0.3470
                      R-squared          =      0.0121
                      Root MSE        =      14.373

```

(Std. Err. adjusted for 72 clusters in SpecimenNumber)

		Coef.	Robust Std. Err.	t	P> t	[95% Conf. Interval]	
FLL							
foottype3		-1.030561	1.088657	-0.95	0.347	-3.201281	1.140159
_cons		159.9444	3.701231	43.21	0.000	152.5644	167.3245

```
. reg FLCM foottype3, cluster(SpecimenNumber)
```

```

Linear regression      Number of obs   =      103
                      F(1, 71)             =      0.07
                      Prob > F           =      0.7945
                      R-squared          =      0.0008

```



```

Prob > F      = 0.0190
R-squared    = 0.1152
Root MSE     = 0.01879

```

(Std. Err. adjusted for 51 clusters in SpecimenNumber)

MLCALxFLCM	Coef.	Robust Std. Err.	t	P> t	[95% Conf. Interval]	
footype3	.0041906	.0017289	2.42	0.019	.000718	.0076632
_cons	.4432894	.0053589	82.72	0.000	.4325256	.4540531

```
. reg BHCALxMLCALx fotype3, cluster(SpecimenNumber)
```

```

Linear regression      Number of obs   =      74
                      F(1, 50)           =      8.19
                      Prob > F         =     0.0061
                      R-squared        =     0.1320
                      Root MSE       =     0.03284

```

(Std. Err. adjusted for 51 clusters in SpecimenNumber)

BHCALxMLCALx	Coef.	Robust Std. Err.	t	P> t	[95% Conf. Interval]	
footype3	.0079172	.0027666	2.86	0.006	.0023603	.0134741
_cons	.572717	.0085068	67.32	0.000	.5556306	.5898035

```
. reg MinAHCALxMLCALx fotype3, cluster(SpecimenNumber)
```

```

Linear regression      Number of obs   =      74
                      F(1, 50)           =      5.63
                      Prob > F         =     0.0215
                      R-squared        =     0.1163
                      Root MSE       =     0.02068

```

(Std. Err. adjusted for 51 clusters in SpecimenNumber)

MinAHCALxM~x	Coef.	Robust Std. Err.	t	P> t	[95% Conf. Interval]	
footype3	-.004638	.0019541	-2.37	0.022	-.0085629	-.0007132
_cons	.2947896	.005203	56.66	0.000	.284339	.3052402

```
. reg MinAWCALxMLCALx fotype3, cluster(SpecimenNumber)
```

```

Linear regression      Number of obs   =      74
                      F(1, 50)           =      0.08
                      Prob > F         =     0.7784
                      R-squared        =     0.0017
                      Root MSE       =     0.02452

```

(Std. Err. adjusted for 51 clusters in SpecimenNumber)

	Coef.	Robust Std. Err.	t	P> t	[95% Conf. Interval]	
MinAWC~LCALx						
footype3	.0006277	.0022189	0.28	0.778	-.0038291	.0050845
_cons	.2853967	.0067746	42.13	0.000	.2717896	.2990038

. reg MinAWCALxMinAHCALx fotype3, cluster(SpecimenNumber)

Linear regression

Number of obs	=	74
F(1, 50)	=	5.08
Prob > F	=	0.0286
R-squared	=	0.0902
Root MSE	=	.09957

(Std. Err. adjusted for 51 clusters in SpecimenNumber)

	Coef.	Robust Std. Err.	t	P> t	[95% Conf. Interval]	
MinAWC~HCALx						
footype3	.01938	.0085988	2.25	0.029	.0021088	.0366512
_cons	.969463	.0279925	34.63	0.000	.9132384	1.025688

. reg MaxLTALxFL fotype3, cluster(SpecimenNumber)

Linear regression

Number of obs	=	68
F(1, 49)	=	6.00
Prob > F	=	0.0180
R-squared	=	0.1073
Root MSE	=	.0147

(Std. Err. adjusted for 50 clusters in SpecimenNumber)

	Coef.	Robust Std. Err.	t	P> t	[95% Conf. Interval]	
MaxLTALxFL						
footype3	.0032534	.0013287	2.45	0.018	.0005832	.0059235
_cons	.2387117	.0048652	49.07	0.000	.2289347	.2484887

. reg MaxLTALxFLCM fotype3, cluster(SpecimenNumber)

Linear regression

Number of obs	=	68
F(1, 49)	=	6.58
Prob > F	=	0.0135
R-squared	=	0.1121
Root MSE	=	.01851

(Std. Err. adjusted for 50 clusters in SpecimenNumber)

```

footype3 | .003806 .0040036 0.95 0.346 -.0042395 .0118514
_cons | .4724274 .0130143 36.30 0.000 .4462743 .4985806
-----

```

```
. reg MaxLHNTALxFL fotype3, cluster(SpecimenNumber)
```

```

Linear regression              Number of obs   =      68
                              F(1, 49)        =      5.37
                              Prob > F              =     0.0248
                              R-squared             =     0.0729
                              Root MSE          =     .0117

```

(Std. Err. adjusted for 50 clusters in SpecimenNumber)

```

-----+-----
MaxLHNTALxFL |           Robust
              |   Coef.   Std. Err.   t    P>|t|   [95% Conf. Interval]
-----+-----
footype3 |   .0020939   .0009039    2.32  0.025   .0002775   .0039104
_cons |   .107623   .0031918   33.72  0.000   .1012089   .1140371
-----+-----

```

```
. reg MaxLHNTALxFLCM fotype3, cluster(SpecimenNumber)
```

```

Linear regression              Number of obs   =      68
                              F(1, 49)        =      5.28
                              Prob > F              =     0.0258
                              R-squared             =     0.0724
                              Root MSE          =     .01525

```

(Std. Err. adjusted for 50 clusters in SpecimenNumber)

```

-----+-----
MaxLHNTALx~M |           Robust
              |   Coef.   Std. Err.   t    P>|t|   [95% Conf. Interval]
-----+-----
footype3 |   .0027184   .0011825    2.30  0.026   .000342   .0050948
_cons |   .1392494   .0040648   34.26  0.000   .131081   .1474179
-----+-----

```

```
. reg MaxWHTALxMaxLHNTALx fotype3, cluster(SpecimenNumber)
```

```

Linear regression              Number of obs   =      68
                              F(1, 49)        =      0.17
                              Prob > F              =     0.6843
                              R-squared             =     0.0021
                              Root MSE          =     .10759

```

(Std. Err. adjusted for 50 clusters in SpecimenNumber)

```

-----+-----
MaxWHTALxM~x |           Robust
              |   Coef.   Std. Err.   t    P>|t|   [95% Conf. Interval]
-----+-----
footype3 |  -.0031846   .0077862   -0.41  0.684   -.0188315   .0124624
_cons |   1.179395   .0260067   45.35  0.000   1.127133   1.231658
-----+-----

```

```

. reg MinWNTALxMaxWHTALx foottype3, cluster(SpecimenNumber)

Linear regression                               Number of obs   =       68
                                                F(1, 49)       =       5.53
                                                Prob > F       =       0.0228
                                                R-squared     =       0.0969
                                                Root MSE     =       .04187

```

(Std. Err. adjusted for 50 clusters in SpecimenNumber)

```

-----+-----
MinWNTALxM~x |          Coef.   Robust          t    P>|t|    [95% Conf. Interval]
               |          Std. Err.
-----+-----
    foottype3 |   -.0087498   .0037219   -2.35  0.023   -.0162292   -.0012703
       _cons |    .9102791   .0095858   94.96  0.000    .8910158    .9295425
-----+-----

```

```

.
end of do-file

```

VITA

David Agoada was born in Brooklyn, New York in 1950. He received a bachelor's degree in anthropology from Brooklyn College in 1972. After spending five years in graduate studies in physical anthropology at the University of Washington in Seattle, he attended the Pennsylvania College of Podiatric Medicine (now Temple University School of Podiatric Medicine), where he received his Doctor of Podiatric Medicine degree in 1981. He completed his surgical residency at New England Deaconess Hospital (now Beth Israel Deaconess Hospital) in 1983. He was a staff podiatrist at Harvard Vanguard Medical Associates, in Boston, for over 30 years. Dr. Agoada is board certified in both podiatric surgery and podiatric orthopedics. He has been actively involved in developing board examinations for the podiatric profession, serving as chairman of the lower extremity anatomy section of the National Board of Podiatric Medical Examiners from 1992 to 2015. Dr. Agoada has a longtime interest in the forensic sciences. He received master's degrees in forensic medicine from the Philadelphia College of Osteopathic Medicine in 2008 and in forensic anthropology from Boston University's School of Medicine in 2011. He resumed his graduate studies in biological anthropology between 1986 and 1990 and completed his dissertation research in 2018. His areas of interest continue to be the form and function of the human foot as well as the evolution of hominin bipedal locomotion.